A STRUCTURAL STUDY OF THE GRØVUDAL FOLD-NAPPE, NORTHERN DOVREFJELL, CENTRAL NORWAY

THESIS
SUBMITTED TO THE FACULTY OF THE
GRADUATE SCHOOL OF THE
UNIVERSITY OF MINNESOTA

BY

FREDERICK WOLFER VOLLMER

IN PARTIAL FULFILLMENT OF THE REQUIREMENTS
FOR THE DEGREE OF
DOCTOR OF PHILOSOPHY

JUNE 1985

ACKNOWLEDGEMENTS

I thank my thesis advisor, Peter J. Hudleston, for his help, friendship, and encouragement during this study, and for his valuable insight and discussion during my stay at the University of Minnesota. Fredrik Chr. Wolff and Alan G. Krill of the Norges Geologiske Undersøkelse provided invaluable aid, direction and hospitality during my stays in Norway, and kindly supplied personal maps, equipment and literature for my studies. The Suisdal family provided generous hospitality during my stays in Grøvudalen, including mail service, and I thank Terje, Torhil and Oddrun Suisdal for their fine milk and cheeses, and Oddrun for the use of her Volkswagon for weekly supply trips in 1983. My fellow graduate students at the University of Minnesota, Stephen F. Wright and Dan Ela, provided moral and intellectual support. Finally, I thank my wife, Debra, for her patience.

Financial support for this study was provided by a research grant from the Geological Society of America, a Haakon Styri Fellowship from the American-Scandinavian Foundation, a Torske Klubben Fellowship, grants from the Minneapolis Foundation-Francis E. Andrews Fund, the University of Minnesota Grants for Research Abroad, and the Chevron Fund. The Norges Geologiske Undersøkelse also provided financial aid and field support. Computer time was provided by a grant from the University of Minnesota Computer Center. Support for my academic studies at the University of Minnesota is gratefully acknowledged from a University of Minnesota Graduate School Fellowship and a Doctoral Dissertation Fellowship, as well as teaching assistantships and a research assistantship under Peter J. Hudleston. I thank the above institutions and individuals for their generous support.

ABSTRACT

The Grøvudal area of the northern Dovrefjell lies within the high-grade core of the Caledonian orogen in western central Norway. The focus of this study is the southern portion of a large infold of cover into basement gneisses. Lithologic units are correlative with a thrust-nappe sequence exposed along the front of the orogen in Sweden, and were derived from the Precambrian continental margin. Mesoscopic structures are dominated by a trans-position foliation, lineations, and subsimilar folds. Fold axes parallel lineations, and sheath folds are present. Folds with finger-like outcrop patterns are also suggested to be sheath folds. The folding history involves a minimum of three coaxial fold phases, formed during one continous deformation, and a later refolding event. Microstructures suggest pervasive ductile flow.

A computer-aided methodology devised for the structural analysis of the area used foliation eigenvectors to define five NW trending cylindrical domains, and revealed the large structure to be a near-recumbent north-facing fold refolded by an east-verging antiform. On a regional scale this implies that the Grøvudal structure is a synformal 'sheath-nappe', and that basement gneisses to the north and south form major basement-cored sheath-nappes.

Computer-generated passive fold models show that

sheath-folds can be generated by the growth of low amplitude irregularities during progressive simple shear. Sections through the models display interference patterns seen in outcrop and map pattern. Kinematic models of active fold generation show that fold axes formed in progressive simple shear will occur in many orientations easily rotated towards the direction of maximum elongation. In a rock body undergoing plastic flow small changes in applied stresses or surface slope can lead to the rotation of slip lines through a developing foliation, leading to buckle or shear fold formation, and refolding of earlier structures.

Field observations, fold geometry, computer simulation of passive folding, and mechanical considerations are all consistent with a continous deformation dominated by simple shear with an easterly direction of transport.

TABLE OF CONTENTS

LIST OF FIGURES

INTRODUCTION

In considering the Earth's mountain belts one is struck by their great diversity in form, lithologic character, and internal structure. However, most of these orogenic belts share a number of common characteristics. Cross-sections through the world's best studied mountain belts, for example the Appalachians, Canadian Rockies, and Alps, show a typical change in structural style from the foreland to the interior (e.g., Price, 1981; Hatcher, 1981; Trümpy, 1980). This involves a change from thin-skinned thrust tectonics within platform and exogeoclinal sediments, through progressively increased thrusting of far-traveled allochthons and involvement of basement rocks, to ductile fold-nappe tectonics where basement and cover may be intricately folded into immense recumbent structures. In general, the tectonics of these high-grade, basement-involved fold-nappes are less well understood than the thrust-tectonics found farther towards the foreland (e.g., papers in McClay and Price, 1981). In part this is due to economic factors, such as the lack of oil and gas in high grade rocks, but also to the extreme complexity of the highly deformed and metamorphosed, multiply-folded orogenic interiors.

This study is an attempt to work out some of the geometric and kinematic aspects of basement-involved fold-nappes in the interior of the Caledonian orogen in western

Norway. The area chosen for study is in the Dovrefjell Mountains within the eastern portion of the Basal Gneiss Complex, also known as the Møre Gneisses or simply the Western Gneiss Region (Oftedahl, 1980; Cuthbert et al., 1983 and references therein). Fold-nappes structures were first recognised in the Dovrefjell Mountains by Muret (1960). Recent compilation of work in this area has lead to the recognition of regionally mappable tectonic units whose areal distribution is now fairly well constrained (Krill, 1980a; in press), however the structural characteristics and nappe geometries are not well understood. Thus, the state of knowledge of the Dovrefjell's geology makes it a prime target for structural analysis. The Dovrefjell is also ideally situated between the relatively homogeneous basement gneisses to the west where stratigraphic horizons are limited, and the cover thrust-nappes of the Trondheim region to the east. The Dovrefjell therefore provides an ideal laboratory for the study of basement-involved fold-nappes. The main focus of the study is a large trumpet-shaped infold of cover sequence rocks (Holtedahl and Dons, 1960) in the Grøvudal area, refered to herein as the Grøvudal structure, or Grøvudal fold-nappe.

The Dovrefjell Mountains of central western Norway expose rocks from some of the deepest portions of the Caledonian-Appalachian orogen. The rocks of this region are part of the core zone of the orogen, where the deformation occurred

under very high temperature and pressure conditions of kyanite to eclogite grade metamorphism (e.g., Cuthbert et al., 1983). The style of deformation is thus dominated by complex and very ductile fold-nappe tectonics. In general, the rock exposure is excellent, due to the intense Pleistocene glaciation that produced spectacular fjords and glacial valleys, often with local relief in excess of one kilometer. The Dovrefjell therefore provides a nearly unique environment for the study of the tectonic processes that operate at depth beneath the world's major mountain belts. The Grøvudal area of the northern Dovrefjell provides good exposures of some of the more highly deformed rocks where the cover, mainly metasedimentary, nappe sequence can be distinguished from the underlying felsic basement gneisses. These cover nappes form a large fold closure in this region (e.g., Holtedahl and Dons, 1960) that is one of the principal foci of this study.

The general methodology used here was to carry out basic lithologic mapping and to collect abundant structural data so that the structural geometry could be tightly constrained using methods of structural analysis (e.g., Ramsay, 1967, p. 461-553; Hobbs et al., 1976, p. 347-375). The orientation data collected included over 1800 measurements of the strikes and dips of various foliations and fold axial planes, and the trends and plunges of lineations and fold axes. This data was then analysed by various

techniques including a computerized eigenvector method devised for this study (Chapter 6). A number of theoretical models were then developed to explain the observations including, a computer-generated passive folding model (Section 8.1), models of active fold generation in simple shear (Section 8.2), and a slip-line fold model relating the plastic slip-line field in an idealized flowing rock body to fold development (Chapter 9).

The area specifically chosen for study was a 12 by 15 kilometer area roughly centered at latitude N 62°25', longitude E 8°55' (Plate 1). The topography of this area is dominated by the kilometer-wide, north-south trending glacial Grøvudal valley, whose walls range from 400 to 700 meters in height. The highest peak within the area is the 1926 meter Grønliskardtinden, which lies within the southern portion of the area, giving a total relief of about 1300 meters. Tree line is at approximately 1000 meters, so that the landscape outside the main valley, roughly 90% of the area, is dominated by mountain tundra, bare rock exposure and boulder fields. The wild life includes pipits, golden plovers, ptarmigan, reindeer and occasional stray musk-ox from the Dovrefjell National Preserve. The unusally calcium-rich soil and relatively sheltered micro-climate of the north-south trending valley also make Grøvudalen one of the richest areas of mountain flora in Norway. The small blooms include an abundance of the rare yellow Grøvu-

dalsvalmue (Grøvuedal poppy), named for the valley.

Access to the valley is about 20 km south by road from the village of Gjøra in the Sunndal valley. This road ends as a dirt road at the mouth of the Grøvudal valley, where a trail leads in six kilometers to a hiking cabin, Grøvudals-hytta, and several small sod-roofed log buildings of Gammelsætra. Gammelsætra is a small summer-farm where a local family, the Suisdals, make butter and cheeses while their sheep and cows are in summer pasture. No other roads approach the area, although there are several cairned hiking trails (Plate 1).

Grøvudalshytta, maintained by the Kristiansund Turist-forening (Hiking Association), is centrally located in the area, and served as a base for the 21 weeks of study during the summers of 1983 and 1984. High camps were used to access higher and more remote portions of the field area, but in general were not feasible for long periods of time because of the frequent rain and high winds. Workers in this area of Norway should be prepared to work under incle-ment conditions; wool and pile clothing and Gore-tex rain-gear were found especially useful, along with a plexiglass map case and waterproof cover. Approximately one day in seven was lost to rain, plus an additional day for supply trips.

Norwegian topographic maps are subdivided into a metric grid system which is especially useful for locating out-

crops. The present map area lies within the Storskrymten 1:50,000 map sheet, and has a grid zone and 100 km square designation 32 V MQ (the easternmost portion of the map falls within 32 V NQ). The map coordinates are then given as 0.1 km grid coordinates within the 100 km square. The northwest corner of the map area is thus designated 089300, and the southeast corner 011150. Rock outcrops can be located to within a 100 meter square by designating a six digit number. True north and grid north are essentially parallel in this area.

The Dovrefjell and neighboring Trollheimen ranges have been included within numerous geologic studies, including those of Goldschmidt (1915), Wegmann (1935, 1959), Barth (1935), Holtedahl (1938), Rosenqvist (1943), Holmson (1955, 1960), and Hansen (1971). A compilation map of the geology of the Oppdal district, which includes the Trollheimen and Dovrefjell, has been made by Krill (1980a; in press; personal communication, 1983). This includes the work of a number of persons who have worked in the area, including PhD dissertations by Hansen (1963), Scott (1967), Wheeler (1973), and Krill (1980b). The Grøvudal area of the northern Dovrefjell has been mapped in reconnaissance (Holtedal and Dons, 1960; Muret, 1960; Krill, personal communication, 1983), so that the first-order lithologic outlines were known, but no detailed structural analyses had been done prior to this study.

REGIONAL GEOLOGY AND TECTONOSTRATIGRAPHY

The regional geology of the Fennoscandian Penninsula can be broadly subdivided into three major provinces: the Baltic Shield, the Caledonian nappes, and the Western Gneiss Region (Figure 1). Post-Silurian rocks are of minor areal extent in Scandinavia (Magnusson et al., 1960; Oftedahl, 1980), and in Norway include small fault-bounded Devonian molasse basins, Permian igneous rocks of the Oslo graben, and Mesozoic and Tertiary sedimentary rocks of the continental shelf (Oftedahl, 1980). Precambrian rocks of the Baltic Shield underlie most of Sweden and form the basement rocks to the Caledonian nappes of Norway and westernmost Sweden. The principal orogenic phase recorded by these basement rocks is now referred to as the Svecokarelian phase, of approximately 1750 to 1950 Ma (Lundqvist, 1979). A late 'post-orogenic' phase (Gothian) of mainly intrusive activity continued until c. 1400 Ma or somewhat younger. A 'Sveconorwegian' event of intrusion and metamorphism is also identified in southern Norway and Sweden at about 1000 Ma (Lundqvist, 1979).

Approximately along the Swedish-Norwegian border the basement rocks of the Baltic Shield are tectonically over-

Figure 1. Regional geology of Scandinavia, after Oftedahl (1980). Study area is indicated by small rectangle in the Western Gneiss Region.

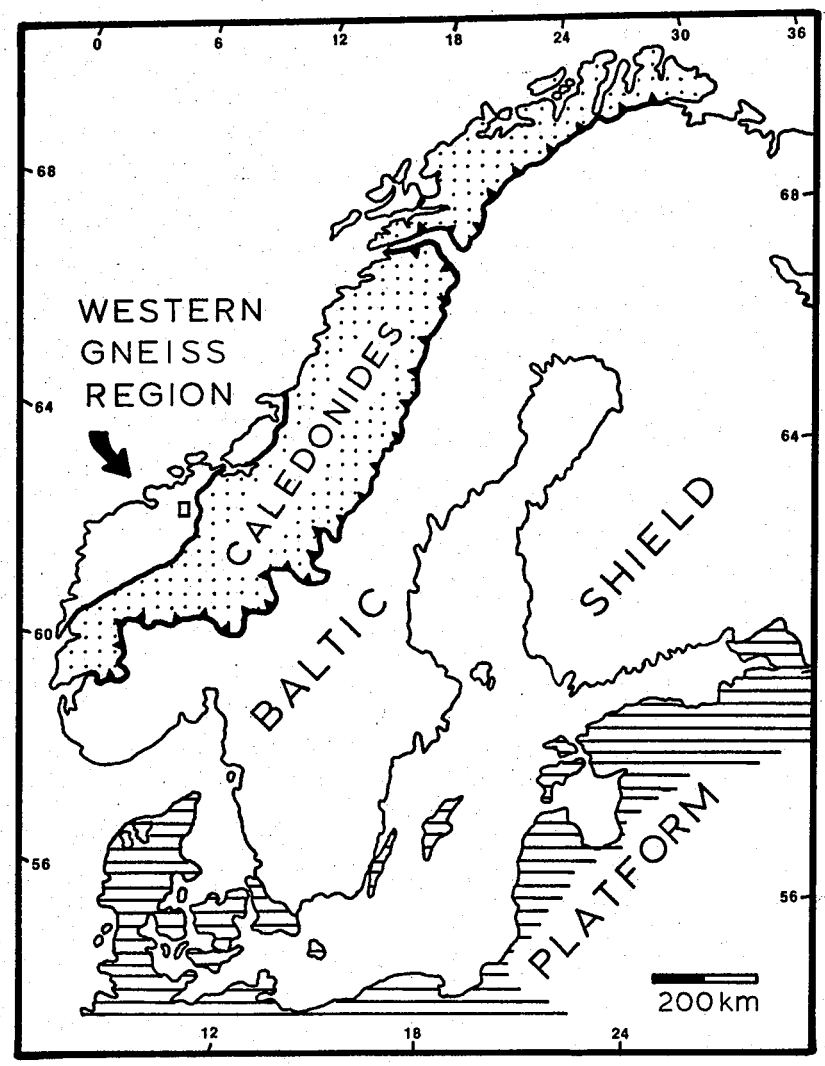
0
6
12
18
24
30
36
68
64
60
56
WESTERN
GNEISS
REGION
CALEDONIDES
BALTIC
SHIELD
PLATFORM
200 km

lain by a series of Caledonian thrust sheets comprising a variety of meta-sedimentary and igneous rocks whose ages range from Middle Proterozoic through Silurian. Dyrelius et al. (1980) have described a traverse through the central Scandinavian Caledonides at approximately 63°N latitude (the Trondheim-Østersund area), and Gee (1975a, 1975b, 1978) has described the distribution and stacking sequence of the principal nappe units in the Trondheim-Østersund area. Hossack (1983) has also redrawn a cross-section through this region using branch-line maps (Figure 2). A generalized nappe stratigraphy and correlation chart is given in figure 3.

The lowermost nappes, emplaced over the crystalline basement in western Sweden, are the Jämtland nappes (Asklund, 1960). This group of nappes includes the Osen-Røa Nappe Complex, or sparagmite nappes, exposed mainly to the south (Roberts and Wolff, 1980). The Jämtland nappes comprise Precambrian to at least late Llandoverian sedimentary rocks (Early Silurian) or possibly Ludlovian (Late Silurian) age (Dyrelius et al., 1980), metamorphosed at the

Figure 2. Geology of the Trondheim region, with cross-section. Geology from Hossack (1983), after Roberts and Wolff (1980); cross-section from Hossack (1983). Rectangle indicates area of study.

Figure 3. Correlation chart of nappe units of the Dovrefjell, the Trondheim region, and Sweden. Correlations after Roberts and Wolff (1980), Krill (1980a), and Dyrelius et al. (1980). See text for discussion.

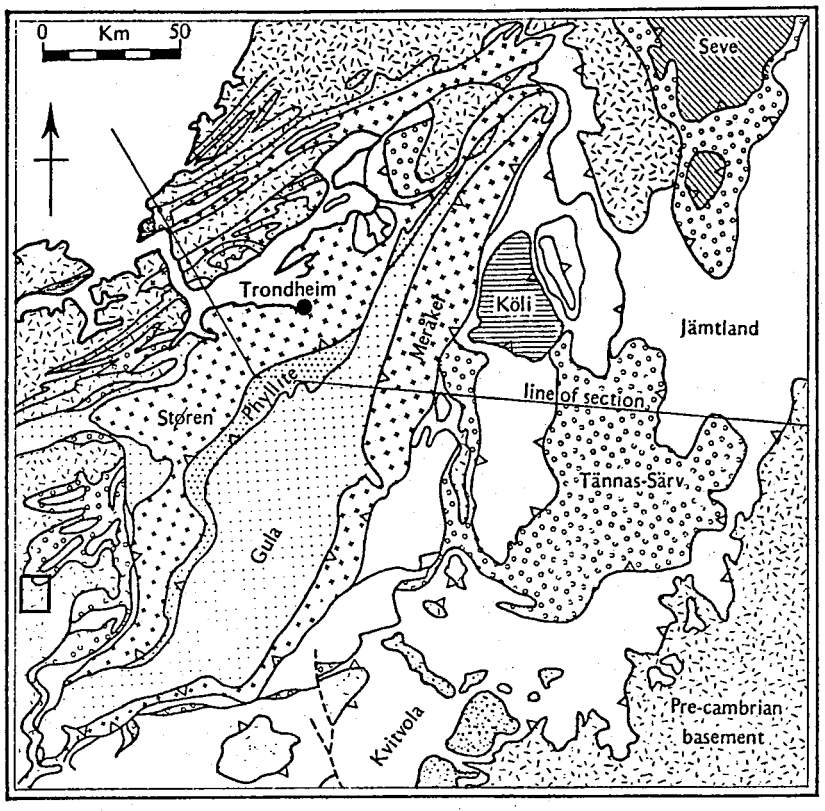
0 Km 50
Seve
Trondheim
Köli
Meråker
Jämtland
line of section
Støren
Phyllite
Tännas-Särv
Gula
Kvitvola
Pre-cambrian
basement

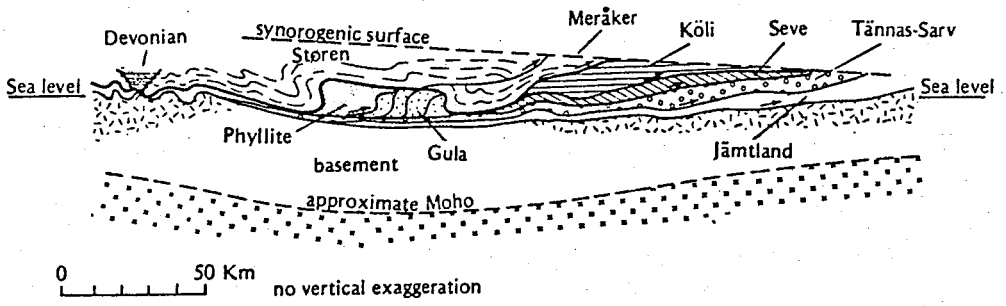
Devonian
synorogenic surface
Støren
Meråker
Köli
Seve
Tännas-Sarv
Sea level
Sea level
Phyllite
basement
Gula
Jämtland
approximate Moho
0 50 Km
no vertical exaggeration

TECTONOSTRATIGRAPHY OF CENTRAL NORWAY

Dovrefjell	Trondheim Region	Sweden
	?Ludlovian - Mid. Devonian sediments	
Tronget-Støren Surna	Trondheim Nappe - Støren-Meraker Gula	
	Levanger-Øyfjell	Köli
Blåhø	Skjotingen-Essandsjo	Seve
Saetra	Leksdal-Remsklepp	Särv Offerdal
Risberget		Tännäs
Åmotsdal	Osen-Røa	Jämtland
Lønset	Precambrian basement with cover	Precambrian basement with cover

Sources: Roberts and Wolff, 1980; Krill, 1980a; Dyrelius et al., 1980

thrust front. Locally this sequence laps on to Precambrian basement, suggesting that these nappes represent the imbrication of a sedimentary basin developed on the Baltic Shield. The nappes have thus been termed parautochthonous by Gee (1975a), although they have suffered considerable translation. The basal thrust horizon is generally within weak Cambrian shales; of particular importance is a black uraniferous shale whose distinctive trace element geochemistry allows correlation with more internal metamorphosed equivalents (Gee, 1980).

Overlying the Jämtland nappes to the west are a series of mylonitized granitic rocks, including the Offerdal (Asklund, 1960) and Tännäs (Törnebohm, 1896; Röshoff, 1978) nappes. The Offerdal nappe includes feldspathic sandstones and local conglomerates, as well as granites, porphyries and gabbro. The Tännäs nappe is dominated by granitic augen gneisses. To the west, structurally above these granitic nappes lies the Särv nappe (Gee, 1975b), largely composed of sandstones intruded by a tholeiitic dike-swarm (Ottfjället dolerites). The sandstones are feldspathic and are probably of shallow marine or fluviatile origin, and on the order of 4500-6000 m in thickness.

The Seve-Köli nappe complex overlies the Särv Nappe along a major tectonic discontinuity, showing a sharp increase in metamorphic grade. This discontinuity, exposed at Åreskutan in Sweden, lead Törnebohm (1888, 1896) to

first apply the nappe theory to the Scandinavian Caledonides. The lower Seve nappe is composed of schists, gneisses and amphibolites, with intercalations of limestone, quartzite and ultramafic rocks. The overlying Köli contains greenschist to lower amphibolite grade phyllites, volcanic rocks, limestones, quartzite, and conglomerates, with ultramafic, gabbroic and minor felsic igneous rocks. Ashgillian (uppermost Ordovician) and Middle to lower Upper Llandoverian (Lower Silurian) fossils have been recovered from part of the Köli nappe.

Higher tectonic units are restricted to the broad Trøndelag depression in central Norway. These upper units are referred to as the Trondheim Nappe Complex (Roberts and Wolff, 1980), and can be broadly subdivided into the lower Gula Nappe and the upper Støren-Meråker Nappe. The Gula Nappe comprises mainly garnet to kyanite or sillimanite grade schists, migmatites and amphibolites with minor marbles, quartzites, conglomerates and ultramafic rocks. Ages of these rocks are not well known, but are thought to be Precambrian to Cambrian (Wolff and Roberts, 1980). The Støren Nappe (Gale and Roberts, 1974) is dominated by a low metamorphic grade submarine sequence including basaltic greenstone, jasper, chert conglomerates and phyllite. An apparent ophiolitic sequence of pillowed greenstones, sheeted dolerite dikes and gabbro also occurs within the nappe. Graptolitic shales overlying the volcanic sequence

give a minimum age of Middle Arenig (Wolff and Roberts, 1980).

The Western Gneiss Region or Basal Gneiss Complex includes large areas of gneissic rocks exposed mainly in western south Norway (Holtedahl and Dons, 1960; Carswell, 1973). The bulk of the Basal Gneiss Complex consists of Svecokarelian age gneisses similar to those of the Baltic Shield, but with varying degrees of Caledonian age deformation (Sturt, 1978). These gneisses apparently form the orogenic core region, showing the highest metamorphic grades and strong ductile deformation, over which the major Caledonian thrust nappes were emplaced (Wegmann, 1935, 1959; Strand, 1961; Wolff, 1976; Krill, 1980; Cuthbert et al., 1983). The origin and age of deformation and metamorphism of the rocks within this terrane have been the subject of considerable debate, and in particular the age and origin of the eclogitic lithologies often found as pods within the gneisses have been the focus of attention (Cuthbert et al., 1983).

In the eastern portion of the Basal Gneiss Terrane a series of nappes are exposed that structurally overlie the main basement gneisses. A regional tectonostratigraphy has been worked out by Krill (1980a, in press; Gee, 1980; Fig-

Figure 4. Geology of the Oppdal district, from Krill (in press). Rectangle indicates area of study.

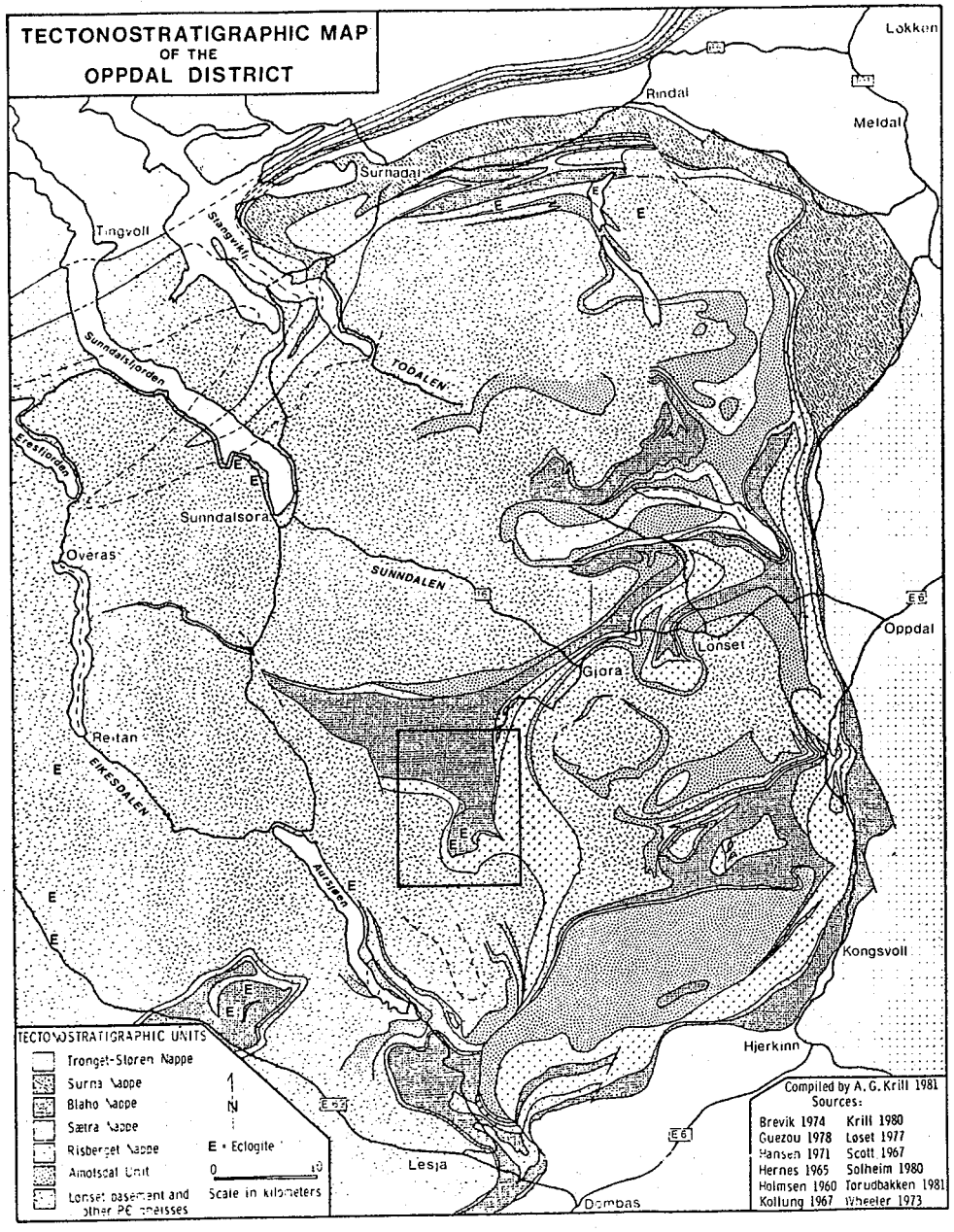
TECTONOSTRATIGRAPHIC MAP
OF THE
OPPDAL DISTRICT
Løkken
Rindal
Meldal
Surnadal
Tingvoll
Stangvik
Sunndalsfjorden
TODALEN
Eresfjorden
Sunndalsora
Overas
SUNNDALEN
Oppdal
Lønset
Gjora
Rennan
EIKESDALEN
Aursjøen
Kongsvoll
Hjerkinn
Lesja
Dombas
E
TECTONOSTRATIGRAPHIC UNITS
Tronget-Storen Nappe
Surna Nappe
Blaho Nappe
Sætra Nappe
Risberget Nappe
Almotsdal Unit
Lonset basement and other PC gneisses
N
E = Eclogite
0
Scale in kilometers
Compiled by A. G. Krill 1981
Sources:
Brevik 1974
Guezou 1978
Hansen 1971
Hernes 1965
Holmsen 1960
Kollung 1967
Krill 1980
Løset 1977
Scott 1967
Solheim 1980
Torudbakken 1981
Wheeler 1973

ures 3 and 4), who has compiled the data of a number of authors including: Hansen (1971), Holmsen (1960), Krill (1980b), Loset (1977), Scott (1967), Solheim (1980), Wheeler (1973), and others. As this tectonostratigraphy was used in the present study a brief summary of the lithologies and known age relationships is presented here.

The Lønset gneiss complex is the lowest unit recognized. It consists of granitic, granodioritic and heterogeneous gneisses. Texturally these rocks vary from relatively homogeneous unfoliated gneisses to well foliated or, in some western areas, migmatitic gneisses. Amphibolitic and gabbroic components are common and locally eclogitic pods are abundant. Rb-Sr geochronology studies have yielded only Precambrian whole-rock ages (Krill, in press), although mineral ages of 447-400 Ma have been reported from eclogite pods collected over a wide area of the lower gneisses (Cuthbert et al., 1983).

The Amotsdal unit is dominated by arkosic, or sparagmitic, psammites. Basal conglomerates have been found in several localities, including a new locality described in this study, suggesting deposition unconformably over the basement gneisses. Cross-bedding can been found in less deformed exposures east of the present field area, and faces upward from the gneisses. These rocks are similar to sparagmites found to the southeast in the Mjøsa area, and by correlation are suggested to be Late Precambrian to

Early Paleozoic in age (Krill, in press). In the Trollheimen area a thin black graphitic schist associated with quartzite and marble (Midtre kam schists of Hansen, 1963, 1971) overlies this unit. Gee (1980) has correlated this unit on the basis of its unusual trace element geochemistry with a similar unit exposed in the Tømmeras basement window northeast of Trondheim, and with the Upper Cambrian black shales of the Jämtland supergroup in Sweden.

The Risberget Nappe is characteristically a coarse augen gneiss, but also includes rapakivi granite, gabbro, anorthosite, felsic granite and heterogeneous gneiss with some calc-silicates (Krill, in press). Numerous Rb-Sr geochronological studies have yielded only Precambrian (c. 1100-1700 Ma) whole-rock ages (Solheim, 1980; Krill, 1980a), including one age determination made on an ultramylonite (Krill, 1983b). However, Solheim (1980) obtained a mineral-isochron of c. 395 Ma on foliated basement and augen gneiss samples, and Krill (1983b) similarly obtained a 358 Ma date on unoriented biotites from rapakivi granite of the Risberget nappe. These latter dates presumably reflect a Caledonian overprint on a Precambrian granulite-facies metamorphism. This unit was correlated with the Precambrian augen gneiss of the Caledonian front (Tännäs Nappe) by Törnebohm (1896) and this has been accepted by most present workers (Gee, 1980; Krill and Röshoff, in press). The idea that the augen gneisses of the Basal

Gneiss Complex formed by granitization through metasomatism was advanced by Barth (1938), Holtedahl (1938) and Rosenqvist (1943), and this notion was accepted by many later workers (e.g., Holmson, 1955; Hansen, 1971). However, Rb-Sr initial ratios for the gneisses suggest a magmatic origin, and igneous textures including rapakivi rims and exsolved minerals are common in potassium feldspar augen of less deformed samples (Krill, 1980b, 1983b). These relationships and the confinement of the augen gneiss to a continously mappable unit make a metasomatic origin unlikely.

The Sætra Nappe consists of feldspathic psammite and amphibolite. Commonly these lithologies are strongly interlayered or laminated, however in less deformed areas (e.g., Eiggen quarries; Krill and Röshoff, in press) the amphibolites can clearly be seen to have originated as dolerite dikes cutting across sedimentary layering in cross-bedded fluvial sandstones. Abundant dikes are confined to the Sætra Nappe and no amphibolite has been described from the underlying Amotsdal unit, demonstrating that the Sætra Nappe must be allochthonous. A Rb-Sr whole-rock isochron for the dolerite dikes gives 745 ± 37 Ma, interpreted as the intrusive age (Krill, 1983a). Identification of a boudin train of eclogite pods within this unit during the present study gives supporting evidence for a Caledonian eclogite-grade metamorphic event, as

the Sætra psammites are clearly younger than the basement gneisses. Correlation of the Sætra Nappe with the Särv Nappe of Sweden is strongly supported on a lithologic basis (Gee, 1980; Krill and Röshoff, in press), and dating of the Ottfjället dolerite dikes has yielded a whole-rock Rb-Sr isochron age of 720 ± 225 Ma.

The Blåhø Nappe (Hansen, 1963, 1971) comprises mainly garnet-mica gneisses with amphibolite and some serpentinite, marble, psammite and mica schists. Its apparent eugeoclinal affinity suggests the Blåhø is likely to have been tectonically emplaced over the Sætra (Krill, 1980a), and the present study suggests tectonic truncation of units along the basal Blåhø contact. Age determinations on the Blåhø rocks have been generally unsuccessful, but suggest a maximum of c. 800 Ma (Krill, in press). The Blåhø Nappe may be in part correlative with the Seve Nappes of Sweden (Gee, 1980), although Krill (in press) suggests this is not supported by existing lithologic evidence.

Above the Blåhø Nappe Krill (in press) has defined a lithologically similar nappe, the Surna Nappe, which is delimited by the presence of abundant dikes and bodies of trondhjemite. Poor isochrons on these rocks suggest a possible Ordovician metamorphic age. In sharp contact along syn- or post-metamorphic faults is the overlying Tronget-Støren Nappe, of much lower, greenschist facies meta-volcanic and meta-volcaniclastic rocks.

REGIONAL TECTONICS

From the preceeding discussion of the regional tectonostratigraphy a number of important consequences become apparent. The well established correlation of the nappes and nappe tectonostratigraphy between the Western Gneiss Region and the frontal nappe sequence of western Sweden (Gee, 1977, 1980; Roberts and Wolff, 1980; Krill and Roshoff, in press; Figure 3) suggests a continuity of the nappe pile for over 200 km across strike. As most of the nappes can be demonstrated to be allochthonous with respect to lower nappes, a simple unstacking of the pile from east-southeast to west-northwest (the general transport direction is east-southeast; Roberts and Wolff, 1980) would suggest total displacements on the order of 600 to 1000 km.

Gee (1978), in fact, has attempted to do this and suggests that displacements on the order of at least 1000 km are required. He emphasizes that a large amount of horizontal stretching may account for perhaps half of this displacement. This stretching component seems evident from the extreme attenuation and apparent boudinage of the nappe units (e.g., Roberts and Sturt, 1980), although Lisle (1984) has suggested that observed strain patterns in the Seve-Köli Nappe complex are not compatible with post-emplacement boudinage of nappe units, and Hossack (1983) has suggested that such "boudins" are more likely to be

horses. Lisle (1984) also shows that flattening strains are common in the Köli Nappe, which he suggests are difficult to reconcile with simple nappe emplacement models. It may be significant, however, that the most intense strains reported by Lisle show west or northwesterly plunging elongation directions. Other finite strain measurements are not abundant, however Hossack (1968) and Chapman et al. (1979) also report strong east-west elongations of up to several hundred percent in other portions of the orogen. Presumably these are related to a large component of simple shear during the eastward directed emplacement of the nappes over the Baltic Sheild.

Hossack (1983) has drawn a balanced cross-section (Figure 2) through the Trondheim region by constructing branch line maps from existing geologic data. This section also incorporates aeromagnetic and Bouger anomaly data for depth to basement, and a model of the synorogenic surface from metamorphic data. Geometrically, Hossack's section seems to better incorporate knowledge of the three-dimensional shape of the nappes than previously published sections (cf., Dyrelius et al., 1980, p. 263; Roberts and Wolff, 1981).

Figure 5 schematically shows the inferred paleogeographic environments on the ancient continental margin from which the nappes of the Oppdal District may have been derived. These are largely based on the interpretations of

Gee (1975a, 1978) and correlations with eastern units (figure 3, Chapter 2). In the following section correlative units are given in parentheses.

The Lønset basement gneisses (Baltic Shield, in part) represent the essentially autochthonous, although now strongly folded, basement to the orogen. Amotsdal feldspathic psammites (Jämtland, in part) were fluvial sandstones deposited on, and presumably largely derived from, these basement rocks. The Risberget nappe (Tännäs) augen gneisses also represent Precambrian basement gneisses, possibly correlative with the type rapakivi gneisses in Finland (Krill, 1983b). These gneisses are believed to be a portion of the old contiental margin basement imbricated into the developing nappe pile, perhaps along old listric normal faults or as an uplifted block clipped off during thrusting (Figure 5).

The Sætra (Särv) nappe may represent the western equivalent of the Amotsdal where intruded by basic dikes (Ott-

Figure 5. Schematic paleogeographic cross-section through the Baltic Shield continental margin prior to the Caledonian collision with Greenland. B = Blåhø nappe, S = Sætra nappe, R = Risberget nappe, A = Amotsdal psammite, and L = Lønset basal gneisses. In this model the Blåhø nappe represents orogenic sediments shed from the approaching orogen, the Sætra nappe represents continental sandstones or rift facies intruded by basic dikes during initial continental breakup c. 740 Ma, the Risberget nappe represents continental basement (either a horst or block thrust along old listric normal faults). The Lønset gneisses and Amotsdal psammite represent Baltic Shield continental basement and cover respectively.

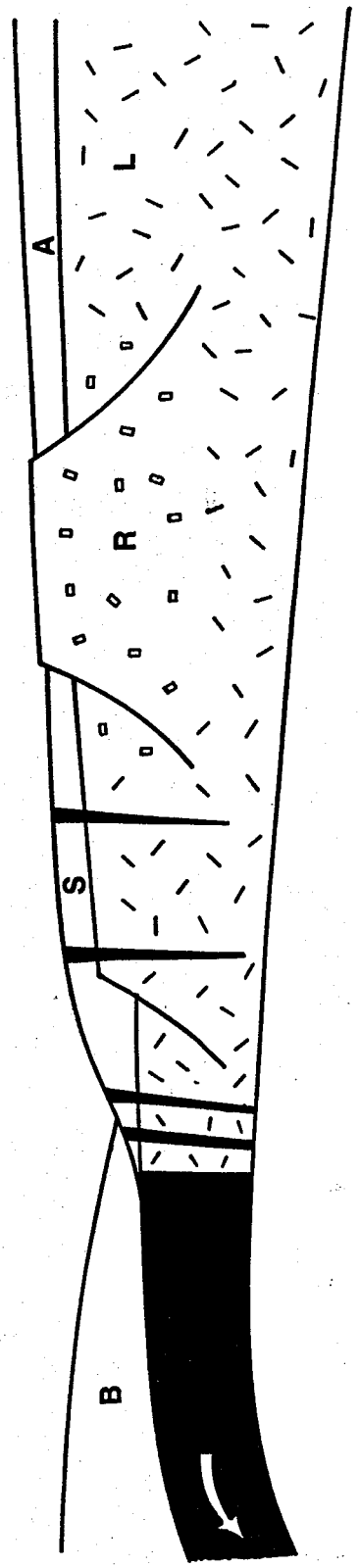
A
L
R
S
B

fjället dikes of the Särv nappe) during the initial continental breakup approximately 740 Ma ago (Roberts and Gale, 1978; Krill, 1983a). Garnet-mica gneisses of the Blåhø (Seve?) nappe were probably derived from a eugeoclinal graywacke sequence (Scott, 1967) including carbonate and mafic volcanic components now preserved as eclogite and talc-carbonate bodies. These may have been orogenic deposits associated with the approach of a convergent margin in the early Paleozoic, possibly Ordovician, times.

Higher nappes, not represented in figure 5, including the Seve-Köli, Støren-Meråker and Gula nappes contain diverse lithologies including metamorphosed Ordovician and Silurian sedimentary rocks, and volcanic and intrusive rocks. Greenstones within the Støren nappe have been inferred to be remnants of ophiolite. These higher nappes have been carried in from areas west of the ancient continental margin (Gee, 1978).

The present boundary between the Western Gneiss Region and these higher nappes of the Trondheim Nappe Complex (Roberts and Wolff, 1980) in the Oppdal District occurs along sharp syn- or post-metamorphic faults (Krill, 1980a). It is suggested here that this faulting may be due to isostatic uplift of the Gneiss Region following crustal thickening due to the emplacement of basement-cored nappes. This is consistent with the observed strain gradient across the area (Chapter 7).

The development of this large nappe pile is a consequence of the collision of two continental masses: present day Greenland and Scandinavia (Dewey, 1969; Gee, 1975a, 1975b; Roberts and Gale, 1978; Mykkeltveit et al., 1980; Roberts and Sturt, 1980; Hurst and McKerrow, 1981; Bartley, 1982; Cuthbert et al., 1983). The present configuration of the orogen is due to the Cenozoic opening of the Norwegian Sea, which split the mountain belt longitudinally along its axis (e.g., Talwani and Eldholm, 1977) The Caledonian mountain belt of eastern Greenland shows predominantly west-directed thrusting of at least 100 km displacement (Haller, 1971, p. 132; Henriksen and Higgins, 1976; Henriksen, 1978; Roberts and Sturt, 1980; Hurst and McKerrow, 1981). The present trace of the suture zone between contrasting basement terranes apparently lies west of the present Norwegian coastline (Gee, 1975a). Westward directed subduction of the former oceanic crust beneath Greenland is suggested by abundant Caledonian granitic bodies intruding basement rocks of East Greenland (e.g., Steiger et al., 1979), and their corresponding absence in the Scandinavian Caledonides (Bartley, 1982).

High pressure kyanite and eclogite metamorphism is regionally developed in the Western Gneiss Region of Norway, and eclogite mineral ages fall mainly within the 420-400 Ma range (Cuthbert et al., 1983, and references therein). This high-pressure metamorphism is therefore

consistent with a Silurian collisional event. Geobarometric studies of the eclogites suggest maximum pressures of about 20 kbar, or burial depths of 65 km (Cuthbert et al., 1983). Mykkeltveit et al. (1980) have modeled the crustal structure across the Basal Gneiss Complex based on a seismic reflection profile line, and find a 4 km thick low velocity layer at 14 km. They suggest that this may best be explained by the presence of low grade eugeoclinal sedimentary rocks, indicating crustal imbrication. This may explain the observed low-pressure reequilibrium of some eclogites (Cuthbert et al., 1983), as well as the fact that they are presently observed at the surface. If crustal imbrication of the Baltic Shield occurred during the final stages of collision the Western Gneiss Region could have been rapidly uplifted. Cuthbert et al. (1983) have modeled this scenario and suggest crustal thicknesses at this time could have reached 80 km, with surface topography locally reaching 8 kilometers, similar to the present Himalaya.

LITHOLOGIC UNITS

The nappe units mapped in the Grøvudal area are lithologically correlative with the regional tectonostratigraphic units outlined in chapter 2, and in most cases are continously mappable on a regional scale (Figure 3; Krill, 1980a). In this chapter the local variations and characteristics of these units are briefly described. Figure 6 is a simplified geologic map of the Grøvudal area, the complete version is given as Plate 1. Map coordinates of some outcrops are given in parentheses.

The lowermost unit is the basal gneiss, or Lønset, unit exposed mainly in the southwestern portion of the map area, and reappearing in the northeast corner. The basal gneisses are mainly medium-grained biotite-bearing felsic gneisses. Amphibole and epidote are common minor phases, and locally occur as clots or stringers (893217, 911162,

Figure 6. Geologic map of the Grøvudal area in the northern Dovrefjell Mountains of central Norway, with cross-sections. Structural symbols indicate foliation and lineation orientations. Triangles (summits) and circles indicate selected elevations in meters. Random dash (L) = Lønset basal gneisses. Random stipple (A) = Amotsdal psammite. Outer white (R) = Risberget nappe. Patterned stiple (S) = Sætra nappe, with eclogite pods indicated as e. Inner white (B) = Blåhø nappe. Zones marked 1-5 are the structural domains described in Chapter 6.

Section lines are indicated on map border. Symbols on the sections are the the same as on the map, except the Risberget nappe is shown with a parallel-dash pattern. Intersections of cross-section lines are shown as vertical lines.

GRØVUDALEN AREA, NORTHERN DOVREFJELL, WESTERN NORWAY

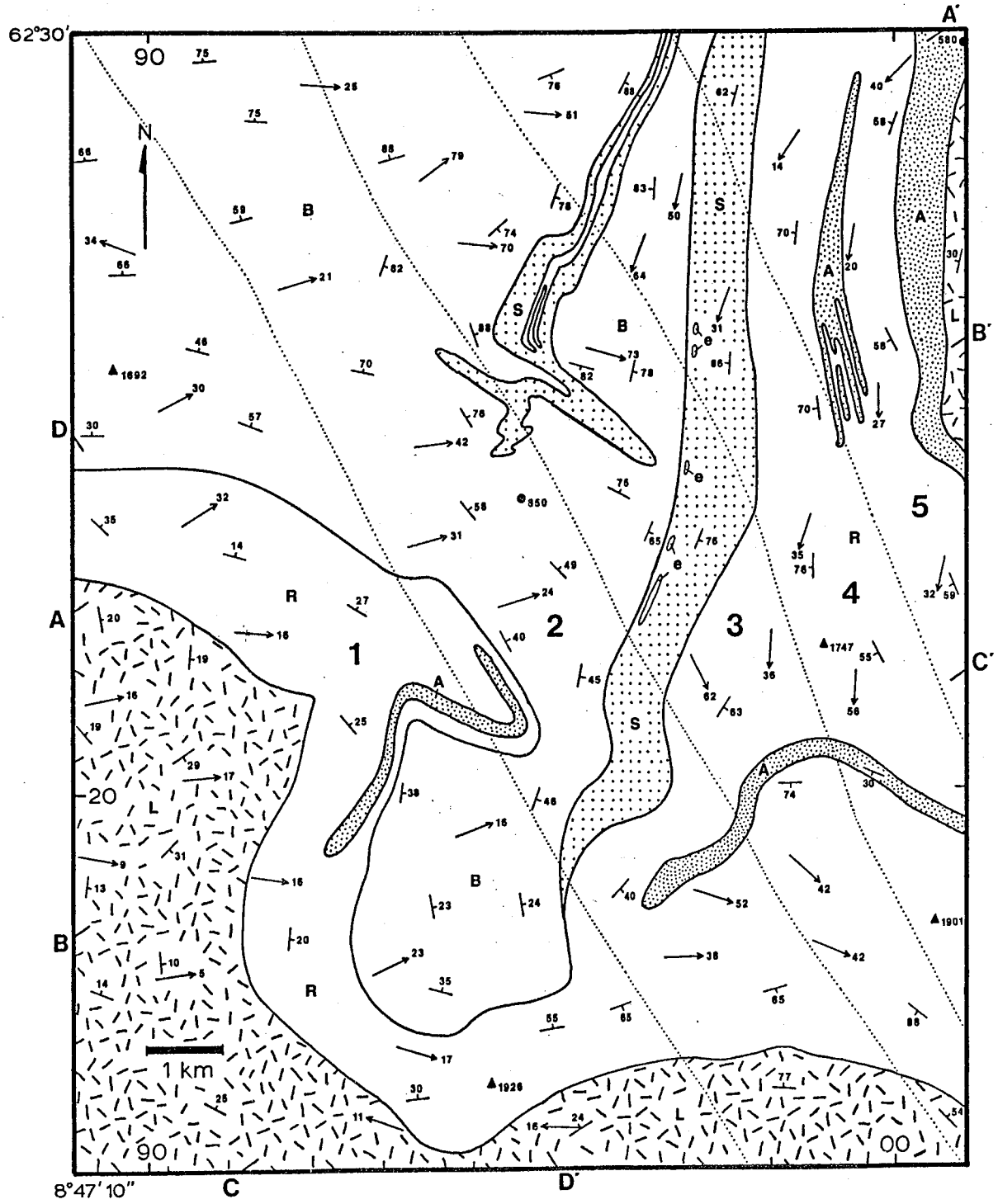

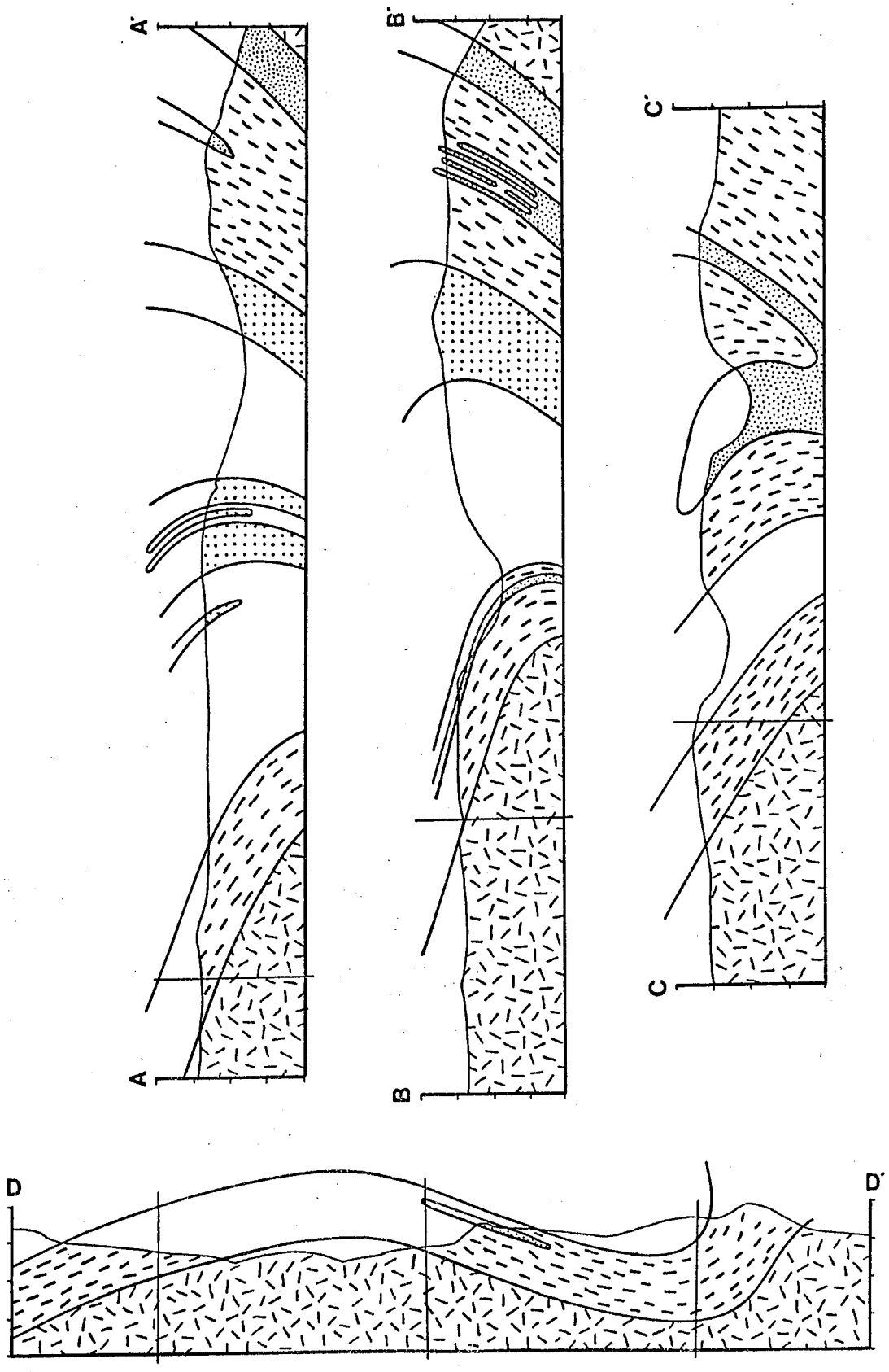
A'
A
B'
B
C'
C
D
D'

994155). Outcrops are commonly massive, poorly or irregularly foliated gneisses (913169, 009286), although many are compositionally layered with complex folding in felsic layering (916153, 892220). No eclogite pods were found within these gneisses.

The Åmotsdal psammite occurs in its regional tectonic position above the basal gneisses (Chapter 2) only in the northeastern portion of the area. Here the psammite forms a stripe narrowing to the south. A horizon of deformed conglomerate, comprising quartzose and felsic cobbles, outcrops here (003265), and is apparently correlative with similar outcrops near Lønset (Figure 3). Three other outcrop areas of Åmotsdal psammite occur as slender fingers within the tectonically higher Risberget nappe (Figure 3; Plate 1). In the northeast one of these fingers terminates in a series of fine interlayers within the Risberget augen gneisses (992251). The most accessible exposures of the Åmotsdal psammite are those at the south end of Grøvudal (946215), which can be reached in late summer by fording Litlgrøvu. The psammite is typically a fine-grained quartz-rich feldspathic gneiss with muscovite and hematite; biotite and epidote occur as minor accessory minerals. Outcrops are generally flaggy and light gray to off-white in color. Flaggy lithologies in the Risberget can appear similar, but the high quartz content, muscovite and characteristic hematite grains of the Åmotsdal psammite

make the unit quite distinctive.

The Risberget nappe forms an extensive band wrapping around the area from southwest to northeast, outlining the major structure. The lower face of Høgtunga, the prominent 700 meter face at the south end of Grøvudal, is formed of this unit. Good accessible exposures occur along the waterfalls on the lower Litlgrøvu (935220). The characteristic lithology in this unit is a distinctive pink augen gneiss with coarse potassium-feldspar phenocrysts. The rock is normally well foliated and lineated. Rather undistinctive grey epidote-biotite gneisses are also common, although subordinate, making a distinction from the basal gneisses difficult locally. In general, the contact of the Risberget nappe with the basal gneisses was mapped as the last occurrence of coarse potassium-feldspar phenocrysts within the gneisses. It is possible that interfingers of the basal gneisses occur within the Risberget nappe that could not be delimited. Other lithologies within the Risberget nappe include light grey to pinkish aplite (922168, 982212), a white cataclastic-appearing felsite or fine-grained anorthosite (975216, 981253), and amphibolite (981280). Additionally, a small body of talc-carbonate occurs in one locality (930171), and at the upper contact with the Sætra nappe (980261) a small peridotite body is preserved. This latter rock is exposed precisely along the contact, suggesting it is a far traveled horse.

Structurally above the Risberget nappe is the Sætra nappe. This unit forms a narrow band along the eastern limb of the major structure, pinching out to the south. Some outcrops of this unit occur along the foot-trail into Grøvudalen (974281), and well exposed folds in this unit outcrop along the Raudbekken access route to the eastern summits (962210). A second area of outcrop occurs along the western edge of the Grøvudal valley, where the Sætra nappe is interlayered within the higher Blåhø nappe. Rocks of the Sætra nappe are distinctively banded and consist of quartzose and amphibolite laminations typically 0.5 to 2 centimeters thick. The felsic layers are quartz-rich with mainly potassium-feldspar and minor amphibole. The amphibolite consists dominantly of a dark green hornblende. Outcrops of the Sætra lithologies are typically flaggy and at the northeast end of Grøvudalen a number of small flagstone quarries have been dug in amphibolite-free outcrops of the Sætra unit (e.g. 978291). In one locality, just south of Nonsfjellkollen (976232), the Sætra contains apparent meta-gabbro. An eclogite boudin train occurs near the top of the nappe, stretching out over five kilometers (975271, 967224). Some calcium carbonate occurs in association with the boudins, suggesting a possible sedimentary derivation.

The final, and structurally highest, unit is the Blåhø nappe. The rocks of this unit are typically rather homo-

geneous grey garnet-muscovite-biotite gneisses. Staurolite and kyanite are found as accessory minerals. This unit is the principal one exposed in the walls of Grøvudalen; the steep cliffs near the south end of Grøvudalen (955216) expose a thick section, and the contact with the underlying Risberget nappe is well exposed in the opposing southern wall (945207). Good outcrops are more accessibly exposed in the vicinity of Litle Aurhøa (928262). Variations within the Blåhø lithologies include more quartzose rock types common at the base of the nappe (973273, 964218), rusty-weathering schistose biotite gneisses (957275, 909240), and amphibolite (899271, 928268). Talc-carbonate pods are fairly common within the Blåhø nappe (962251, 920297, Plate 1), and outcrops of dolomite locally occur in association with the pods (909267, 914265, 897268).

It should be noted here that reference to these lithologic units as "nappes" is largely based on correlation with units outside the field area (e.g., Krill, 1980a; Chapter 2). The lower contact of the Amotsdal with the Lønset gneisses is thought to be an unconformity on the basis of local conglomerates; thrusting along this contact is suggested if correlations with the sparagmite or Jamtlandian nappes are made. The Sætra unit is assumed to be allochthonous on the basis of the correlation with the Sætra nappe east of the field area; the abundant mafic dikes in this nappe (amphibolites in the Grøvudal area) are

not found within lower units, suggesting they were intruded before the nappe was emplaced. The Sætra nappe can also be convincingly correlated with the Särv Nappe (Chapter 2). Similarly, the augen gneisses found within the Risberget unit are not found within lower units, and can be correlated with the augen gneisses of the Tännäs Nappe. The lower contact of the Bláhø unit could possibly be an unconformity, however the justiposition of the apparent eugeoclinal lithologies with fluvial sandstones of the Sætra Nappe suggests tectonic emplacement. It is felt that the best interpretation of the lithologic contacts in the Grøvudal area is that they are tectonic. This interpretation, however, does not effect the main focus of this thesis, which deals with the later ductile behavior of these rocks (Sections 5.2, 5.3, and Chapters 6-9).

STRUCTURAL STYLE

The structural style of the Grøvudal area, and of the Western Gneiss Region in general, is similar to that of other orogenic core zones, such as the Pennine zone of the Alps (e.g., Huber et. al, 1980) or the ductile nappe area of the central New England Appalachians (e.g., Thompson et al., 1968). Ductile structures such as complex flow folding, gneissic and transposed layering, stretching lineations, boudinage and shear zones clearly predominate over faulting or other brittle phenomena.

Major brittle structures within the region appear to be late stage post-metamorphic faults that have little effect on the regional map pattern. The principal exception is the contact with the Tronget nappe, here the structurally highest nappe correlative with portions of the Trondheim Nappe Complex. This contact has been described by Krill (1980b) as occurring along low and high angle faults with cataclastic textures and local pseudotachylite, in contrast to the contacts between lower nappes that show no evidence of cataclasis.

5.1 Nappes

The occurence of Pennine style nappes in the eastern portion of the Western Gneiss Region was first recognised by Muret (1960). Subsequent mapping up through 1980 has

been compiled by Krill (1980a; in press), resulting in clarification of the regional nappe distribution (Figure 4). The characteristic style is that of a complexly inter-folded sequence of thrust-nappe sheets. Thus two stages of evolution can be usefully defined, an early thrust-nappe phase and a later fold-nappe phase.

The general continuity of the individual nappe sheets through the Oppdal District is remarkable, and even more so if correlations with the nappes of the Caledonian front in Sweden are valid. Locally individual nappe sheets are less than one kilometer thick, yet may be traced for over 200 km across the regional strike. Additionally, there remains a continuity of the sequence order; the tectono-stratigraphic order at the Caledonian front is the same as that in the Oppdal District (Krill and Röshoff, in press; Figure 3).

These observations suggest thinning of the nappes after, or during, their emplacement. Gee (1977) cited the pinch-and-swell and "mega-boudin" geometry of several nappes as evidence for late structural thinning. However, as pointed out by Hossack (1983), such pinch-and-swell geometries could appear in cross-sections taken across oblique ramps on a basal thrust, while "mega-boudins" may actually be horses produced during thrusting. Addition-ally, Lisle (1984) has suggested that measured strain patterns within one such "mega-boudin" are not compatible

with a boudinage origin. Despite these criticisims, there does seem to be a regional pattern of strong ESE-WNW stretching through much of the orogen, presumably reflecting a large component of simple shear associated with allochthon emplacement (Roberts and Sturt, 1980).

In the Grøvudal area textural evidence for the initial brittle thrust-stacking event has been obliterated. That is, the nappe contacts presently show no evidence of localized cataclasis, and appear welded with no textural contrast with rocks internal to the nappes. The rocks in general show a penetrative protomylonitic to mylonitic texture (Sibson, 1977), and the nappe contacts show show a similar texture. This is particularly well displayed at the Sætra-Risberget contact exposed 2 km north of Nonsfjellkollen (981255). Here the psammite-augen gneiss contact is a knife sharp discontinuity, with no apparent textural gradation away from the contact. Similar relationships can be observed for the Blåhø-Sætra contact (949251, 956269, 9733269), and the Risberget-Amotsdal contact (947214, 933204). This can also be observed in the Trollheimen mountains, for example on Blåhø (158593); and in the Oppdal District in general (Krill, 1980a).

As the nappe sheets are allochthonous with respect to each other, with relative displacements of 10's to 100's of kilometers (Chapters 2 and 3), this suggests recrystallization of the nappe contacts during the development of a

pervasive protomylonitic fabric. Presumably then, during the initial emplacement of the sheets the contacts were characterized by a high strain or high strain-rate induced fabric; either cataclastic or mylonitic in nature. With increasing strain, temperature or strain-rate (White et al., 1980) the zones of shear progressively widened, and new zones may have been initiated internal to the nappes, until a pervasive flow fabric developed. This would then represent a transition from localized brittle behavior characteristic of thrust-nappe tectonics, to pervasive ductile flow characteristic of fold-nappe tectonics.

Although the small-scale structures associated with an early phase of thrusting may have been obliterated, the larger scale geometry of the nappe contacts may retain more information about the early thrust-nappe geometries. Throughout the Oppdal District there are many examples of tectonostratigraphic excision, or loss of one nappe unit along a contact (Figure 4). In the district as a whole, this may be locally explained by lack of map control in difficult terrain with complex geology, however, these relationships may be observed near Kongsvoll and in Grøvudalen where the control is good (Figures 4 and 6; Plates 1 and 2).

The significance of this is as follows. In thrust belts certain geometric rules have been observed to hold. These include that thrusts always cut up section in the

direction of transport, and that younger thrusts occur beneath older thrusts (Dahlstrom, 1970; Boyer and Elliott, 1982). These rules may be understood mechanically in terms of a "snowplow model". The thrust belt forms a wedge of material thickened until it reaches a critical taper, after which it slides stably. The critical taper is reached when the wedge is on the verge of failure everywhere. As the wedge thickens it maintains its taper by constantly breaking out new thrusts in front of, and beneath, the wedge (Davis et al., 1983). According to these geometric rules it is not possible to thin a stratigraphic section, as has apparently happened in the Grøvudal area. If thrusting follows a progression from higher to lower levels, with thrusts emplaced in piggy-back fashion, sections may be repeated or thickened but never thinned.

To see how this might apply to the Grøvudal area consider the basic geometry of the thrust-nappes taken prior to folding, schematically shown in figure 7a. As already demonstrated (Chapter 3) the stacking order Blåhø-Sætra-Risberget-Åmotsdal/Lønset (B-S-R-L) may be interpreted to represent a sequence of nappes stacked from west to east, with the highest being the furthest traveled (Figure 5). Thus the Blåhø nappe must have been initially

Figure 7. Geometric models for thrust excision. A - present geometry of thrust nappes. B - out of sequence thrusting. C - boudinage. D - extensional faulting.

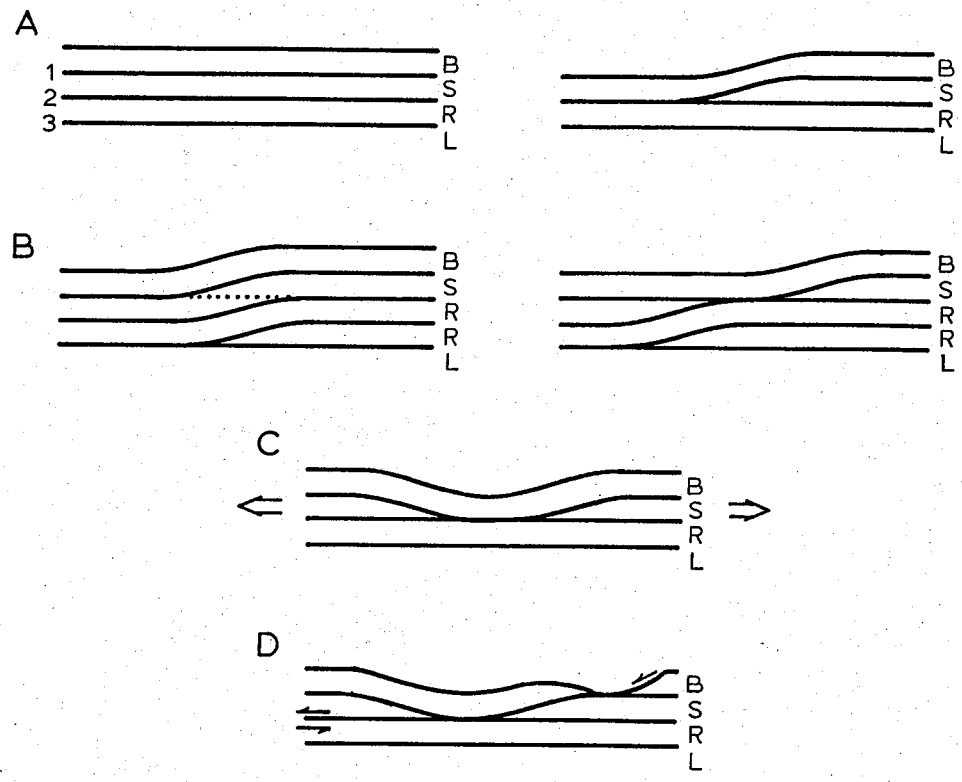
A
1
2
3
B
S
R
L
B
S
R
L
B
S
R
R
L
B
S
R
R
L
C
B
S
R
L
D
B
S
R
L

emplaced onto the Sætra nappe, and the two then emplaced ensemble onto the Risberget nappe. Finally these three nappes were emplaced as a package on to the Åmotsdal and underlying Lønset basement. The thrust sequence would then be: B on S, B+S on R, and B+S+R on L.

Possible origins of the observed geometric relationship of figure 7a include: out of sequence thrusting, thrusting a folded thrust, boudinage, extensional faulting, or as a thrust sheet boundary (branch line). Several of the more plausible possibilities are schematically shown in figure 7. Figure 7a shows the general tectonostratigraphic sequence of the Oppdal District with inferred emplacement order, and the observed excised sequence of the Grøvudal area. Figure 7b shows a possible history where ramping along the basal thrust results in folding of the higher nappes, and is then followed by out of sequence reactivation of the higher Blåhø thrust. This results in the correct structural order, however this explanation is mechanically unlikely as it disobeys the geometric rules of thrust sequence. A similar senario, however, has been suggested for a portion of the Moine thrust belt by McClay and Coward (1981). There reactivation of older thrusts is believed to have resulted in such a reversal of the stacking sequence.

Figures 7c and 7d represent boudinage and extensional faulting hypotheses. Gee (1978) has attributed lens-shaped

and pinch-and-swell type geometries to late stage stretching of the nappe pile during gravitational collapse. An alternative explanation is that stretching is a normal component of extensional flow associated with the nappe emplacement process (section 8.3).

The final possibility is simply that the excision point, or line, is a branch line defining the limit of the nappe volume. In this case the branch line would represent the westernmost limit of the Sætra nappe. Of the possibile alternatives this is perhaps the most plausible. While an extensional origin could be argued for by the presence of abundant stretching lineations and by the boudinaged eclogite pods, there is no additional evidence of boudinage or pinch and swell of the nappe itself as might be expected. Also, there are presently no mapped occurrences of Sætra lithologies west of this point.

The presence of large-scale ductile fold-nappes in the Oppdal District was first described by Muret (1960), and Krill (in press) has published some schematic sections through the Oppdal District showing the major east-verging recumbent structures. While the internal geometries of the nappes are not yet completely understood, the vergence and general style seem clear. Primary facing indicators (cross-bedding) are well preserved in the Lønset and Kongsvoll areas (Figure 4) indicating an upward facing structures. Similar relationships are observed for the synformal

structure near Gráho (Krill, 1980a). To the west are over-printing fold relationships, with later steeply inclined folds refolding the early isoclines. The significance of the Grøvudal structure and implications for the regional nappe geometries will be discussed in Chapter 7.

5.2 Foliations, Lineations and Folds

The rock units of the Dovrefjell are all well layered, generally showing a compositional banding and a linear fabric. To the east of the area, for example along the main road E-6 at Eiggen quarry (Krill, 1980b), layering within the Sætra nappe can be demonstrated to be primary, with cross-bedded arkosic sandstones cross-cut at high angles by basic dikes. In the Grøvudal area, however, the same map unit consists of centimeter-scale banded psammite and amphibolite. In most outcrops it is possible to find isoclines, suggesting the banding is due to high strains and transposition of primary layering. The other lithologic units similarly show evidence of transposition and high strain, including isoclines in most outcrops and a flattened conglomerate section in the Amotsdal unit (003265). The main foliation (S_1) in the Grøvudal area is clearly a transposition fabric, and is the result of high strains.

The identification of later (S_2) foliations is somewhat problematic, as locally (e.g., 965245 area and 935265 area)

"S_2" foliations intensify and become dominant in outcrop, while obscuring older foliations. Also, where the relationship to folds can be observed, an S_2 foliation is typically subparallel to the long limbs of folds, and hence to S_1, so that it is well defined only near fold hinges. In general, a strict correlation of foliation ages was not possible. In part this is due to the paucity of micas in most of the units so that foliation generations are not well defined. Also, as primary layering is not well defined in the area the age of the oldest foliation with respect to bedding is not known. As all foliation orientations can vary stongly from outcrop to outcrop, because of intense folding, no correlation can be made on the basis of orientation.

The procedure adopted here was to designate the oldest foliation observed in a given outcrop as S_1, and a later cross-cutting foliation as S_2. In most cases S_1 was the dominant compositional banding, and S_2 was a later foliation. In the following analysis of foliation data (section 6.3) it will be shown that there is no significant statistical difference between the two populations (including fold axial planes), suggesting a continous sequence of foliation formation and folding.

The designation S_3 was used for kink bands and crenulations that post-date other foliations. This data set, including the kink axes, was relatively small, quite vari-

able, and difficult to analyse (section 6.5).

Linear features within the rocks include intersection lineations, mineral lineations, elongation lineations and fold axes. Typically, lineations measured were some combination of the above. Mineral and elongation lineations appear the most common, including quartz segregations, tailed feldspar augen, and aligned amphibole needles. In some cases the origin of the lineations was not always clear, for example whether quartz rods initiated as stretched clasts, fold hinges or intersection lineations. Lineations clearly originating as fold hinges, however, were included within the fold axes data set. Intersection lineations were both measured in outcrop and calculated from outcrop measurements of foliations. In general, lineations are subparallel to fold axes in outcrop. Their variations are analysed in section 6.4.

Folds are common within the Doverfjell, varying from isoclines to open folds and kink folds. Typically, folds are similar or subsimilar. Fold axes and axial planes were measured when possible, and style and symmetry noted. In general no orientation differences could be detected on the basis of style or symmetry, although isoclinal fold axes apparently tend to be more closely parallel to lineations (section 6.4). Coaxiality of folds of various styles and generations appears typical of the Trollheimen-Dovrefjell area (Hansen, 1963, 1971; Scott, 1967; Wheeler, 1973;

Krill, 1980b). As is shown in section 6.3, folds in fold axial planes and secondary foliations have the same orientations as earlier folds, suggesting at least three phases of coaxial folding: initial isoclinal folding to form the transposition fabric, followed by folding of the transposition fabric, and finally folding of these fold axial planes. Bell and Hammond (1984) found similar relationships in a study of folded mylonitic rocks, and used the designation $F_M{}^M$ for folds in the mylonitic foliation with the mylonitic foliation as an axial plane, suggesting that the folds and foliations had been produced in one continous deformation. The folds in the Dovrefjell region may have formed in a similar fashion. A possible exception here is that of kink folds, whose orientations tended to be more erratic. These were analysed separately.

Locally, fold-interference patterns can be observed in outcrop. Type 3 interference patterns (Ramsay, 1967, p. 531) appear common, as refolded isoclines (Figure 8a). In fact, their general presence can be inferred in that all refolded layering is a transposition fabric, and that the

Figure 8. Fold interference patterns from the Grøvudal area, traced from photographs. A - type 3 interference pattern in banded amphibolite and metapsammite (962211). B - type 3 interference pattern in tightly folded quartz vein shortened to approximately 10% of its original length. C - type 1 interference pattern, a sheath fold in banded amphibolite and metapsammite. All fold axes plunge steeply into the page.

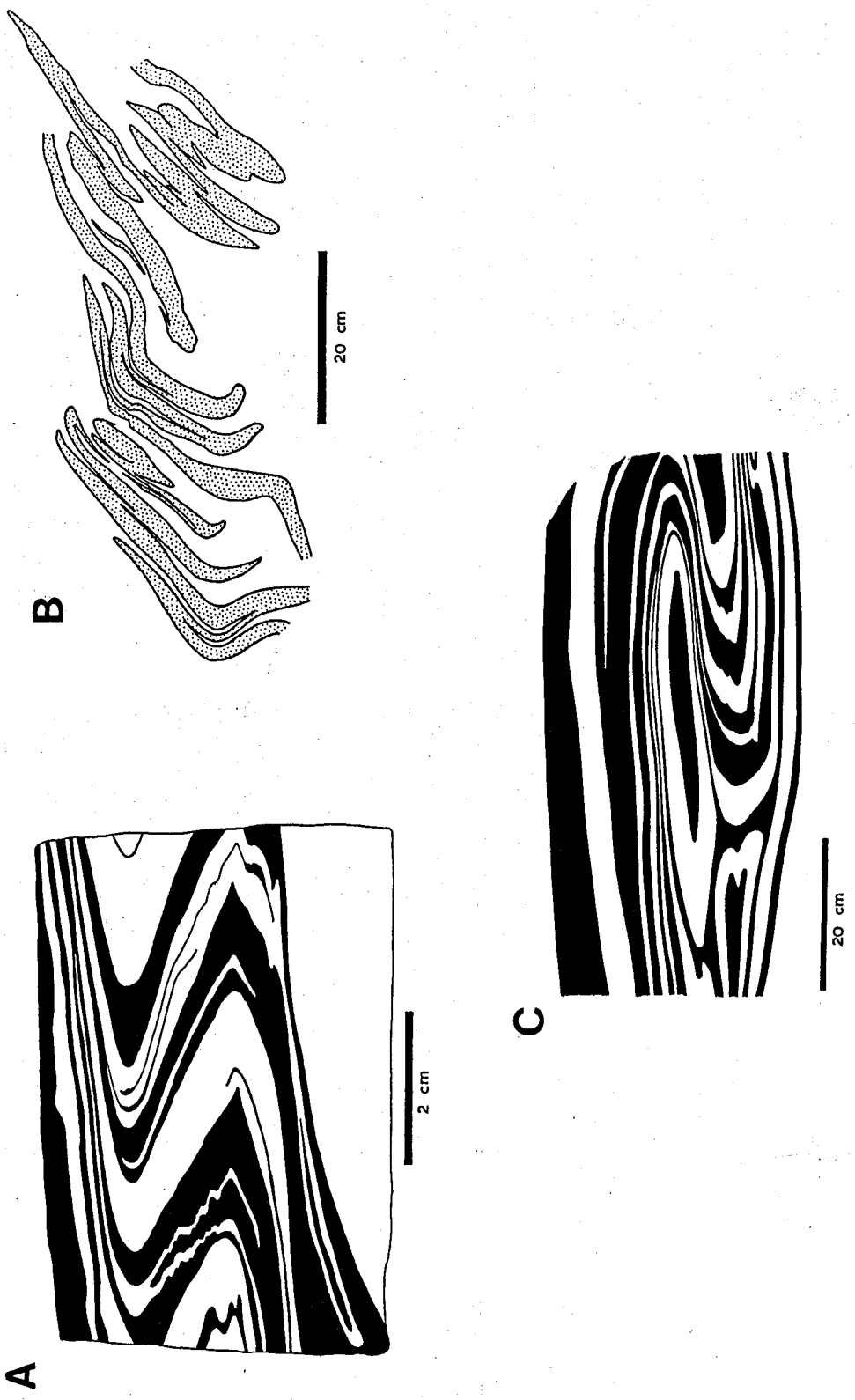
A
2 cm
B
20 cm
C
20 cm

fold axes are typically parallel. A refolded quartz vein (989219) is shown in figure 8b. This vein has been shortened to approximately 10% of its original length.

Of particular interest is the presence of closed, type 1, interference patterns (Figure 8c). The one pictured is from a particularly good exposure where ice-polished outcrops of the banded Sætra nappe are exposed with lineations and fold axes plunging into the mountain side (962211). These folds plunge steeply into the outcrop, and are of the type known as sheath folds (Cobbold and Quinquis, 1980). Similar tubular folds exist elsewhere in the Dovrefjell (e.g., Krill and Röshoff, in press), and a spectacular outcrop on Blåhø in the Trollheimen has been described by Hansen (1963, 1967). While not well displayed elsewhere in the Grøvudal area (e.g., 976267), their presence may be inferred by parallel-plunging folds of opposite symmetry, which are common. The general parallelism of lineations and fold axes, in fact, suggests a sheath fold environment, although this is perhaps not sufficient evidence alone. The significance of this is further explored in chapter 8, but it is noted here that sheath folds typically occur in association with shear zones (e.g., Minnigh, 1979; Bell and Hammond, 1984, and references therein).

5.3 Microstructures

Microstructures of the rocks of the Grøvudal area give

additional evidence for the highly plastic nature of the deformation. In general, the quartzo-feldspathic components are fine-grained, typically less than 0.5 mm, with coarser porphyroblasts or porphyroclasts of garnet, amphibole, feldspar, and lesser staurolite and kyanite. The groundmass in many samples is largely equigranular, suggesting annealing, however nearly all samples display extremely elongate domains of recrystallized ribbon quartz. Most of the samples also display textures within the quartz grains that are indicative of dynamic recrystallization, including mortar textures, deformation lamelli, undulose extinction, and subgrain development.

Porphyroblasts of amphibole in some cases are granulated or recrystallized at their boundaries, forming extensive tails trailing away from the host grains. Garnets typically show quartz pressure shadows, and are generally rotated. Kyanite and mica grains are kinked in some cases.

The textures within all thin sections (43 examined) thus suggest large ductile strains. The general textures are largely mylonitic, and many rocks appear equivalent to protomylonites of Higgins (1971) and Sibson (1977; but not of Wise et al., 1984), gradational into mylonitic gneisses.

Twenty-nine oriented samples were collected to determine the sense of shear parallel to the foliation, and hence the sense of nappe displacement. Eighteen of these samples were collected from the garnet-mica gneisses of the Blåhø

nappe from which rotated garnets had been reported by Krill (personal communication, 1983). In preparation of the samples it was assumed that the plane perpendicular to the foliation and containing the lineation also contained the displacement direction. Samples were accordingly cut perpendicular to the foliation and parallel to the lineation. Although most garnets appear rotated, it is not always clear in what sense, as sigmoidal inclusion trails are not always well preserved. In some cases the asymmetry of pressure shadows on the garnets could be used as a supplementary method. The garnets, however, are not always well preserved and are commonly anhedral with irregular boundaries.

Several other sense of shear indicators were found to be useful, however, and all samples were checked for interpretable asymmetric structures (e.g., Simpson and Schmid, 1983). Asymmetric pressure shadows aided in the interpretation of some rotated garnets, although these were often equivocal. Asymmetric porphyroclast trails were also difficult to reliably interpret. Several samples showed shear bands (White et al., 1980) inclined at angles of 10 to 30° from the foliation, and some samples of felsic gneiss showed recrystallized subgrains flattened oblique to the main foliation.

Eighteen of the oriented samples could be interpreted for the sense of shear with a reasonable degree of confid-

ence. Ten of these samples are from the mainly gently to moderately east-dipping rocks of domains 1 and 2; seven of these indicated a west-over-east sense of displacement, and three suggested the reverse. Two samples from domain 3 similarly indicate a northwest-over-southeast displacement sense, although layering is inclined steeply to the east giving a down-to-the-east sense. Finally, in the vertical to overturned rocks of domain 4 two samples give down-to-the-east senses, while four samples indicate the opposite sense.

Thus, within domains 1 through 3 nine out of twelve samples (75%) indicate west-over-east displacements, while in domain 4 four out of six indicate the reverse sense of displacement. Although the data set is not large, it does suggest that the displacement direction of the nappes was to the east. The possible reversal in domain 4 may or may not be significant (see chapter 7).

ANALYSIS OF ORIENTATION DATA

The orientation data collected in this area comprises over 1800 measurements of the strikes and dips of compositional layering (mainly transposition foliation), cleavage, fold axial planes and kink bands; and trends and plunges of mineral, stretching and intersection lineations, and fold and kink axes. These orientation measurements have been plotted on equal-area stereographs to give a visual representation of their angular variations (Appendix A).

Plotting of orientation data was done using the FORTRAN program STGRAPH (Appendix B). Strike and dip data, stored in computer files, were transformed into trends and plunges of the plane normals. The ambiguity of the trend direction which results from using the strike and dip values alone is resolved by assigning the dip direction (a string input as N, NE, etc.) its azimuthal value, and comparing this number with one of the two possible trend directions. The program STGRAPH then plots lineations or poles to foliations using the equation for an equal-area stereographic projection (e.g., Hobbs et al., 1976, p.501), where in polar coordinates:

$$r = R\sqrt{2} \sin (\pi/4 - \delta/2)$$

where R is the radius of the net, r is the radial coordinate and δ is the plunge. In Cartesian coordinates:

$$x = r \cos (\pi/2 - \theta)$$
$$y = r \sin (\pi/2 - \theta)$$

where θ is the trend.

6.1 Eigenvalue Analysis

In order to quantify the data distributions eigenvalues and eigenvectors were calculated for each plot using a Fortran program, EIGEN (Appendix B). After converting foliation data to foliation pole plunges and trends, direction cosines for each lineation or pole to foliation were calculated for a coordinate system with x north, y east, and z down :

$$l = \cos \theta \cos \delta$$
$$m = \sin \theta \cos \delta$$
$$n = \sin \delta$$

where θ is the trend and δ is the plunge.

A matrix of the sum of the products of the direction cosines was then calculated:

$$M = \begin{bmatrix} \Sigma\, l_i^2 & \Sigma\, l_i m_i & \Sigma\, l_i n_i \\ \Sigma\, m_i l_i & \Sigma\, m_i^2 & \Sigma\, m_i n_i \\ \Sigma\, n_i l_i & \Sigma\, n_i m_i & \Sigma\, n_i^2 \end{bmatrix} \qquad i = 1,n$$

where the summation is over n, the number of measurements. The eigenvectors [V_1, V_2, V_3] and eigenvalues [s_1, s_2,

s_3] are then calculated, where $s_1 \geq s_2 \geq s_3$. The eigenvalues have the property that:

$$s_1 + s_2 + s_3 = n$$

and, for comparative purposes are more usefully given in normalized forms $S_i = s_i/n$ (Woodcock, 1977), so that:

$$S_1 + S_2 + S_3 = 1$$

If the individual measurements are considered as point masses on the surface of a unit sphere, then V_1, the eigenvector associated with the maximum eigenvalue, may be considered as the axis about which the moment of inertia of the distribution is minimized. Similarly, V_3 represents the axis about which the moment of inertia is maximized (Watson, 1966; Mardia, 1972, p. 224). It can also be shown that the eigenvectors effectively give a best fit line or plane to the data by minimizing the sum of the squares of the cosines of the angular residuals (Mancktelow, 1981).

The eigenvalues can then be used to represent the type of distribution. Woodcock (1977) suggested a graphical technique in which $\ln(S_1/S_2)$ is plotted against $\ln(S_2/S_3)$. On this graph random distributions will plot near the origin, while stronger fabrics plot further out. The parameter, C, where:

$$C = \ln(S_1/S_3)$$

can thus be used to quantify the fabric strength. A second parameter K (c.f., Flinn plot in Ramsay, 1967, p. 137):

$$K = \frac{\ln(S_1/S_2)}{\ln(S_2/S_3)}$$

can be used to quantify the type of fabric. Girdle distributions plot below the K = 1 line, while clustered distributions plot above the K = 1 line. This plot is particularly useful for visual comparison of a number of distributions (Section 6.3, Figure 14, Appendix A).

6.2 Confidence Regions

More rigorous statistical methods are available for the characterization and comparison of orientation data distributions; these are also mainly based on eigenvalues (Mardia, 1972). The most generally useful is based on the Bingham distribution (Bingham, 1974; Mardia and Zemroch, 1977; Ela, 1984, personal communication). Briefly, we can calculate the estimated confidence intervals about the eigenvectors as follows. Let τ_i be the normalized eigenvalues such that $\tau_1 < \tau_2 < \tau_3$. Then let:

$$\delta_{ij} = (\tau_i - \tau_j)(k_i - k_j)$$

where k_i are maximum likelihood estimates for the Bingham distribution. k_i values have been tabulated by Mardia and Zemroch (1977). A standard deviation is then given by:

$$\sigma_{ij} = (2n\ \delta_{ij})^{-\frac{1}{2}}$$

and confidence regions may be calculated as:

$$R_{ij} = \sigma_{ij}\ [X^2_{1-\alpha}(2)]^{\frac{1}{2}}$$

where the X^2 (chi squared) term is taken from standard statistical tables for two degrees of freedom, and $1-\alpha$ as the confidence interval (e.g., for $1-\alpha$ = 95%, $X^2(2)$ = 5.99147). R_{ij} will then be the semiaxes of approximately elliptical confidence regions about the eigenvectors.

Confidence regions have been determined for the eigenvectors of orientation data within each domain using this method (Figure 16, Appendix A). This allows a simple, easily visualized summary of the data distribution showing the degree of confidence about each eigenvector.

6.3 Determination of Domain Boundaries

In areas of complex or polyphase folding the standard method for geometric analysis is to subdivide the map area into smaller domains. In general, these domains are defined as areas in which the folding can be described as approximately cylindrical; i.e., all surfaces within that domain share a common line, the fold or π-axis (Turner and Weiss, 1963; Whitten, 1966; Ramsay, 1967; Hobbs et al., 1976). The terms "π-axis" and "β-axis" are nearly synonomous, however a distinction is usually made on the basis of how they are

found. A π-axis represents the pole to a great circle of poles to foliations (π diagram), while a ß-axis represents the intersection of foliation planes (ß diagram). The latter method can be shown to be statistically invalid, and as the term "ß-axis" has this connotation it will not be used here (see Ramsay, 1967, p.9-14).

Subdivision into domains is generally accomplished by an iterative process where initial domain boundaries are chosen by visual inspection of the strike and dip variations over the mapped area (e.g., Ramsay, 1967, p. 552). The data from each domain is then plotted on stereographs to determine the degree of cylindricity; ideally poles to planes will lie on a great circle, and fold axes will cluster near the pole to the great circle. The domain boundaries can then be adjusted until a satisfactory fit is obtained.

This process, apart from being rather subjective, becomes especially difficult when domain boundaries are gradational or where a constant gradient exists. Additionally, if the scale of folding is larger than an average outcrop, but small with respect to the map area then the definition of domains by visual inspection becomes much harder. To illustrate this point figure 9 shows a plot of a portion of the foliation data collected for the area. Each data type was stored in a computer file with its grid reference coordinates, and a simple graphics plotting

routine, LINEPL, was used to prepare maps of the data (Appendix B). Figure 10 is a similar plot of the lineation measurements. The data in stereographic form is shown in Appendix A. Note the near complete variation in the foliation data and the wide distribution of lineation orientations on the stereoplots, indicating little preferred orientation of these elements at this scale. The areal distribution of elements shown in the two maps indicate trends within the data, but it is not apparent where, or if, one could define domains of cylindrical folding.

In this case, then, it is apparent that a manual search for domain boundaries would involve a large degree of subjectivity, and an inordinate amount of iterative plotting and replotting of data. This approach was initially attempted, however, it soon became clear that a more objective search procedure would be required. Charlesworth et al. (1975) and Langenberg et al. (1977) have suggested a statistical test based on work by Watson (1965) to determine domain boundaries. For this test the null hypothesis

Figure 9. Map of selected foliation data from the Grøvudal area. Dip tick marks are proportional to the cosine of the dip, giving their projection onto the map surface. The distance between tick marks on the map border is 10 kilometers.

Figure 10. Map of selected lineation data from the Grøvudal area. Lineation arrows are proportional to the cosine of the plunge, giving their projection onto the map surface. The distance between tick marks on the map border is 10 kilometers.

FOLIATIONS

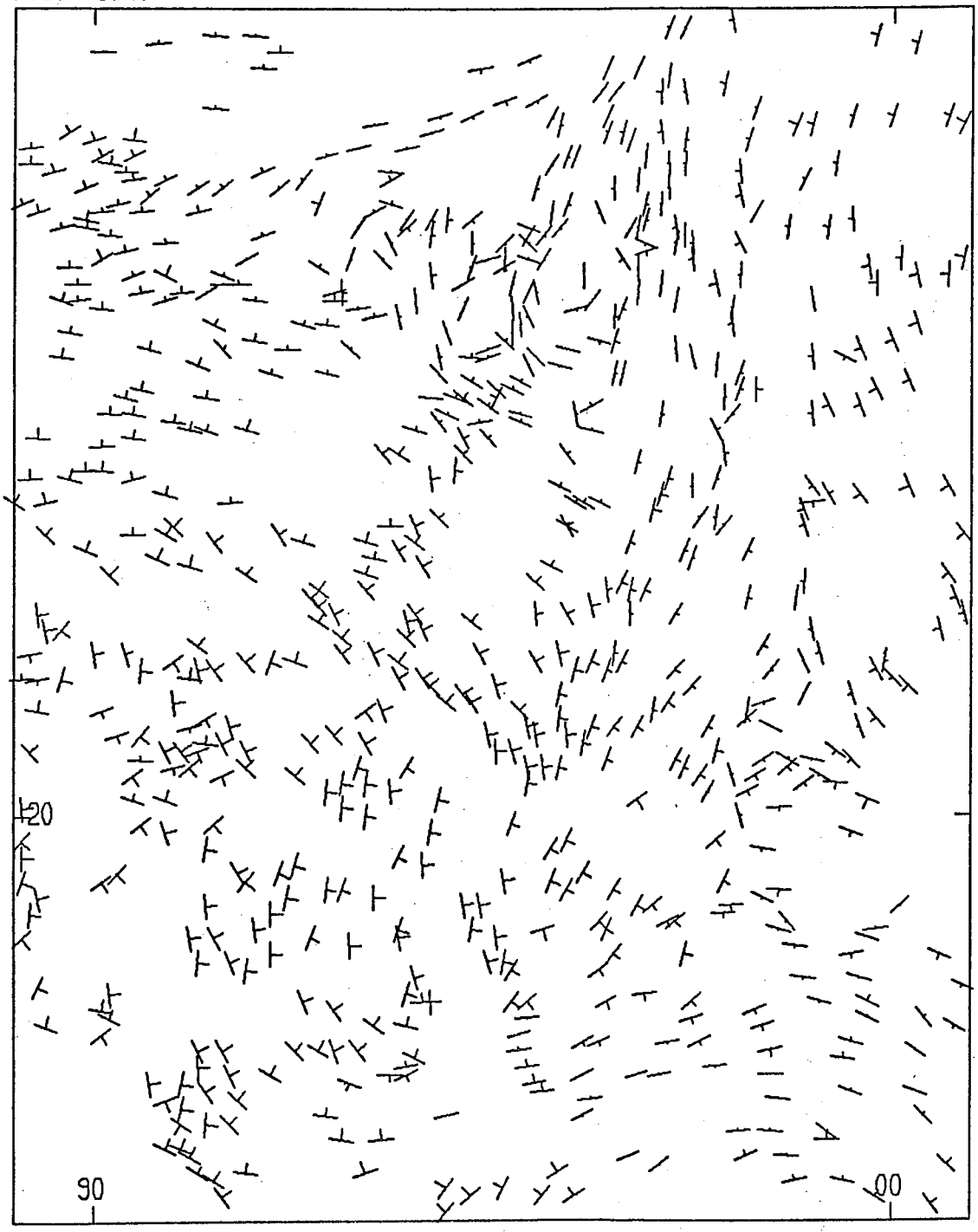

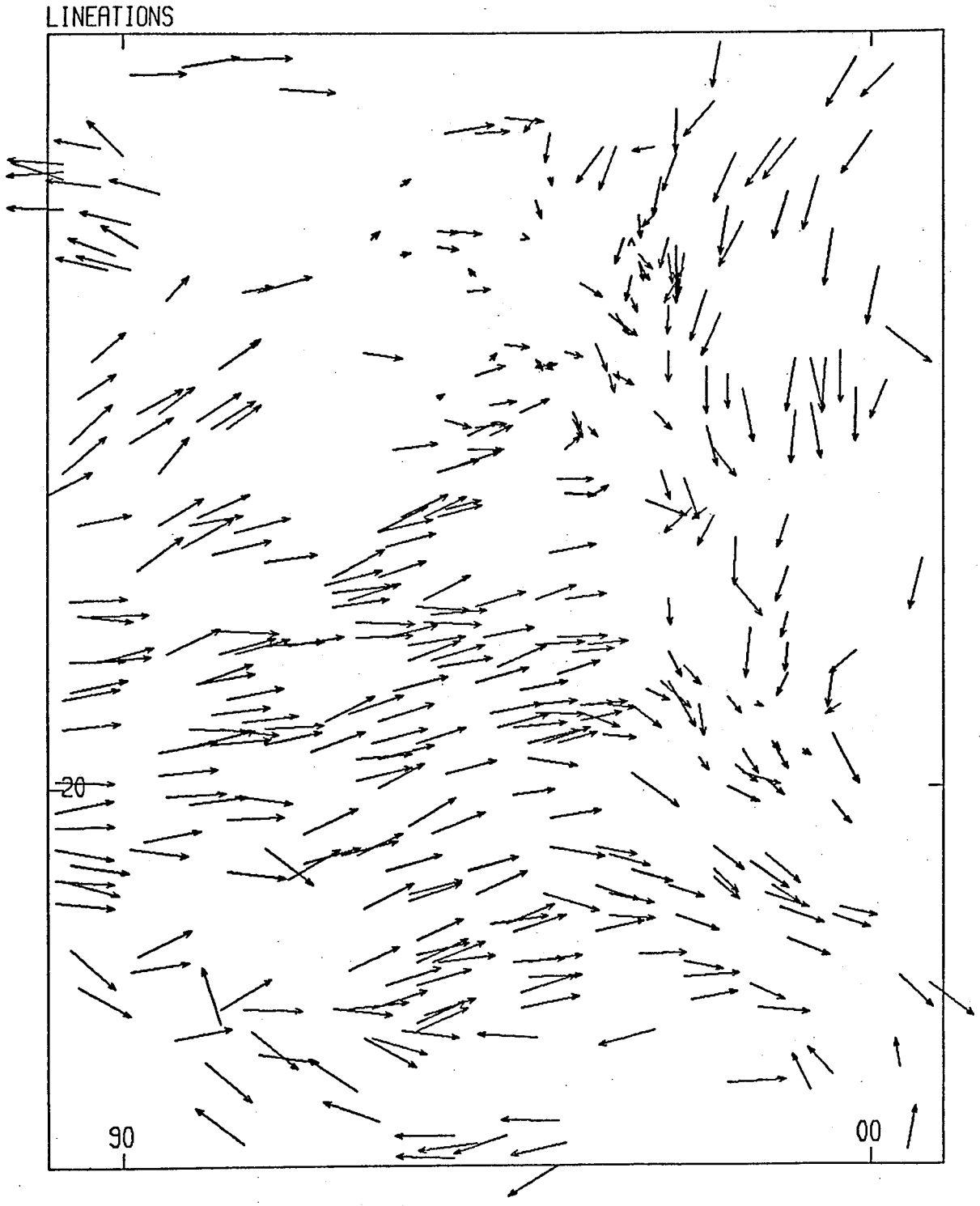
LINEATIONS
20
90
00

of coplanarity of S-poles is rejected with confidence $1-\alpha$ if:

$$k\, s_3 > X^2(n-2)$$

where k is an empirical constant dependent on measurement and roughness errors. As k is difficult to determine where the features producing roughness occur at a scale larger than individual outcrops, a second test for coaxiality is generally required. For this test a fold is divided into two segments and the null hypothesis for coaxiality is rejected with confidence $1-\alpha$ if:

$$\frac{(n-4)\ (s_3 - s_{3a} - s_{3b})}{2(s_{3a} + s_{3b})} > F_{2,\ n-4(\alpha)}$$

where s_{3a} and s_{3b} are the minimum eigenvalues for the two subareas and $F_{2,\ n-4(\alpha)}$ is the upper 100 percentile point of the F distribution with 2 and n-4 degrees of freedom. Two further tests are then required to determine whether the two segments have equal scatter, and whether each segment has coplanar S-poles.

Several problems with this method make it difficult to apply in the present case. First, the apparent scatter in the data at a scale larger than single outcrops precludes a straightforward determination of k. Also, the variation in lithologies from interlayered schists and gneisses of the Blåhø nappe to more homogeneous gneisses of the Amotsdal

nappe suggests that k will not be a constant. Secondly, the coaxiality test requires initial definition of a major fold, thus precluding a general search. In the present field area it is not clear how to initially define the fold limbs. If, for example, a late large scale fold is superimposed on early folds, the major lithologic contacts will show a more complex pattern than the actual kinematic pattern of the late folding event alone (e.g., Ramsay, 1967, p. 531).

In view of these problems a more generally applicable search procedure was developed. The first step was to divide the area into square kilometer areas. Eigenvectors were then calculated for the foliation and lineation data from each square kilometer. This provides a method of reducing scatter, including folding at the outcrop scale, to better delimit large scale trends in the data. This also provides a more easily manipulated data set. Figures 11, 12, and 13 are maps of the average foliations (plane whose normal is V_1 for S-plane data), π-axes (V_3 for S-plane data), and average lineations (V_1 for L data) respectively. The lineation and π-axis plots clearly show a marked variation across the field area, presumably associated with the major fold structure. However, note that the area of the strongest gradient in lineation orientations does not correspond with any structure obvious from the outcrop pattern of lithologic units (cf. Figure 6, Plate

1). The π-axis plot is the least well defined of the three plots, as the axes are not always well defined for each square kilometer, however they clearly indicate the same trends as do the lineation data. The significance of this and an analysis of their deviations will be discussed further in section 6.4.

The plot of average foliations (Figure 11) was analyzed to locate cylindrical domains using a FORTRAN program DSEARCH (Appendix B). Initial domains were arbitrarily defined as squares 3 kilometers on a side. π-axes were then calculated for these 20 domains, and several of them were immediately combined if their eigenvectors differed by less than 10°. The data for such domains were combined and their π-axes recalculated. The π-axes of the resulting 15 domains were then used in the search for the final domains.

The list of average foliations in each square kilometer

Figure 11. Map of eigen-foliations calculated for each square kilometer of the Grøvudal area. Dip tick marks are proportional to the cosine of the dip, giving their projection onto the map surface. The distance between tick marks on the map border is 10 kilometers.

Figure 12. Map of eigen-π-axes calculated for each square kilometer of the Grøvudal area. Lineation arrows are proportional to the cosine of the plunge, giving their projection onto the map surface. The distance between tick marks on the map border is 10 kilometers.

Figure 13. Map of eigen-lineations calculated for each square kilometer of the Grøvudal area. Lineation arrows are proportional to the cosine of the plunge, giving their projection onto the map surface. The distance between tick marks on the map border is 10 kilometers.

EIGEN FOLIATIONS

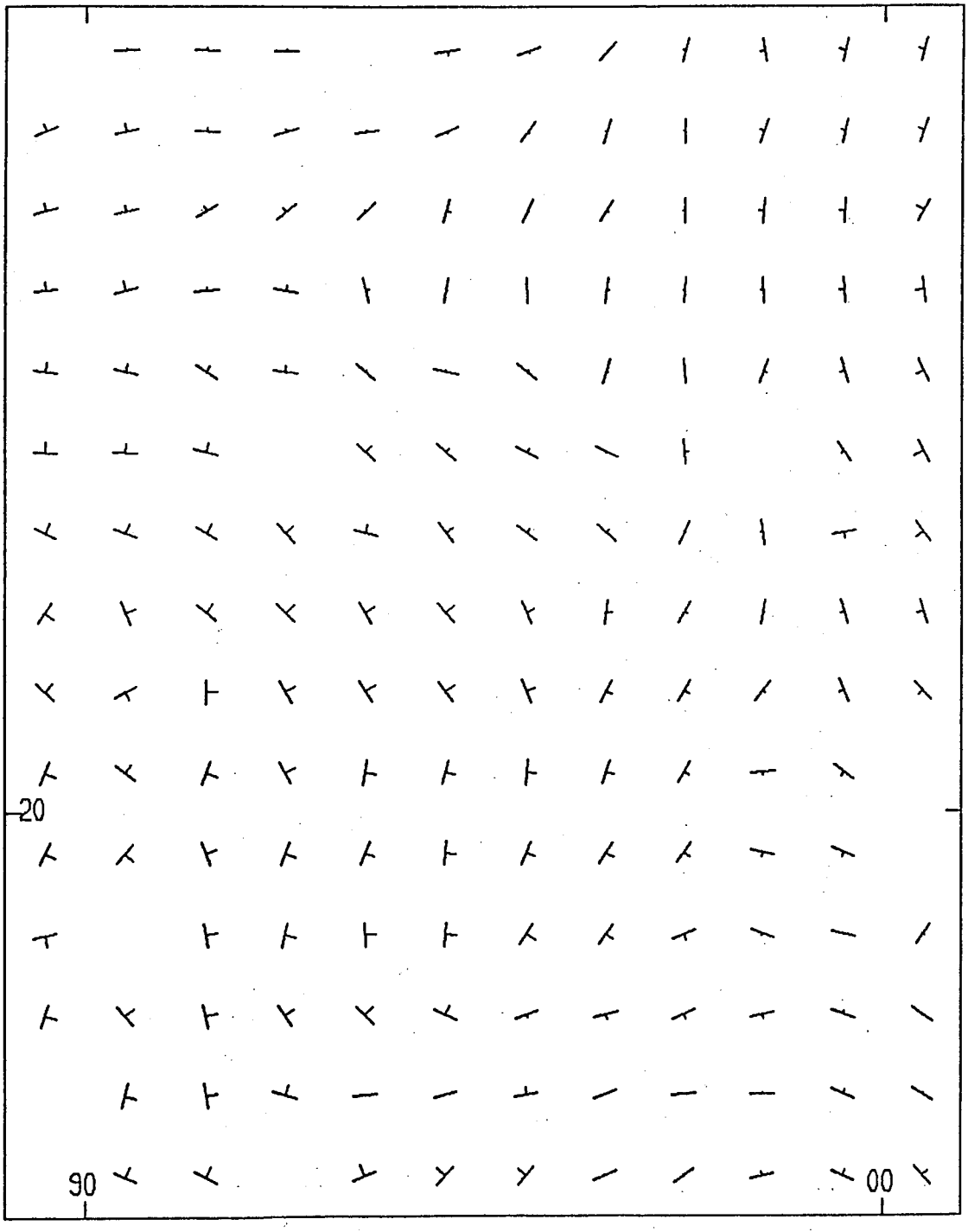

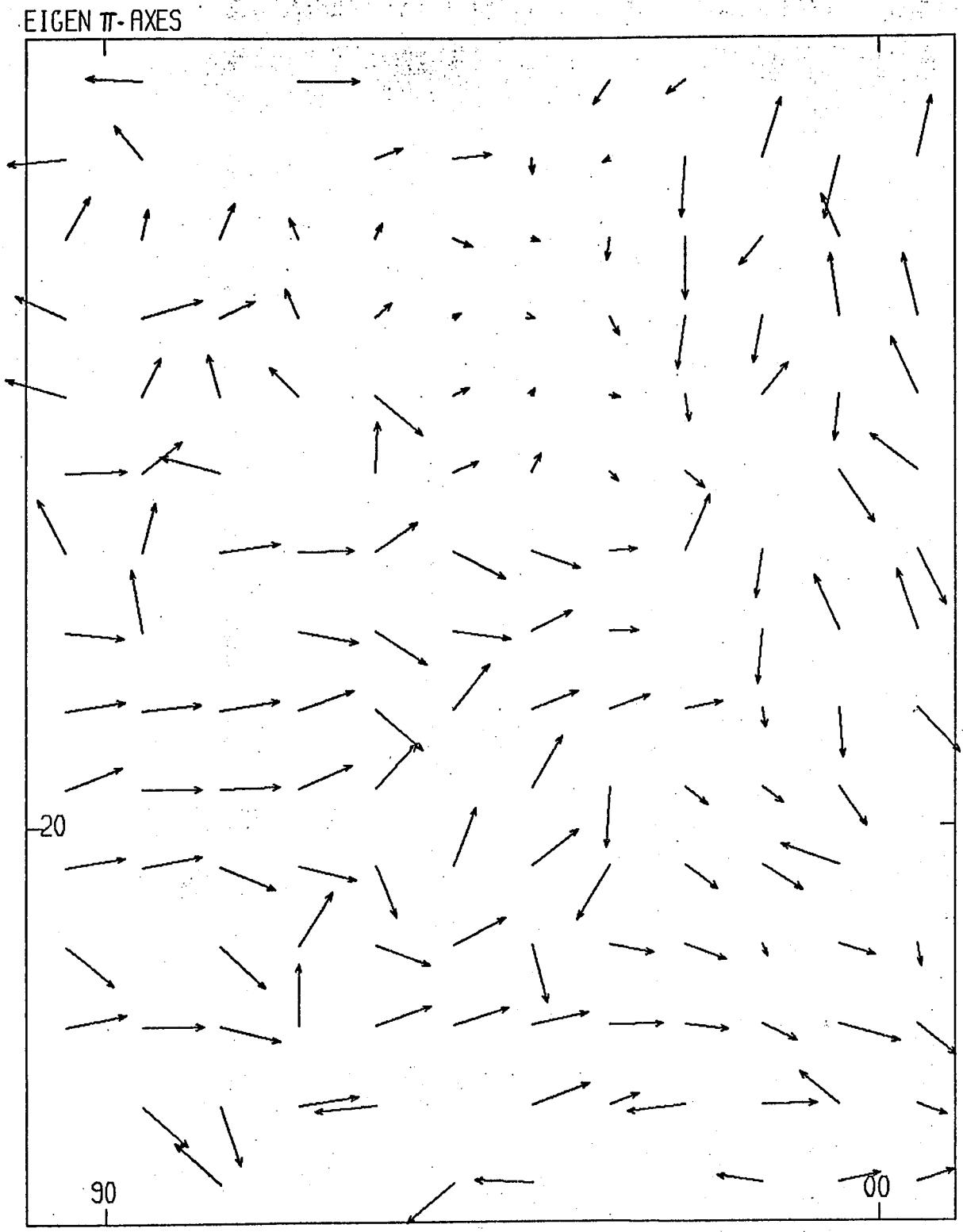
EIGEN π-AXES
20
90
00

EIGEN LINEATIONS

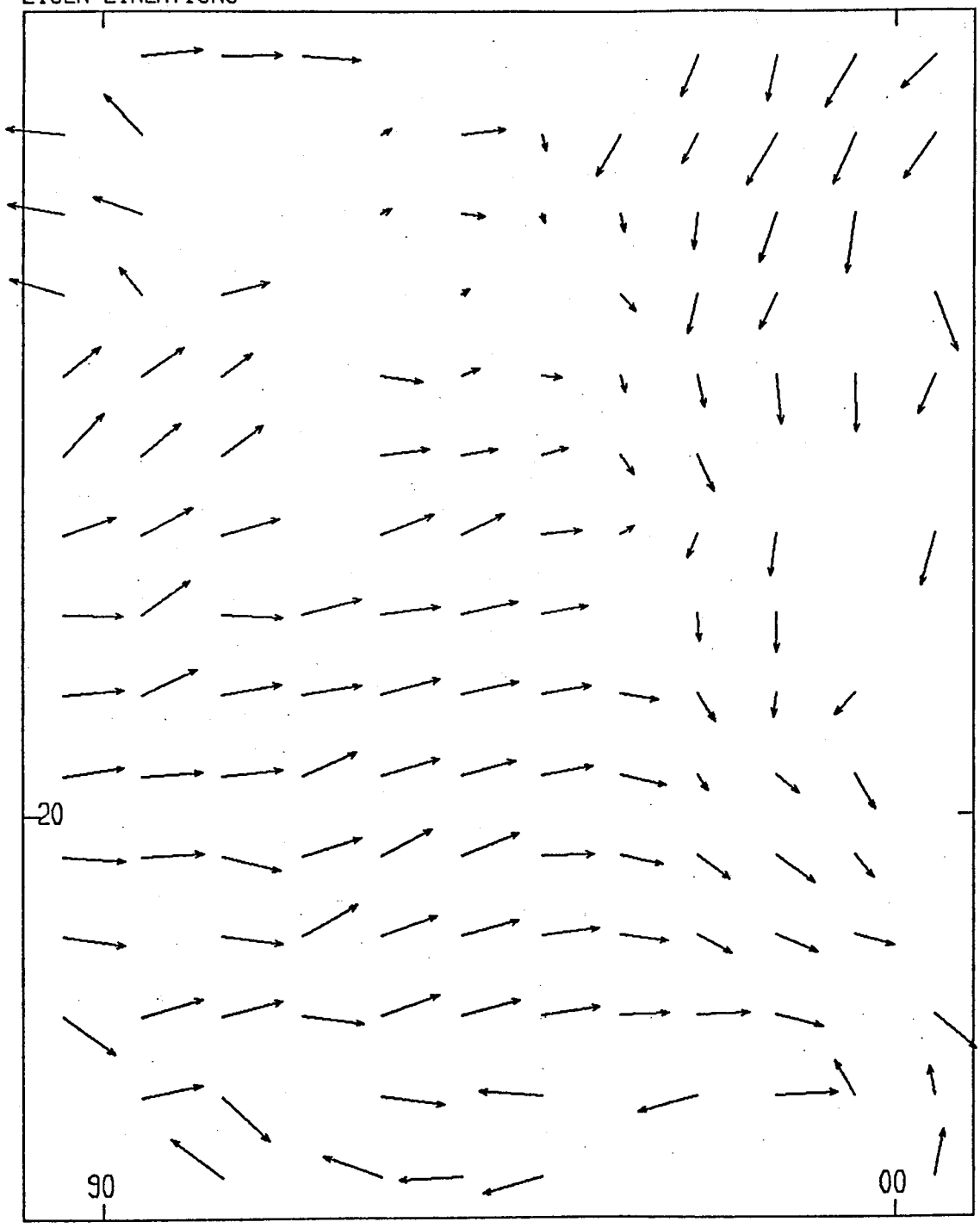

was then compared to each of these 15 π-axes in turn, to determine which foliations were within 10° of perpendicular to a given domain π-axis. Thus 15 lists of all average foliations compatible with each respective domain (i.e., within 10° of perpendicular to the domain axis) were compiled. These 15 lists were plotted on grid paper by outlining each square kilometer on the list. Ten of these plots produced irregular, scattered and discontinuous domains, indicating that the π-axes used to produce them were unsuitable for defining domains.

The remaining five plots which produced more continuous polygons were then used by outlining the continuous portion of the plot, while ignoring scattered outlying areas. π-axes were then calculated for these new domains, and a new plot of compatible average foliations was prepared. Additional square kilometer areas could then be added if they were continuous with the old domain and appeared on the plot, or subtracted if they did not appear on subsequent iterations. In this fashion the π-axes defining the cylindrical domains were modified until they included continuous polygonal areas. To test for uniqueness the process was repeated using different initial domains; it was found that the solution converged on the same polygonal domains. These final polygonal domains were finally altered slightly so no overlap occurred, and so all of the area was covered. This produced five elongate domains trending

NNW across the area.

The final step was to apply the process to the entire foliation data set. This data set was similarly compared to the five domain π-axes and five plots of foliations were made using the program LINEPL showing all the data which were compatible with each domain axis. These plots were superimposed on a light table and boundaries were drawn between the domains. This process required some degree of subjectivity, but generally only at a local scale. The eigenvectors for these final domains were then calculated.

The results of the domain boundary analysis can be evaluated in two ways; by considering the type and strength of the resulting fabrics, and by considering the orientations of the eigenvectors. The resulting fabric intensities can be qualitatively seen in the domain stereograms shown in Appendix A. Clearly the strong girdle patterns of the domainal foliation plots contrast strongly with the near random fabric of the whole area plot. Similarly, the lineation and fold axes plots show strong point maxima within each domain. It should be emphasized here that the domains were defined using the foliation data only; correlation of fold and lineation data is thus taken as confirming evidence for the validity of the search procedure.

Fabric intensities and type can be more quantitatively compared on a eigenvalue plot, as shown in figure 14. Here

distance from the origin as measured by the parameter C = $\ln(S_1/S_3)$ is a measure of fabric intensity. In this case C for the foliation data has increased from 0.67 in the whole area to a range of 1.97 to 2.91 within the domains, or 2.9 to 4.3 orders of magnitude. The second quantity represented on the graph is the fabric type. For example, total lineations plot just within the girdle field, while lineation data for domains 2 to 4 plot as strong clusters. In general, there is a good clustering of linear data within the domains and strong girdle patterns within the foliation data.

Several deviations from this behavior are worth noting however. A traverse across the domains from 1 to 5 reveals an apparent change in fabric type, with little change in fabric intensity. Lineation clustering is strongest in the central three domains, falling off to either side. Similarly, the strongest foliation girdle patterns are found in domains 2 and 3. The pattern in fold axes is less well defined, but still present (the fold axis eigenvalue for domain 5 is based on only 4 measurements). The significance of these patterns is discussed in chapter 7. A

Figure 14. Eigenvalue plot for foliation, lineation and fold axis data from the Grøvudal area. S_1, S_2, and S_3 are respectively the maximum, intermediate, and minimum normalized eigenvalues. The total data eigenvalues (T) and the eigenvalues of data for each domain (1 to 5) are plotted by their eigenvalue ratios.

Eigenvalue Plot of
Grøvudalen Orientation Data

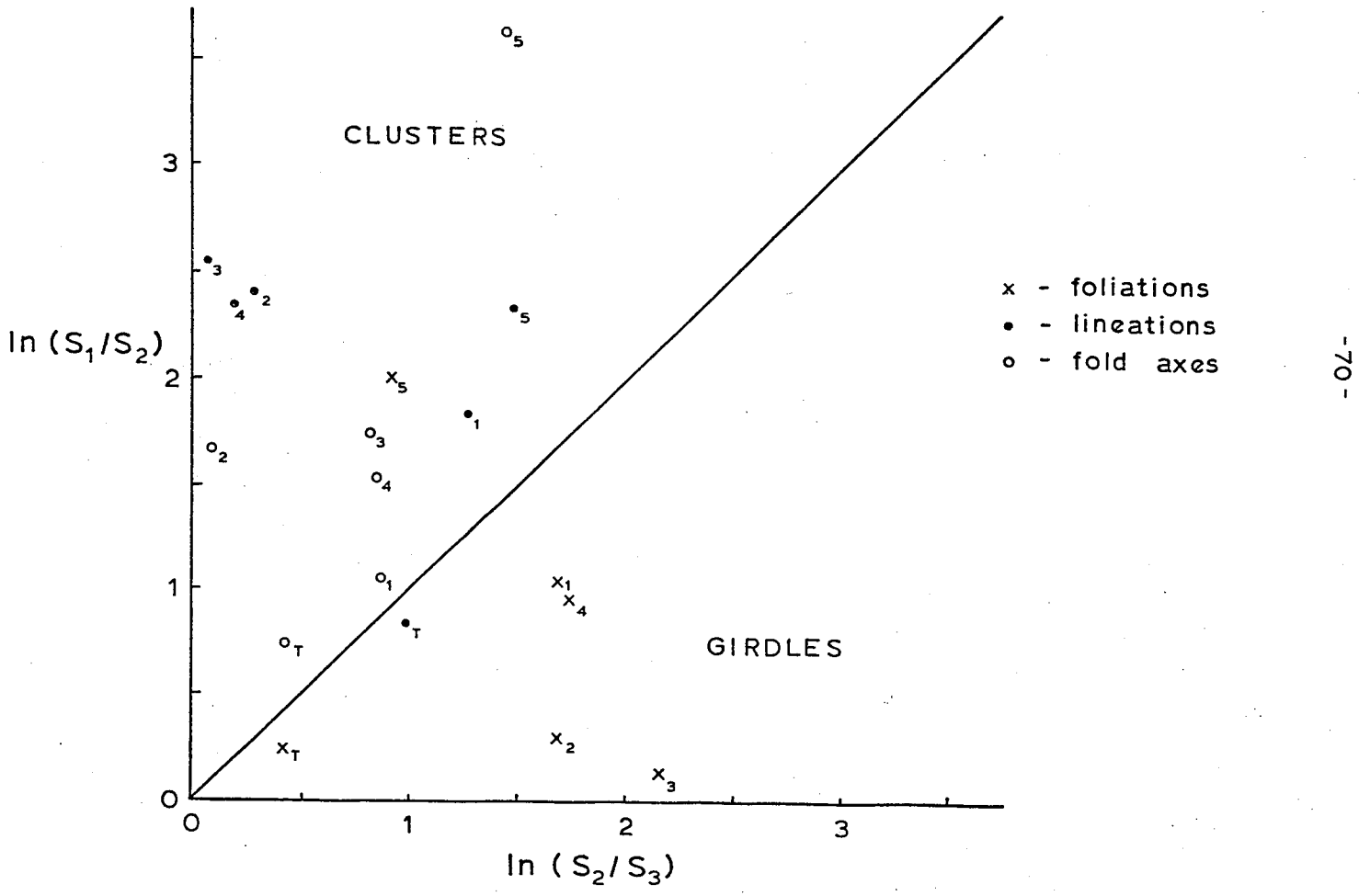

similar plot for the other orientation data sets is given in Appendix A.

Finally, the eigenvectors for foliation, lineation and fold axis data have been plotted in figure 15, and their 95% confidence regions are shown in figure 16. Within each domain there is a close correspondence between the foliation π-axis, and the lineation and fold axes eigenvectors. At the 95% confidence level they are indistinguishable. Most significantly, however, there is a clear progressive change in these orientations across the area. This strongly suggests a reorientation of an early fabric across the area. Note also the change in foliation maxima, and that S_1 and S_2 foliation maxima are indistinguishable at the 95% level of confidence. The significance of these patterns will be discussed further, the main point here is that a strong and statistically valid pattern has emerged from the data.

The domain search procedure analysed the orientations and locations of foliation data with no inital assumptions about the domain boundaries. This was deemed essential as

Figure 15. Equal-area stereogram of the maximum eigenvectors for lineation and fold data, and the minimum eigenvectors for foliation data in each domain. The best-fit small circle to the plotted points has an axis of 06-146.

Figure 16. Equal-area stereograms of the 95% confidence regions for eigenvectors of data distributions within each domain, based on a Bingham distribution.

Eigenvectors of Grøvudalen Orientation Data

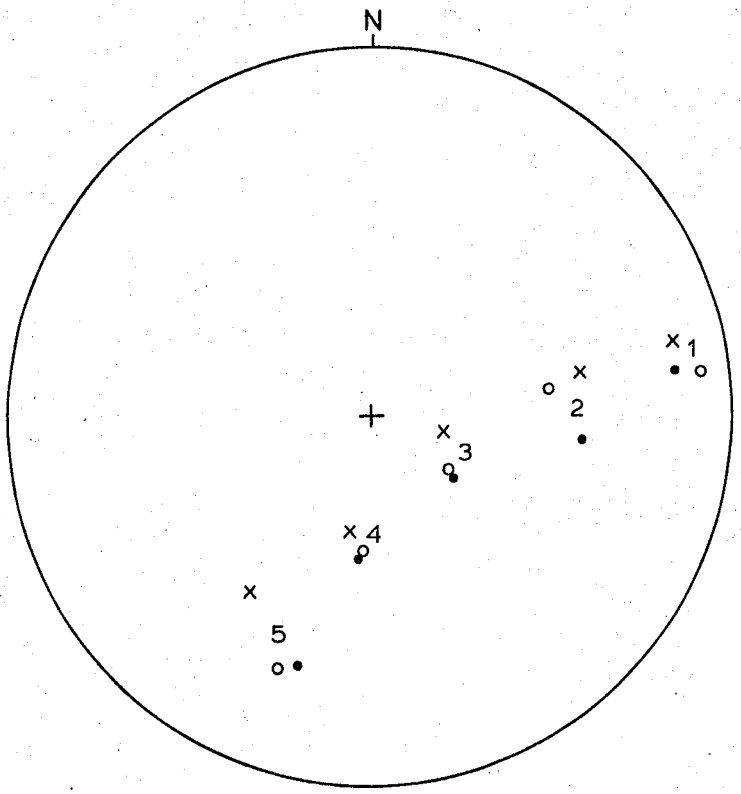

x - foliation minima (957)
o - fold axes (199)
• - lineations (439)

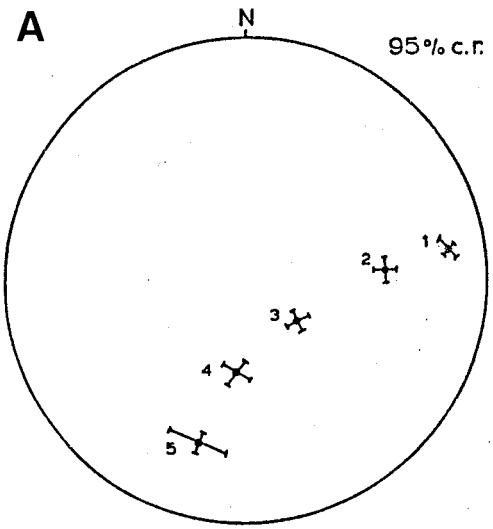

Lineation maxima n=439

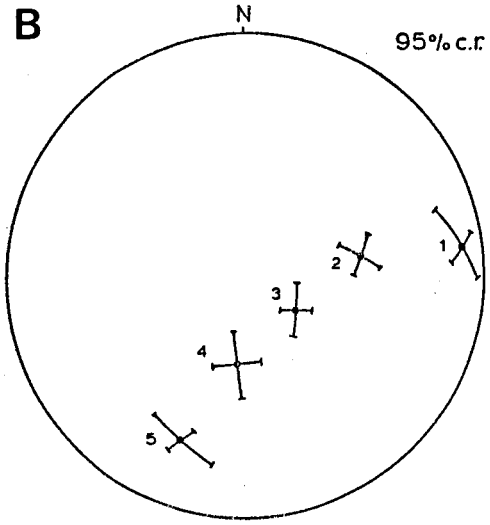

Fold axes maxima n=199

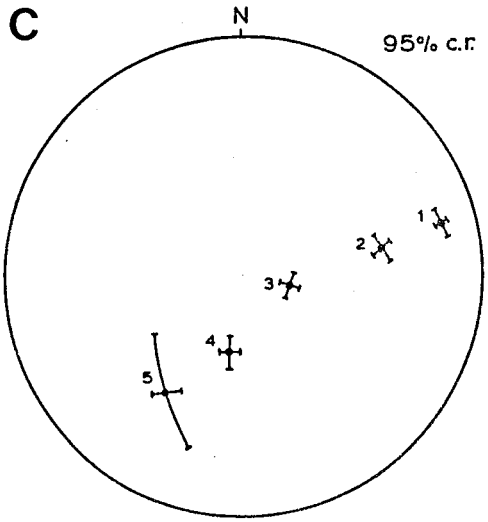

Foliation (S_1) minima n=957

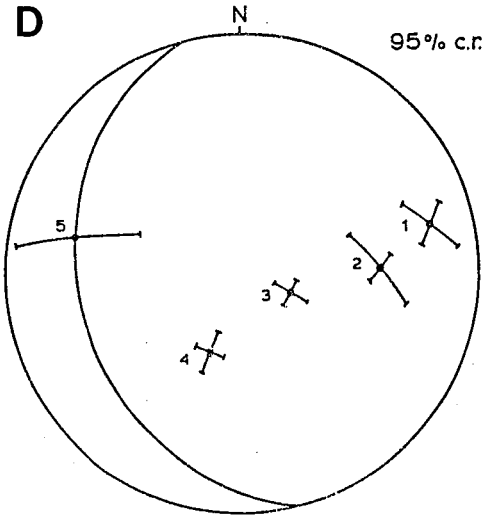

Axial plane and cleavage (S_2) minima n=125

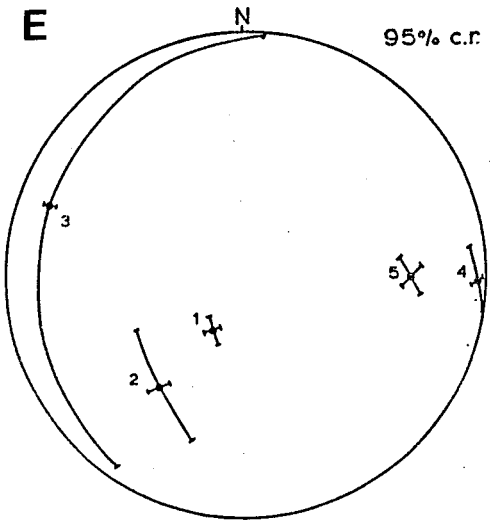

Foliation (S_1) maxima n=957

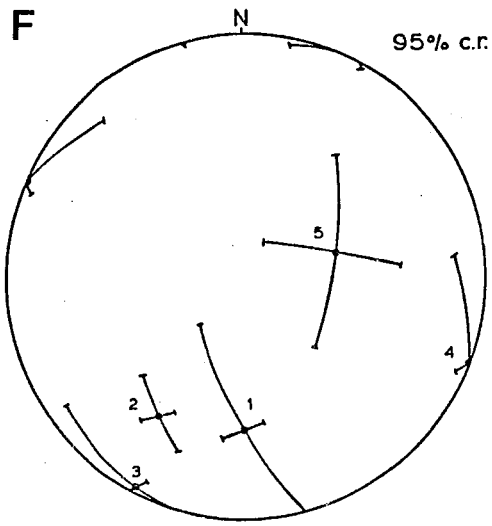

Axial plane and cleavage (S_2) maxima n=125

there were no clear initial choices for such boundaries. Clearly, lithologic contacts were of little aid (Figure 6); and while in retrospect the lineation pattern shows a trend parallel to the domain boundaries, the largest and most significant data set is that of foliation orientations. The major assumption made was that the domains were cylindrical; while this is the standard type of domain encountered in the literature, there are other possibilities such as conical domains. In the Grøvudal area however it appears that the regional fabric can be approximated by cylindrical domains at a mappable scale.

6.4 Fold and Lineation Data

In section 6.3 it was demonstrated that within each domain fold axes and lineations are statistically parallel. This includes π-axes derived from both foliation data sets, S_1 and S_2. The only indication of any deviation from statistical parallelism is that lineation maxima are consistently about 8° closer to the apparent small circle axis (06-146) than the foliation minima (Figure 15). This is, however, statistically significant at the 95% level only in domain 3, and is not regarded as a resolvable difference. The only other deviation from this trend is the intersection data (S_1/S_2, Appendix B). In general, these intersections would be expected to parallel fold axes. Their deviation here may be attributed, perhaps, to the small

data set and errors inherent in calculating them from field data.

In any event, there is clearly a strong parallelism of fold axes with lineations, and no clearly resolvable deviations occur at the scale of the domains. An additional, and somewhat remarkable, result is that there appears to be no resolvable difference between the S_1 and S_2 foliation data sets; their 95% confidence regions overlap in all domains for both maximum and minimum eigenvectors. This suggests that both sets were operated on by the same deformation, and that both foliation and fold development may have been a continous process with early foliations and isoclines folded to form new folds and foliations, and subsequently refolded in a similar fashion.

In order to further analyze the deviation of fold axes from lineations, a number of attempts were made to identify any possible correlation of style or symmetry with orientation. This is of particular interest because, in general, the lineations are largely stretching lineations that represent the maximum finite elongation direction, while fold axes are presumed to have been rotated towards the maximum elongation direction (Chapter 8). Tighter folds, for example, might be expected to lie closer to the lineations than more open folds (e.g., Grocott and Watterson, 1980). Also, Hansen (1963, 1967) was able to relate the symmetry of folds to a movement direction by considering asymmetric

folds to have rotated towards a movement direction.

Figure 17 is a histogram of the angular deviation of fold axes from lineations measured in the same outcrop. These calculations were made on a Sharp EL-512 programable calculator using the relationship:

$$\cos \alpha = \cos \delta_1 \cos \theta_1 \cos \delta_2 \cos \theta_2 + \cos \delta_1 \sin \theta_1 \cos \delta_2 \sin \theta_2 + \sin \delta_1 \sin \delta_2$$

where θ and δ are the trend and plunge respectively. The histogram shows a clear tendency for parallelism of fold axes and lineations in outcrop, and further suggests a tendency for isoclines to be more closely parallel to lineations than other folds.

To test for any trend in areal distribution of such deviations, the foliation minima eigenvector set (Figure 12) was compared to the lineation maxima eigenvector set (Figure 13) for each square kilometer of the area. After discarding clearly spurious data points, the angular deviations were hand contoured (Figure 18). The resulting map does not give any clearly defined pattern, although there is a general tendency for the lowest angular deviations to

Figure 17. Histogram of the angular deviation of fold axes from lineations as measured in outcrop.

Figure 18. Map of Grøvudal area contoured for the angular deviation of eigen-lineations (Figure 13) from eigen π-axes (Figure 12) calculated for each kilometer of the area.

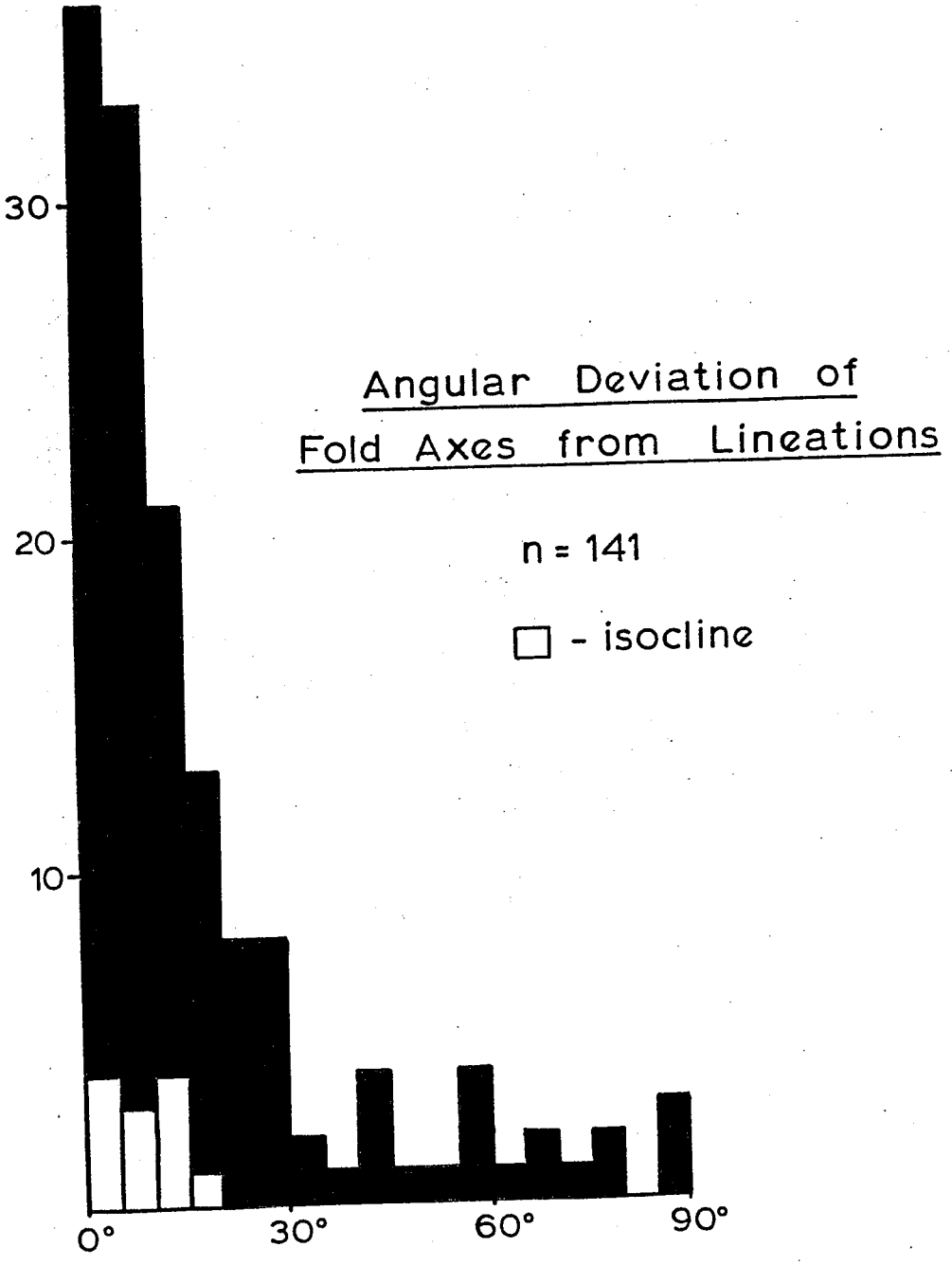
30
20
10
0°
30°
60°
90°
Angular Deviation of
Fold Axes from Lineations
n = 141
□ - isocline

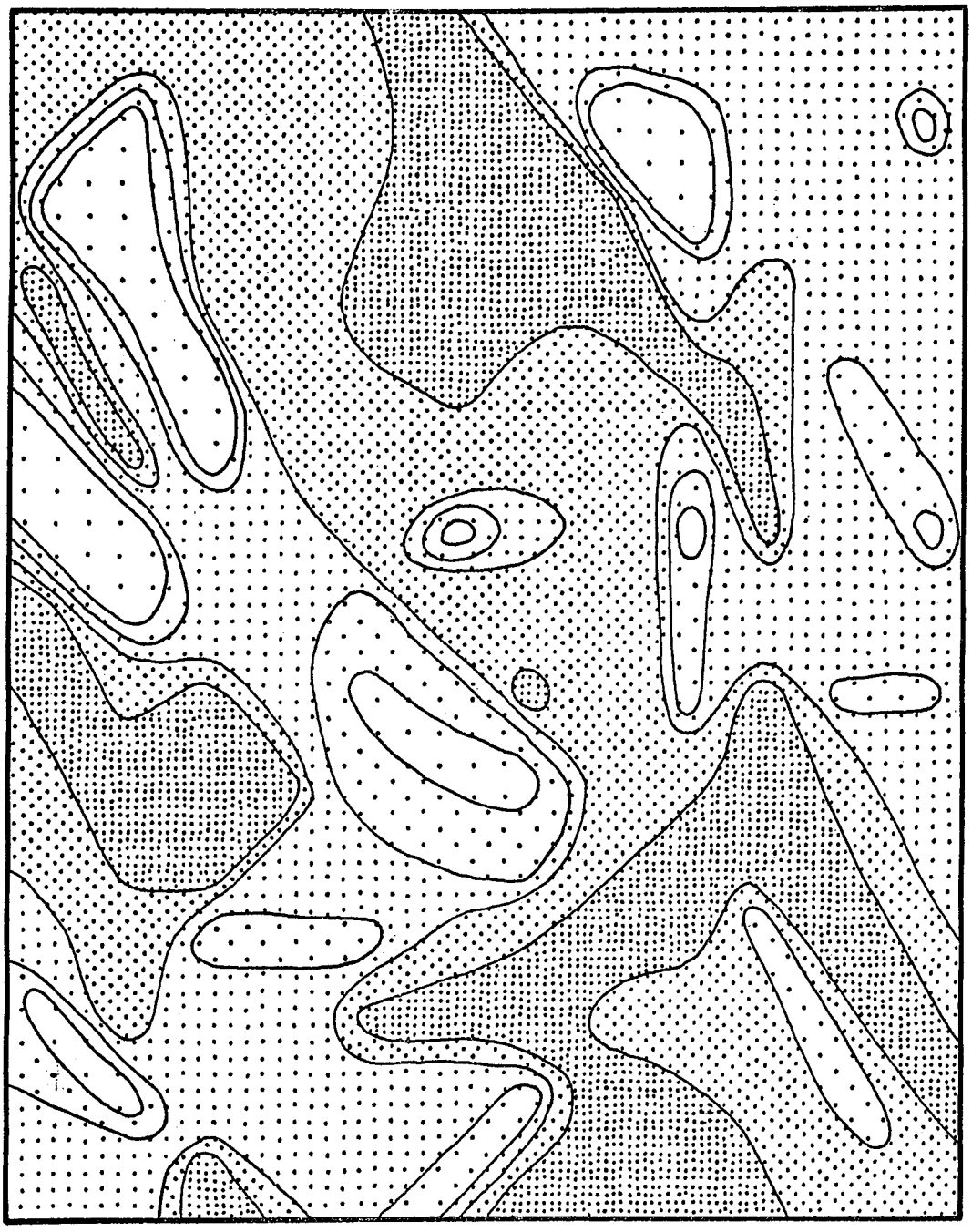

0 - 9°
10 - 19°
20 - 29°
30 - 39°
40 - 90°

occur approximately in domain 3. There may be a correlation here with the eigenvalue analysis, which suggests a stronger linear fabric in domain 3 (Figure 14).

Finally, a number of attempts were made to see if a correlation existed between fold tightness or symmetry and orientation within each domain. The data from each domain were plotted on stereonets by fold symmetry, as S or Z, and isoclines were plotted as separate symbols. No general correlation was found. This may in part be attributed to the presence of well developed sheath folds, such that folds of opposite symmetry have been rotated into parallelism.

To summarize these relationships, all fold axes and lineations are essentially parallel, and at least three early fold phases folded and refolded layering under apparently identical circumstances, interpreted to represent a continous deformation sequence. The first fold phase is associated with isoclinal folding and transposition of primary layering. The second is open to isoclinal folding of the secondary layering. The third is associated with refolding of the later foliations and fold axial planes. These are not presumed to be regionally distinct phases, and probably represent continous $F_M{}^M$ fold development in response to local flow heterogeneities.

Thus far, we have not considered kink folds or the later major refolding event which lead to the present re-

oriented distribution of structural fabric across the domain boundaries, these are considered in section 6.5 and chapter 7 respectively.

6.5 Kink Folds

A relatively small population of the folds in the Grøvudal area (30 measured axes) have pronounced angular kink-like geometries, suggesting they may have formed in a different environment than the more common, typically rounded subsimilar folds found throughout the area. The distributions and orientations of these folds are shown in Appendix A as maps and stereograms of kink fold (crenulation) axes, axial planes (S_3), and their domainal eigenvectors.

It is difficult to draw any convincing conclusions from these data. The map of kink axes suggests the kink fold population is similar to that of all fold axes, however, the confidence regions for the kink fold data set suggest that this correlation may not be statistically valid.

An attempt was made to see if a consistent stress orientation, or trajectory, could account for the kink fold orientations by using an empirical relationship derived by Weiss and Gay (1974). From experimental data the approximate relationship:

$$\bar{\Omega} = 60^{\circ} + 0.57\ \alpha$$

was obtained where α is the angle between the folded surface and σ_1, and $\bar{\varrho}$ is the angle between the folded surface and the kink band boundary, both measured in the same direction. This equation was used to find the σ_1 orientations for 23 folds for which $\bar{\varrho}$ was known. Of these, six had angles of significantly less than 50°, suggesting their origin was unrelated to processes observed under the experimental conditions. Six others were regarded as questionable, lying outside or marginal to the experimental data field. These and the remaining eleven points showed no significant correlation or trend across the area. This would seem to rule out an origin due to the imposition of a late stress field.

SYNTHESIS AND STRUCTURAL HISTORY

It has been shown in Chapter 6 that the Grøvudal area can be divided into five north-northwest trending elongate domains (Figure 6). Within each of these domains the poles to foliations form a great circle whose axis is parallel to the lineation and fold axes maxima. Poles to fold axial planes and secondary cleavages also form a great circle with a similarly oriented axis. It was further shown that the orientations of these domainal axes change from domain to domain in a regular fashion, forming a well defined small circle pattern. This chapter attempts to interpret these patterns, in particular the pattern of the domainal axis variations. Cross-sections through the area (Figure 6) are heavily based on these interpretations.

The implications of the orientation data within each domain for the folding history have been discussed in section 6.4. Following, or transitional to, an early thrust-nappe history (Section 5.1), primary layering was transposed into a new layering defined by isoclines, this layering has been folded to form the girdle pattern of poles to foliations, and refolded to form the girdle pattern of poles to fold axial planes. Rather than three distinct episodes, however, the general parallelism of all axes and foliations suggest a continous process of folding and foliation formation. Similar histories have been suggested for

mylonite zones (Bell and Hammond, 1984, and references therein). The parallelism of fold axes with the stretching lineation is believed to be due to a number of processes discussed in Chapter 8, and is commonly observed in high strain zones and areas of sheath folding (Bell and Hammond, 1984, and references therein).

The well ordered change in axis orientation across the domain boundaries suggests large scale folding or re-orientation of the fabric. The five poles to the domain eigen-foliations form a rather poorly defined girdle pattern, but clearly show a progressive steepening of the average layering from west to east (Figure 16). The simplest explanation for this is an antiformal structure overturned to the east; with a shallow east-dipping western limb defined by domain 1, and a steep overturned eastern limb defined by domain 5. This clearly requires some elaboration, however, as the tectonostratigraphic order suggests a synformal structure (e.g., Krill, in press). Furthermore, the domains do not correspond with the apparent limbs of the observed major structure (Figure 6), so that a simple antiformal structure can not be a valid solution.

The second pattern that requires explanation is the small circle pattern of the axes (Figure 15). This pattern is very well defined, and is unlikely to be fortuitous. A small circle drawn for the π-axis eigenvectors about the

pole 06-146 has a standard deviation of less than 3°, and including lineaton and fold axis eigenvectors the standard deviation is about 6°.

Geometrically, the simplest way to generate a small circle pattern is by rotation. In figure 19 the eigen-lineations have been rotated to horizontal by first rotating the cone axis 6° to horizontal, and then rotating the eigen-lineations progressively to horizontal about the axis. The eigen-lineations then lie within a 14° range, trending almost due east (Rotation of the eigen π-axes instead of the lineations would produce an even tighter clustering). The poles to the eigen-foliations were unrolled along with the lineations; that is the data within each domain was rotated as a whole about the cone axis until the lineations were horizontal. When this is done the poles to eigen-foliations lie on a vertical great circle striking about 163°, with two maxima (Figure 19).

This unrolling sequence can be explained by the model shown in figure 19B. The early sequence of transposition

Figure 19. Refolding model for the Grøvudal fold-nappe. A - foliation and lineation data unrolled about 06-146. B - refolding of early east-trending north-facing fold with elongation lineations (L_1) parallel to fold axes (F_1). During refolding the upper, south-dipping limb (S_1') follows the path from S_1', forming the present foliation maxima in domains 4, 5, and part of 3. The lower, gently north-dipping limb (S_1'') follows the path from S_1'', forming the present distribution of foliation maxima in domains 1, 2, and part of 3. See text for further explanation.

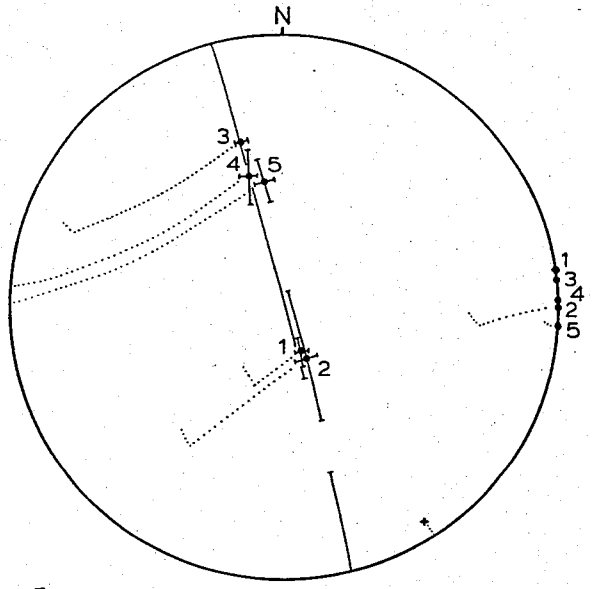

A

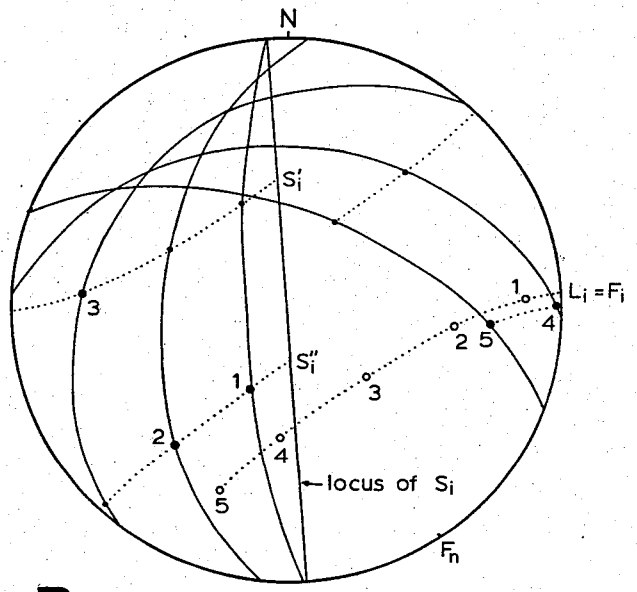

B

and folding produced an average horizontal foliation with east-trending lineations and fold axes, while the entire locus of foliations forms a vertical great circle. During, or possibly following, this deformation a large nearly recumbent north-facing fold developed with an upper limb dipping 40° south and a lower limb dipping about 15° north to produce the pattern of foliation data seen in figure 19A. This large fold presently closes to the south, and forms the major obvious closure pattern.

Refolding of this major east-trending fold then lead to the present distribution of orientation data. In figure 19 this is simulated by successive rotations in the 5 domains of 15, 45, 80, 115 and 145° respectively, giving a fold with a tighter hinge curvature than limb curvature. Thus the five domains represent successive positions on the large late east-verging antiform. The lower limb of the early fold now lies mainly within domains 1 and 2, while the upper limb of the early fold lies mainly within domains 4 and 5. Domain 3 contains about equal portions of both limbs.

This folding sequence can be visualised by folding a piece of paper lengthwise to simulate the first fold. Holding the folded paper horizontal with the crease towards oneself, fold the right side down along a crease angling off about 45° to the left (NW if east is to the right).

This model explains a number of peculiarities in the

data set. First, compare the foliation data set from figure 6 with figure 19. The foliations in the central portion of domain 2 are largely dipping moderately northeast. To the south the foliations become moderately southeast dipping. These are the orientations predicted for the orientations of foliations by refolding the two limbs of the early fold, and a change occurs in crossing the early fold axial plane. To the north another, more open, early fold exists (e.g., Figure 6, section D-D'). Second, the orientations of the domain eigen-foliations become clear, as they lie on two small circles rather than one great circle. That is, the foliation maxima of figure 16E correspond closely with the foliation maxima predicted in the model of figure 19B (large filled circles). Third, the pattern of the foliation eigenvalues (Figure 14) can be explained, as the domains cut across the early fold axial plane. Thus, domain 3 shows the strongest girdle pattern because it contains both limbs of the major early fold. Finally, the peculiar outcrop pattern can be explained as a result of a folded axial plane that dips steeply in the east, and dips shallowly in the west (Figures 4 and 6).

One possible problem with the model, however, is that it may be too simple. The distribution of data has been explained by pure rotation with no attendant strain. In rock bodies of a finite thickness this creates a compatibility problem. One solution to this is by flexural

flow folding, in which the space problem is alleviated by simple shear tangential to the folded surface (as in bending a telephone book). This shear will result in strains that will effect the orientations of all fabric elements not parallel to the folded surface, but not of fabric elements parallel to the surface (e.g., Ramsay, 1967, p. 492). In the present case the folded surfaces correspond to imaginary horizontal planes, with respect to the early near-recumbent fold.

The amount of simple shear required to maintain constant length of these planes is simply related to the amount of rotation (Ramsay, 1967, p. 393):

$$g = \tan \mu = \theta$$

where g is the shear strain, μ is the angular shear, and θ is the rotation in radians. This shear strain could be distributed in many possible ways around the fold. For example, one limb could be held fixed while the other accommodates the strain, or the shear strain could be distributed equally, but with opposite senses, on both limbs.

The total rotation within the Grøvudal structure, as recorded by the lineations, is about 130°. Distributed equally on both limbs this would give maximum shear strains of g = 1.1 in domains 1 and 5. These shear strains would have opposite senses on either limb, possibly explaining

the reversed sense of shear indicated by microstructures of domain 4 (Section 5.3). A simple shear of g = 1.1 gives a strain ellipsoid ratio of about 1.7:1.0:0.6. These strains are presumably quite small compared to the total cumulative strain.

The effect of the fold-induced shear strains on the orientations of the fabric would be quite small in this case, because the lineations are assumed to have been originally horizontal, and the foliations strike at low angles to the shear direction. Using the above model the amount of rotation of inclined planes due to the required simple shear can easily be calculated (e.g., Section 8.2, Figure 27). In this case, the model shown in figure 19B would only have to be modified slightly by taking the upper limb of the early fold to dip about 30° south rather than 40° south. The orientation of the lower limb would only be changed by a few degrees. While this is not a unique solution, it does show that a flexural flow mechanism is compatible with the data.

To summarize, then, following the initial thrust-stacking event, early folding produced a sequence of east-directed sheath folds and a large scale north-facing near-recumbent synform. This synform was then refolded about a south-southeast trending axis, possibly by a flexural flow mechanism, to form an east-verging antiform. This late antiform can only be recognised by its effect on the older

structures, as brought out by the domain analysis.

A few further points are worth making here concerning, first, the significance of the fold mechanics, and second, the regional implications. The mechanics of the first folding event can be explained in terms of a west-over-east shear or sheath-fold regime; this topic is discussed in some detail in Chapters 8 and 9. The late phase of folding, however, appears to be the result of quite a different process, although the vergence of the structure is consistent with the earlier folding.

While the kinematic interpretation of this late fold structure required an elaborate analysis of the data, it is difficult to envision an alternative folding mechanism. In particular, the conical pattern of lineations strongly suggests a rigid rotation, and can not easily be explained by other processes (e.g., Ramsay, 1967; Lisle, 1974). Flexural flow or flexural slip folding, however, is typically associated with well layered sequences that have well defined slip planes. In this case, while the folded surface may have been parallel to earlier flow planes (Figure 19), there is no apparent layering parallel to these surfaces.

One possible way of generating the late fold might be through heterogeneous simple shear. That is, if the rock were flowing from west to east under horizontal simple shear and strain-rates became lower to the east, perhaps

because of dehydration, then folding might occur as the strain compatibility conditions are met by rotation. This explanation, however, still requires the layering to retain a preferred shear plane, whether a fabric or crystallographic anisotropy.

The recognition of the Grøvudal structure as an antiformally refolded north-facing near-recumbent synform has a number of important implications for the regional geology and tectonics. First, the deformation sequence can clearly be explained as an orderly consequence of the west to east emplacement of the Caledonian nappes. No complex displacement history is required to explain the deformation sequence (cf. Scott, 1967; Wheeler, 1973). Secondly, the peculiar trumpet-shaped outcrop pattern of the entire Grøvudal structure (Holtedahl and Dons, 1960; Krill, in press; Figure 4) can be explained as a large, nearly recumbent sheath fold, generally plunging to the east, which has been folded into an east-verging asymmetric antiform. The present form of the Grøvudal fold-nappe is thus due to the interference of the two fold phases, resulting in a type 2 interference pattern of Ramsay (1967). The interference pattern is particularly difficult to see in map pattern because the axial plane traces of the two fold phases are at low angles.

The southern fold closure in the Grøvudal area now plunges to the south-southeast beneath the basement

gneisses (Figure 4), so that the present structure is anti-formal rather than synformal. While it is difficult to accurately extrapolate in such noncylindrically folded rocks, this suggests a below-surface connection with Blåhø exposures to the south. In this interpretation, then, the entire Lønset dome area of basement gneisses must be allochthonous, forming an extensive sheath-like fold-nappe overlying the Blåhø and other cover nappes. Thus, the outcrop areas of cover nappes are unlikely to be simple infolded synclines (c.f., Krill, in press), and are more likely to represent early recumbent structures exposed by later folding.

This also explains the extreme strain gradient observed between outcrops exposed east of the Lønset area and those of the Grøvudal area. That is, outcrops of the Sætra nappe showing primary layering, cross-bedding and cross-cutting dikes occur east of the Lønset nappe (Chapter 2); correlative amphibolite-banded psammites of the Grøvudal area lie structurally below the nappe, and have been completely transposed by high shear strains (Section 5.2).

This sheath-nappe interpretation may be extended to the north, implying that the basement gneisses of the Trollheimen range form an extensive fold-nappe carried to the east over cover nappes. This can be visualized by viewing figure 4 down-plunge from west to east. Two major antiformal sheath fold-nappes then become apparent: the

Trollheimen and Lønset fold-nappes (see figure 21 in Chapter 8 for the geometry of a sheath fold-nappe). These are separated by three major synformal sheath fold-nappes, from north to south: the Surnadal, Grøvudal and Lesja fold-nappes. Later refolding on steeper axial planes has resulted in combined type 2 and 3 fold interference patterns. Further detailed structural analyses will be required to work out the details of these nappes. Such large 'sheath-nappes' have not been generally recognised elsewhere, although they have been suggested to occur in the Canadian Rockies (Mattauer et al., 1983) and the Pennine zone of the Alps (Cobbold, 1979). One final suggestion offered here is that the low velocity zone of Mykkeltveit et al. (1980) represents an extension of these isoclinally infolded cover nappes.

FOLDING IN STEADY FLOW

The structural style of the Western Gneiss Region indicates that the nappe structures are associated with large scale eastward transport of material, and that this movement involved large strains and very ductile behavior. The large scale Pennine-style nappe structures (Muret, 1960; Krill, 1980a), nearly ubiquitous isoclinal folding and transposition are clear evidence for this. In particular, the centimeter-scale interlamination of originally arkosic sandstones and cross-cutting basic dikes in the Sætra Nappe is impressive evidence for large ductile strains. Large strains are also suggested by the strong linear fabric, and by the parallelism of this fabric with fold axes (section 6.4). The apparent annealing of nappe contacts, protomylonitic textures, and high temperatures (Chapter 5 and section 8.3) argue for very ductile behavior of the rocks during deformation. Of particular interest, in terms of folding behavior, is the presence of sheath folds (Figure 8; Hansen, 1967, p. 78-80; Krill, 1980b). This style of fold is common in zones of high shear (Minnigh, 1979 and references therein), and Cobbold and Quinquis (1980) have experimentally produced sheath folds in a layered silicon putty subjected to simple shears of about 10 to 30.

Simple shear is probably a reasonable, if oversimpli-

fied, model for a deformation history of the Dovrefjell nappes. This is the simplest type of deformation that could explain the large horizontal displacements and the strong lineation. A large component of simple shear would also be expected in an orogeny involving large horizontal displacements as is suggested by the regional geology (Chapter 3).

8.1 Passive Folding in Simple Shear

In order to test whether the first-order geometric characteristics of the folded nappes in the Dovrefjell could have been produced by a deformation history approximating simple shear, a series of deformation experiments were done by computer simulation. The folding simulated in these experiments was purely passive, the layering acting only to mark relative positions. The material itself is assumed to be homogenous and isotropic. To produce folding an initially perturbed, or non-planar, surface was defined and subjected to varying amounts of rotation and strain. These transformations were accomplished by defining the coordinates of 2048 to 8192 points on the initial surface, and subjecting these to displacements described by transformation equations. The results were displayed as a distorted grid using a three-dimensional plotting package, MNCORE, on a CYBER 845, and a Varian Statos 42 electrostatic paper plotter. The MNCORE graphics package is a

University of Minnesota Computer Center library routine that is designed to be largely machine independent. The fortran program used for this, SHEATH, is given in Appendix B.

Most of the plots for the experiments were orthographic projections. However, a number of perspective projections were done of several plots using different view points, allowing stereoscopic viewing with a standard stereoscope. Several of these are shown in Plate 3. Cross-sections in various orientations were obtained by specifying extremely narrow clipping planes, so that only an essentially two-dimensional plane within the figure would be viewed. For these plots the grid lines were more closely spaced (twice as many in the x direction and four times as many in the z direction); and three or five parallel surfaces were defined to simulate layering. This gives a figure defined by closely spaced dashes that represent the intersection of the grids with the cross-section plane. These plots were then traced and alternating layers colored.

The initial surface was defined as a double sine surface, giving an undulose dome and basin topography. The equation:

$$y = 0.06283\ (\cos x + \cos z)$$

was used for this with z ranging from $-\pi$ to π. The range of x depended on the experiment, for most cases $\pm 2\pi$ or $\pm 8\pi$

was sufficient, although larger values were used when generating cross-sections. This choice of coordinate scaling gives a surface topography symmetric about the origin, thus simplifying the equations for ensuing rotations and shear (Figure 20). The coefficient used here gives a maximum amplitude to wavelength ratio of 1:50, or a maximum surface dip of about 3.6°.

Before discussing the experiments some justification for the choice of the initial state is required. The initial form of the perturbations was chosen to simulate an unspecified irregularity in the surface. This irregularity could be a relict sedimentary structure, such as a ripple or channel, a larger feature due to topographic relief on an erosional surface, or a deformational feature such as a boudin or buckle fold. Such perturbations are assumed to die out in all directions, that is, it is assumed that all irregularities have finite dimensions. The idealization of such features as sine waves will increase the symmetry of the resulting forms, but should not alter their basic character.

The amplitude to wavelength ratio of 1:50 is considered to be sufficiently low to represent a wide variety of such

Figure 20. Surface contours of the initial irregularity, or perturbation, in the passive fold model. In the model the surface is scaled so the maximum amplitude/wavelength ratio is 1/50. Dashed line outlines ¼ waveform used for calculation of orientation data.

$Y = \cos X + \cos Z$

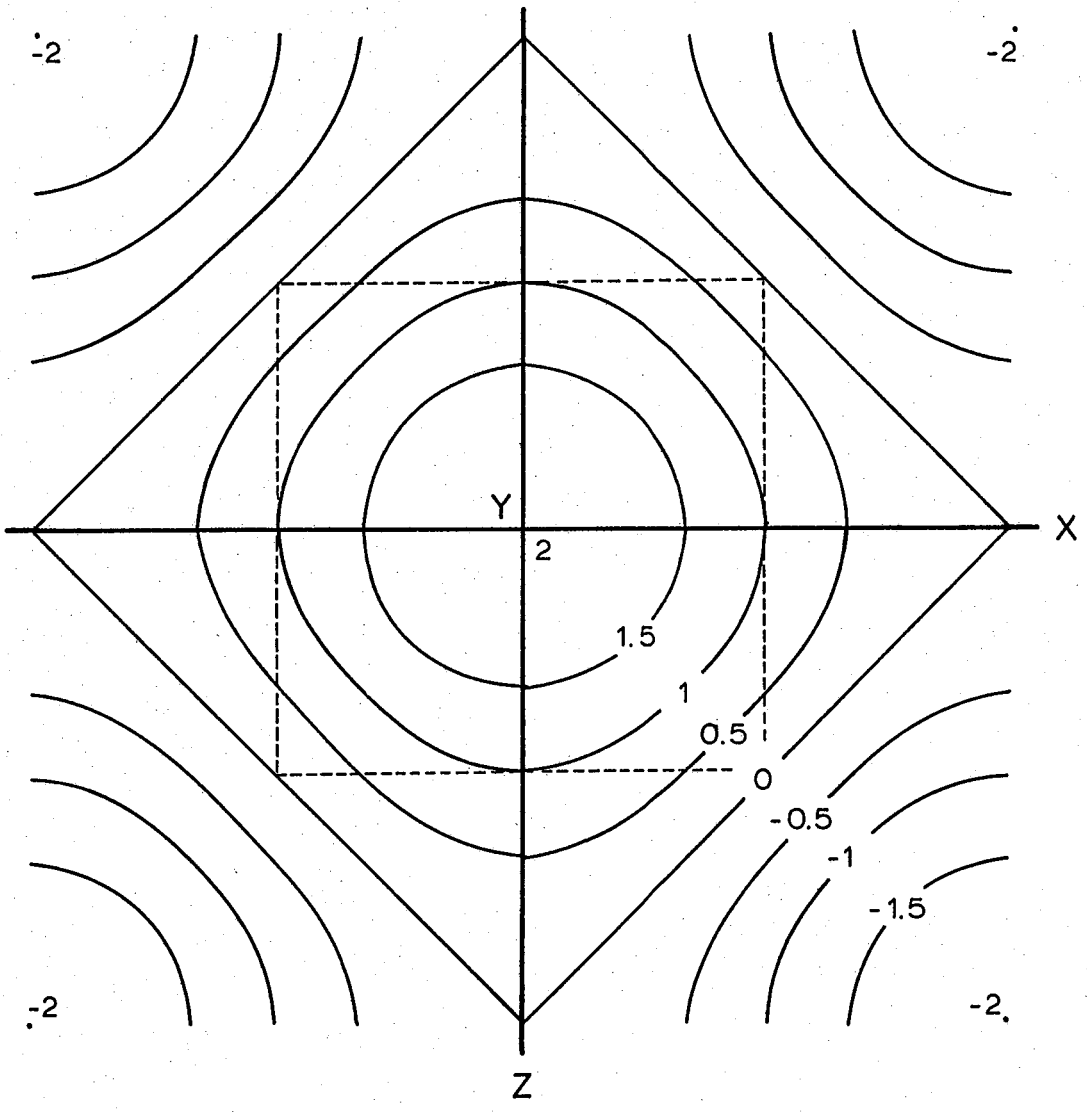

perturbations; primary and secondary structures of this amplitude appear common in most geologic formations. Discussion of the imposed rotations is left to the following section where it is shown that the imposed sequence can be explained as a progressive change in boundary conditions. It should be noted, however, that the sense of rotation causes the original foliation plane to move into the shortening field; thus any viscosity contrasts between layers should lead to buckling. This then would cause active amplification of irregularities (e.g. Smith, 1975) in addition to the purely passive amplification described here.

This initial surface was then rotated about the z axis using the transformation:

$$\begin{bmatrix} x' \\ y' \end{bmatrix} = \begin{bmatrix} \cos\theta & \sin\theta \\ -\sin\theta & \cos\theta \end{bmatrix} \begin{bmatrix} x \\ y \end{bmatrix}$$

A rotation of 2° was used for most of the experiments. A simple shear was then applied using the transformation:

$$\begin{bmatrix} x' \\ y' \end{bmatrix} = \begin{bmatrix} 1 & g \\ 0 & 1 \end{bmatrix} \begin{bmatrix} x \\ y \end{bmatrix}$$

where g, the shear strain, was varied from 1 to 1000.

A final heterogeneous simple shear was added in some of the experiments to simulate a late phase of folding. This

involved a rotation of 20°, followed by the superposition of a half-wavelength sine curve and a corresponding constant y value at values greater than or less than the peak sine wave values:

$$\begin{aligned} y' &= y + \sin(2x) && \pi/4 > x > -\pi/4 \\ y' &= y + 1 && x > \pi/4 \\ y' &= y - 1 && x < -\pi/4 \end{aligned}$$

This gives a heterogeneous shear at 90° to the plane of simple shear, simulating an asymmetic fold (Figure 21D).

The final geometric forms of these deformed surfaces were further analyzed by calculating the surface normals at specified intervals using the FORTRAN program SHEAROR (Appendix B) and plotting these on stereographic nets. This allows the plots to be visualized in a form equivalent to stereographs of S-surface normals, as used in standard structural analysis. For this purpose 8192 grid intersection points on the range $x = \pm\pi/2$, $z = \pm\pi/2$ (one quarter waveform; figure 20) were used. These points were more closely spaced in the x direction, as the surface form changes most rapidly in this direction.

For each grid point the components of two vectors were calculated. The vectors were defined by the grid point and two closest neighboring points. The cross product of these two vectors then gives a surface normal:

$$N = V_1 \times V_2 = \begin{vmatrix} i & j & k \\ x_1 & y_1 & z_1 \\ x_2 & y_2 & z_2 \end{vmatrix}$$

This was then converted to direction cosines:

$$l = (y_1z_2 - y_2z_1)/ N$$
$$m = (z_1x_2 - z_2x_1)/ N$$
$$n = (x_1y_2 - x_2y_1)/ N$$

converted to plunges, δ, and trends, θ, where:

$$\delta = \sin^{-1} n$$
$$\theta = \tan^{-1} (l/m)$$

and plotted on stereonets using the STGRAPH program (Appendix B).

Figure 21 shows the results of applying progressive simple shears of g = 10 and 20 on an initial surface with a maximum amplitude/wavelength ration of 1:50, and an initial rotation of 2°. At g = 10 asymmetric folds with strongly curved hinge lines are well developed. At g = 20 the folds are strongly overturned and form pocket-like projections. The final state in this sequence results from a rotation of 20° followed by a heterogeneous simple shear in a sense conjugate to that of the simple shear plane. Figure 22 shows the effects of increased shear on the initial perturbation. These results are also given in Plate 3 as stereo-pairs for three-dimensional viewing.

From these experiments it is clear that sheath folds

are readily generated from small amplitude perturbations subjected to large shear strains. Under these conditions any small undulation in the surface subjected to shear becomes strongly amplified. Additionally, the lines of maximum curvature on the surface, i.e., the fold hinge lines, progressively rotate into the shear direction. Passive rotation of hinge lines under conditions of simple shear has been suggested by a number of authors to account for the apparent parallelism of fold axes with stretching lineations (e.g., Escher and Watterson, 1974; Williams, 1978; Bell, 1978), and a similar effect is shown here. It should be noted, however, that fold hinge lines here are not passive markers or material lines, as they are defined by the locus of points of maximum curvature on a passively deforming surface. Initially the fold hinge lines are defined only as points at the sine wave maxima. With increasing strain anticlinal hinge lines migrate slightly forward in the surface (toward the shear direction), and then back toward the fold crest.

Cobbold and Quinquis (1980) have done similar shear

Figure 21. Passive fold model for a simple shear of 0, 10, 20, and a refolding in heterogeneous simple shear. The initial perterbed surface (Figure 20) is rotated 2° into the shear direction before the simple shear is imposed.

Figure 22. Passive fold model for a simple shear of 30, 40, 60, and 100. The initial state is the same as that for figure 22.

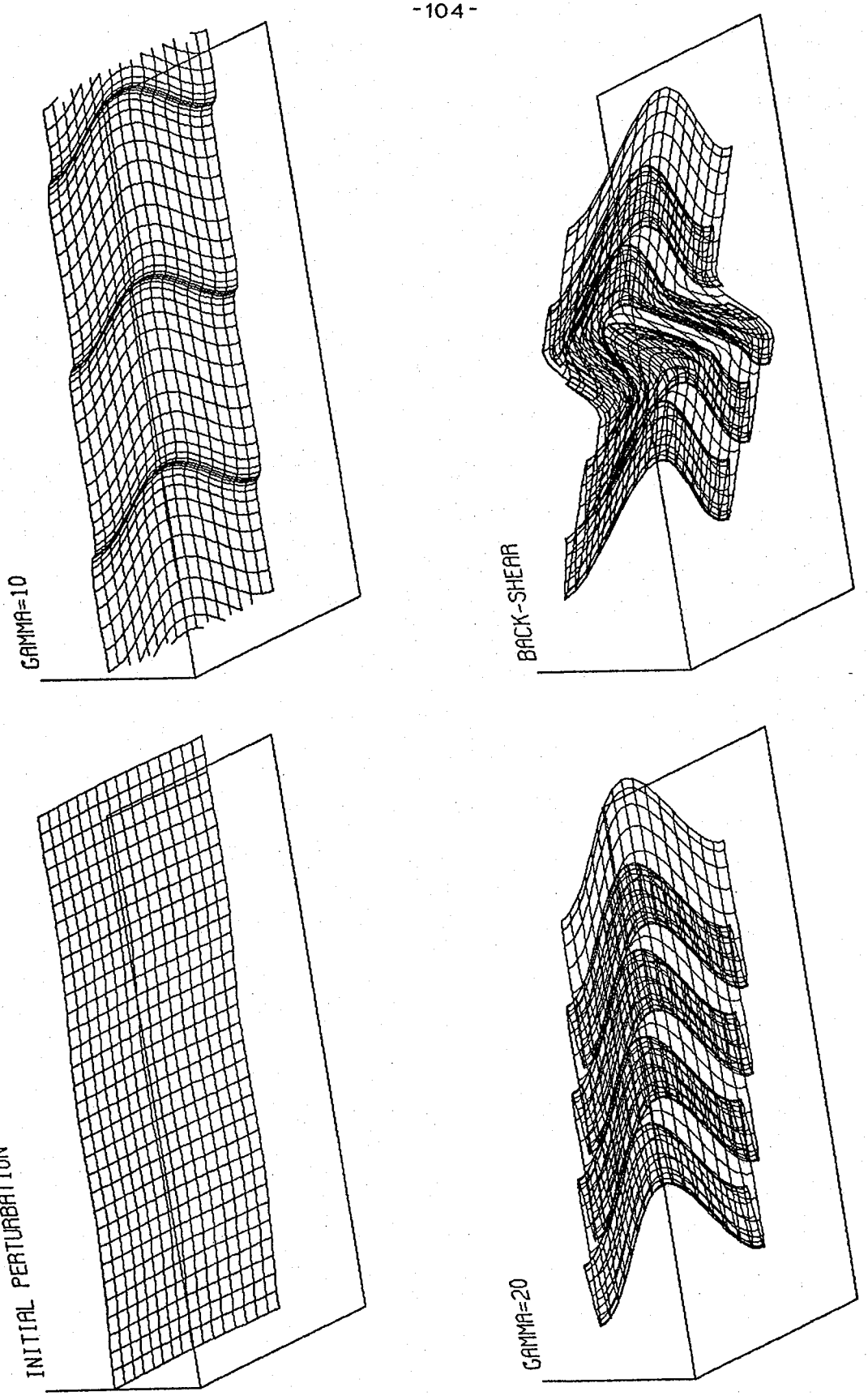
INITIAL PERTURBATION
GAMMA=10
BACK-SHEAR
GAMMA=20

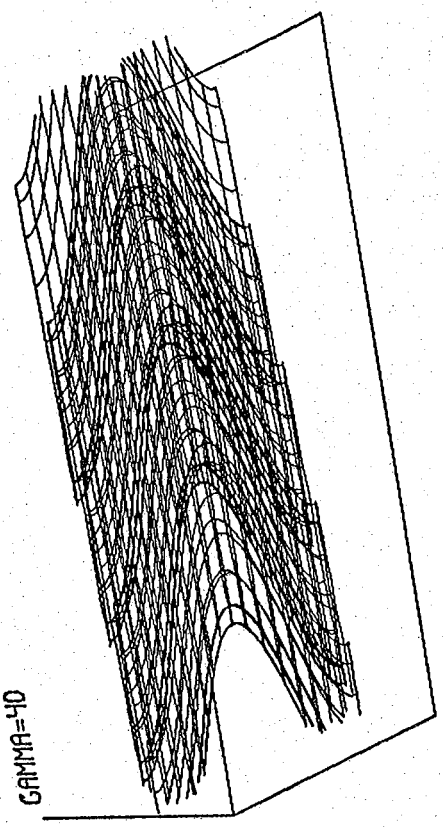
GAMMA=40

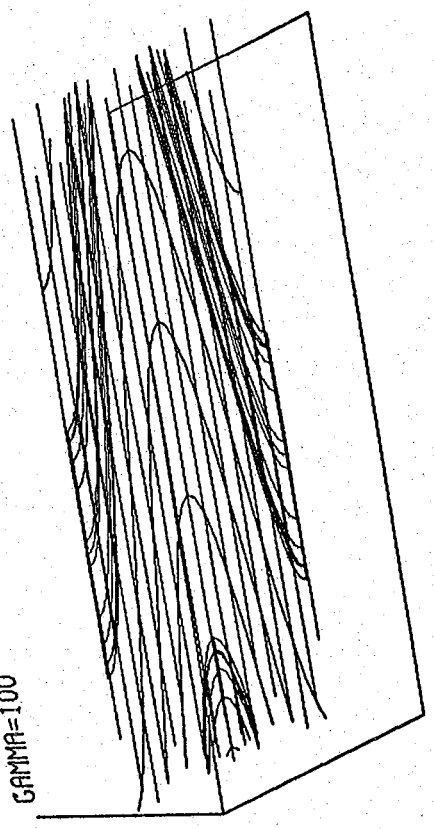
GAMMA=100

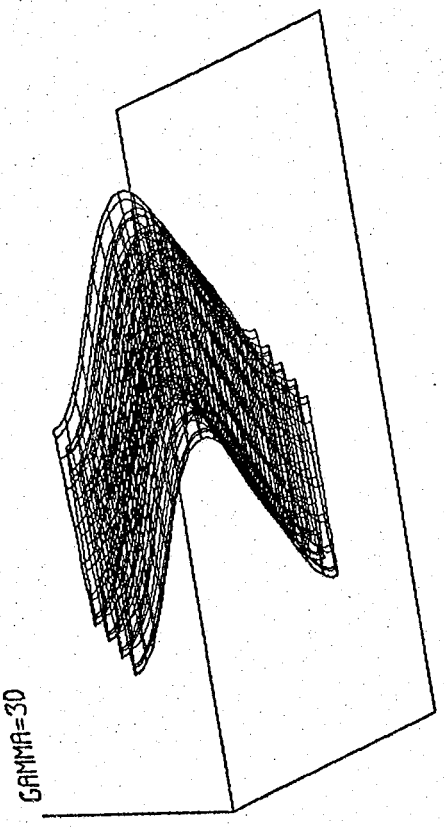
GAMMA=30

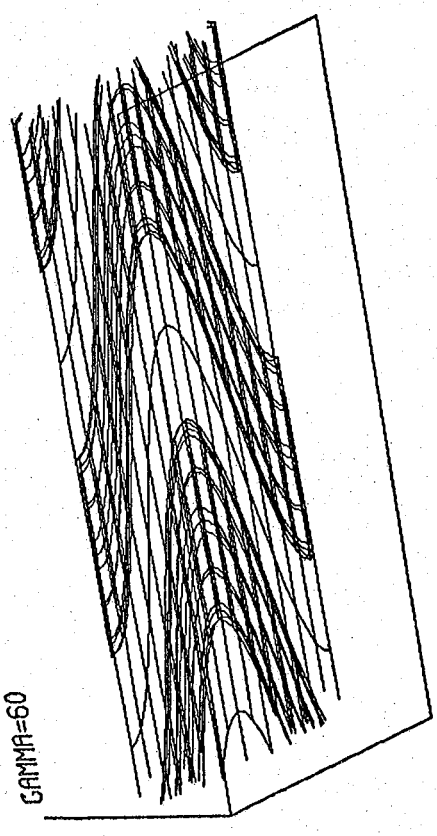
GAMMA=60

experiments on models composed of layered silicon putty and Plasticine. Initial irregularities were imposed on the layering, and shear strains up to 30 were applied parallel to the layering. This resulted in strong sheath-like forms similar to those of the present experiments.

Once the folds form they become more strongly flattened and stretched, with the hinge lines moving closely towards parallelism with the shear direction as the strain is increased. If a secondary perturbation were then introduced into the new foliation plane defined by the strongly flattened isoclines, a second set of folds would overprint the first. If perturbations can be successively introduced, this gives a mechanism for repeated refolding, flattening and transposition. Such a process could well explain, for example, the finely interlaminated dikes and arkose of the Sætra Nappe.

This additionally suggests that the folds may show overprinting and style characteristics that are only indicative of local fold development, rather than regional phases. That is, the tightness or style of a particular fold may reflect only the strain since its initiation. Since such initial perturbations may be small, they are likely to be initiated by relatively random fluctuations in the deformation history. Therefore regional correlation of folds by tightness or height to width ratios (e.g., Hansen, 1971) is unlikely to be successful (see also Williams,

1970).

Figures 23 and 24 are a series of vertical cross-sections through the shear experiments. Five parallel layers were deformed in the experiment to simulate layering. The geometrical resemblence of figure 24 to sheath folds observed in outcrop (figure 8) is striking, and the orientation of hinge lines is similarly steeply into the page. Figure 25 shows sub-horizontal sections, or map views, through the refolded (back-shear) model. The section dips 15° in a direction perpendicular to the shear, to simulate a map view of a north plunging fold pair.

The most notable features of figure 25 are the narrow, elongate fingers and discontinuous bands of lithologies.

Figure 23. Vertical cross-sections through the passive fold model parallel to the shear direction for simple shears of 0, 10, 20, and 30. Five parallel surfaces were simultaneously deformed to simulate layering. Length of the sections is 14 units.

Figure 24. Vertical cross-sections through the passive fold model perpendicular to the shear direction for a simple shear of 20. Five parallel surfaces were simultaneously deformed to simulate layering. Compare to figure 8c. The width of the sections is 2π units; the spacing of the sections is 0.5 units.

Figure 25. Sub-horizontal section through the refolded passive fold model of figure 21. Three parallel surfaces were simultaneously deformed to simulate layering. The cross-section plane dips 15° to the south (down), effectively making the late fold plunge north 15°. The narrow isolated fingers are believed to be analogous to those observed in the Grøvudal area (Figure 6). Length of the sections is 14 units, and spacing of the sections is 0.5 units. Sense of shear is above page to right.

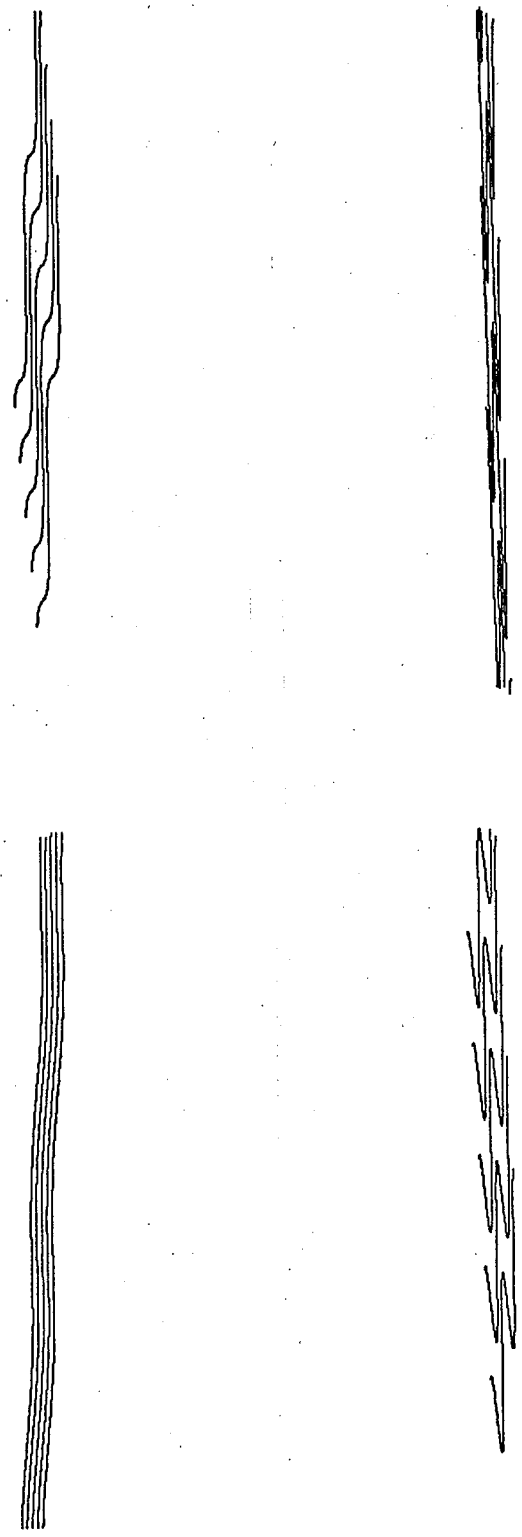

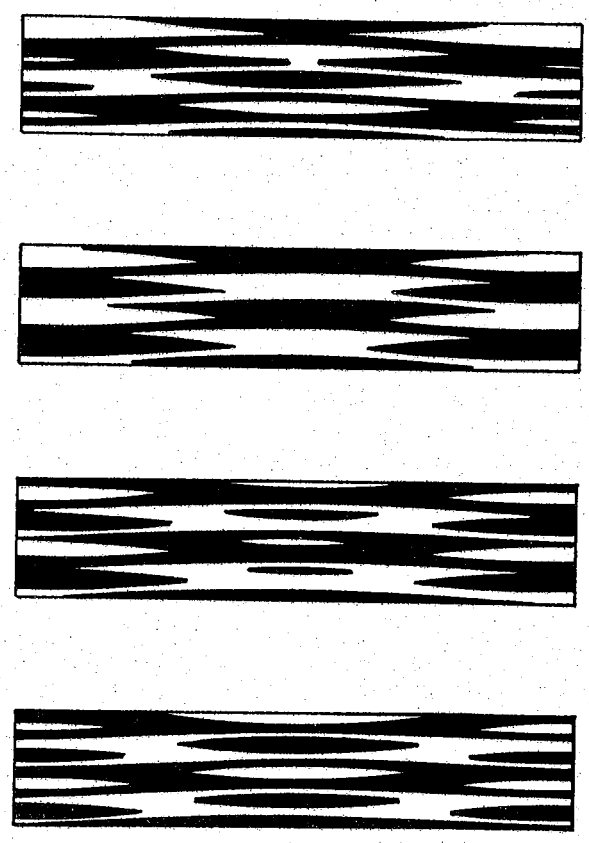

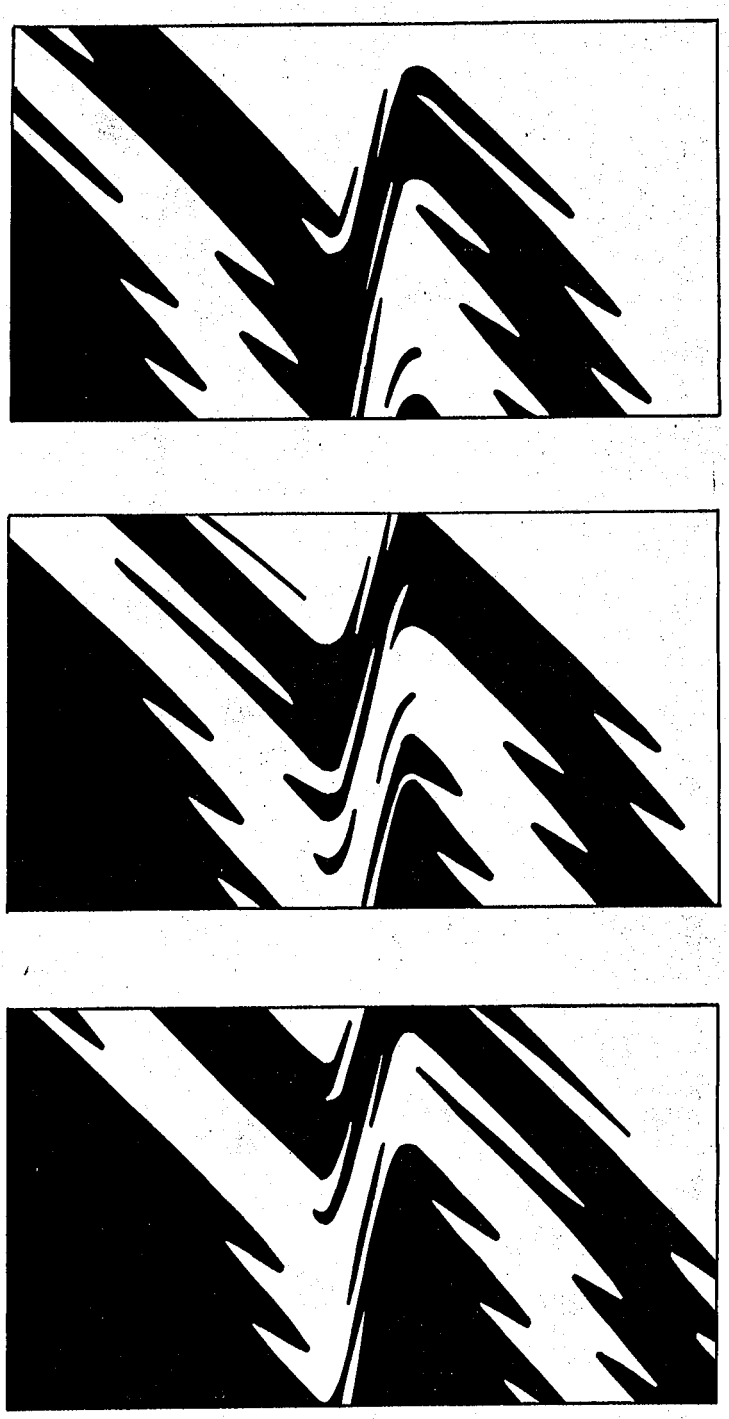

These bands are isoclines plunging into the section at their terminations. Narrow bands like these are characteristic of the Dovrefjell map patterns. Four major ones occur in the Grøvudal area (Figure 6, Plate 1), and they appear common in the district as a whole (Figure 4). In the Amotsdal arkose finger of the northeast portion of the Grøvudal area (Figure 6, Plate 1) the termination of one such finger can be observed. Here there is complex interlayering and folding, suggestive of an isoclinal hinge region. Similarly, in the Trollheimen area at the summit of Blåhø there is an excellent exposure of the termination of an arkosic "thumb." Here again the folding is intense and spectacular (Hansen, 1971) suggesting strong folding in the hinge region of an isocline.

The Z-like outcrop of Amotsdal psammite in the central portion of the Grøvudal map area (Figure 6) gives confirmation of the sheath-like form of these infolds, as this forms a tongue plunging to the east-northeast. The Z shape is due to the topographic effect as the psammite cuts through the mountain-side of Høgtunga (Plate 1). This suggests that these narrow fingers are isoclines, rather than thrust slivers, and that their origin can be accounted for by this model.

Figure 26 shows stereographs of 8192 poles to foliations at various stages of shear, calculated using the SHEAROR program (Appendix B). On these plots the shear

plane is horizontal and the shear direction is to the right. The plots clearly show the progression towards a girdle pattern with higher shear strains, corresponding to a progressive reorientation of hinge lines towards the shear direction. A strong girdle pattern, however, does not develop until shear strains of approximately 60 are reached. Therefore, if this model is an appropriate one to explain the early folding phase in the Dovrefjell, very large strains would seem to be required to get the observed strong girdle patterns (Appendix A). A shear strain of 60, for example, would require 60 kilometers of displacement over a one kilometer thickness of rock. While local strains of this magnitude may not be unreasonable, it seems unlikely that the entire thickness of the nappe pile could have been subjected to this magnitude of strain.

Two possible explanations for this discrepancy are that the initial amplitudes of the model are too low, and that active folding of layers has not been considered. The maximum initial amplitude to wavelength ratio was chosen as 1:50, which corresponds to a maximum surface dip of about 3.6°. This was chosen as a reasonably low value for common primary structures. While it might be reasonable to use maximum dips as high as 10°, the probability of such larger

Figure 26. Equal-area stereogram of poles to layering for the passive fold model, shown for simple shears of 20, 40, 60, and 100.

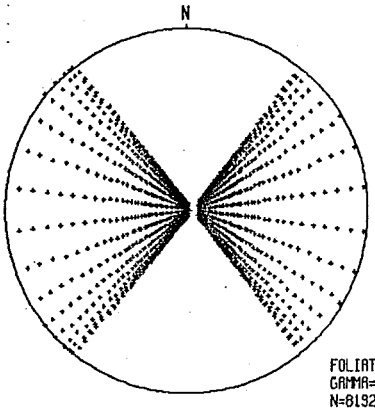

FOLIATIONS
GAMMA=20
N=8192

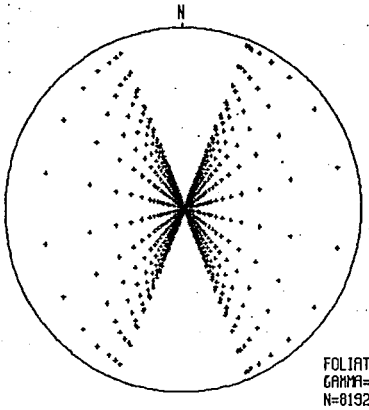

FOLIATIONS
GAMMA=40
N=8192

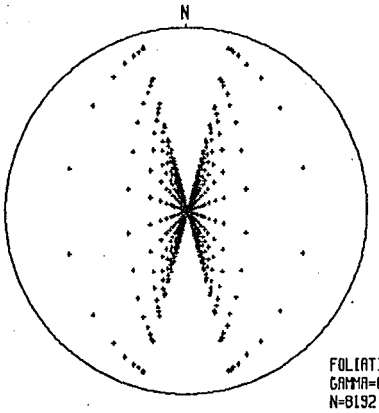

FOLIATIONS
GAMMA=60
N=8192

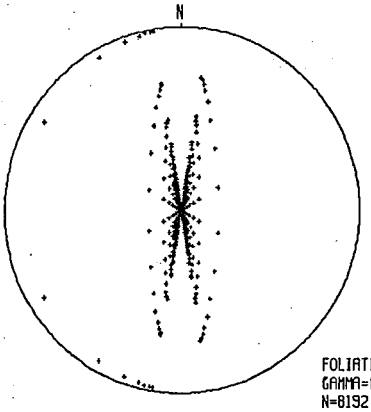

FOLIATIONS
GAMMA=100
N=8192

perturbations becomes somewhat more questionable. Although the angle of repose for loose sediments is about 30°, the most common structures with such large surface dips are folds. If such folds exist, they will be amplified, however we are then faced with the problem of their generation. We therefore become concerned with the active generation of folds, which is the subject of the next section.

In summary, the passive folding model demonstrates that relatively small amplitude irregularities, which should be common as primary structures in rocks, will be strongly amplified under large shear strains. At a larger scale such irregularities might be present as topographic variations along depositional surfaces or unconformities, such as the Åmotsdal-Lønset contact. New perturbations can also be intruduced during deformation by common structural processes, although these can not be generated in a purely passive model. The form of the final fold shapes after a simple shear deformation is strongly sheath-like. With the superimposition of secondary folding, maps and cross-sections through the models display geometric features similar to those observed in map and outcrop patterns of the Dovrefjell. The common elongate "fingers" observed in map pattern are thus believed to be sheath-like isoclines, rather than thrust slices. As only small perturbations are required to initiate folding, it is argued that fold gener-

ation will occur in response to local conditions. This implies that folds of different tightness or amplitude would be expected in association with a single deformation. Additionally, if perturbations are introduced during the deformation overprinting and multiple fold generations should be common.

Style groups based on tightness, height to width ratios, refolding, or presence of an axial plane foliation are likely to represent local histories and are therefore unlikely to be regionally correlative. This would also explain the general coaxiality of the style groups defined in the Trollheimen-Dovrefjell area by other workers (Hansen, 1963, 1971; Scott, 1967; Wheeler, 1973; see also Krill, 1980b).

8.2 Active Folding in Simple Shear

The previous section considered only the effects of passive amplification of irregularities to form folds during simple shear. The main problem that arises from this approach is that a strong parallelism of fold axes with the shear direction is not reached until very high shear strains, on the order of 60. While this may not be a problem if larger initial perturbations are allowed, there is still some point at which folds seem to be required to produce folds, a rather unsatisfactory explanation. Perhaps a more critical point is that, while the passive model

can generate folds from initial primary irregularities, there is no provision for the introduction of secondary perturbations.

Hudleston (1976) has shown how passive folds may develop in flowing ice due to a change in boundary conditions. If flow is initially non-planar, for example in ice flowing over a bedrock irregularity, then a change in flow lines will cause folding of layering formed parallel to the original flow lines. Ablation or accumulation rate changes will cause a change in the flow lines; a similar condition might be found in flowing rock with the addition or loss of overlying material. This is a simple way of forming passive folds, and may be quite important in high grade rocks such as those of the Dovrefjell. Cobbold and Quinquis (1980) and Platt (1983) have discussed several other ways of initiating folds in flowing rocks, including the development of perturbations during boudinage. In this section we will consider only the formation of folds by active buckling in ideal simple shear. In particular, the objective is to demonstrate that fold axes will tend to form in orientations such that they easily rotate into the shear direction.

Throughout this section the standard convention (e.g., Skjernaa, 1980) for simple shear axes will be used. The shear plane is the ab plane, a is the shear direction and c is the normal to the shear plane. All diagrams are con-

structed so that planes above the page are sheared to the right with respect to planes below the page. X, Y and Z are respectively the maximum, intermediate and least principal strain or strain-rate axes.

A number of authors have approached the problem of the parallelism of fold hinge lines with a stretching lineation or shear direction by assuming passive rotation in simple shear (Escher and Watterson, 1974; Williams, 1978; Skjernaa, 1980). The general assumption is that buckle folds initiate with hinge lines near the b = Y direction, and progressively rotate towards a = X. Figure 27 shows this relationship for two passive fold hinges plunging 10 and 20° towards Y, the intermediate strain axis. After a simple shear of g = 10 the axes have been strongly reoriented, and at g = 20 the axes are within 16° of the a direction. An important point to also note here is that the principal strain axis, X, becomes within a few degrees of the shear direction, a, at shear strains greater than 10. Williams (1978) and Vollmer and Bosworth (1984) have good field evidence suggesting that a similar process occurs in nature, showing the reorientation of fold hinge lines through approximately 90° with increasing strain near

Figure 27. Passive rotation of two linear features with inital plunges of 10 and 20° towards Y after simple shears of 5, 10, and 20. The orientations of the X and Z finite strain axes are also shown.

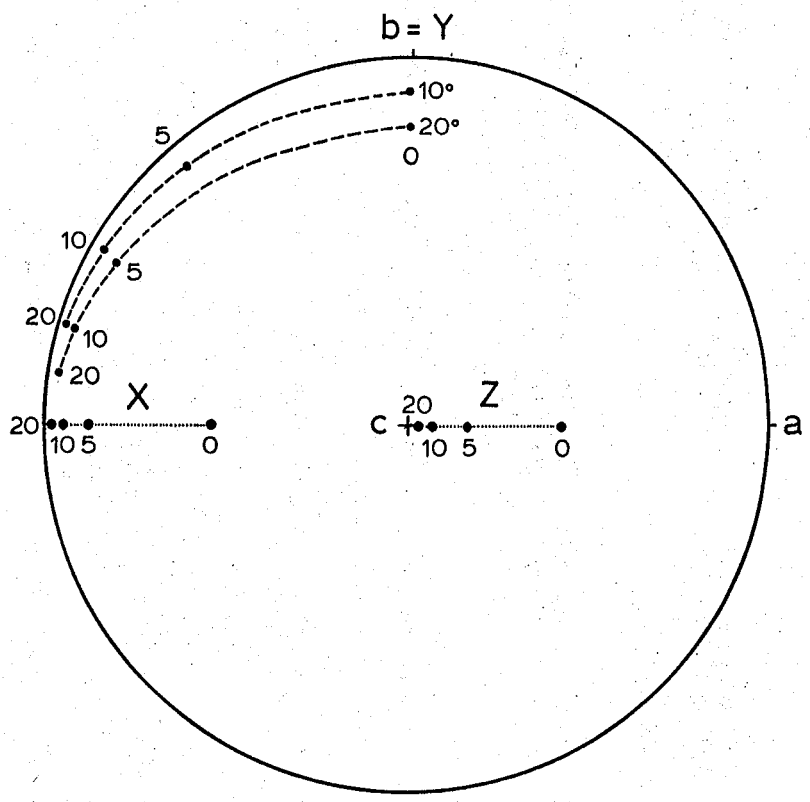

Passive rotation in simple shear

γ = 0 to 20

major overthrusts.

In ideal simple shear, however, fold axes forming exactly parallel to the Y axis would not be expected to rotate at all, and considerable variation of initial fold axes would be required to produce a strong reorientation at reasonable strains, of perhaps 10 to 20. Sanderson (1973) approached this problem in the pure shear case by considering an initial normal frequency distribution of fold axes about the Y strain axis, in the XY plane. For a pure shear of $X/Y > 5$ the distribution becomes strongly clustered about the X axis. For example, a normal distribution with a standard deviation of 10° about the Y axis will have a frequency distribution with two strong maxima at about 10° to X after a strain of $X/Y = 20$. This distribution includes a sampling factor calculated by Sanderson (1973) to take into account the variable elongation of lines of different orientations. Although not directly applicable to simple shear strain paths, it is clear that in shearing a normal-type distribution of axes, outlying orientations would rotate quickly into the shear direction (e.g., figure 27) forming maxima near X (for comparison, $g = 20$ gives $X/Y = 20.05$).

What has not been considered in these treatments, however, are the probable orientations of developing buckle folds in simple shear. The rotation model of Escher and Watterson (1974), for example, assumes fold formation with

axes near the b = Y direction without further analysis. In general we can assume that buckle folds will develop perpendicular to the maximum shortening direction in a given layer at the instant of formation (e.g., Treagus and Treagus, 1981), and that fold amplification will depend on the two-dimensional state of strain perpendicular to the fold axis (e.g., Hudleston, 1973). The main problem encountered here is that while fairly good theoretical relationships exist for the buckling of layers oriented parallel to principal strains (e.g., Biot, 1961; Sherwin and Chapple, 1968; Smith, 1977), none have been derived for the more complex case of layers inclined to strain axes (although, see Treagus, 1973, and criticism of Smith, 1975). We will, then, here consider two qualititative models that predict the orientations of developing folds in simple shear; one where the strain-rate or state of infinitesemal strain controls the orientation of fold axes, and one in which the orientations of fold axes are functions of the cumulative state of strain.

For a state of infinitesimal strain we can write (e.g., Jaeger, 1969, p. 48):

$$e = l_i l_j e_{ij}$$

or for principal strains:

$$e = l^2 e_1 + m^2 e_2 + n^2 e_3$$

where e_1 are principal elongations and l, m, and n are the direction cosines of the line with the X, Y and Z strain axes respectively. By differentiating with respect to time we may write:

$$\epsilon = l^2\epsilon_1 + m^2\epsilon_2 + n^2\epsilon_3$$

where ϵ_1 are the principal strain-rates, and l, m and n now refer the line to strain-rate axes. For conditions of plane strain and constant volume we impose the conditions:

$$\epsilon_2 = 0$$
$$\epsilon_1 + \epsilon_2 + \epsilon_3 = 0$$

so that:

$$\epsilon_1 = -\epsilon_3$$

therefore:

$$\epsilon = \epsilon_1 (l^2 - n^2)$$

or, if we normalize to ϵ_1:

$$\epsilon/\epsilon_1 = (l^2 - n^2)$$

Figure 28 is a contoured stereograph illustrating this relationship for simple shear (or any other plane strain). In this case the line of maximum elongation rate, where $\epsilon/\epsilon_1 = 1$, is at X; and the line of minimum elongation rate or maximum shortening rate is at Z, where $\epsilon/\epsilon_1 = -1$. Lines

of zero strain-rate lie within the horizontal ab plane, and within the vertical bc plane. Any plane, plotted as a great circle on this net, will contain one line of maximum elongation rate perpendicular to a line of maximum shortening rate (see Flinn, 1962, for related calculations).

We now make two assumptions. First, that if buckling occurs, it will occur in a direction perpendicular to the maximum shortening rate in that layer; and second, that the probability of buckling is related to the ratio of the maximum layer shortening rate to the shortening rate normal to the layer. That is, if buckling is to occur, extension perpendicular to the layer must be sufficient to accommodate buckling; if a layer is flattened faster than it is shortened no buckling will occur. The first assumption seems reasonable, as buckling is a direct response to layer shortening. The second assumption here is based on infinitesemal buckling theory, which suggests the growth rate of buckle folds is dependent on the two-dimensional state of strain perpendicular to the fold hinge line rather than on the layer shortening alone (e.g., Hudleston, 1973). We are thus implicitly assuming that the strain-rate parallel

Figure 28. Equal-area stereogram of strain-rate contours for simple shear (or any similarly oriented plane strain such as pure shear). Contours are normalized to the maximum principal strain rate. The two directions of principal strain-rate for any plane may rapidly be found by plotting the plane (as a great circle) and locating the maximum and minimum values indicated by the contours.

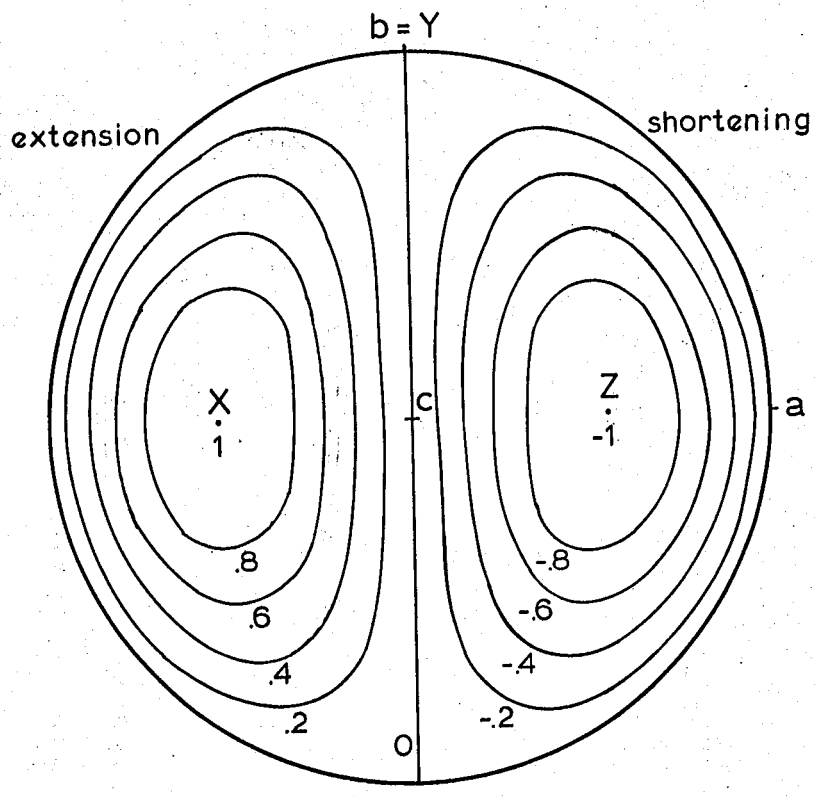

Normalized strain rate, $\dot{\epsilon}/\dot{\epsilon}_1$

to the fold hinge does not strongly effect buckling behavior.

Perhaps the main weakness in the second assumption is that the direction of strain-rate normal to the layer is not a principal one in the plane perpendicular to the fold axis; in general there will be a component of shear strain as well. The effect of layer parallel shear on buckling theory has not been adequately treated, despite the work of Treagus (1973, see criticism by Smith, 1975)). It is suggested that the following results derived from kinematic arguments qualitatively represent the probable orientations of developing fold axes.

Figure 29 is a stereograph giving the orientations of 39 planes dipping at 10, 20 and 30° with variable strikes, and the orientations of the probable fold axes within those planes. The fold axes are calculated as the directions of maximum elongation rate within each layer, perpendicular to the direction of maximum shortening rate. These directions can be found by plotting the planes as great circles; the principal directions within the planes must bisect the

Figure 29. Equal-area stereogram of potential fold axis orientations and normalized differential strain-rate, ϵ_N, calculated for 39 planes dipping at 10, 20, and 30° from the simple shear plane, ab. The normalized differential strain-rate varies from −1 to +1, where negative values have potential for folding. ϵ_{min} is the minimum layer strain-rate, and ϵ_n is the strain-rate perpendicular to the layer. Values of ϵ_N are given for only half of the axes as the figure is symmetrical about the ac plane.

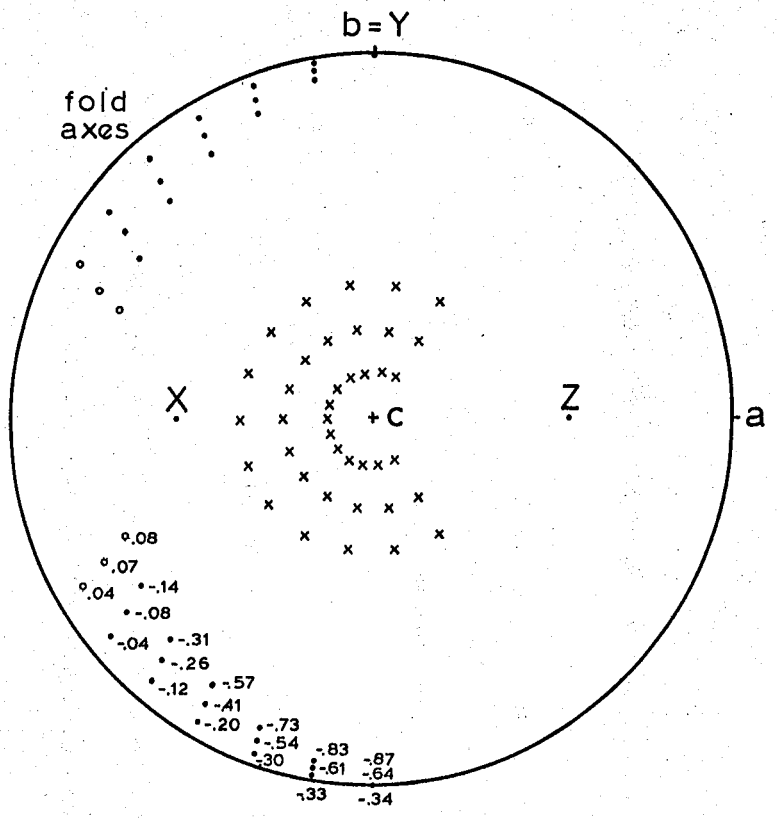

Normalized differential strain rate,

$$\frac{\dot{\epsilon}_{min} - \dot{\epsilon}_n}{\dot{\epsilon}_1 - \dot{\epsilon}_3}$$

lines of no infinitesemal strain-rate, contained within the vertical bc plane and the horizontal ab plane.

For each fold axis an indication of the probability of fold formation, the 'normalized differential strain rate,' ϵ_N, was calculated as:

$$\epsilon_N = \frac{\epsilon_{min} - \epsilon_n}{\epsilon_1 - \epsilon_3}$$

or:

$$\epsilon_N = \tfrac{1}{2} \left[\frac{\epsilon_{min}}{\epsilon_1} - \frac{\epsilon_n}{\epsilon_1} \right]$$

where ϵ_{min} is the minimum layer elongation rate, and ϵ_n is the elongation rate perpendicular to the layer. This gives a range of ϵ_N from +1 to −1. The layer with $\epsilon_N = -1$, then, is the one containing the Y and Z axes (ϵ_2 and ϵ_3), in the best position for fold development. The layer containing the X and Y axes (ϵ_1 and ϵ_2) would correspondingly be in the worst position for folding, with $\epsilon_N = +1$. The case of $\epsilon_N = 0$ corresponds to the cross-over between layer buckling and layer flattening.

It is apparent from Figure 29 that although folds may most easily form parallel to b = Y, these can only form in planes initially containing the b axis. All planes of other orientations will develop fold axes in orientations

closer to the a axis, and with continued shear these will be rotated towards the a direction (e.g., Figure 27). This suggests that during a progressive simple shear active fold development will occur forming axes in many orientations away from the b direction, and therefore that these folds are easily rotated towards the shear direction.

The second case considered here is where fold orientations are related to the state of finite strain within a layer. This is the argument used by Treagus and Treagus (1981), i.e., that a fold hinge will remain perpendicular to the direction of maximum finite shortening within a layer. This assumes that a fold migrates through a layer, rather than acting as a passive marker. This assumption necessarily leads to the conclusion that folding is path independent, as the state of finite strain is; and that the fold reflects the total finite strain rather than the strain increments. Presumably this can only be true in the case of a perfectly elastic layer where stress is proportional to the total strain, and therefore the layer can respond to the stress at any given stage in the deformation. In all other cases the fold becomes at least partially a passive material marker. As deforming material lines, in general, rotate at different rates than finite strain axes, a material line will not remain parallel to any given axis of finite strain. Thus, here we are concerned with the hypothetical opposite end-member from

passive folding, i.e. purely active folding.

In this case we will assume that the maximum shortening within a plane represents a measure of the probability of folding within that layer. A standard measure of finite strain, s, the stretch, is used here:

$$s = l_f/l_i$$

where l_f and l_i are respectively the final and initial lengths of a given line.

Figure 30 is a contoured stereonet of s after a simple shear of 5. This is a graphic solution to the equation for the elongation of lines in simple shear, as given by Skjernaa (1980):

$$1/s^2 = g^2 \sin^2 \delta' + 2g \sin \delta' \cos \delta' \sin \theta' + 1$$

where δ' and θ' are the plunge and trend of a line as measured in the deformed state. The stereonet is simply a projection of a strain ellipsoid, and therefore all great circles are elliptical sections representing the two dimensional strain in a plane. All planes, then, have maximum and minimum values of s at 90° apart.

Figure 31 illustrates the effect of this strain on 39 planes, again initially making angles of 10, 20 and 30°

Figure 30. Equal-area stereogram of finite strain (stretch) contours for a simple shear of 5 (or any plane strain with similar values of X and Z.

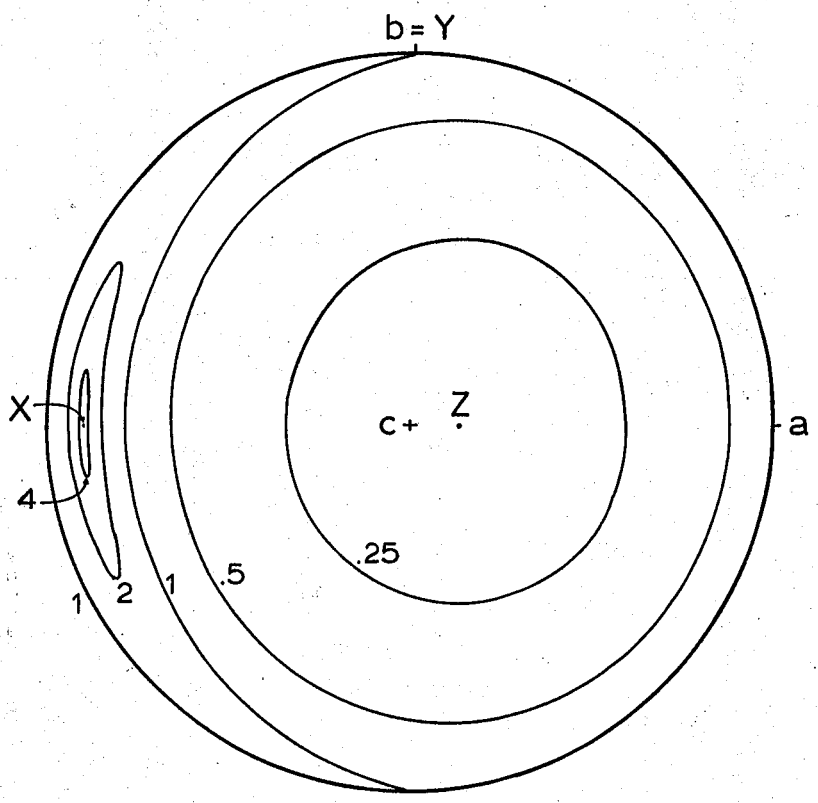

Finite strain ($\sqrt{\lambda}$), $\gamma = 5$

with the shear plane. The normal to each plane after deformation is shown. Also shown is the line perpendicular to the maximum shortening direction in the plane, i.e., the maximum elongation direction, which will be the fold axis. The stretch representing the maximum layer shortening is given for each fold axis.

The orientation of planes after simple shear was found using the equation given by Skjernaa (1980):

$$p' = \tan^{-1} (\tan (p-90) + g|\cos v|) + 90$$

where p and p' are the angles between the given plane and the horizontal shear plane, in the undeformed and deformed states respectively. This is analogous to the dip, but is measured from the positive a direction only, giving a range of 0 to 180°. V is strike of the plane, measured clockwise from b.

The location of the principal axes in these planes was found by first calculating the orientations of the planes of no finite strain. In simple shear one plane of no

Figure 31. Equal-area stereogram of fold axes and finite layer strain in 39 layers initially dipping 10, 20, and 30 degrees from the simple shear plane, ab (see figure 29). The fold axes shown are perpendicular to the directions of maximum shortening within a given layer. The values of maximum layer shortening are given as the stretch perpendicular to the fold axes. The final positions of poles to layering are shown as x's. Values of stretch are only given for half of the diagram because of symmetry about the ac plane.

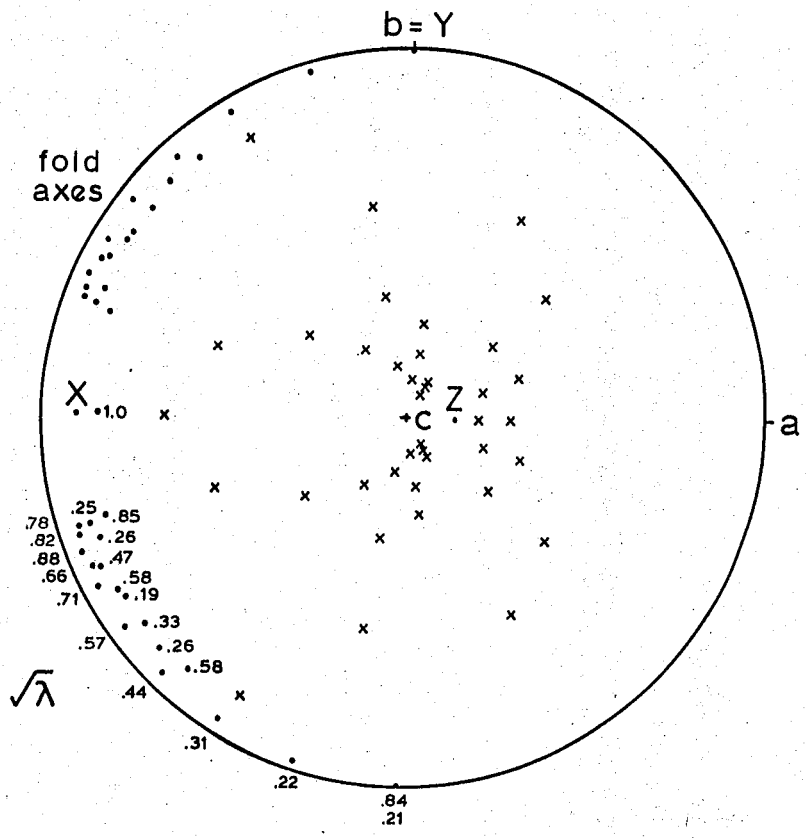

Finite strain, $\gamma = 5$

finite strain is the ab plane, the shear plane. The second plane of no finite strain must contain the b axis, and the two planes are bisected by the X and Y strain axes. The inclinations of the X and Y axes may be found using equations 3.67 and 3.70 of Ramsay (1967):

$$s_2^2,\ s_1^2 = \frac{g^2 + 2 \pm g(g^2 + 4)^{\frac{1}{2}}}{2}$$

$$\tan \theta = g/(1 + g^2 - 1/s_1^2)$$

The second plane of no finite strain can then be located.

Similarly, for each plane the principal axes must bisect the lines of no finite elongation. The axes, then, can be found by plotting each plane in the deformed state and finding the bisectors of the lines of no finite elongation. The elongations of these lines can then be calculated using the equation previously given.

In this example there is a clear tendency for fold axes to be oriented approximately mid-way between the X and Y axes; actually somewhat closer to the X axis. Many of these have stretches significantly less than 0.5, indicating that they have been shortened to less than half of their original length. While other factors, such as the complete three-dimensional state of strain, have not been taken into account, these shortening values should give a reasonable indication of the folding magnitudes.

These two approaches differ in that the strain-rate

model predicts the likelihood of buckle fold initiation at any instant of time, while the finite strain model predicts the orientations of folds after a given amount of strain (active rotation). Both approaches, however, suggest that folds developing in planes inclined at low angles to the shear plane will plunge gently into the -ab-c and -a-b-c quadrants. Thus fold initiation (Figure 29), active rotation (Figure 31) and passive rotation (Figure 27) all contribute towards the formation and movement of fold axes towards the X = a direction. Presumably an individual fold will form and rotate at a rate, and in a path, dependent on its material contrast with the surrounding rock, in some compromise between active and passive behavior.

One final model for folding should be mentioned here, involving differential shear. Coward and Kim (1981) have suggested a model of strain for the rocks of the Moine thrust area involving horizontal simple shear. That is, differential displacement along strike leads to a component of simple shear in a horizontal plane parallel to layering (Figure 32). This leads to a two dimensional finite strain within the layering with a maximum elongation direction at

Figure 32. Two-dimensional layer strain in planes parallel to the bulk simple shear plane, ab. If layering parallel to the shear plane is subjected to shear as a result of variable amounts of displacement parallel to a, layer strains and folding may result with fold axes at less than 45° to a.

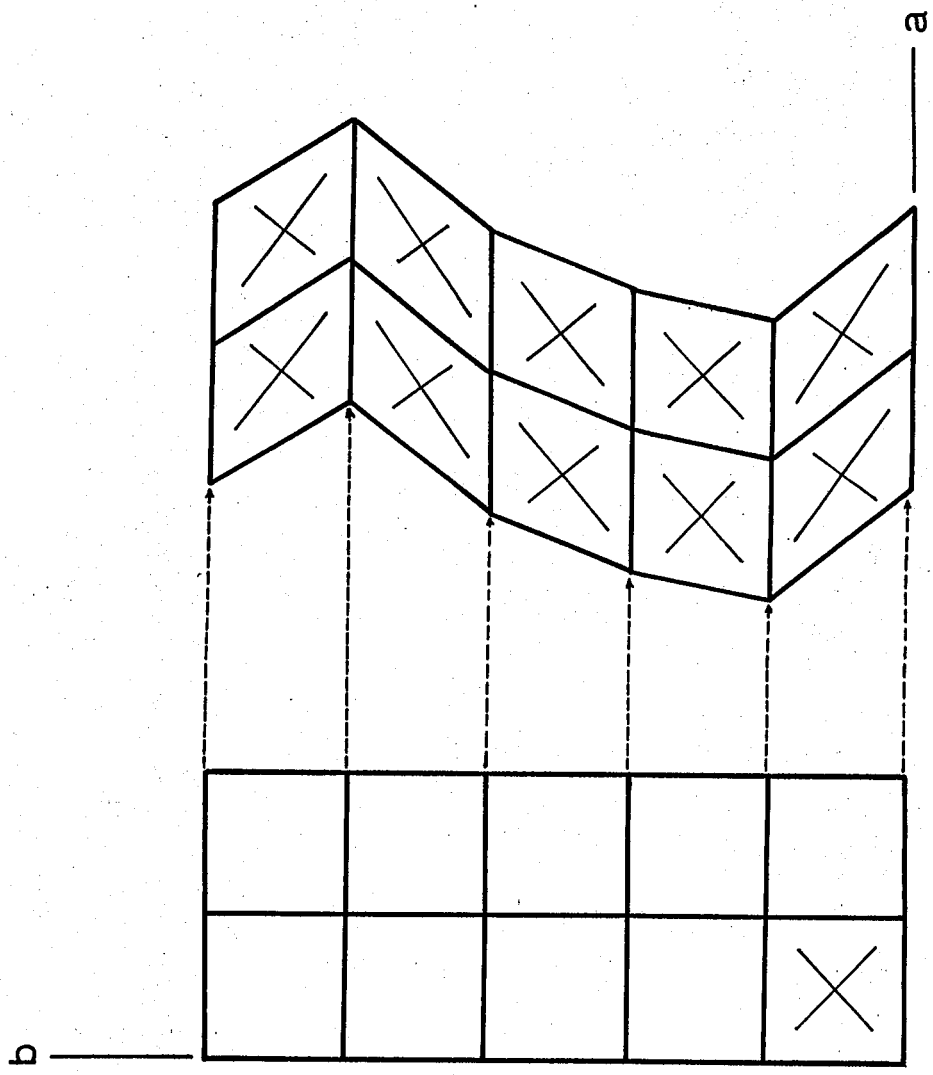
a
b

less than 45° to the displacement direction. In this case then, if the differential movement is large enough folds will be initiated at 45° or less to the displacement direction. This offers an additional mechanism for fold formation in areas where the deformation may be more complex than simple shear alone.

FOLDING IN UNSTEADY FLOW

The preceding chapter on fold development has shown how folds may form in simple shear, and how rotation of fold hinge lines occurs leading to the formation of sheath folds, and to general parallelism of fold axes with the elongation and shear directions. The basic requirements for this type of folding are sufficient ductility, and some deviation of layering from the shear plane. Initial deviation of primary layering from an imposed shear is probably unavoidable, given the heterogeneous nature of sedimentary rocks. In high grade metamorphic rocks, however, there is likely to be a mechanistic relationship between the foliation and the state of finite strain. Under conditions of high strain planar elements are rotated towards the plane of maximum flattening, leading to the formation of a foliation. This process may be aided by chemical diffusion, recrystallization and growth of minerals in the foliation plane.

The generally observed relationship between cleavage and finite strain is that, at least to within the limits of observation, cleavage lies parallel to the principal flattening plane (e.g. Tullis and Wood, 1975, although see Hobbs et al., 1976, p.233-246, and Ghosh, 1982). As the mechanisms of formation are thought to be similar (e.g., Hobbs et al., 1976, p. 252), this relationship is likely to

hold as well for other foliations, such as schistosity and gneissic banding. In transposition foliation the layering is defined by isoclines, again suggesting that it lies parallel to the principal flattening plane. In the northern Dovrefjell this relationship is born out by the presence of flattened augen and pebbles (003265) parallel to the foliation plane.

In simple deformation paths, where strain-rate axes are constant and the vorticity is less than or equal to that of simple shear (Ramsay and Pfiffner, 1982), the finite strain axes are either constant in orientation (coaxial deformation path) or asymtotically approach some constant orientation (noncoaxial deformation path). This implies that a foliation is a stable feature, and will not become folded. Such a foliation may develop under conditions of steady-state flow, even though strain-rate axes may vary spatially. This has been demonstrated for flowing glacier ice by Hudleston and Hooke (1980). If strain-rate axes are allowed to vary through time, however, an old foliation may be placed in a shortening field and become folded.

The following is a simple two-dimensional model of a rock mass flowing under gravity and an induced tectonic stress to demonstrate the general instability of strain-rate axes, and thus the inherent tendency for fold development. The material is assumed to be isotropic and homogeneous. The principal equations used are those of Nye

(1957). A complete derivation is given here, as they are not fully derived in Nye's paper. The equations are not restricted to a specific type of flow law, and the flow law may vary with depth, so that temperature and pressure dependent changes can be accommodated. In the example given here the equations are first solved for a single depth, and strain-rates for equivalent conditions are calculated using experimentally derived flow laws for quartzite and granite. A second calculation is then made to determine the strain-rate axes throughout a rock body assuming further boundary conditions, a temperature gradient, and a specified longitudinal strain-rate.

9.1 Slip-line Orientations

The coordinate reference frame is shown in Figure 33. The rock mass is considered to be semi-infinite with a surface slope α. This allows the calculation of the orientation of the principal strain-rate axes. A more complete solution including the strain-rate distribution requires a complete specification of the boundary conditions. As appropriate boundary conditions are highly

Figure 33. Coordinate system for the plastic flow model, showing positive stress and velocity (u and v) components parallel to axes inclined at α degrees to the horizontal. The block is an infinite half-space with no velocity components in the z direction. Additional assumptions are that the shear stress, τ_{xy}, and the effective stress, τ, are functions of y only; see text.

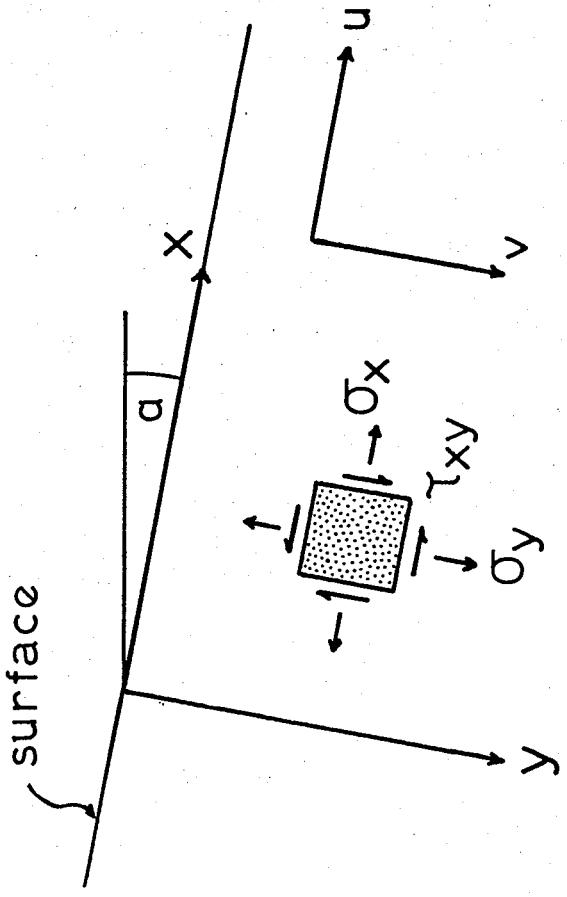
u
v
x
α
σx
τxy
σy
surface
y

speculative only the orientations of the principal strain-rate axes will initially be calculated.

For the orientations of strain-rate axes a single set of slip-lines will be found. Slip-lines are lines of maximum shear strain rate as defined in plastisity theory (e.g., Jager and Cook, 1979, p.233). A second set of slip-lines exists perpendicular to the one chosen, and both are at 45° to the principal strain-rate axes. The set of slip-lines chosen here corresponds closely to a shear plane in simple shear, although the deformation path also contains a component of pure shear. That is, the set chosen is that with the lowest rate of rotation with respect to parallel material lines. This set of slip-lines will be here referred to as the "primary slip-lines". These planes of maximum shear strain-rate are those along which shear zones would be most likely to develop. As shear zones constitute one of the major modes of deformation in rock (e.g., Ramsay, 1980; White et al., 1980), the primary slip-line orientations are considered to be of importance.

Following Nye (1957, eqs. 6-8) a general flow law may be written:

$$\dot{\epsilon} = f(\tau)$$

where $\dot{\epsilon}$ is the effective strain-rate:

$$2\dot{\epsilon}^2 = \dot{\epsilon}_{ij}\,\dot{\epsilon}_{ij}$$

τ is the effective stress, similarly written:

$$2\tau^2 = \sigma'_{ij}\,\sigma'_{ij}$$

where σ'_{ij} are the deviatoric stresses. For conditions of plane strain this simplifies to (Nye, 1957, eq. 16; Jaeger, 1969, p. 143):

$$4\tau^2 = (\sigma_x - \sigma_y)^2 + 4\tau^2_{xy}$$

The stress equilibrium equations, with a term for gravitational body forces, may be written for the two-dimensional case as (Nye, 1957, eqs. 13, 14):

$$\frac{\delta\sigma_x}{\delta x} + \frac{\delta\tau_{xy}}{\delta y} + pg \sin\alpha = 0$$

$$\frac{\delta\tau_{xy}}{\delta x} + \frac{\delta\sigma_y}{\delta y} + pg \cos\alpha = 0$$

where p is the density. For simplicity in the following calculations p is assumed constant, although they could easily be modified so that p varies with depth. These equations must be satisfied for any internally consistent stress solution. Taking the partial derivatives of the equilibrium equations gives:

$$\frac{\delta^2\sigma_x}{\delta x\delta y} + \frac{\delta^2\tau_{xy}}{\delta y^2} = 0$$

$$\frac{\delta^2 \tau_{xy}}{\delta x^2} + \frac{\delta^2 \sigma_y}{\delta x \delta y} = 0$$

Setting these equal and rearranging:

$$\frac{\delta^2 \tau_{xy}}{\delta x^2} - \frac{\delta^2 \tau_{xy}}{\delta y^2} = \frac{\delta^2 (\sigma_x - \sigma_y)}{\delta x \delta y}$$

Or, by rearranging the effective stress equation, we may write:

$$\frac{\delta^2 \tau_{xy}}{\delta x^2} - \frac{\delta^2 \tau_{xy}}{\delta y^2} = \frac{\delta^2}{\delta x \delta y} \pm 2(\tau^2 - \tau^2{}_{xy})^{1/2}$$

Now the simplifying assumption is made that the shear stress τ_{xy} and the effective stress τ are functions of y only. The principal effect of this assumption is that longitudinal strain-rate variations are neglected. These variations are probably important structurally as, for example, Nye (1952) predicts a change from thrusting to crevasse formation in glaciers due to a corresponding change in longitudinal strain-rates. We will consider here, however, only the structural effects in a localized area, and will neglect longitudinal variations. Budd (1970) gives a complete solution including longitudinal strain-rate variations.

Using this simplifying assumption it follows from the above equation that:

$$\frac{\delta^2 \tau_{xy}}{\delta y^2} = 0$$

Therefore a linear dependence of τ_{xy} only is required:

$$\tau_{xy} = ky$$

The equilibrium equations may now be rewritten as:

$$\frac{\delta \sigma_x}{\delta x} + k + pg \sin \alpha = 0$$

$$\frac{\delta \sigma_y}{\delta y} + pg \cos \alpha = 0$$

Integrating these gives:

$$\sigma_x = -kx - pgx \sin \alpha + f(y)$$
$$\sigma_y = -pgy \cos \alpha + g(x)$$

To determine f(y) and g(x) these equations are substituted into the effective stress equation (see Jaeger, 1969, p. 146):

$$4\tau^2 = (-kx - pgx \sin \alpha + pgy \cos \alpha + f(y) - g(x))^2 + 4(ky)^2$$

or:

$$f(y) - g(x) - kx - pgx \sin \alpha + pgy \cos \alpha = \pm 2 [\tau^2 - k^2 y^2]^{1/2}$$

therefore:

$$f(y) = -pgy \cos \alpha \pm 2[\tau^2 \; k^2 y^2]^{1/2}$$
$$g(x) = -kx - pgx \sin \alpha$$

Replacing these functions back into the stress equations gives the stress solution:

$$\sigma_x = -kx - pgx \sin \alpha - pgy \cos \alpha \pm 2[\tau^2 - k^2 y^2]^{1/2}$$
$$\sigma_y = -pgy \cos \alpha - kx - pgx \sin \alpha$$
$$\tau_{xy} = ky$$

Applying the boundary condition that there is no stress applied to the upper surface, or $\sigma_y = 0$ at $y = 0$, then:

$$k = -pg \sin \alpha$$

The complete stress solution may now be written (Nye, 1957, eq. 19):

$$\sigma_x = -pgy \cos \alpha \pm 2[\tau^2 - (pgy \sin \alpha)^2]^{1/2}$$
$$\sigma_y = -pgy \cos \alpha$$
$$\tau_{xy} = -pgy \sin \alpha$$

To determine the orientation of slip-lines we use the standard assumption of plasticity theory that strain-rate axes are parallel to stress axes. The orientation of the principal stress axes is given by (e.g., Jager, 1969, p. 7):

$$\tan 2\theta = \frac{2\tau_{xy}}{\sigma_x - \sigma_y}$$

or, in this case:

$$\tan 2\theta = \frac{-2pgy \sin \alpha}{\pm 2[\tau^2 - (pgy \sin \alpha)^2]^{1/2}}$$

For the orientations of the slip-lines, then:

$$\phi = \theta - 45^\circ$$

Figure 34 is a plot of $\phi - \alpha$, or the true dip of the primary slip-lines, versus the effective stress for a depth of 20 km and with various surface slopes. The depth of 20 km is chosen as an approximate minimum for the stable assemblage kyanite + staurolite (e.g., Winkler, 1967, p. 242), observed in the mica gneisses of the Grøvudal area. Depths of up to 65 km have been inferred for eclogite-bearing gneisses west of the area (Cuthbert et al., 1983). A density of 2900 kg/m^3 is used as an average value for high grade gneisses (e.g., Daly et al., 1966). The range in surface slopes is chosen as representative of the range of average regional slopes of modern mountain belts (Davis et al., 1983).

This graph (Figure 34) shows steep slopes at low values of effective stress, indicating large changes in the dip of slip-lines with small changes in effective stress. The

Figure 34. Slip-line dip versus effective stress for various surface slopes, at a depth of 20 km. I_{ss} indicates the amount of simple shear versus pure shear, assuming that $\delta v/\delta x = 0$.

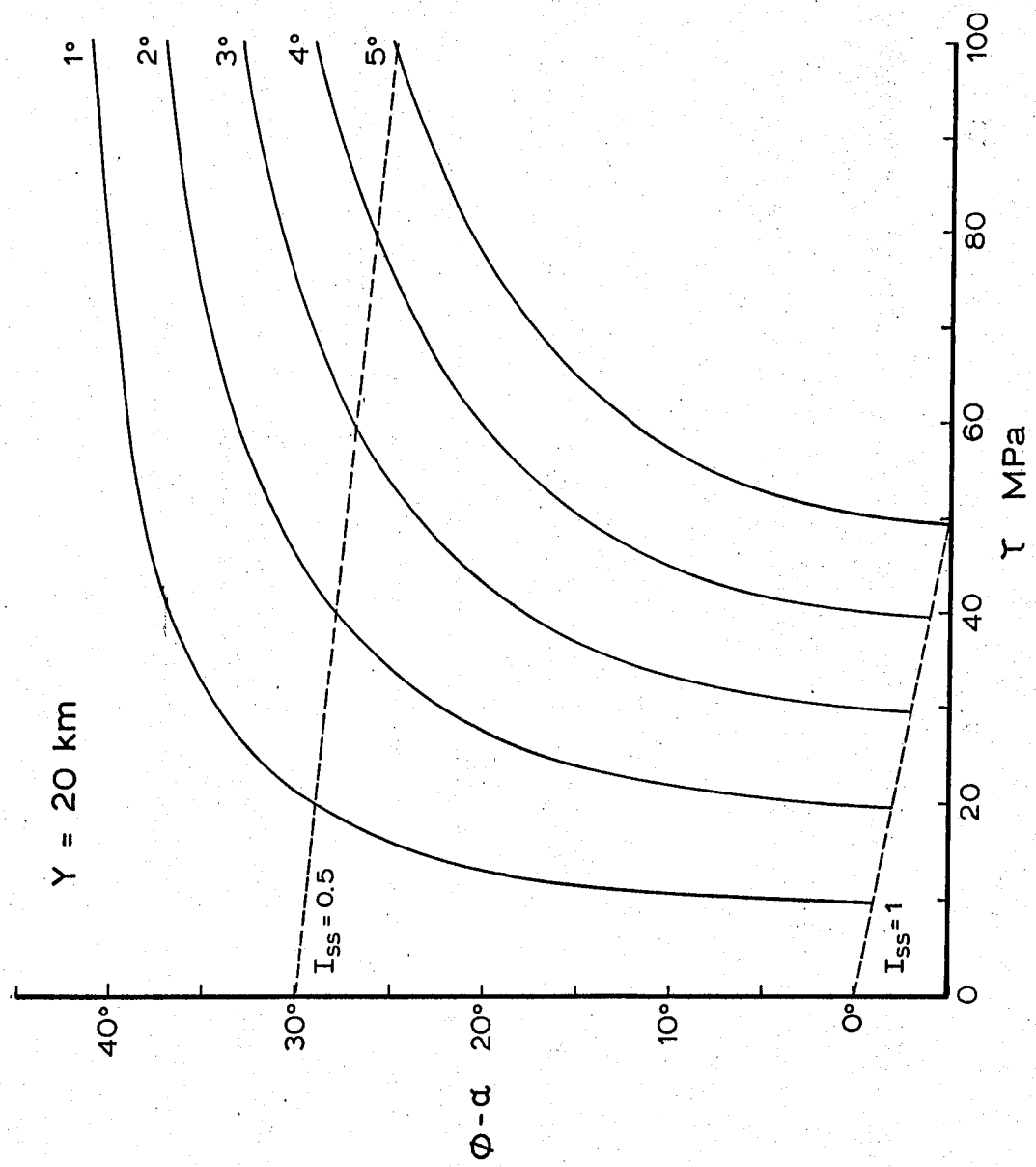
Y = 20 km
1°
2°
3°
4°
5°
I_{ss} = 0.5
I_{ss} = 1
40°
30°
20°
10°
0°
Φ - α
0
20
40
60
80
100
τ MPa

dashed lines indicate values of I_{ss}, an index of simple shear explained further below. The index assumes no change in velocity parallel to the x direction, and varies from $I_{ss} = 1$ for simple shear to $I_{ss} = 0$ for pure shear.

In figure 35 this variation has been expressed in terms of the effect of an increasing deviatoric stress in the x direction on the orientation of the primary set of slip-lines. The graph is a plot of $\emptyset - \alpha$ versus the deviatoric stress σ'_x, where:

$$\sigma'_x = \sigma_x - \frac{\sigma_x + \sigma_y}{2}$$

or:

$$\sigma'_x = [\tau^2 - (\rho g y \sin \alpha)^2]^{1/2}$$

The graph is also plotted for different surface slopes, α, using a depth of y = 20 km.

The principal features of note in this graph are, similarly, the steep slopes at low deviatoric stresses. Therefore relatively small fluctuations of horizontal deviatoric stress on the order of 10 MPa (100 bars), can lead to changes in the dip angles of slip-lines of from 6 to 21

Figure 35. Slip-line dip versus deviatoric stess in the x direction for various surface slopes, at a depth of 20 km. I_{ss} indicates the amount of simple shear versus pure shear, assuming that $\delta v/\delta x = 0$.

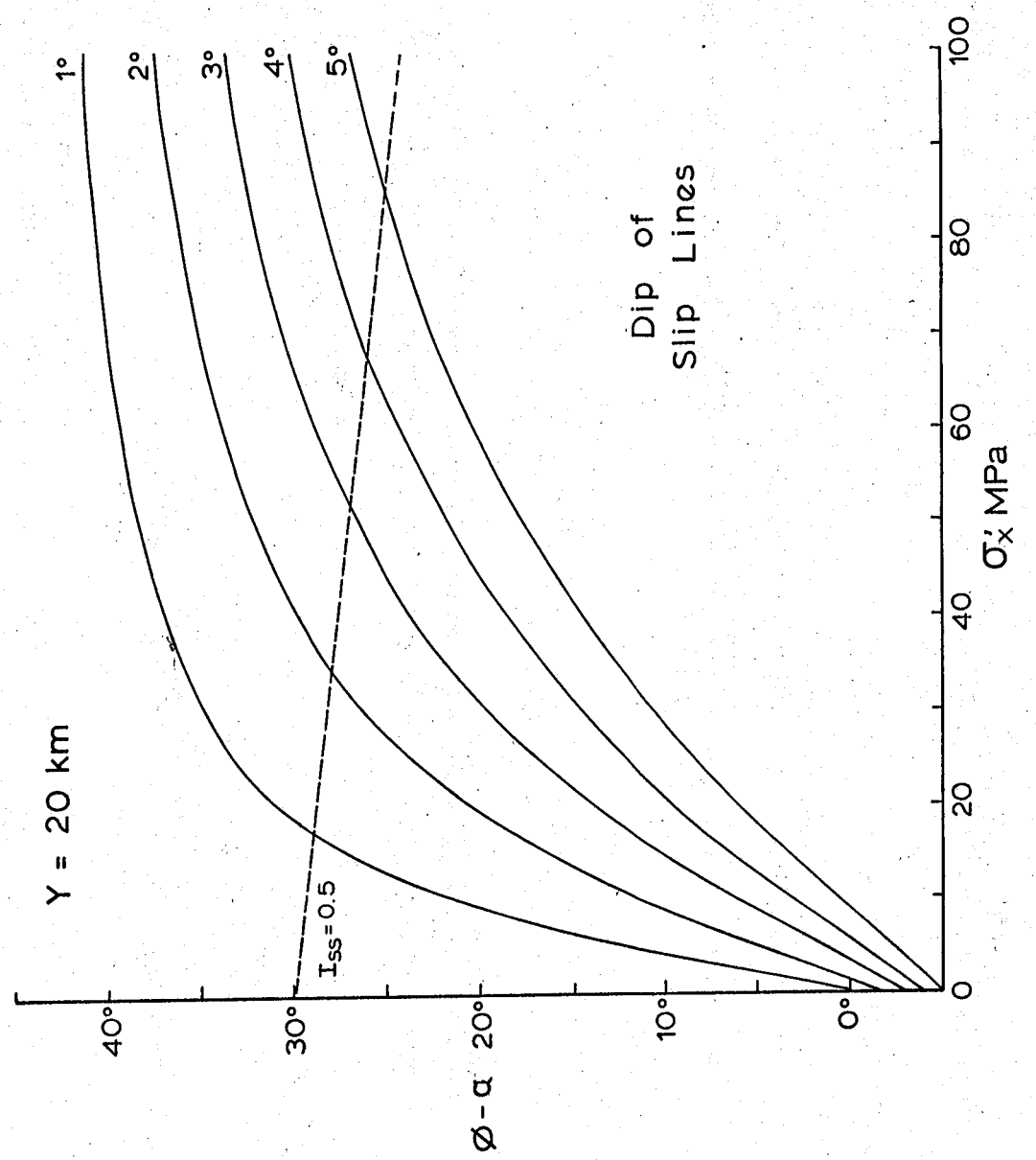
Y = 20 km
Dip of
Slip Lines
1°
2°
3°
4°
5°
I_{ss}=0.5
Ø-α
40°
30°
20°
10°
0°
0
20
40
60
80
100
σ'_x MPa

degrees. The graph is symmetric about its vertical axis, so that tensile deviatoric stresses will have a similar effect, although in the opposite sense. Such variations in stress are probably common in active orogenic zones and represent relatively small fluctuations in the stress field; estimates of the maximum differential stress in deep crustal (20 to 30 km) shear zones are on the order of 100 to 200 MPa (Kohlstedt and Weathers, 1980; Zoback, 1983), or maximum shear stresses of 50 to 100 MPa (cf. figure 34). For the above model this would correspond to approximately 40 to 95 MPa of horizontal deviatoric stress for a 3° surface slope; the ranges of stress on the graphs were chosen as reasonable estimates for the deformation of deep crustal rocks.

To determine the feasibility of fold formation at these stress levels flow laws for granite (Carter et al., 1981) and quartzite (Koch et al., 1980) have been plotted in figure 36. Temperature estimates in the Grøvudal area from garnet-biotite pairs range from about 500 to 660° C (Krill, in press), and about 750° C for the majority of the Basal Gneiss Region (Cuthbert et al., 1983). To flow at a geologically realistic strain-rate of 10^{-13} s^{-1} granite at 500° C requires only a flow shear stress of about 3 MPa (30

Figure 36. Strain-rate versus shear stress curves for granite (after Carter et al., 1981) and quarzite (after Koch et al., 1980).

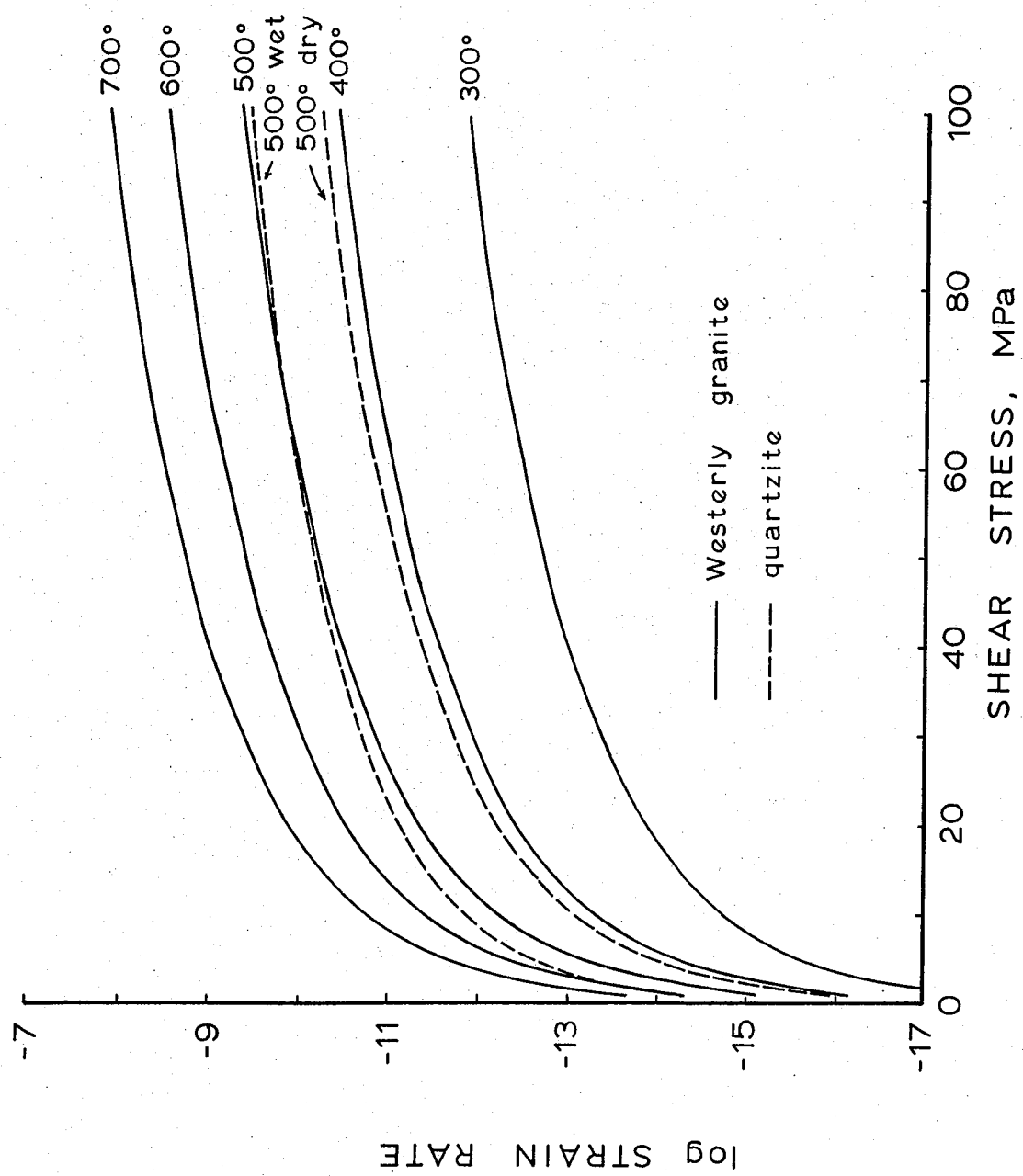
700°
600°
500°
500° wet
500° dry
400°
300°
Westerly granite
quartzite
log STRAIN RATE
-7
-9
-11
-13
-15
-17
0
20
40
60
80
100
SHEAR STRESS, MPa

bars).

9.2 Slip-line Field

Before discussing the implications of these calculations (section 9.1) for folding, a final set of calculations is made to determine a vertical profile of the slip-line orientations given the granite flow law, a geothermal gradient, and assumed longitudinal strain-rates.

To incorporate a flow law into the model assume a Levi-Mises type plasticity relationship of the form (Nye, 1957, eq. 5):

$$\epsilon_{ij} = k\sigma'_{ij}$$

and a flow law of the form:

$$\epsilon = B\tau^n$$

from the definitions of effective stress and strain-rate then:

$$\begin{aligned} 2\epsilon^2 &= k^2\sigma'_{ij}\sigma'_{ij} \\ &= 2k^2\tau^2 \\ \epsilon &= k\tau \\ k &= B\tau^{n-1} \end{aligned}$$

By again assuming plane strain, and that $\delta v/\delta x = 0$, these equations can be solved to give the relationship (Nye, 1957, eq. 24):

$$\epsilon = \frac{r\tau}{(\tau^2 - (\rho g y \sin\alpha)^2)^{1/2}} = B\tau^n$$

where $r = \delta u/\delta x$, the longitudinal strain-rate (see figure 33). This equation, the flow law for granite (Carter et al., 1981):

$$\epsilon = 1.4 \times 10^{-9} \exp(-25.3/RT \times 10^{-3})(2\tau)^{2.9}$$

(R is the Universal Gas Constant and T is the temperature in degrees Kelvin), a temperature gradient of 15° C/km, and the equations previously given for slip-line orientations were then solved using a BASIC program on an IBM-PC to give the slip-line orientations as a function of depth.

Figures 37 and 38 show the primary slip-line orientations, Ø, as a function of depth for surface slopes of 2° and 1° respectively, at various longitudinal strain-rates. The orientation of slip-lines increases with longitudinal strain rate, and a comparison of figure 37 with figure 38 shows that a change in the surface slope of 1° produces an

Figure 37. Slip-line field assuming a Westerly granite flow-law, a $15°km^{-1}$ thermal gradient and a 2° surface slope, shown for various longitudinal strain-rates. I_{ss} indicates the amount of simple shear versus pure shear, assuming that $\delta v/\delta x = 0$.

Figure 38. Slip-line field assuming a Westerly granite flow-law, a $15°km^{-1}$ thermal gradient and a 1° surface slope, shown for various longitudinal strain-rates. I_{ss} indicates the amount of simple shear versus pure shear, assuming that $\delta v/\delta x = 0$.

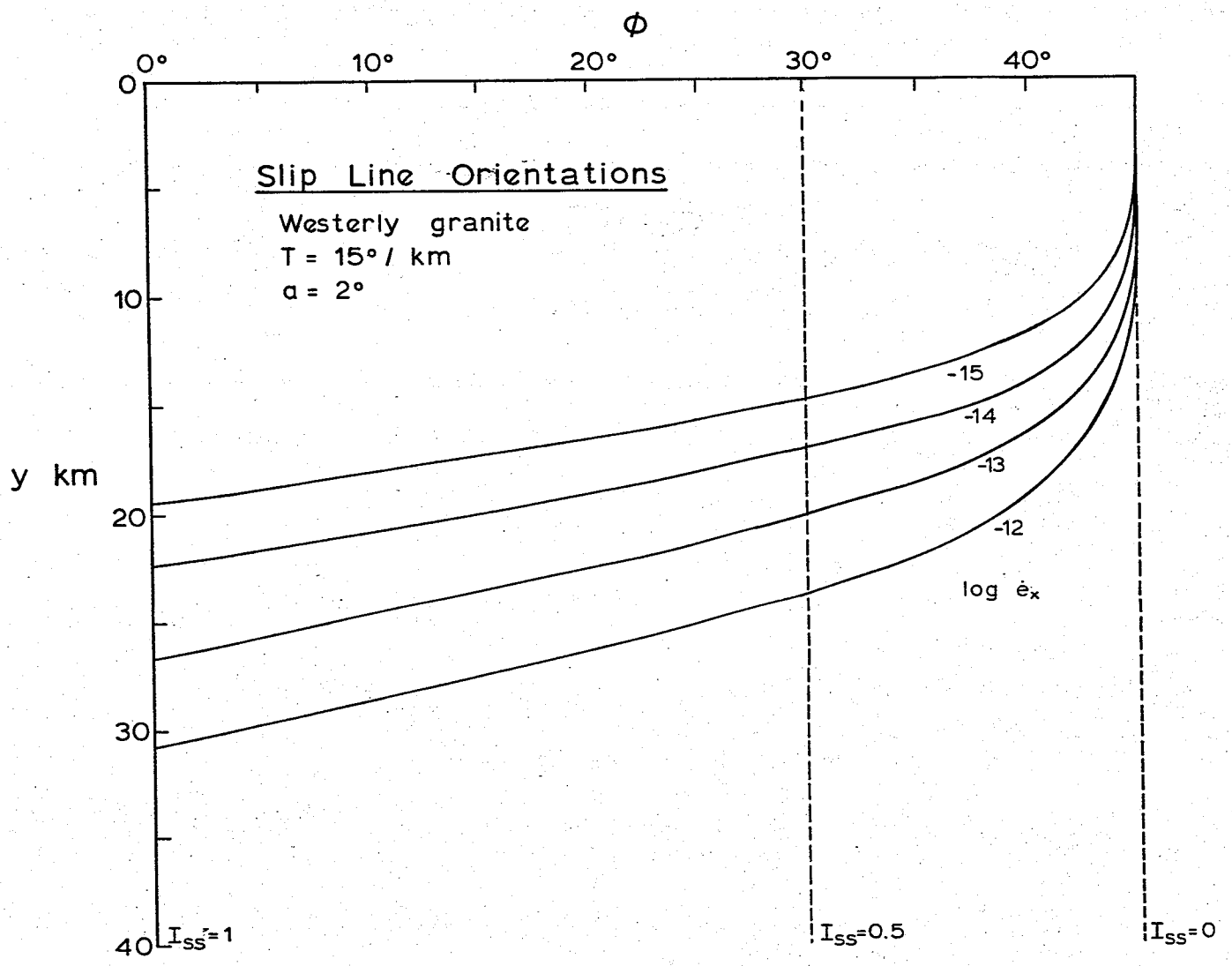
Φ
0°
10°
20°
30°
40°
0
10
20
30
40
y km
Slip Line Orientations
Westerly granite
T = 15° / km
a = 2°
-15
-14
-13
-12
log ėx
Iss=1
Iss=0.5
Iss=0

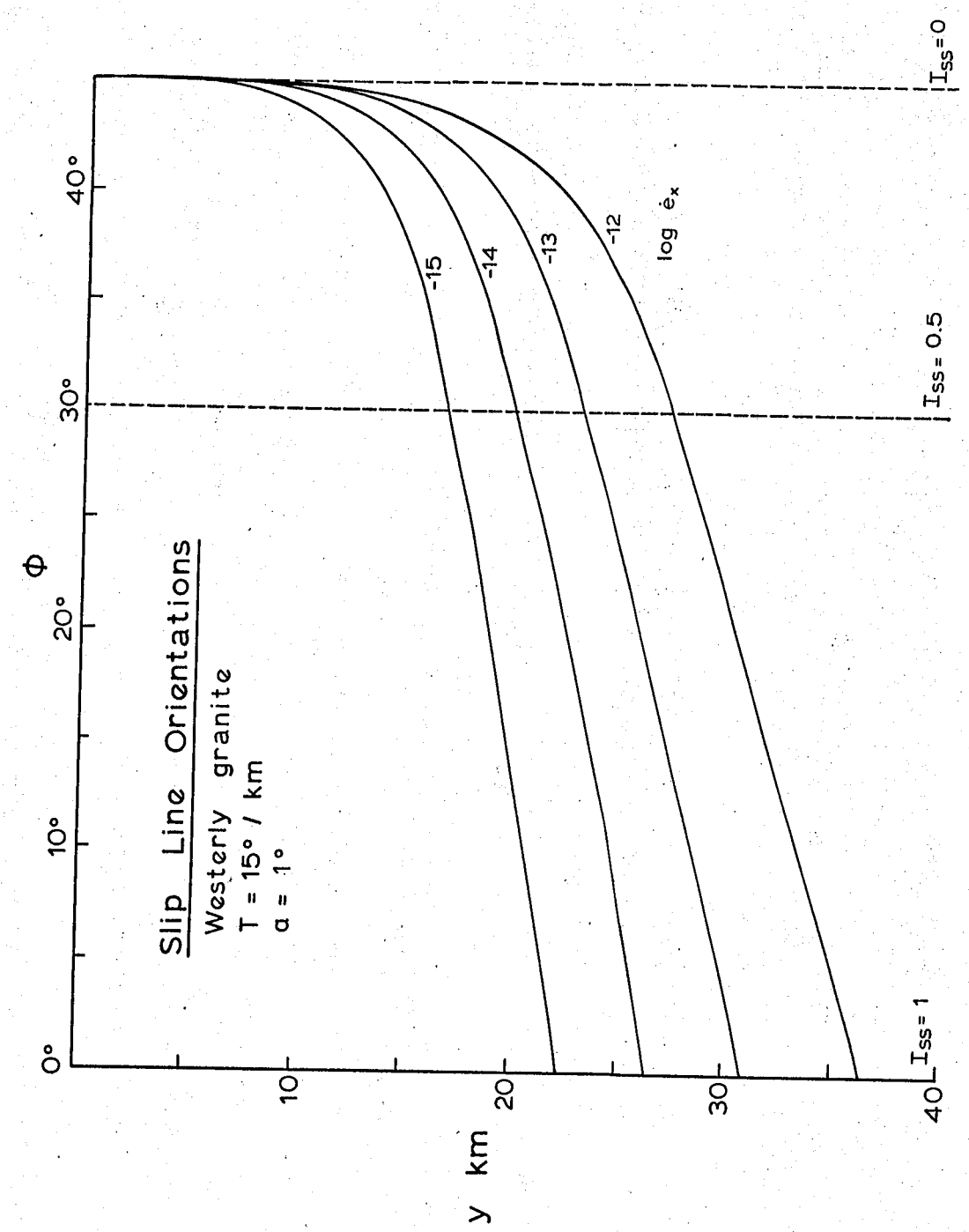
Slip Line Orientations
Westerly granite
T = 15° / km
a = 1°
Φ
0°
10°
20°
30°
40°
y km
10
20
30
40
log $\dot{e}_x$
-15
-14
-13
-12
I_{ss}=0
I_{ss}= 0.5
I_{ss}= 1

approximately 5° change in the orientation of slip-lines. These models also predict the proportion of simple shear; for example with a 2° surface slope and a longitudinal strain-rate of 10^{-13} s^{-1} simple shear will occur at a depth of approximately 27 km. Also, under these conditions pure shear deformation paths would be dominant to depths of about 20 kilometers, where $I_{ss} = 0.5$, with a narrower zone of simple shear dominated deformation below. It should be noted however that I_{ss} varies smoothly with depth (see below) and no sharp break occurs between pure and simple shear dominated regimes.

9.3 Simple Shear Index

A simple shear index, I_{ss}, was defined by Hudleston and Hooke (1980) as:

$$I_{ss} = 2w_{xy}/(\epsilon_1-\epsilon_2)$$

where w_{xy} is the component of the vorticity tensor:

$$w_{xy} = \tfrac{1}{2}(\delta u/\delta x - \delta v/\delta y)$$

To relate this to the present problem, the matrix for a plane strain rate of deformation (or stretching) tensor can be written (e.g. Mase, 1970, p. 112):

$$\epsilon_{ij} = \begin{bmatrix} \delta u/\delta x & \tfrac{1}{2}(\delta u/\delta y + \delta v/\delta x) \\ \tfrac{1}{2}(\delta u/\delta y + \delta v/\delta x) & \delta v/\delta y \end{bmatrix}$$

$$= \begin{bmatrix} \epsilon_x & \Gamma \\ \Gamma & \epsilon_y \end{bmatrix}$$

Using equations for a general Mohr construction (e.g., Jaeger, 1969, p. 10):

$$\tfrac{1}{2}(\epsilon_1 - \epsilon_2) = \tfrac{1}{2}[(\epsilon_x - \epsilon_y)^2 + 4\Gamma^2]^{1/2}$$

For a constant volume deformation $\epsilon_x = -\epsilon_y$, so that:

$$(\epsilon_1 - \epsilon_2) = 2(\epsilon_x^2 + \Gamma^2)^{1/2}$$

and:

$$I_{ss} = \frac{w_{xy}}{(\epsilon_x^2 + \Gamma^2)^{1/2}}$$

Now the equation for I_{ss} can be rewritten by using the plastic stress-strain rate relationship assumed earlier. In plane strain (Nye, 1957, eq. 15):

$$\epsilon_x = -\epsilon_y = \tfrac{1}{2}k(\sigma_x - \sigma_y)$$
$$\Gamma = k\tau_{xy}$$
$$= w_{xy} \qquad \text{(if } \delta v/\delta x = 0\text{)}$$

so that:

$$I_{ss} = \frac{\tau_{xy}}{\tau}$$

Means et al. (1980) have used a similar quantity called the kinematical vorticity number:

$$W_k = \frac{w}{(2II_m)^{1/2}}$$

where w is the vorticity magnitude:

$$w = (\delta u/\delta y - \delta v/\delta x) = 2w_{xy}$$

and II_m is an invariant quantity called the second moment of the stretching tensor (Means et al., 1980, eq. 20 contains an error):

$$II_m = I^2 + 2II = tr(\epsilon_{ij}\epsilon_{ij}^T)$$

which in this case is:

$$II_m = \epsilon_x^2 + \epsilon_y^2 + 2r^2$$

so that:

$$W_k = \frac{w}{[2(\epsilon_x^2 + \epsilon_y^2 + r^2)]^{1/2}}$$

and for constant volume:

$$W_k = \frac{w}{2(\dot{\epsilon}_x^2 + \dot{\gamma}^2)^{\frac{1}{2}}}$$

$$= \frac{w_{xy}}{(\dot{\epsilon}_x^2 + \dot{\gamma}^2)^{\frac{1}{2}}}$$

Therefore in a plane-strain constant-volume deformation path the index of simple shear, I_{ss}, is equivalent to the kinematical vorticity number, W_k.

9.4 Folding

The principal implications of the above calculations in terms of fold generation are that the orientations of slip-lines are dependent on a number of variables, and are therefore unlikely to remain constant through time. Figure 35 shows this variation as a function of deviatoric stress, σ'_x. The effect of increasing stress is to increase the dip of slip-lines. Other variables will also effect the slip-line orientations. Decreasing the surface slope, as has been mentioned, causes a strong increase in slip-line dips. Similarly, a decrease in depth or temperature, or an increase in horizontal strain-rate (largely a function of stress), will result in slip-line dip increases.

In considering the effect of increased slip-line dip on folding assume that an initial transposition foliation has developed under conditions of local steady-state flow, thus establishing an initial isoclinal and intrafolial stage of

folds (Chapter 8). In figure 39 this is shown as occurring in a flow approximating simple shear. With an increase in dip of slip-lines of several degrees, two important folding mechanisms may operate. Both mechanisms depend on the slip-lines rotating through the layering. The easiest way for slip-lines to rotate through the layering is if the initial deformation path approximates simple shear. In this case the initial transposition layering will form close to the primary slip-lines, and the slip-line orientations are the most unstable (Figures 34, 35, 37, and 38).

The first mechanism is passive folding, which will occur if shear zones are generated parallel to the new primary slip-line orientation (Figure 39). As shear zones are commonly initiated in rocks due to their inherently heterogeneous nature, this is a likely mechanism. The second mechanism is active folding, or initiation of buckle folds followed by flattening. By passing through the slip-lines the layering, which was previously in an

Figure 39. Folding model from slip-line theory. An initial foliation forms through transposition, rotation, and chemical processes in a deformation close to simple shear. The orientation of this foliation will lie approximately parallel to the principal flattening plane, which asymtotically approaches some orientation close to the principal slip-lines. After a change in the flow boundary conditions, increasing the horizontal deviatoric stress or decreasing the surface slope, the strain-rate axes and slip-lines change orientations (Figure 35). If the slip lines move through the layering folds will form either through heterogeneous shear, or by buckling as the foliation is placed in a shortening field.

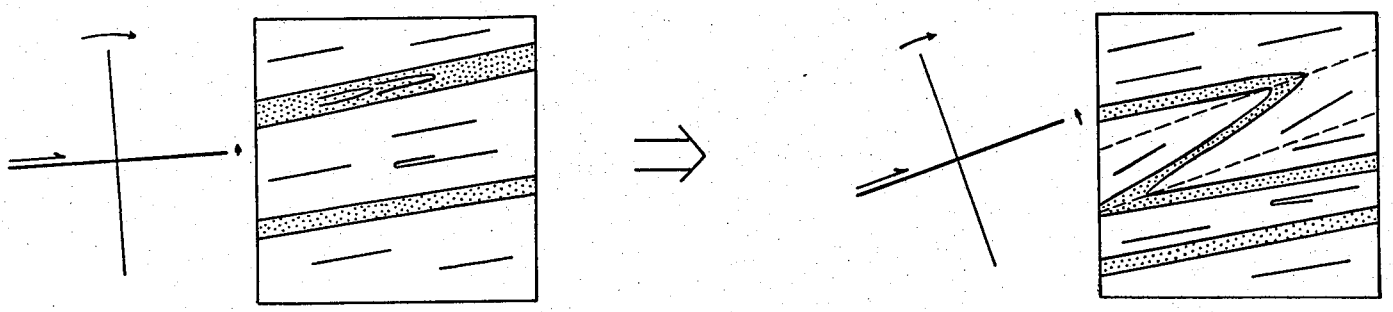
Initial transposition fabric
inc. σ_x' , $\dot{\epsilon}_x$
dec. a , y , T
Refolding

instantaneous elongation field parallel to the maximum finite shortening plane (c.f., Ramsay, 1967, p. 114-120), has been placed in a position of instantaneous shortening. In this field the layers will begin to buckle and form folds. In this way then, relatively small changes in the conditions of flow can result in refolding, and multiple phases of folding are easily accommodated within a single deformation event.

CONCLUSION

The conclusions derived from this study fall into three main categories: the local geology and regional tectonic implications, data analysis, and fold modeling. This section briefly summarizes the principal conclusions.

The geology of the Grøvudal area can be described in terms of five lithotectonic, or tectonostratigraphic, units correlative with those of the Oppdal district in general as described by Krill (1980a), and with similar units at the Caledonian front in Sweden. These tectonic units originated as stacked thrust-sheets derived from the ancient continental margin, and were carried in from west to east during a Silurian continental collision involving the A-type (Bally, 1981; Hodges et al., 1982) subduction of the Norwegian continental margin beneath Greenland. This initial thrust-nappe phase of tectonics was transitional into a ductile fold-nappe phase in which progressive mylonitization of the nappes occurred until a pervasive ductile flow fabric developed.

The ductile fold-nappe phase of deformation involved the formation of large sheath-like basement cored fold-nappes during the general eastward flow of rock in a deformation approximating simple shear. Components of compressive and extending flow, however, are required as simple shear requires special boundary conditions unlikely

to be met over large areas. The deformation involved the progressive development of transposition foliations and fold phases. A minimum of three coaxial fold phases occurred forming sheath folds whose axes dominantly parallel a strong stretching lineation. Larger sheath folds commonly form elongate closed outcrop patterns, with complex interfingering at their terminations. This sequence of folding was the result of a continous progressive deformation, with folding and refolding of the transposition foliation as it developed.

During this phase of deformation a large north-facing near-recumbent fold-nappe developed with an east-west axis parallel to the shear direction. This fold is the southern portion of the sheath-like Grøvudal fold-nappe in which the cover thrust-nappe sequence forms a major recumbent infold beneath the basement gneisses of the Lønset gneiss 'dome'. This interpretation further suggests that the two large regions of basement gneisses in the Lønset and Trollheimen areas are major recumbent basement-cored sheath-nappes carried in from the west. The rocks of the Grøvudal area thus lie structurally beneath the basement-cored Lønset nappe, and have undergone extreme deformation in comparison with correlative units east of the basement nappes (e.g., the Sætra Nappe). This sheath-like geometry of fold-nappes has not been widely recognised in other mountain belts, although such nappes have been suggested to occur in

the Canadian Rockies (Mattauer et al., 1983) and the Pennine zone of the Alps (Cobbold, 1979).

Following this phase of fold and nappe development the early nappe was refolded by a major east-verging asymmetric fold with a north-northeast striking axial plane. The overall symmetry of this late fold is consistent with the earlier deformation, but there is some difference in style. The refolding resulted in a redistribution of structural elements, giving the present complex geometry of the area. The present form of the Grøvudal fold-nappe is due to the resulting interference pattern, a type 2 interference of Ramsay (1967). The regional pattern of fold interference is probably characterised by recumbent sheath folding (type 1), overprinted by steeper asymmetric folds, resulting in combined type 2 and type 3 interference patterns. The mechanics of the late folding event appear more 'active' than the earlier folding, in that structural elements have been rotated about a well defined axis forming a small circle pattern, thus suggesting a large component of external rotation. This rotation requires additional internal deformation for strain compatibility; one compatible solution is a flexural flow mechanism.

The present boundary between the Western Gneiss Region and the Trondheim Nappe Complex occurs as sharp syn- or post-metamorphic faults. It is suggested that these may be related to isostatic uplift of the Gneiss Region following

crustal thickening caused by fold-nappe emplacement.

Analysis of the orientation data was of primary importance in establishing the structural geometry and history outlined above. In particular, the interpretation of the late refolding event and interference patterns became clear only through this analysis, and analysis of the first phase of ductile deformation could only proceed after the domains were established. The goal of the data analysis was to locate spatial domains of coaxial foliations. In order to perform an objective search on the large amount of data, a computerized methodology was developed. Because the data consist of a complex field with large variations in data density, the initial step was to create a simplified field consisting of eigen-foliations for sub-domains chosen as one kilometer squares.

The resulting field was then analysed by compiling maps of all sub-domains compatible with a given axial vector, or π-axis. The iterative search proceeded by defining a domain from connected sub-domains, calculating a new axial vector from the domain data set, and compiling a new map of compatible sub-domains. This was repeated until self-consistent solutions emerged. The final step involved the same process using all data points. The domains that emerged from the analysis showed a systematic change across the area indicating a NNE trending antiform as a late phase structure; an entirely unanticipated result. The existence

of the fold is further verified by an eigenvalue analysis that indicates the relative position of the domains on the early fold limbs. Further analysis of the data within each domain, including calculation of confidence regions based on a Bingham distribution, revealed information about the initial phase of progressive ductile deformation as outlined above.

A number of models were developed to explain the characteristics of the folds and nappes in the area, in particular the extensive early phase of recumbent sheath folding. A computer-generated passive fold model was used to explain some of the geometric features, including the type 2 interference patterns found in outcrop and the common elongate finger-like patterns. This model shows that these geometric features may form by the passive amplification of small amplitude irregularities on an interface deformed in simple shear. The question of active fold generation and rotation of fold axes in simple shear was then explored with several kinematic models involving layer buckling in relation to maximum strain-rate axes, and rotation of fold axes in response to finite strains. These models show that fold axes may form in many orientations during simple shear, and that, although the b direction is statistically preferred for fold generation, it is an unstable one from which fold axes will migrate. Thus, the parallelism of fold axes and stretching lineations may be

explained by the combined effects of both passive and active initiation and rotation.

The final type of fold modeling done involves the calculation of stress axes, strain-rate axes, and slip-line orientations for an idealized flowing rock body. These calculations show that small changes in the magnitudes of stress, strain-rate or surface slope can cause large changes in the orientations of the strain-rate axes or slip-lines. This is significant in that during a progressive deformation a foliation will develop with an orientation approximately parallel to the maximum finite flattening plane, whose orientation asymmtotically approaches an orientation defined by the orientation of the strain-rate axes and the vorticity of the deformation. In an area of compressive flow with a large component of simple shear (i.e., I_{ss} approaches 1) the foliation will develop in an orientation close to the primary slip-lines, analogous to the shear plane in simple shear. With an increase in horizontal stress (5-10 MPa) or decrease in surface slope (1° or less), the slip-lines may rotate through the foliation. Two folding mechanisms may then operate: heterogeneous simple shear parallel to the new primary slip-lines, or buckling and flattening as the new foliation is placed in a shortening field. Thus, multiple generations of folding and transposition are easily generated by small fluctuations in the boundary conditions, or

by local perturbations.

APPENDIX A - ORIENTATION DATA

The orientation data collected for the Grøvudal analysis comprise over 1800 measurements of planar and linear fabric elements. These are presented here in summary stereonets of the domain eigenvector orientations, as maps and stereograms of all eigenvector orientations, and as maps and stereograms of the complete data set. The foliation (S_1) and lineation data sets have been edited on the maps only, so that overlapping data points are largely eliminated. These data are also displayed in part on plate 1. The data set is retained by the author in the form of punched card, and 5¼ inch magnetic disk format.

The map data are presented graphically in projection, so that the length of arrows and dip tick marks is proportional to the cosine of the plunge or dip. This gives an accurate visualization of the three-dimensional attitude variations. The distance between the tick marks on the map borders is 10 kilometers.

Larger crosses on all stereonets are the eigenvector orientations, which are also given at the lower right corners. The normalized eigenvalues are given at the lower left.

S_2 foliation data are the combined S_2 foliation and F_2 fold axial plane measurements. They are distinguished on the stereograms as: o = pole to fold axial plane, + = pole

to foliation.

page

Eigenvectors of Grøvudalen Orientation Data

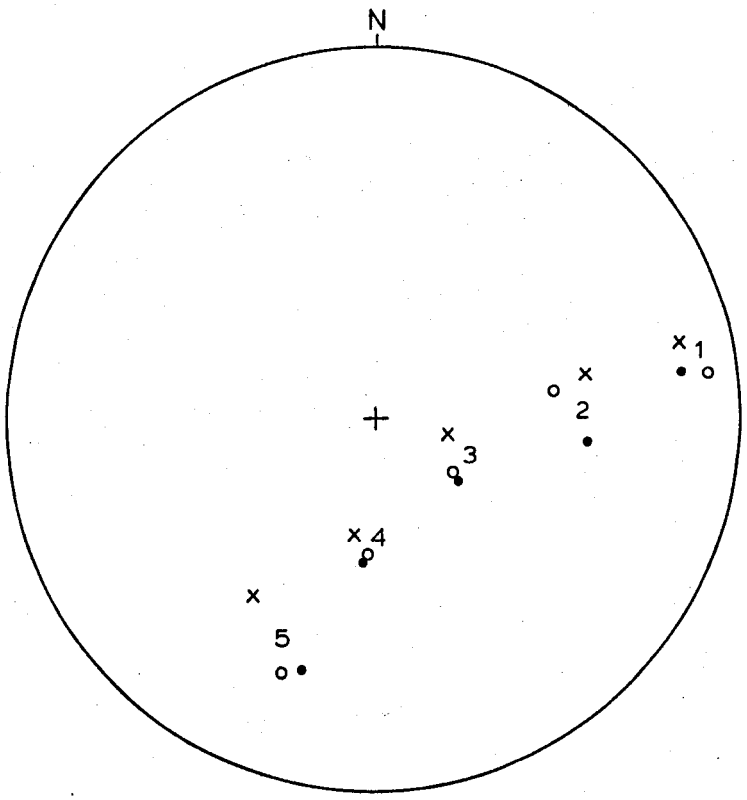

x - foliation minima (957)
o - fold axes (199)
• - lineations (439)

Eigenvalue Plot of
Grøvudalen Orientation Data

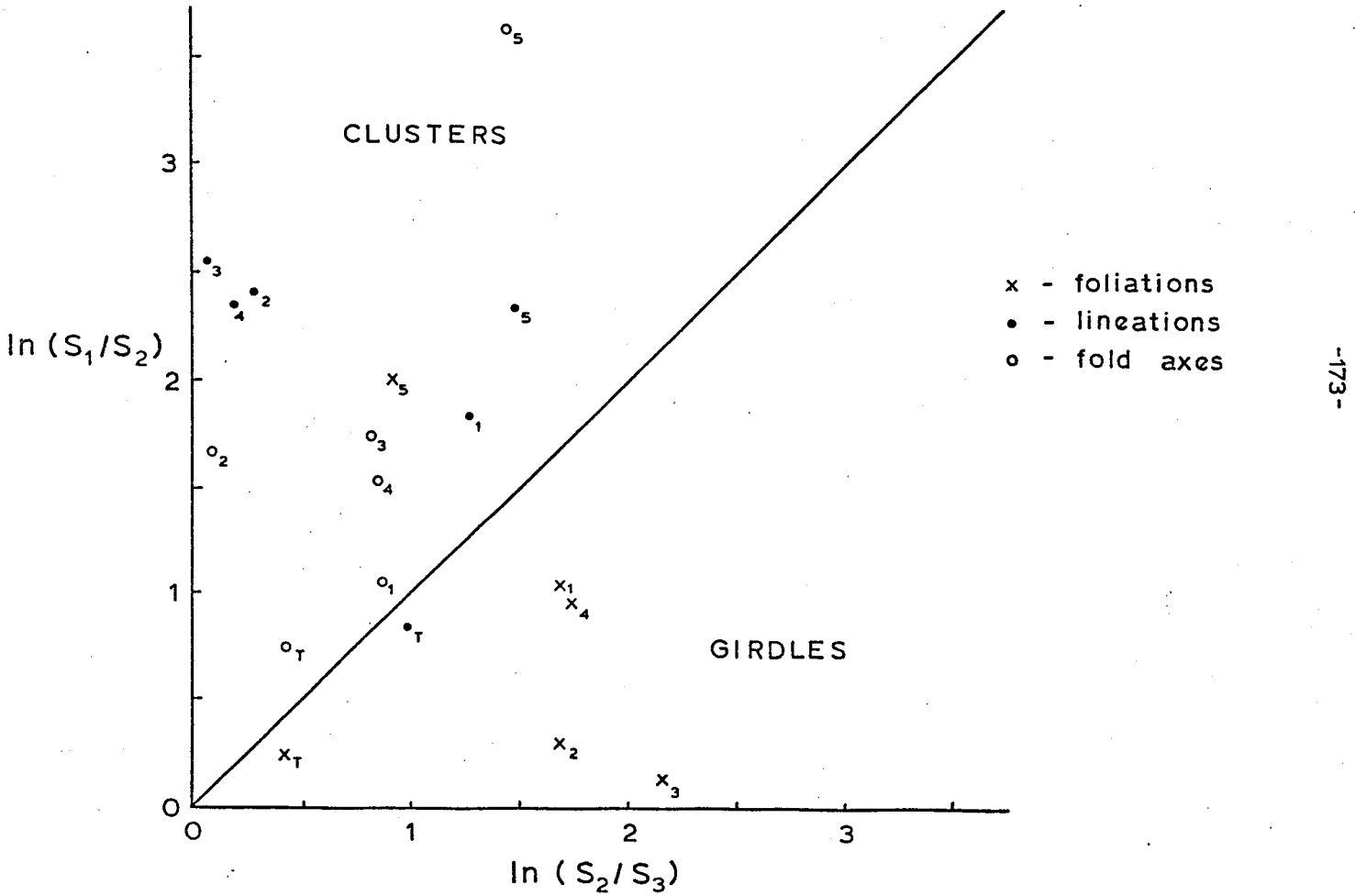

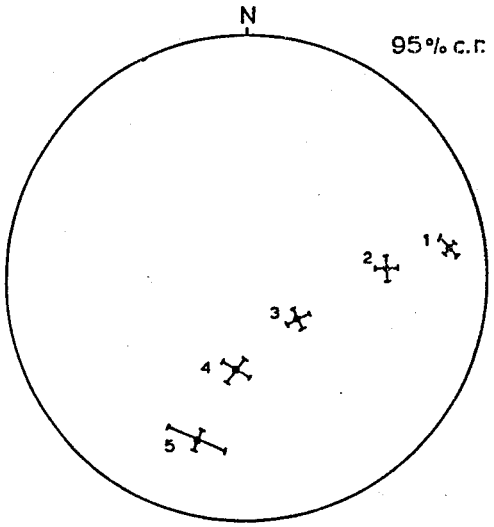

Lineation maxima n=439

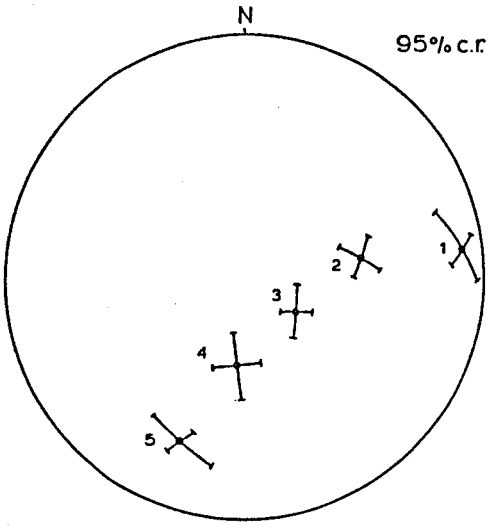

Fold axes maxima n=199

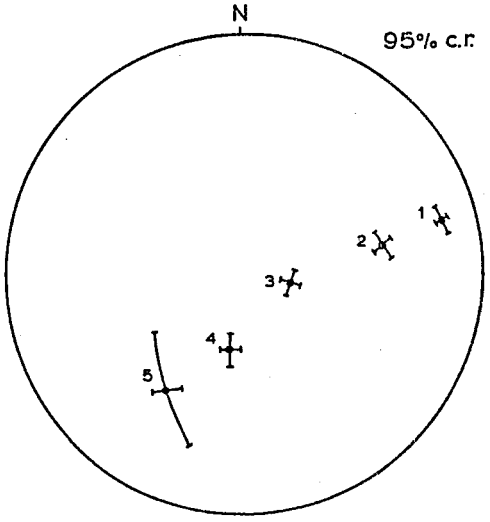

Foliation (S_1) minima n=957

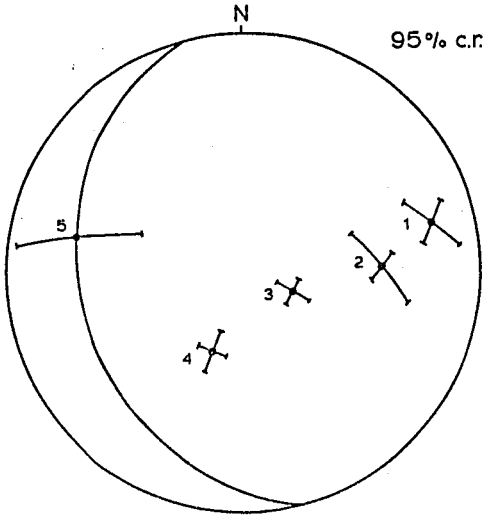

Axial plane and cleavage (S_2) minima n=125

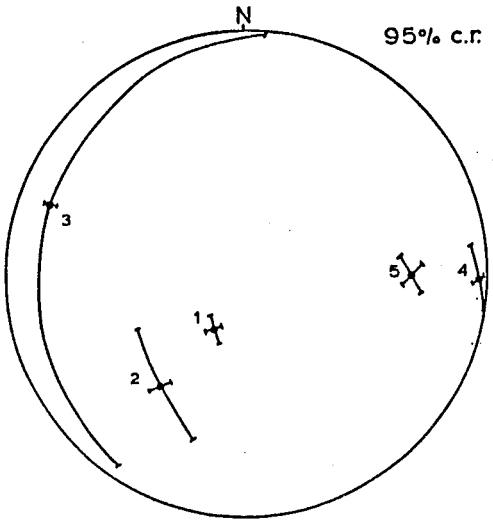

Foliation (S_1) maxima n=957

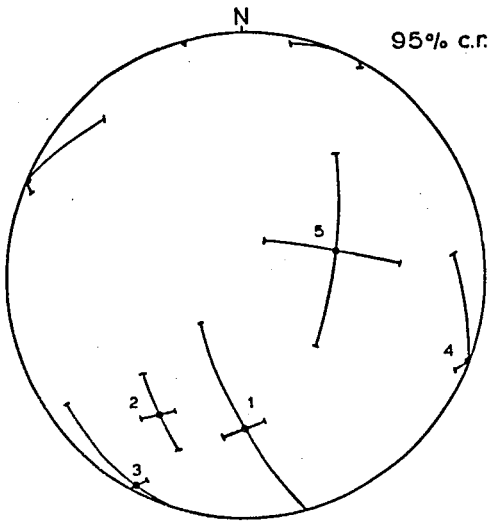

Axial plane and cleavage (S_2) maxima n=125

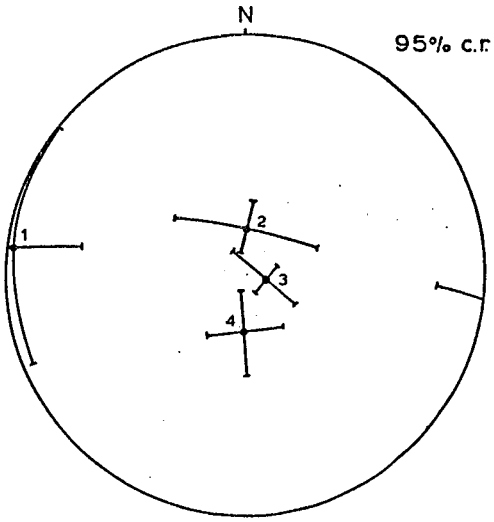

S_1/S_2 Intersections n = 50

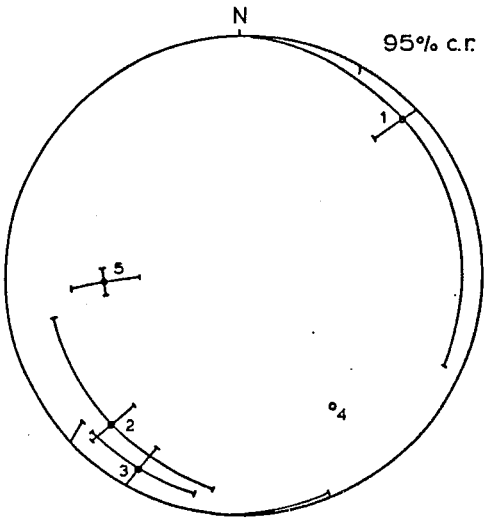

Kink band (S_3) maxima n = 23

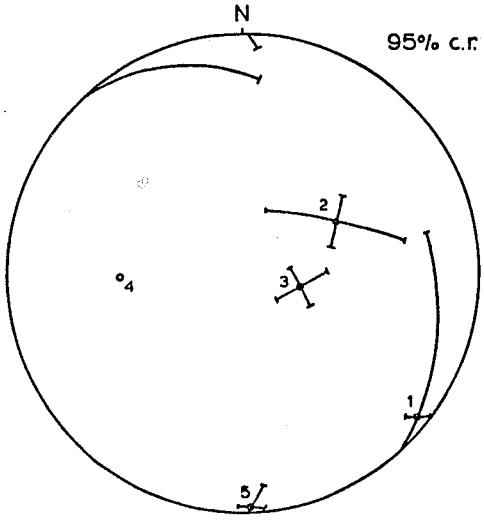

Kink axes maxima n = 30

EIGEN FOLIATIONS

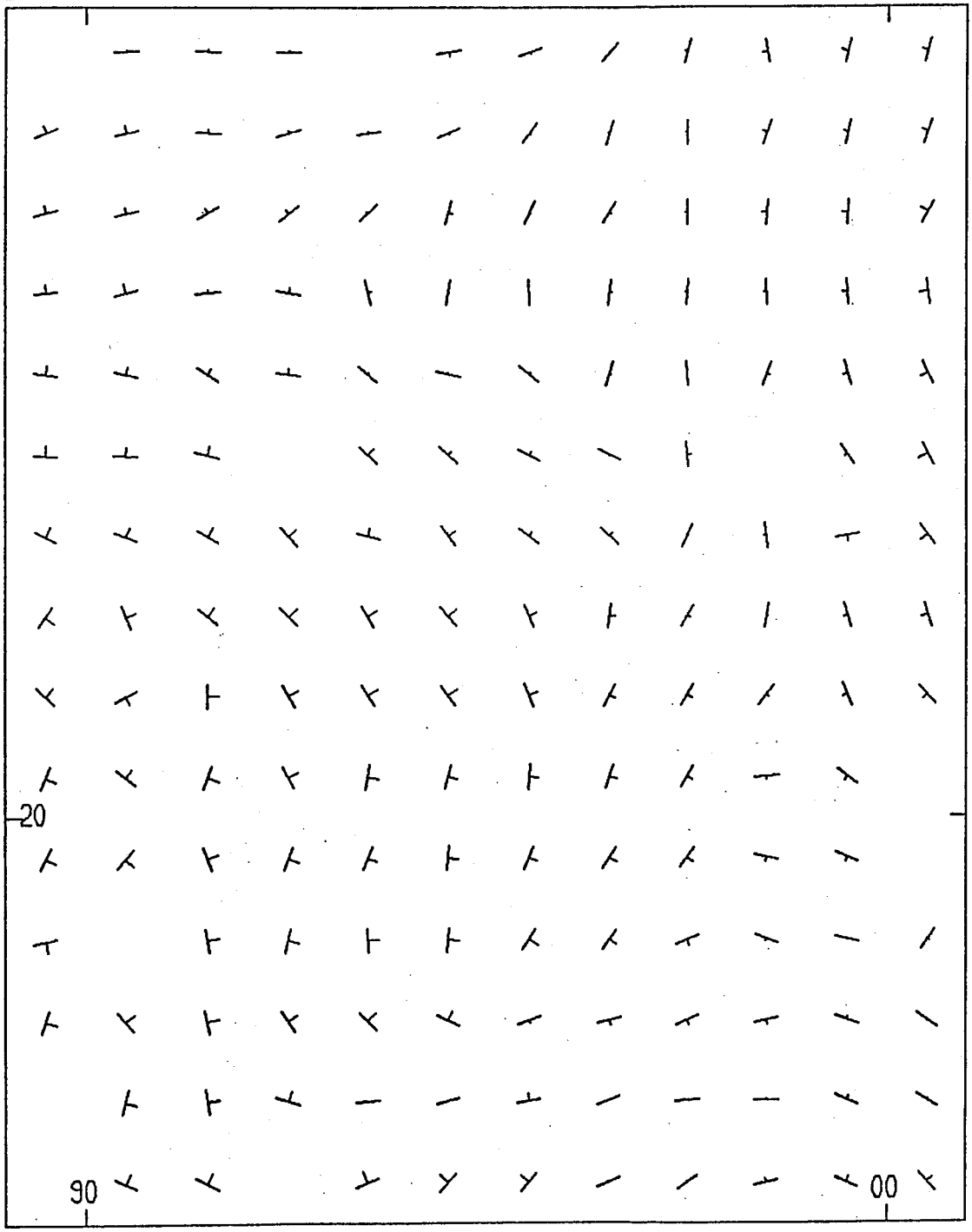

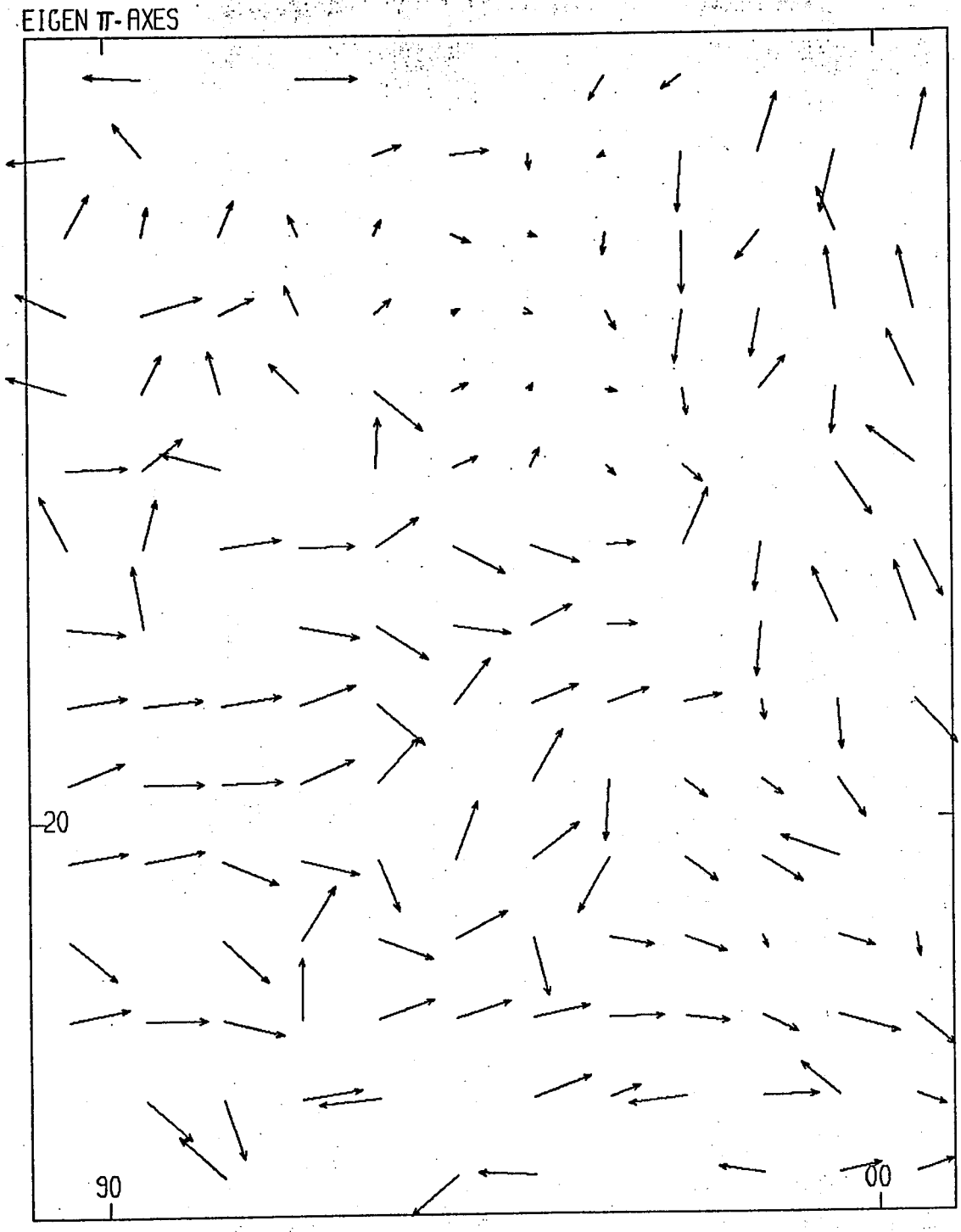
EIGEN π-AXES
20
90
00

EIGEN LINEATIONS

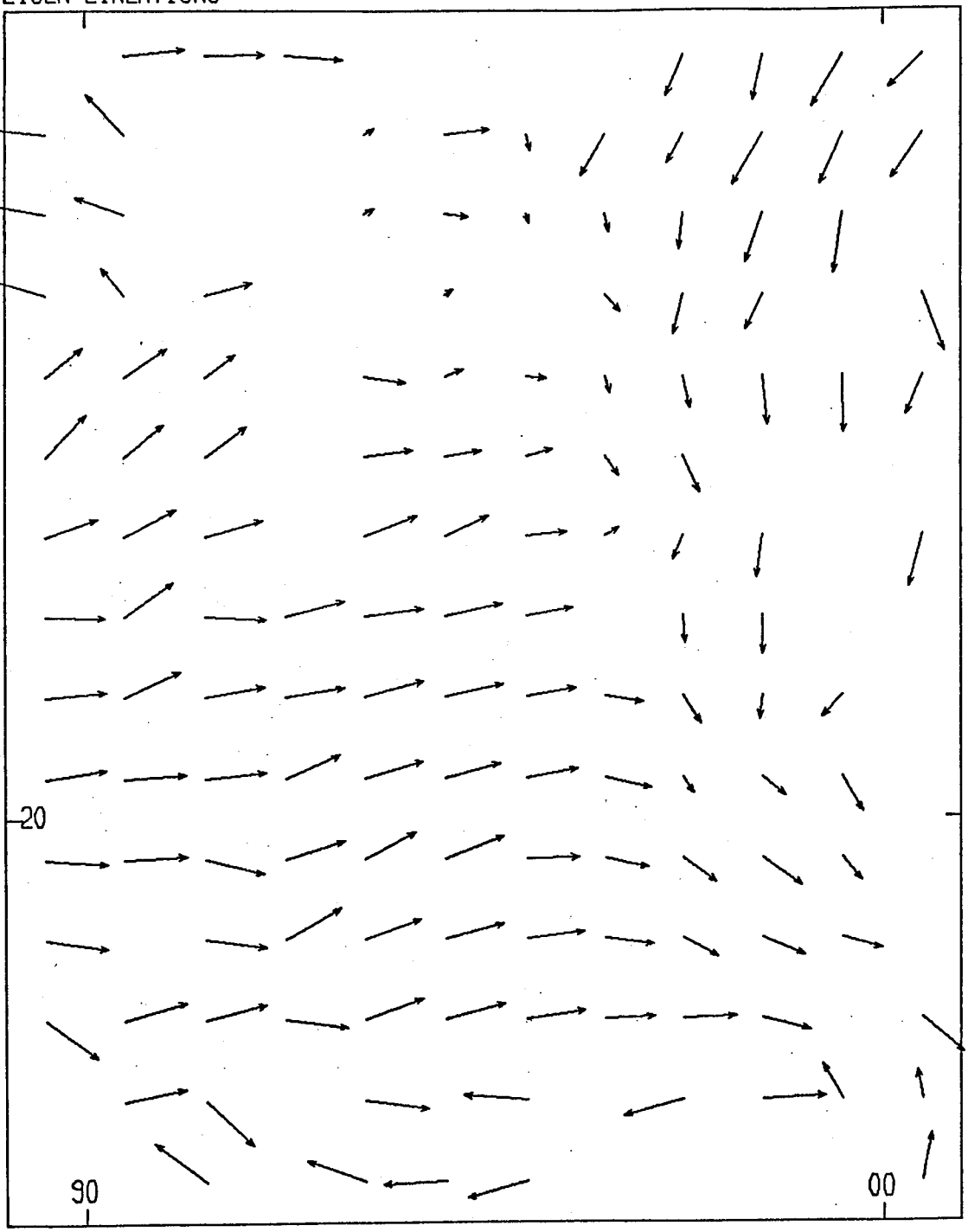

EIGEN FOLD AXES

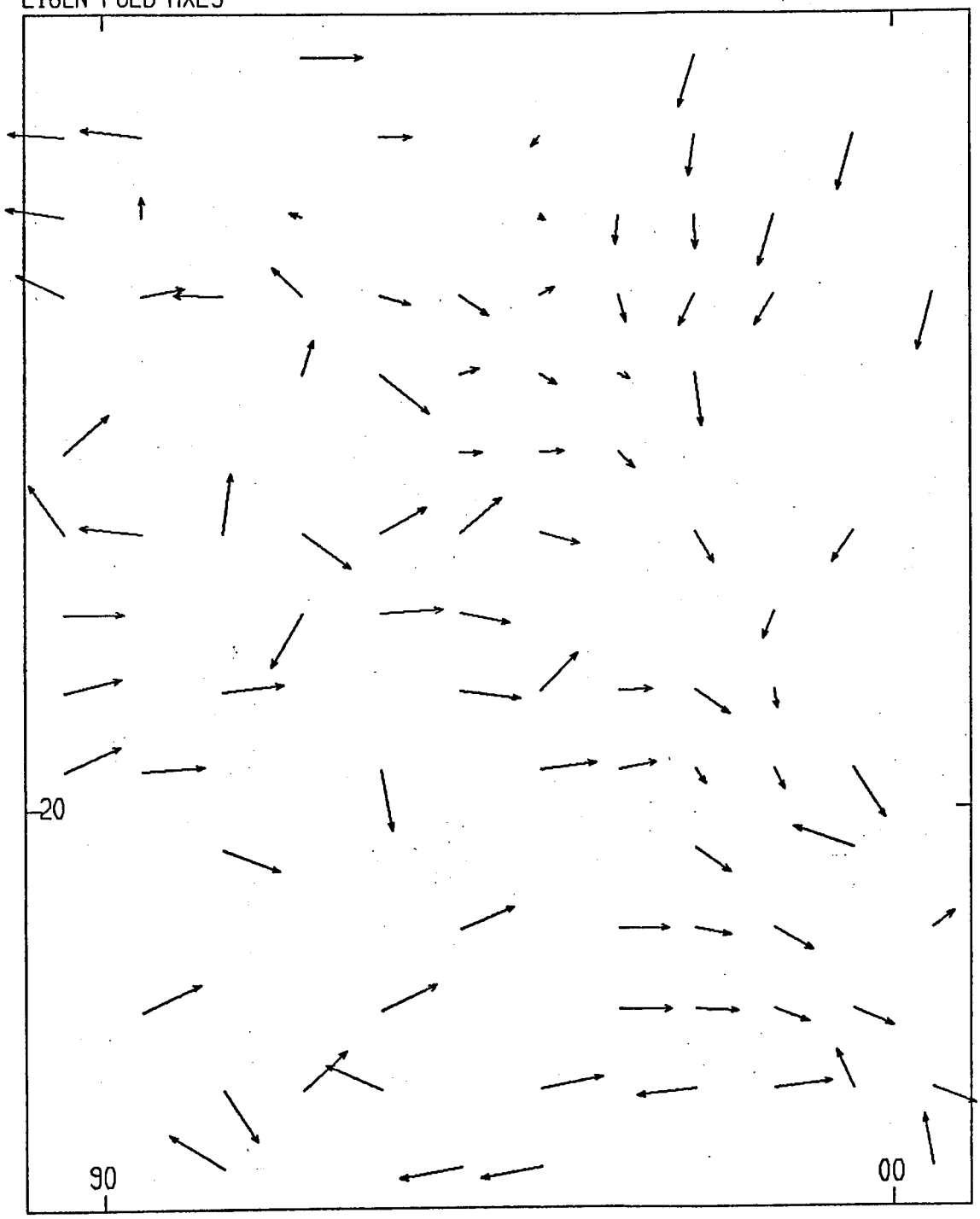

FOLIATIONS

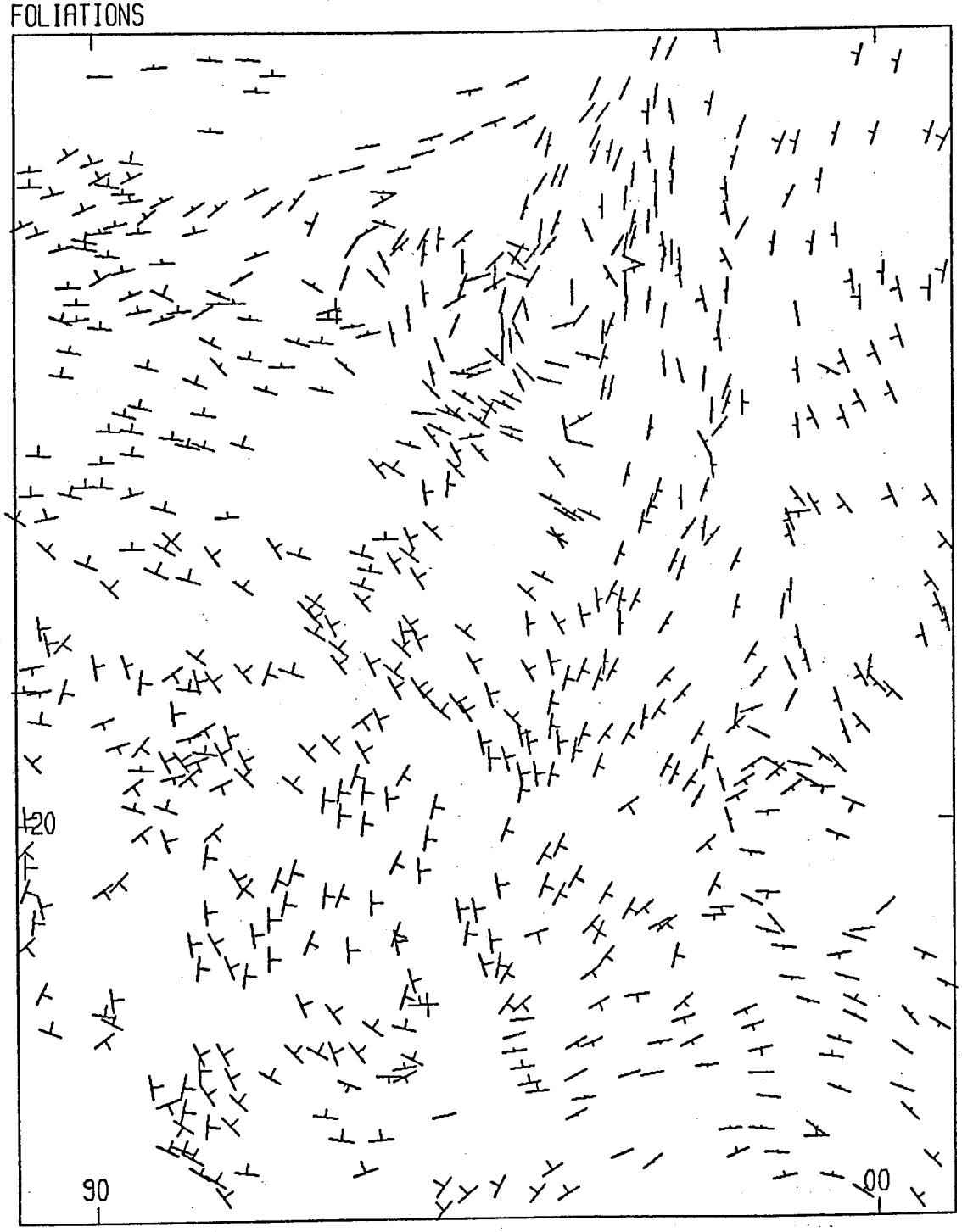

FOLIATIONS
WHOLE AREA
N=957

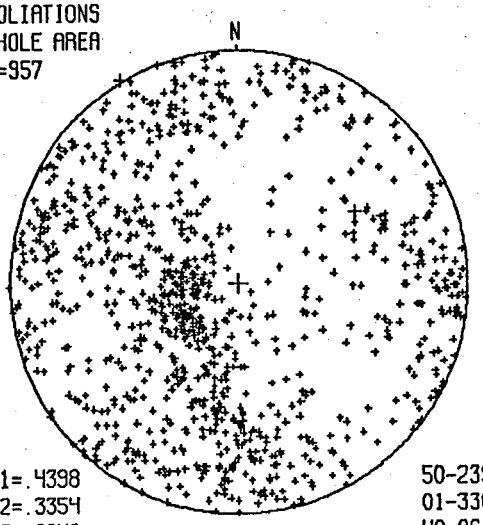

S1=.4398 50-239
S2=.3354 01-330
S3=.2248 40-061

FOLIATIONS
DOMAIN 1
N=351

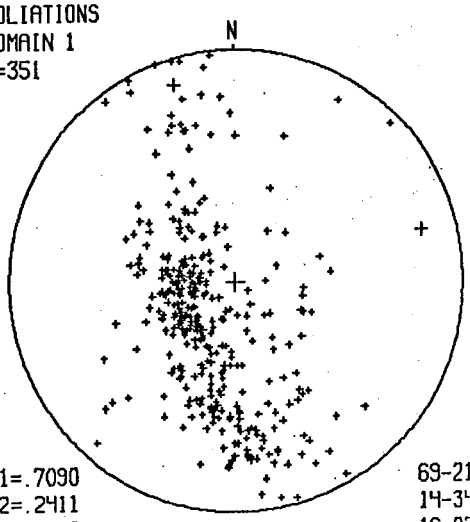

S1=.7090 69-213
S2=.2411 14-343
S3=.0499 16-076

FOLIATIONS
DOMAIN 2
N=206

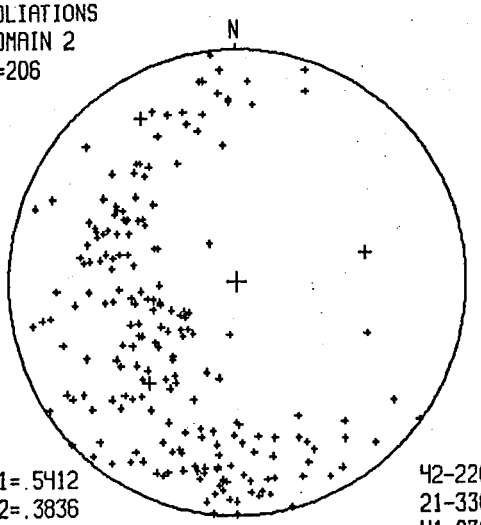

S1=.5412 42-220
S2=.3836 21-330
S3=.0752 41-079

FOLIATIONS
DOMAIN 3
N=221

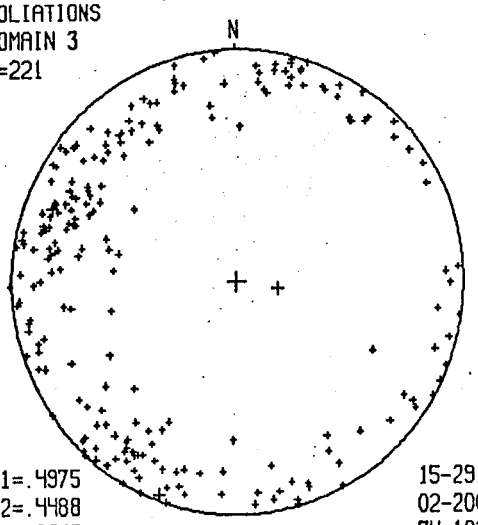

S1=.4975 15-291
S2=.4488 02-200
S3=.0537 74-102

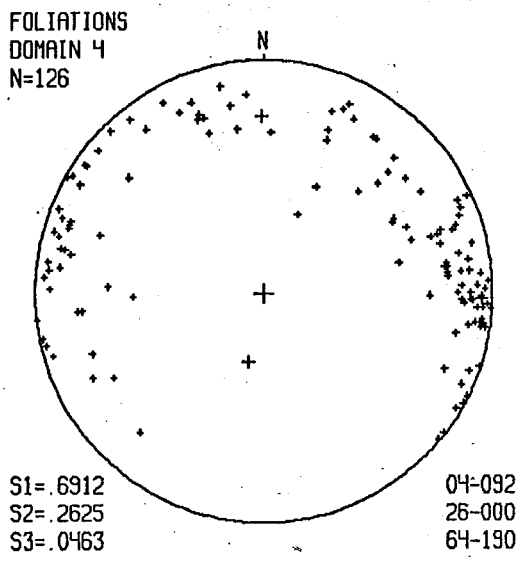
FOLIATIONS
DOMAIN 4
N=126
N
S1=.6912
S2=.2625
S3=.0463
04-092
26-000
64-190

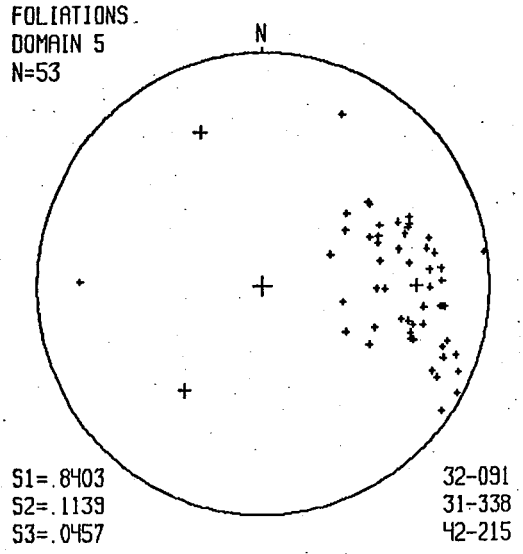
FOLIATIONS
DOMAIN 5
N=53
N
S1=.8403
S2=.1139
S3=.0457
32-091
31-338
42-215

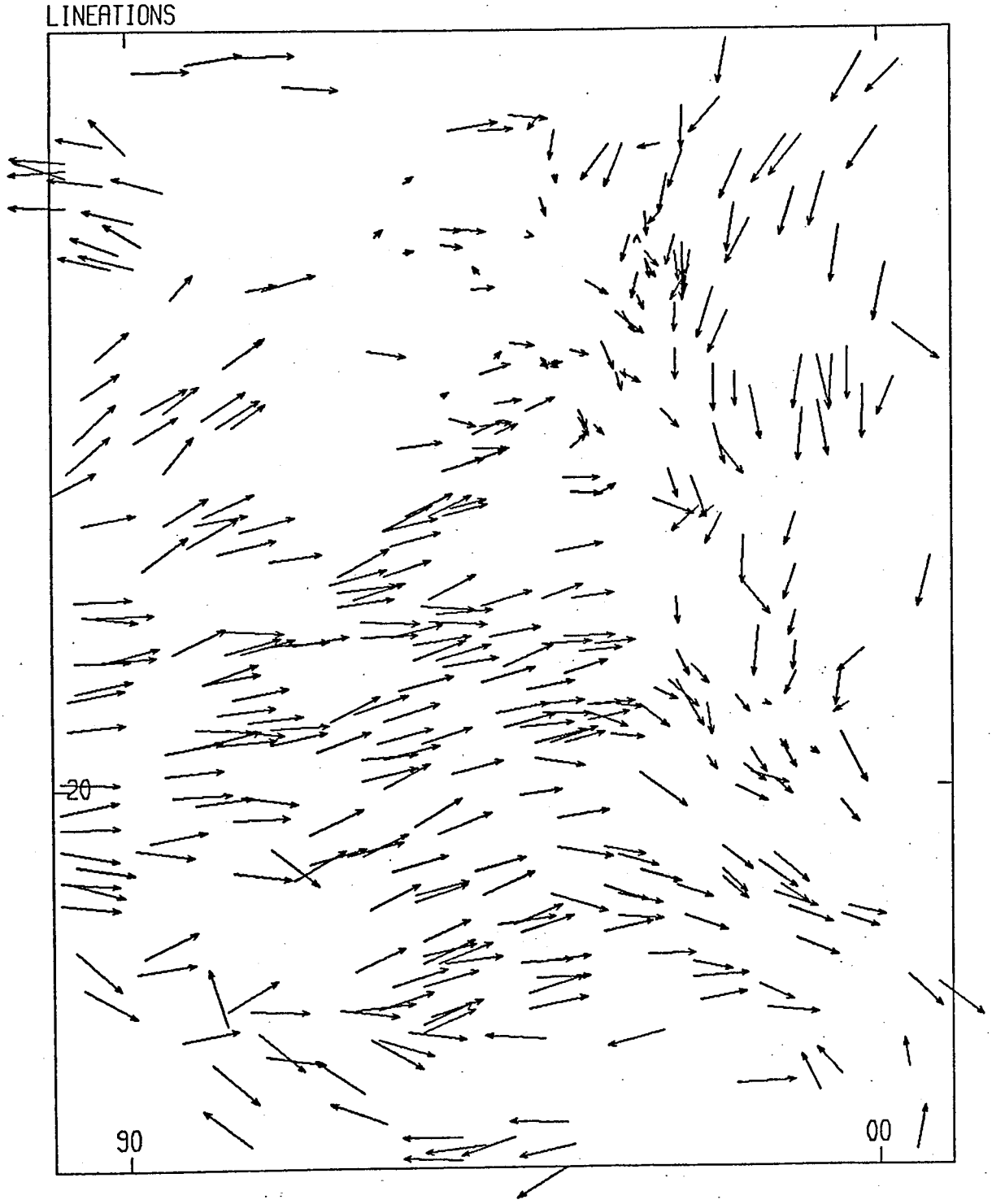
LINEATIONS
20
90
00

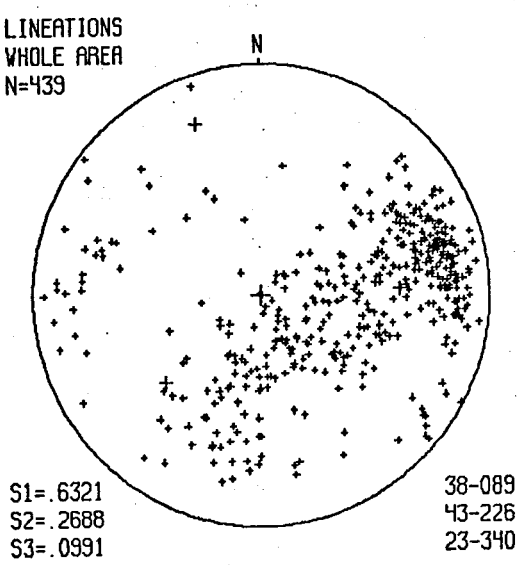
LINEATIONS
WHOLE AREA
N=439
N
S1=.6321
S2=.2688
S3=.0991
38-089
43-226
23-340

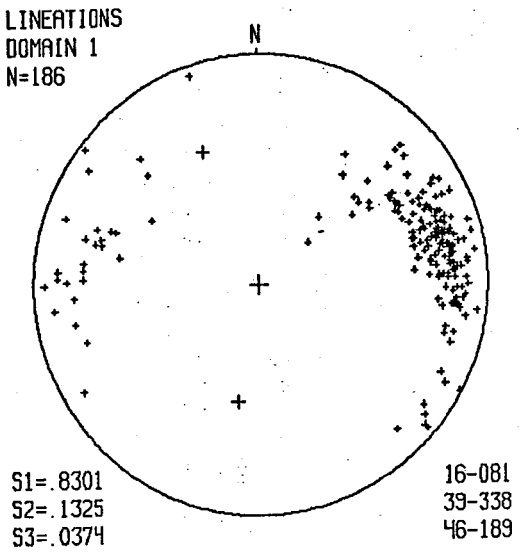
LINEATIONS
DOMAIN 1
N=186
N
S1=.8301
S2=.1325
S3=.0374
16-081
39-338
46-189

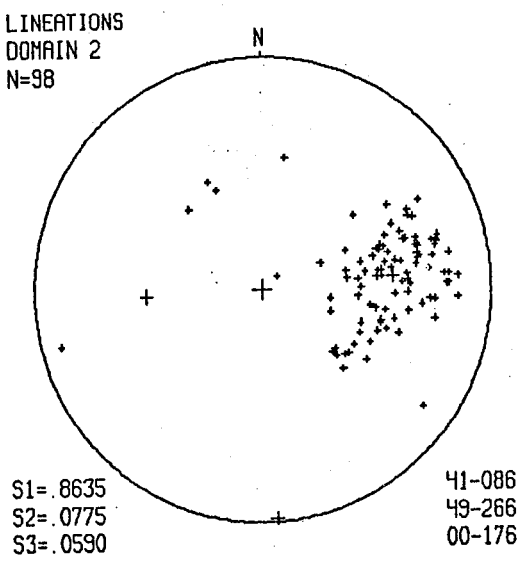
LINEATIONS
DOMAIN 2
N=98
N
S1=.8635
S2=.0775
S3=.0590
41-086
49-266
00-176

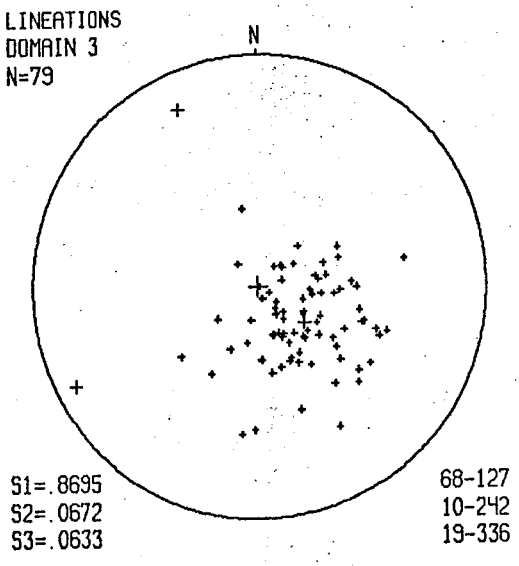
LINEATIONS
DOMAIN 3
N=79
N
S1=.8695
S2=.0672
S3=.0633
68-127
10-242
19-336

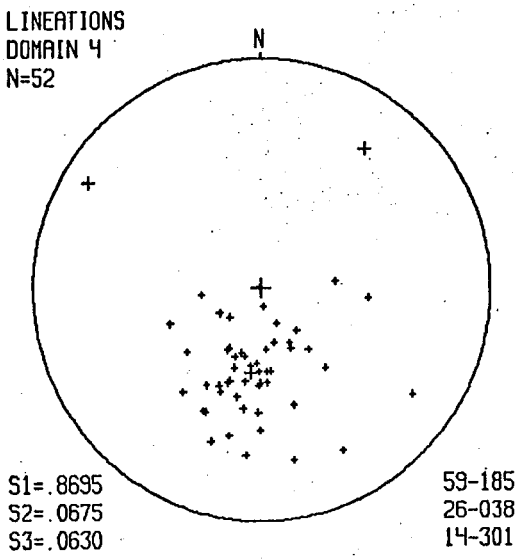
LINEATIONS
DOMAIN 4
N=52
N
S1=.8695
S2=.0675
S3=.0630
59-185
26-038
14-301

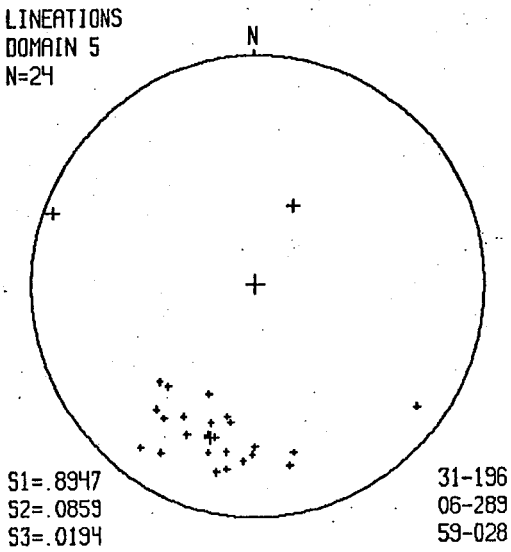
LINEATIONS
DOMAIN 5
N=24
N
S1=.8947
S2=.0859
S3=.0194
31-196
06-289
59-028

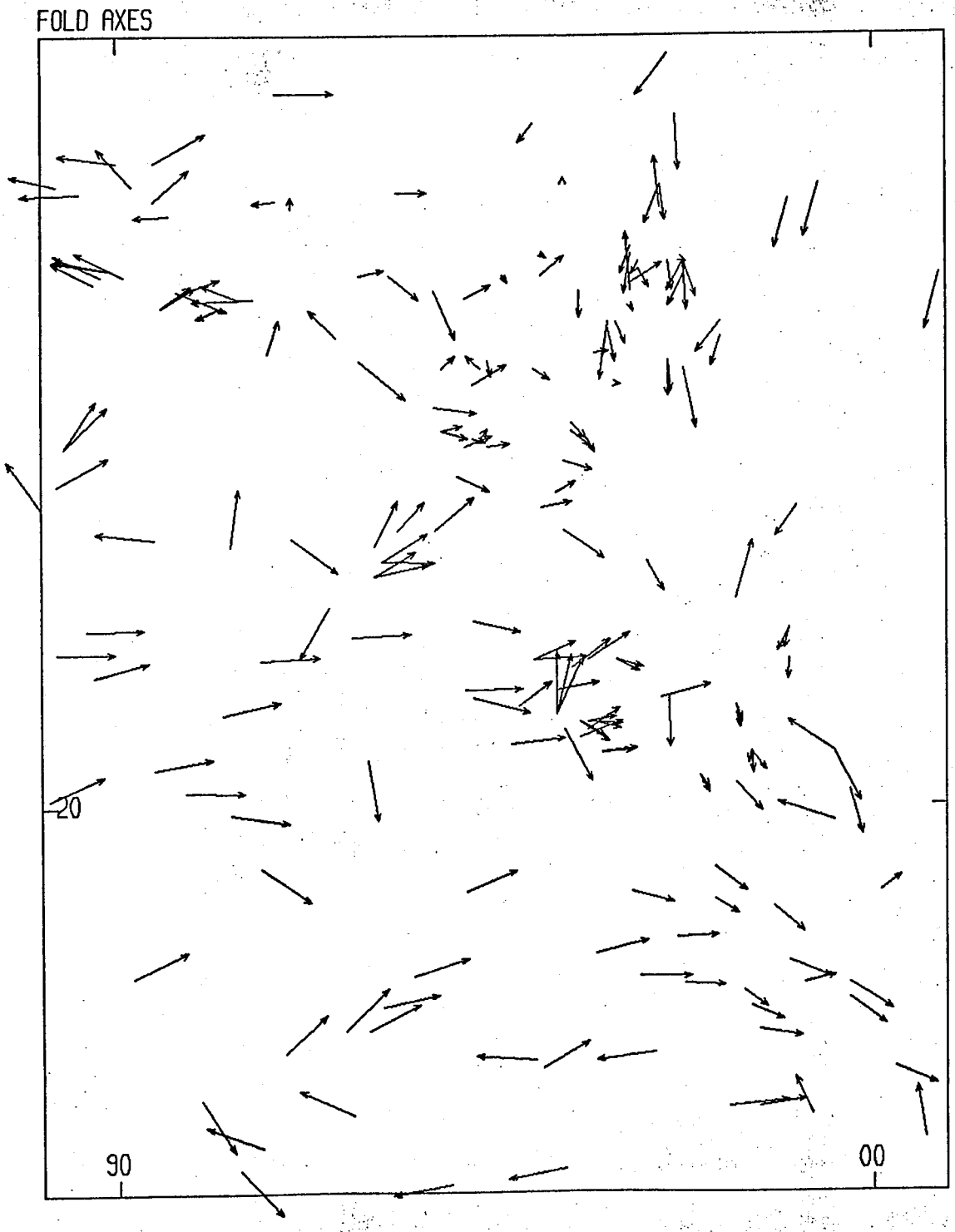
FOLD AXES
20
90
00

FOLD AXES
WHOLE AREA
N=199

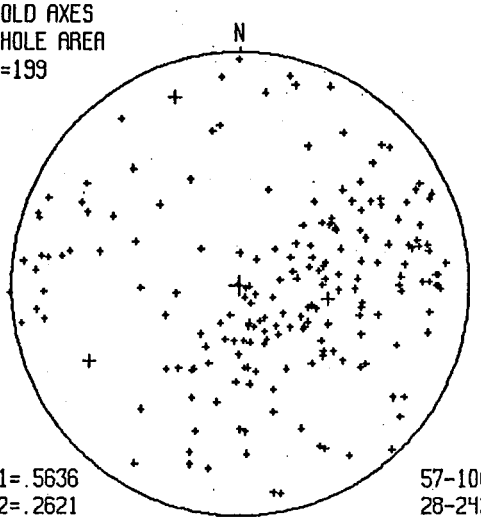

S1=.5636 57-100
S2=.2621 28-242
S3=.1743 17-341

FOLD AXES
DOMAIN 1
N=58

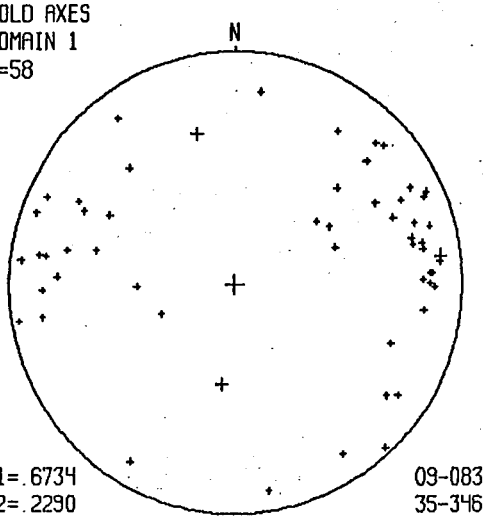

S1=.6734 09-083
S2=.2290 35-346
S3=.0976 53-185

FOLD AXES
DOMAIN 2
N=58

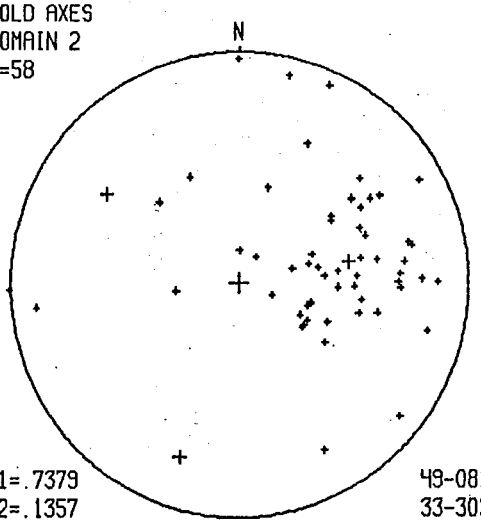

S1=.7379 49-081
S2=.1357 33-303
S3=.1264 22-198

FOLD AXES
DOMAIN 3
N=47

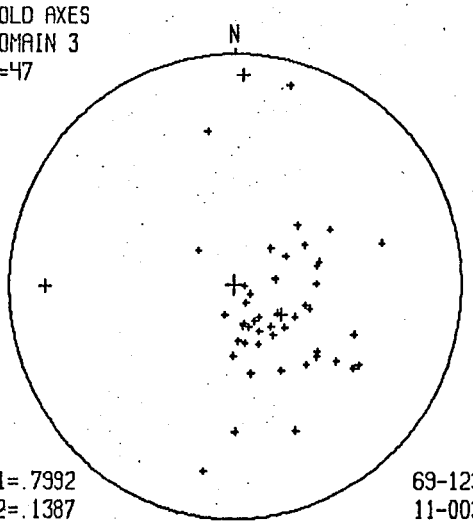

S1=.7992 69-123
S2=.1387 11-003
S3=.0621 18-269

FOLD AXES
DOMAIN 4
N=32

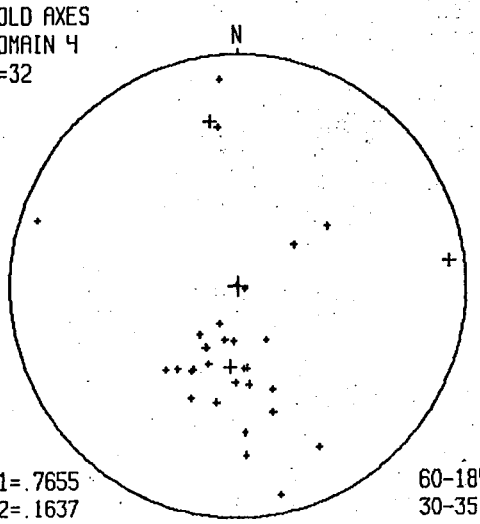

S1=.7655
S2=.1637
S3=.0708

60-184
30-351
06-084

FOLD AXES
DOMAIN 5
N=4

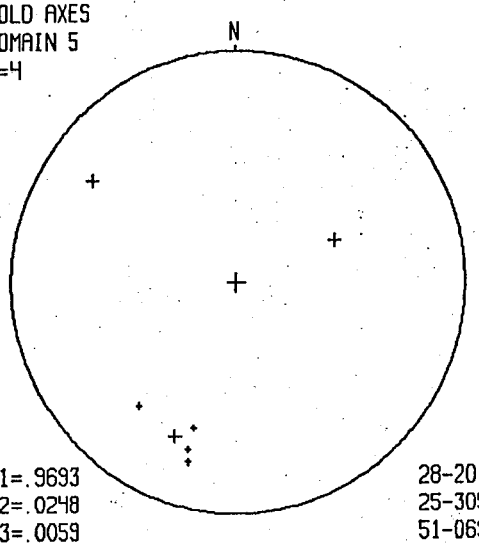

S1=.9693
S2=.0248
S3=.0059

28-201
25-305
51-069

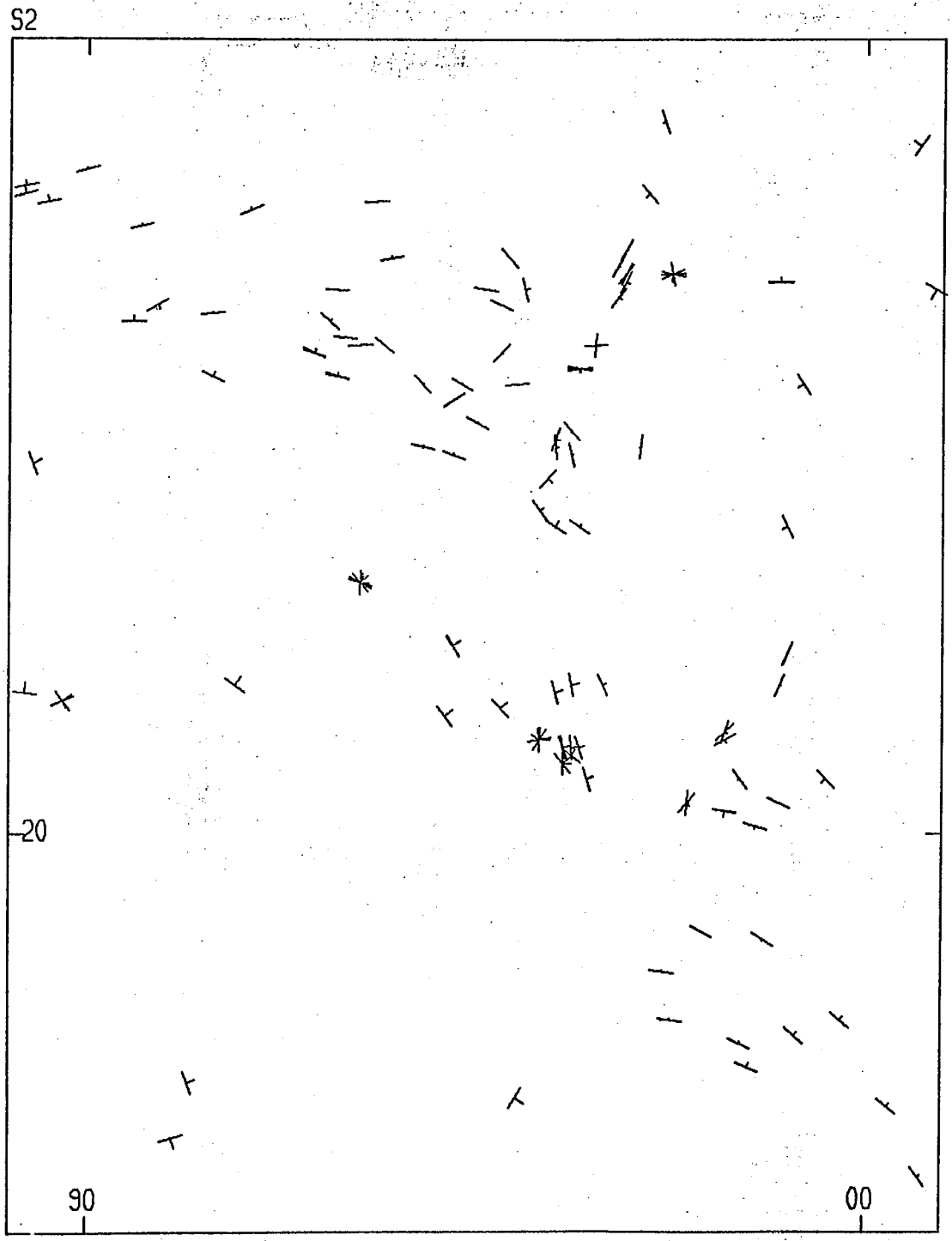
S2
20
90
00

S2
WHOLE AREA
N=125

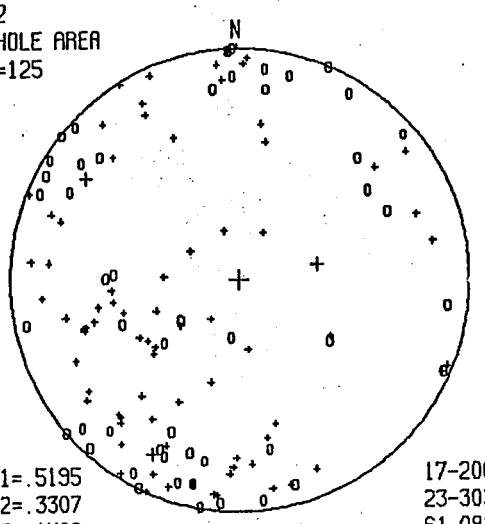

S1=.5195
S2=.3307
S3=.1499

17-206
23-303
61-082

S2
DOMAIN 1
N=18

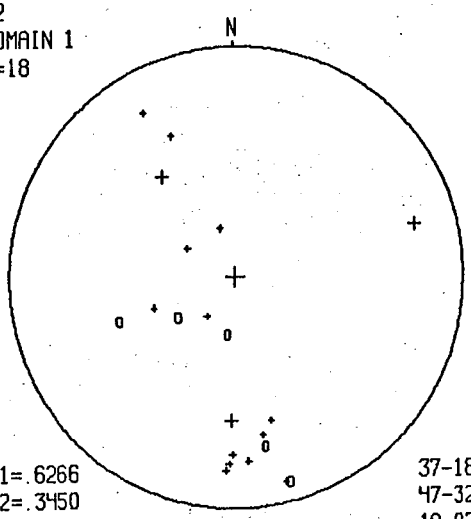

S1=.6266
S2=.3450
S3=.0285

37-181
47-324
19-076

S2
DOMAIN 2
N=42

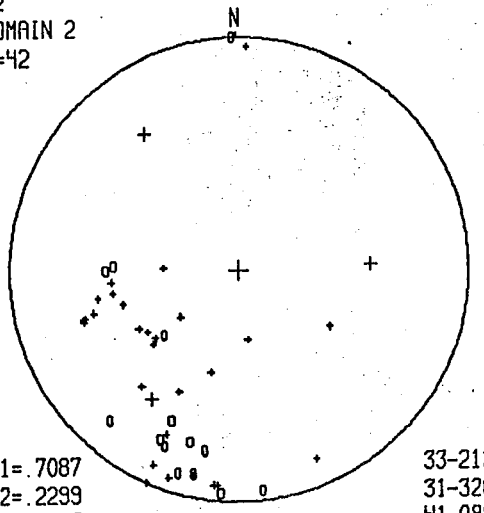

S1=.7087
S2=.2299
S3=.0615

33-213
31-326
41-089

S2
DOMAIN 3
N=44

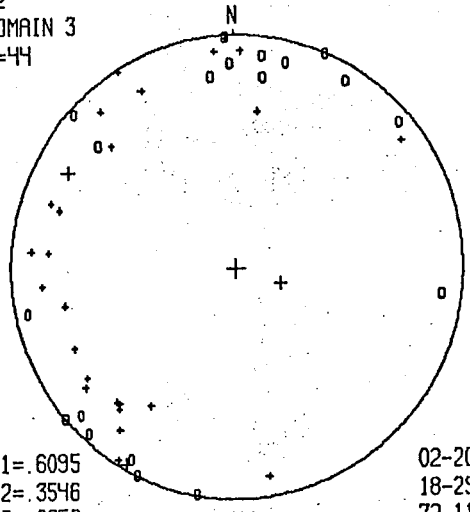

S1=.6095
S2=.3546
S3=.0359

02-209
18-299
72-111

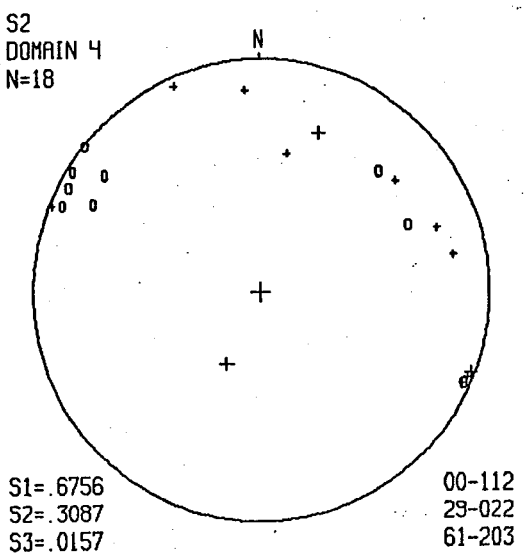
S2
DOMAIN 4
N=18
N
S1=.6756
S2=.3087
S3=.0157
00-112
29-022
61-203

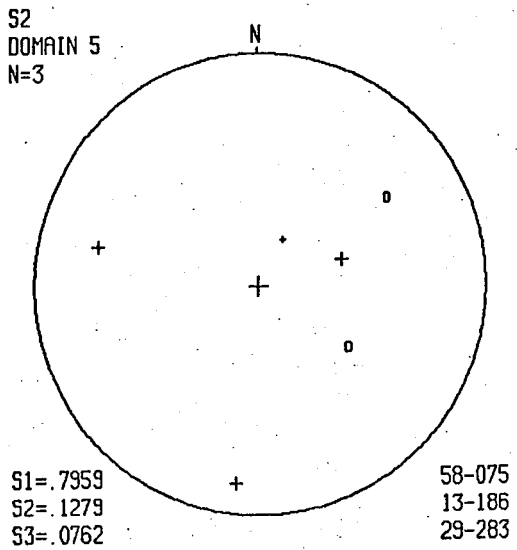
S2
DOMAIN 5
N=3
N
S1=.7959
S2=.1279
S3=.0762
58-075
13-186
29-283

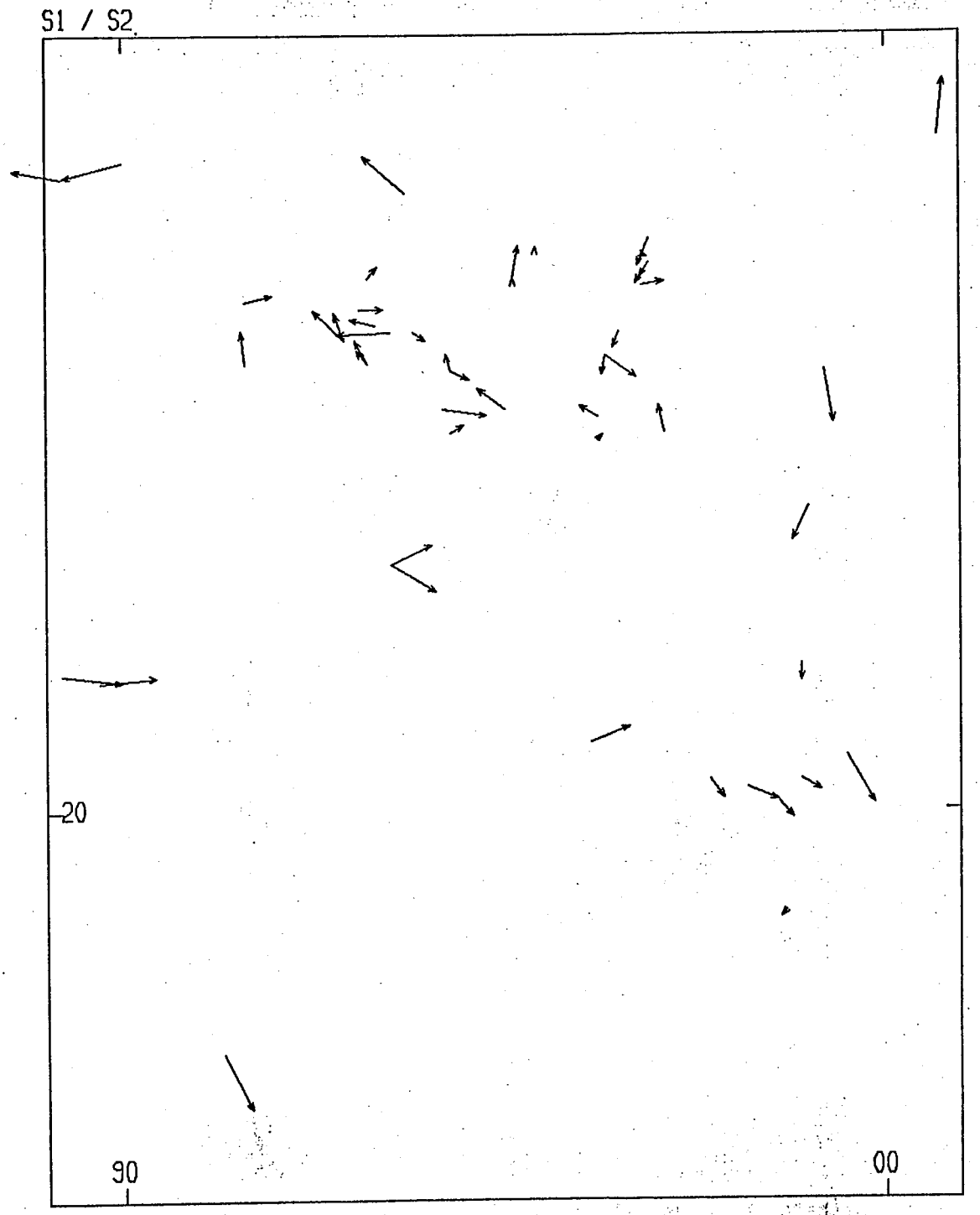
S1 / S2
20
90
00

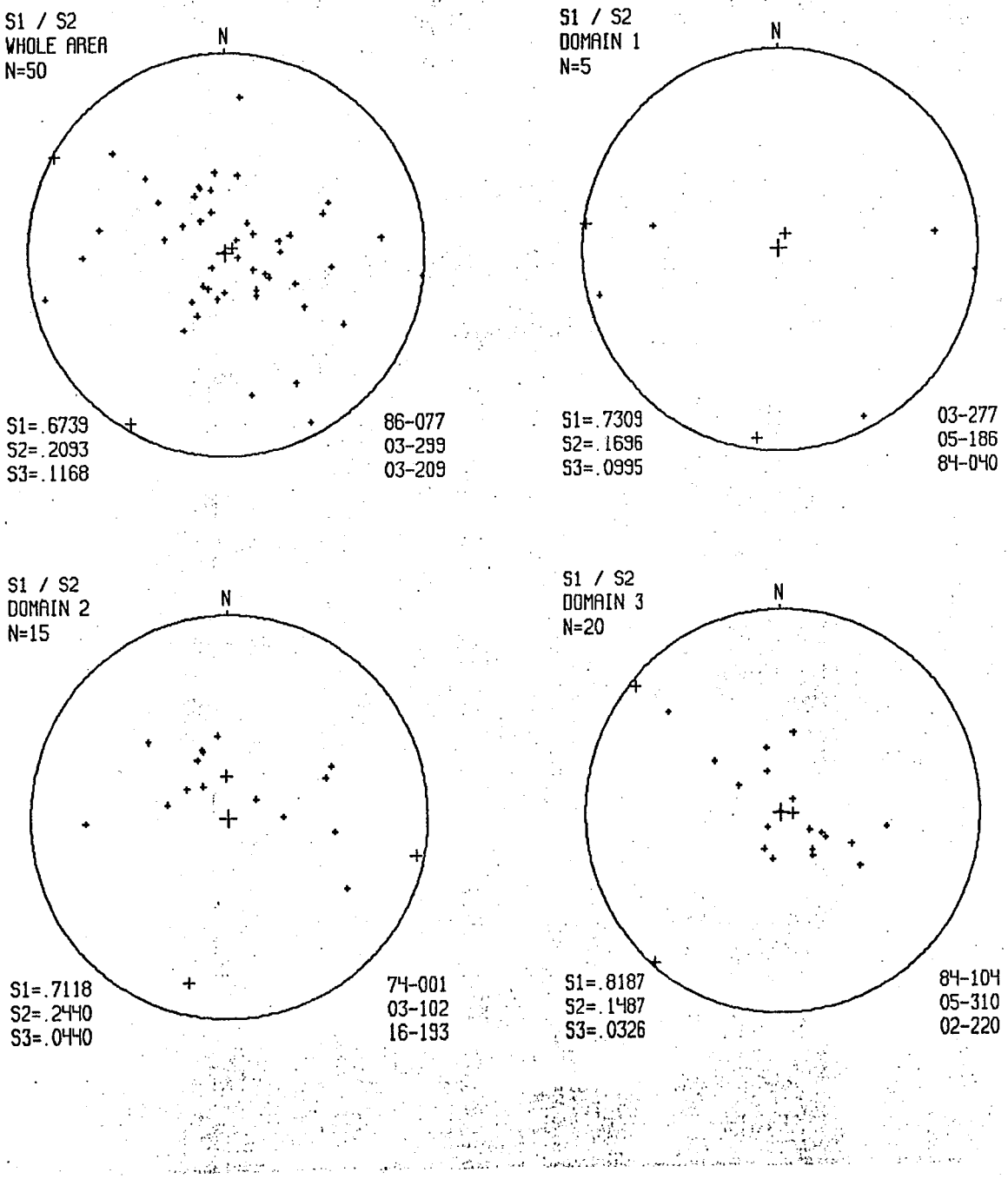
S1 / S2
WHOLE AREA
N=50
N
S1=.6739
S2=.2093
S3=.1168
86-077
03-299
03-209
S1 / S2
DOMAIN 1
N=5
N
S1=.7309
S2=.1696
S3=.0995
03-277
05-186
84-040
S1 / S2
DOMAIN 2
N=15
N
S1=.7118
S2=.2440
S3=.0440
74-001
03-102
16-193
S1 / S2
DOMAIN 3
N=20
N
S1=.8187
S2=.1487
S3=.0326
84-104
05-310
02-220

S1 / S2
DOMAIN 4
N=8

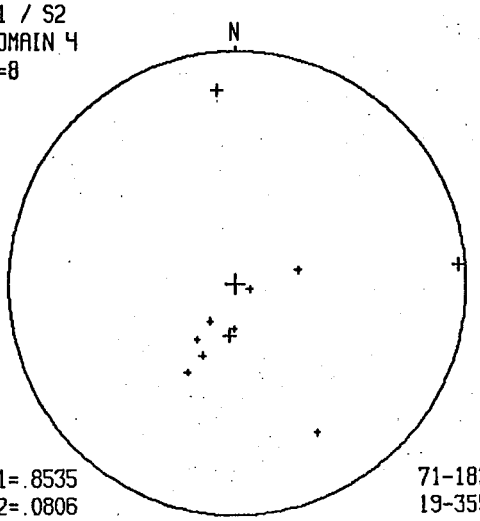

S1=.8535
S2=.0806
S3=.0660

71-183
19-355
02-086

S1 / S2
DOMAIN 5
N=2

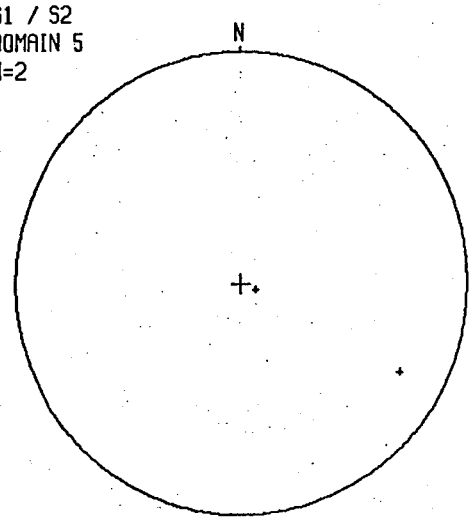

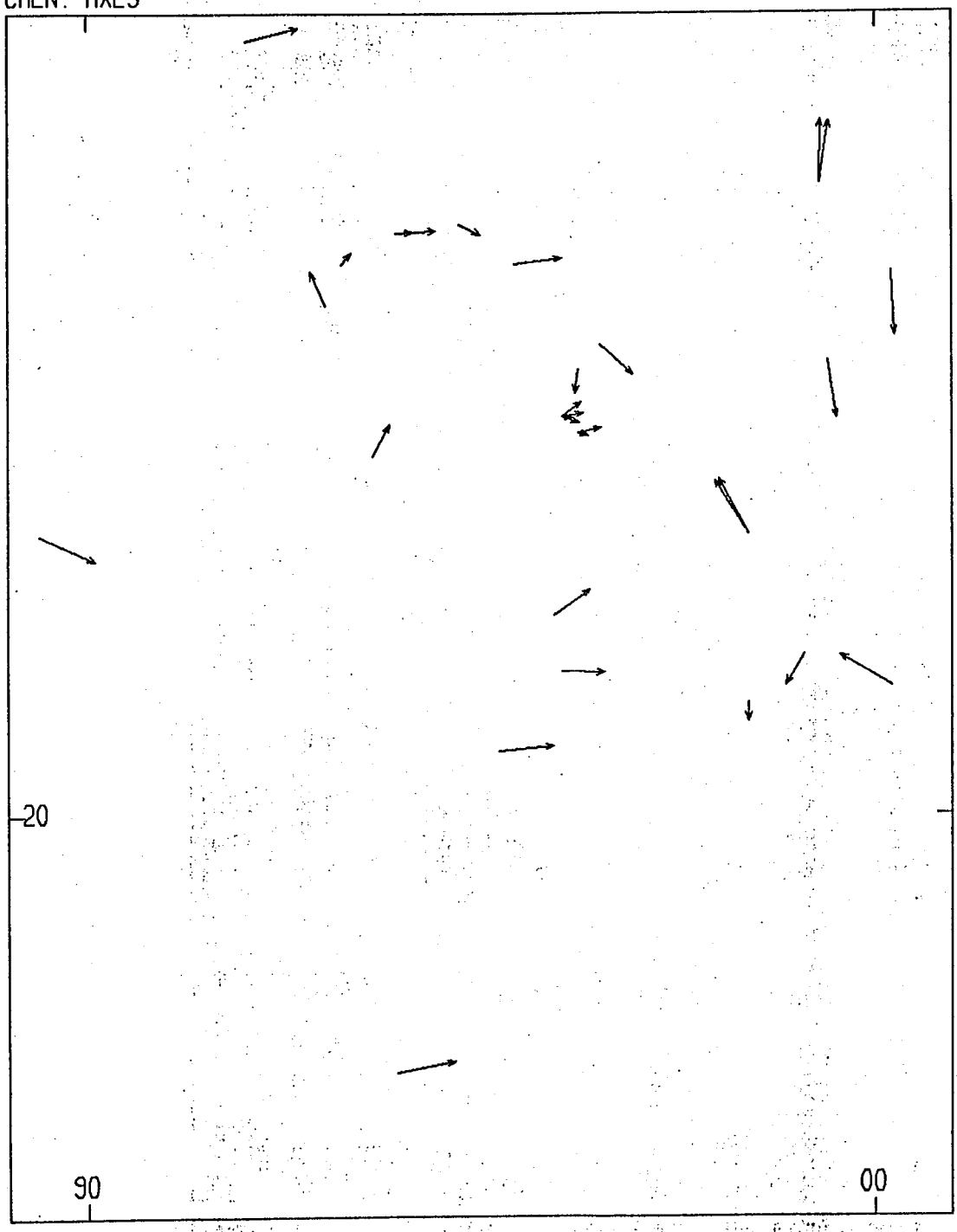
CREN. AXES
20
90
00

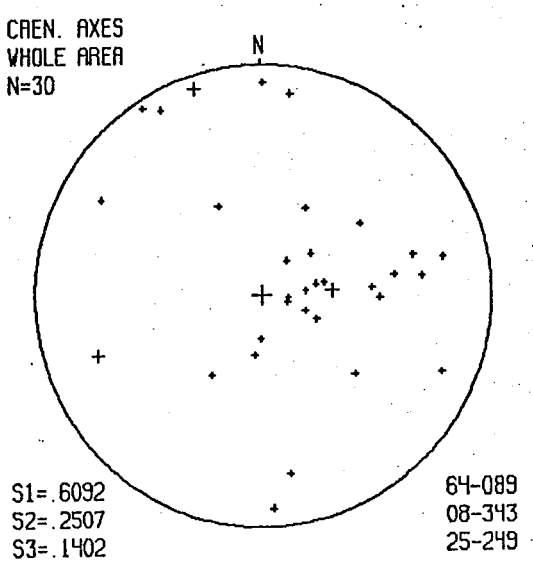
CREN. AXES
WHOLE AREA
N=30
N
S1=.6092
S2=.2507
S3=.1402
64-089
08-343
25-249

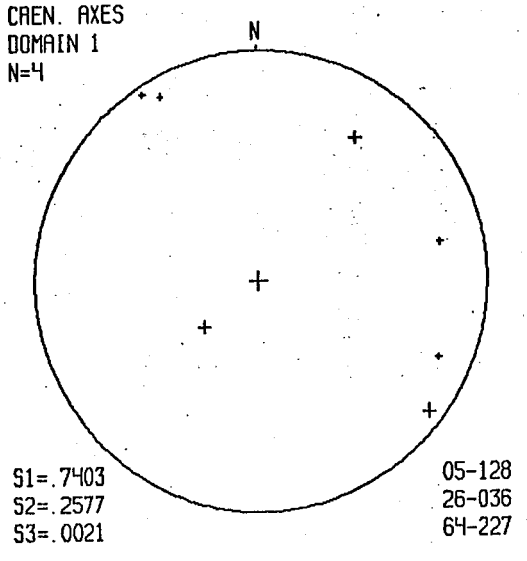
CREN. AXES
DOMAIN 1
N=4
N
S1=.7403
S2=.2577
S3=.0021
05-128
26-036
64-227

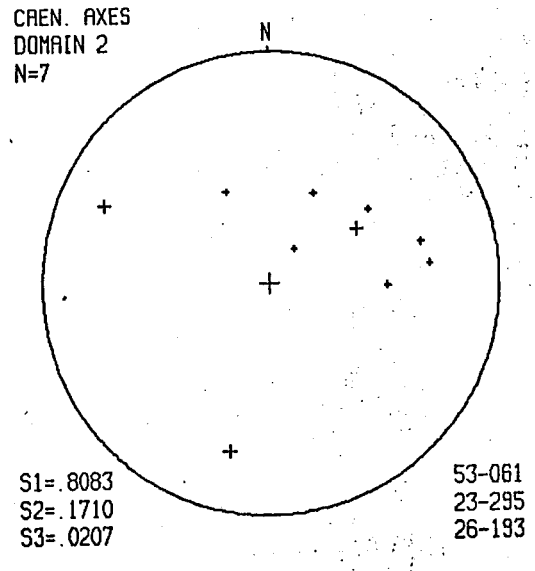
CREN. AXES
DOMAIN 2
N=7
N
S1=.8083
S2=.1710
S3=.0207
53-061
23-295
26-193

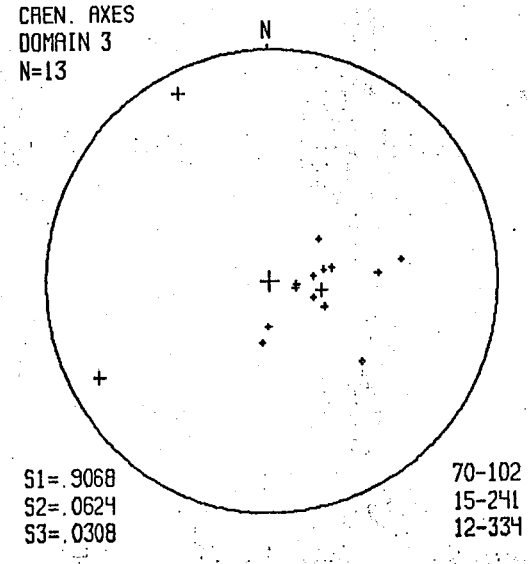
CREN. AXES
DOMAIN 3
N=13
N
S1=.9068
S2=.0624
S3=.0308
70-102
15-241
12-334

CREN. AXES
DOMAIN 4
N=2

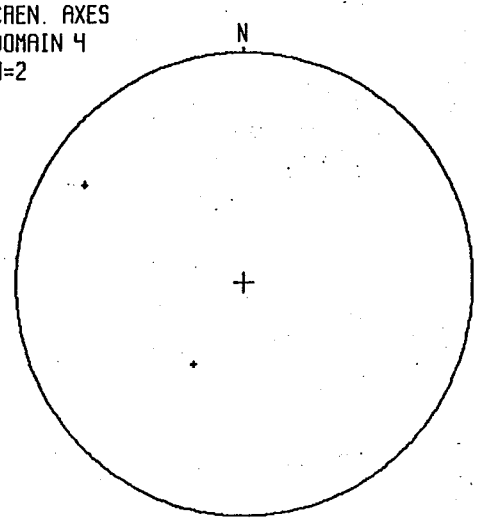

CREN. AXES
DOMAIN 5
N=4

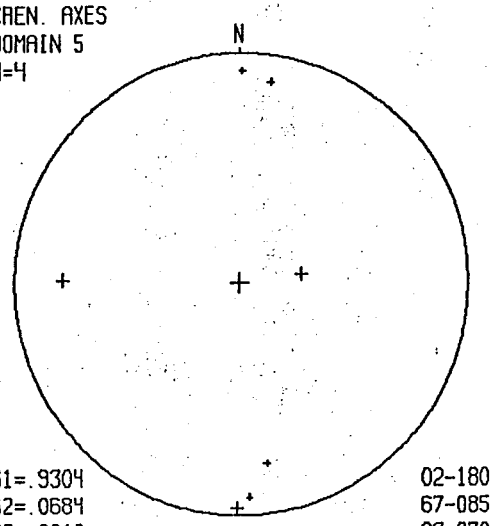

S1=.9304
S2=.0684
S3=.0012

02-180
67-085
23-270

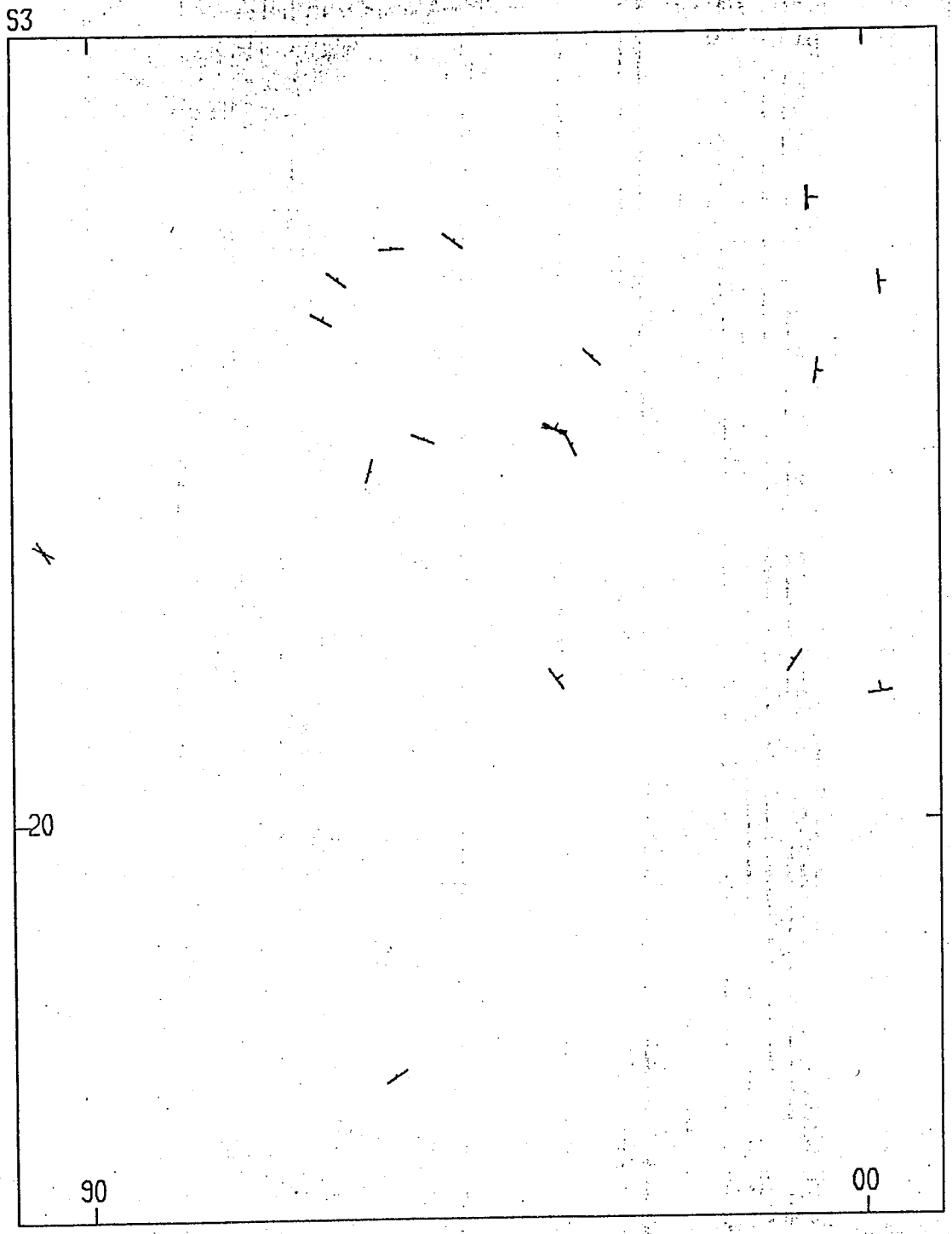
S3
20
90
00

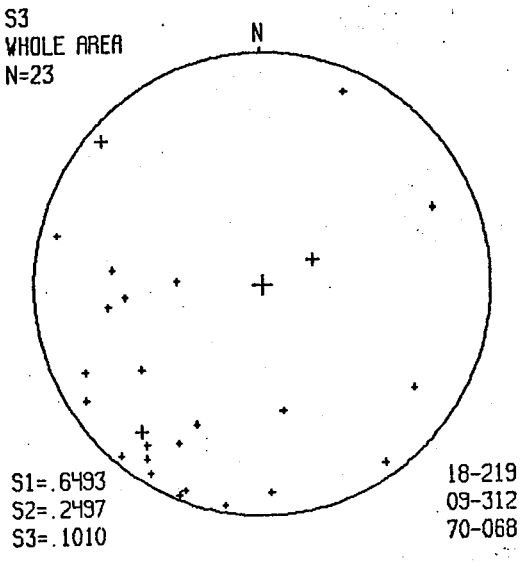
S3
WHOLE AREA
N=23
N
S1=.6493
S2=.2497
S3=.1010
18-219
09-312
70-068

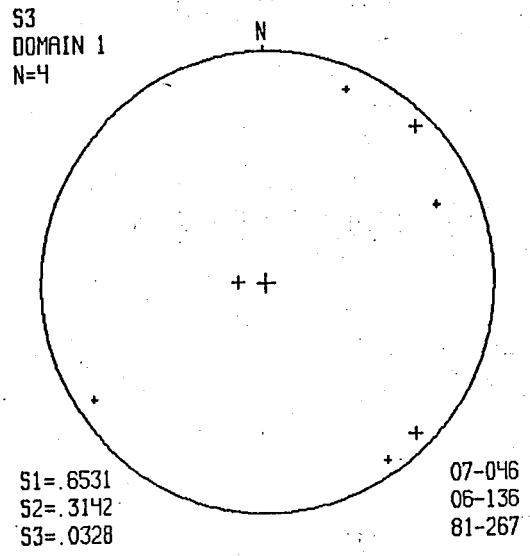
S3
DOMAIN 1
N=4
N
S1=.6531
S2=.3142
S3=.0328
07-046
06-136
81-267

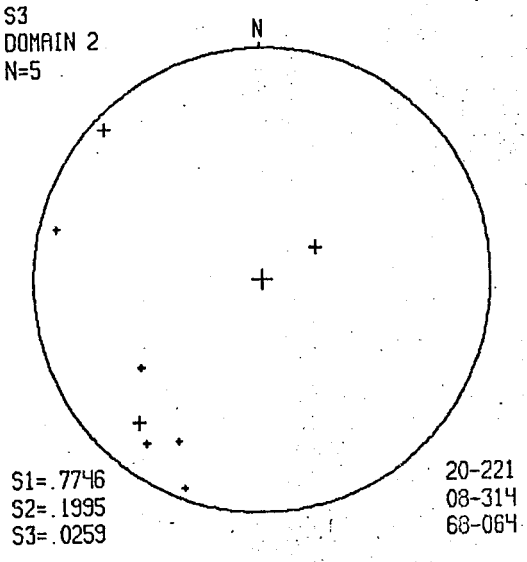
S3
DOMAIN 2
N=5
N
S1=.7746
S2=.1995
S3=.0259
20-221
08-314
68-064

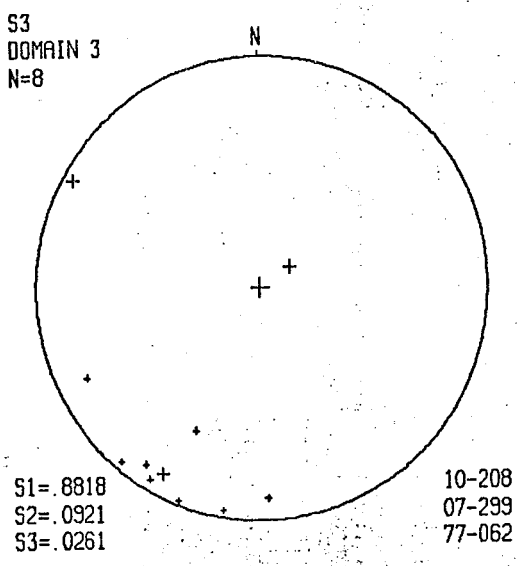
S3
DOMAIN 3
N=8
N
S1=.8818
S2=.0921
S3=.0261
10-208
07-299
77-062

S3
DOMAIN 4
N=2

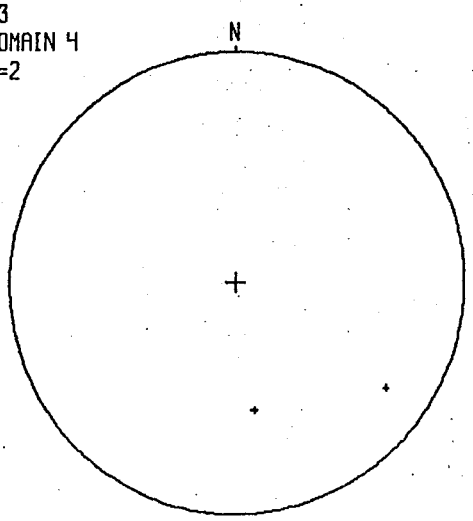

S3
DOMAIN 5
N=4

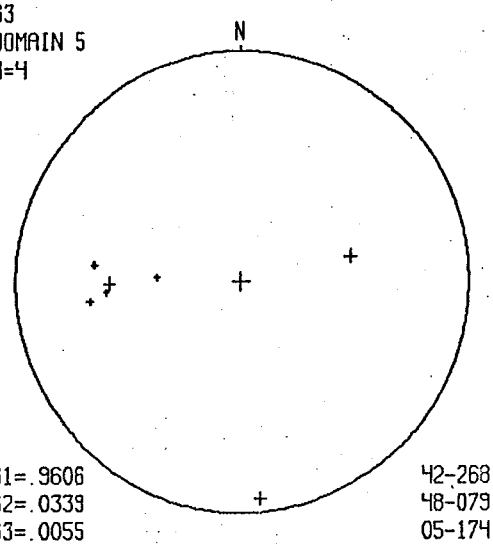

S1=.9606
S2=.0339
S3=.0055

42-268
48-079
05-174

APPENDIX B - COMPUTER PROGRAMS

The following programs were written in FORTRAN 77, and run on the University of Minnesota Cyber system. The main system-dependent functions that might require modification for other systems are as follows. Programs EIGEN and EIGLIST require an eigenvalue function, the one used here is the International Mathematic and Scientific Library function EIGRS. Programs STGRAPH and LINEPL require a simple two-dimensional graphics plotting package, the University of Minnesota Computer Center MNCORE package was used here. Program SHEATH requires a three-dimensional plotting package, also provided in the MNCORE package.

EIGEN calculates the eigenvectors and eigenvalues for any given set of linear or planar orientation data. EIGLIST creates a list of eigenvectors, with factors for their analysis, for each square kilometer of the map area. DSEARCH creates a list of of all foliations, or eigen-foliations, compatible with a given π axis for a domain boundary search. STGRAPH and LINEPL plot orientation data in the form of equal-area stereograms and maps respectively.

SHEATH deforms a specified surface and displays the result in the form of a three-dimensional object, or as variously oriented cross-sections. SHEAROR calculates simulated orientation data for the given deformed surface.

The final page is a sample of a short data file.

```
      PROGRAM EIGEN(INPUT,OUTPUT,TAPE5=INPUT,TAPE6=OUTPUT)
C     THIS PROGRAM IS FOR CALCULATION OF EIGENVALUES AND
C  EIGENVECTORS OF STRUCTURAL ORIENTATION DATA. A FILE OF
C  FOLIATION OR LINEATION DATA IS INPUT; NORMALISED
C  EIGENVALUES AND EIGENVECTORS ARE OUTPUT. EIGENVECTORS
C  ARE GIVEN BOTH AS VECTOR COMPONENTS AND AS PLUNGE AND
C  TRENDS. THE SUM AND THE SUM OF THE PRODUCTS OF THE
C  DIRECTION COSINES ARE ALSO GIVEN. THE PROGRAM USES AN IMSL
C  FUNCTION EIGRS FROM THE LIBRARY; USE FETCH,IMSL/V=M77.
C
C     THE INPUT FILE MUST CONTAIN THREE LABELS, DATA TYPE
C  (1-5 FOR LINEATIONS, >5 FOR FOLIATIONS), NUMBER OF
C  MEASUREMENTS, AND THE DATA. THE DATA IS IN THE FORM:
C  E-W MAP COORDINATE, N-S MAP COORDINATE, PLUNGE, TREND
C  (OR STRIKE, DIP, DIP DIRECTION). DUMMY MAP COORDINATES
C  MAY BE USED.
C                  -F.W. VOLLMER, 1984, U OF MN
C
      DIMENSION EIGVAL(3),EIGVEC(3,3),EPL(3),ETR(3),WK(10)
      INTEGER TYPE,PL,TR,STR,DIP,AZ,ANG
      REAL L(3),M(6),N(3)
      CHARACTER*2,DIR
      CHARACTER*10,LABEL1,LABEL2,LABEL3
      R=0.017453293
      N(1)=N(2)=N(3)=0
      DO 5 I4=1,6
    5 M(I4)=0
      READ(5,10)LABEL1
      READ(5,10)LABEL2
      READ(5,10)LABEL3
   10 FORMAT(A10)
      READ(5,*) TYPE,NUM
      DO 60 I=1,NUM
      IF (TYPE.GT.5) GO TO 20
      READ(5,15) IX,IY,PL,TR
   15 FORMAT(I3,1X,I3,1X,I2,1X,I3)
      GO TO 30
   20 READ(5,25) IX,IY,STR,DIP,DIR
   25 FORMAT(I3,1X,I3,1X,I3,1X,I2,1X,A2)
C  CONVERT STRIKE TO TREND OF NORMAL.
      TR=STR+90
      IF (TR.GT.360) TR=TR-360
      IF (DIR.EQ.'N ') AZ=0
      IF (DIR.EQ.'NE') AZ=45
      IF (DIR.EQ.'E ') AZ=90
      IF (DIR.EQ.'SE') AZ=135
      IF (DIR.EQ.'S ') AZ=180
      IF (DIR.EQ.'SW') AZ=225
      IF (DIR.EQ.'W ') AZ=270
      IF (DIR.EQ.'NW') AZ=315
      IF (DIR.EQ.'  ') AZ=0
      ANG=ABS(TR-AZ)
      IF (ANG.GT.180) ANG=360-ANG
      IF (ANG.LT.90) TR=TR+180
```

```
      IF (TR.GT.360) TR=TR-360
      PL=90-DIP
C  CALCULATE DIRECTION COSINES.
   30 L(1)=COS(TR*R)*COS(PL*R)
      L(2)=SIN(TR*R)*COS(PL*R)
      L(3)=SIN(PL*R)
C  CALCULATE DIRECTION COSINE PRODUCT MATRIX.
      M(1)=M(1)+L(1)**2
      M(2)=M(2)+L(2)*L(1)
      M(3)=M(3)+L(2)**2
      M(4)=M(4)+L(3)*L(1)
      M(5)=M(5)+L(3)*L(2)
      M(6)=M(6)+L(3)**2
      N(1)=N(1)+L(1)
      N(2)=N(2)+L(2)
   60 N(3)=N(3)+L(3)
      CALL EIGRS(M,3,2,EIGVAL,EIGVEC,3,WK,IER)
      DO 90 I2=1,3
      EPL(I2)=ASIN(EIGVEC(3,I2))/R
      ETR(I2)=ATAN2(EIGVEC(2,I2),EIGVEC(1,I2))/R
      IF (EPL(I2).LT.0.0) ETR(I2)=ETR(I2)+180
      EPL(I2)=ABS(EPL(I2))
      IF (ETR(I2).LT.0.0) ETR(I2)=ETR(I2)+360
      IF (ETR(I2).GT.360.0) ETR(I2)=ETR(I2)-360
   90 EIGVAL(I2)=EIGVAL(I2)/NUM
      WRITE(6,100)LABEL1
      WRITE(6,100)LABEL2
      WRITE(6,100)LABEL3
  100 FORMAT(A10)
      WRITE(6,110)M(1),N(1),M(2),M(3),N(2),M(4),
     +M(5),M(6),N(3)
  110 FORMAT(/7X,1HL,10X,1HM,10X,1HN/
     +1HL,1X,F10.5,25X,F10.5/
     +1HM,1X,F10.5,1X,F10.5,14X,F10.5/
     +1HN,1X,F10.5,1X,F10.5,1X,F10.5,3X,F10.5//)
      WRITE(6,*)'EIGENVALUES'
      DO 130 J=1,3
  130 WRITE(6,140) EIGVAL(J),EIGVEC(1,J),EIGVEC(2,J),
     +EIGVEC(3,J),EPL(J),ETR(J)
  140 FORMAT(F7.5,1X,1H(,F7.5,1X,F7.5,1X,F7.5,1H),
     +1X,F5.2,1X,F6.2)
      WRITE(6,150)IER
  150 FORMAT(/12HERROR FACTOR,1X,I5)
      STOP
      END
```

```
      PROGRAM EIGLIST(INPUT,OUTPUT,TAPE5=INPUT,TAPE6=OUTPUT)
C     THIS PROGRAM CALCULATES EIGENVECTORS FOR ORIENTATION
C   DATA IN EACH SQUARE-KILOMETER OF THE MAP AREA. THESE
C   ARE GIVEN AS BEST-FIT FOLIATIONS AND FOLD AXES FOR
C   FOLIATION DATA, AND AS BEST-FIT LINEATIONS FOR
C   LINEATION DATA. K AND C PARAMETERS, WHICH ARE MEASURES
C   OF DATA CLUSTERING, ARE ALSO CALCULATED FOR EVALUATION
C   OF THE VECTORS.
C     THE PROGRAM USES AN IMSL FUNCTION EIGERS FROM THE
C   LIBRARY; USE FETCH,IMSL/V=M77.
C     THE INPUT FILE MUST CONTAIN THREE LABELS, DATA TYPE
C   (1-5 FOR LINEATIONS, >5 FOR FOLIATIONS), NUMBER OF
C   MEASUREMENTS, AND THE DATA. THE DATA IS IN THE FORM:
C   E-W MAP COORDINATE, N-S MAP COORDINATE, PLUNGE, TREND
C   (OR STRIKE, DIP, DIP DIRECTION). THE DATA MUST BE
C   ORDERED BY SQUARE KILOMETER, LISTED FROM NORTH TO
C   SOUTH BY COLUMN.
C                          - F.W. VOLLMER, U. OF MN., 1984
C
      DIMENSION EIGVAL(3),EIGVEC(3,3),WK(10)
      INTEGER TYPE,PL,TR,STR,DIP,AZ,ANG,EPL(3),ETR(3),
     +ESTR,EDIP,PLO,TRO,STRO,DIPO
      REAL L(3),M(6),K
      CHARACTER*2,DIR,EDIR,DIRO
      CHARACTER*10,LABEL1,LABEL2,LABEL3
      R=0.017453293
      NCT=PL=TR=STR=DIP=0
      DIR='  '
      DO 5 I4=1,6
    5 M(I4)=0
      READ(5,10)LABEL1
      READ(5,10)LABEL2
      READ(5,10)LABEL3
      WRITE(6,10)LABEL1
      WRITE(6,10)LABEL2
      WRITE(6,10)LABEL3
   10 FORMAT(A10)
      READ(5,*) TYPE,NUM
      DO 200 I=1,NUM
      IF (TYPE.GT.5) GO TO 20
C  READ IN LINEATION DATA.
      READ(5,15) IX,IY,PL,TR
   15 FORMAT(I3,1X,I3,1X,I2,1X,I3)
      IF (I.EQ.1) IXKM=(INT(IX/10))*10
      IF (I.EQ.1) IYKM=(INT(IY/10))*10
      IF (((IY-IYKM).GT.9).OR.((IY-IYKM).LT.0)) GO TO 60
   17 PLO=PL
      TRO=TR
      NCT=NCT+1
      GO TO 30
C  READ IN FOLIATION DATA.
   20 READ(5,25) IX,IY,STR,DIP,DIR
   25 FORMAT(I3,1X,I3,1X,I3,1X,I2,1X,A2)
      IF (I.EQ.1) IXKM=(INT(IX/10))*10
```

```
      IF (I.EQ.1) IYKM=(INT(IY/10))*10
      IF (((IY-IYKM).GT.9).OR.((IY-IYKM).LT.0)) GO TO 60
   26 STRO=STR
      DIPO=DIP
      DIRO=DIR
      NCT=NCT+1
C  CONVERT STRIKE TO TREND OF NORMAL.
      TR=STR+90
      IF (TR.GT.360) TR=TR-360
      IF (DIR.EQ.'N ') AZ=0
      IF (DIR.EQ.'NE') AZ=45
      IF (DIR.EQ.'E ') AZ=90
      IF (DIR.EQ.'SE') AZ=135
      IF (DIR.EQ.'S ') AZ=180
      IF (DIR.EQ.'SW') AZ=225
      IF (DIR.EQ.'W ') AZ=270
      IF (DIR.EQ.'NW') AZ=315
      IF (DIR.EQ.'  ') AZ=0
      ANG=ABS(TR-AZ)
      IF (ANG.GT.180) ANG=360-ANG
      IF (ANG.LT.90) TR=TR+180
      IF (TR.GT.360) TR=TR-360
      PL=90-DIP
C  CALCULATE DIRECTION COSINES.
   30 L(1)=COS(TR*R)*COS(PL*R)
      L(2)=SIN(TR*R)*COS(PL*R)
      L(3)=SIN(PL*R)
C  CALCULATE DIRECTION COSINE PRODUCT MATRIX.
      M(1)=M(1)+L(1)**2
      M(2)=M(2)+L(2)*L(1)
      M(3)=M(3)+L(2)**2
      M(4)=M(4)+L(3)*L(1)
      M(5)=M(5)+L(3)*L(2)
      M(6)=M(6)+L(3)**2
      GO TO 200
   60 IXK=IXKM+5
      IYK=IYKM+5
      IXKM=(INT(IX/10))*10
      IYKM=(INT(IY/10))*10
      IF (NCT.EQ.1) THEN
         EPL(3)=PLO
         ETR(3)=TRO
         ESTR=STRO
         EDIP=DIPO
         EDIR=DIRO
         EPL(1)=ETR(1)=0
         K=C=0.0
         GO TO 100
      ENDIF
      CALL EIGRS(M,3,2,EIGVAL,EIGVEC,3,WK,IER)
      DO 90 I2=1,3
      EPL(I2)=NINT(ASIN(EIGVEC(3,I2))/R)
      ETR(I2)=NINT(ATAN2(EIGVEC(2,I2),EIGVEC(1,I2))/R)
      IF (EPL(I2).LT.0.0) ETR(I2)=ETR(I2)+180
```

```
      EPL(I2)=ABS(EPL(I2))
      IF (ETR(I2).LT.0.0) ETR(I2)=ETR(I2)+360
   90 IF (ETR(I2).GT.360.0) ETR(I2)=ETR(I2)-360
      IF (EIGVAL(1).LT.0.000000001) THEN
         K=C=0.0
         GO TO 100
      ENDIF
      K=ALOG(EIGVAL(3)/EIGVAL(2))/ALOG(EIGVAL(2)/EIGVAL(1))
      C=ALOG(EIGVAL(3)/EIGVAL(1))
  100 IF (TYPE.GT.5) GO TO 140
C  PRINT OUT LINEATION DATA.
      WRITE(6,130)IXK,IYK,EPL(3),ETR(3),NCT,K,C
  130 FORMAT(I3,1X,I3,1X,I2,1X,I3,3X,I3,1X,F6.3,1X,F6.3)
      DO 135 I4=1,6
  135 M(I4)=0
      NCT=0
      GO TO 17
C  CALCULATE FOLIATION STRIKE AND DIP.
  140 IF (NCT.EQ.1) GO TO 145
      ESTR=ETR(3)+90
      IF (ESTR.GT.360) ESTR=ESTR-360
      IF (ETR(3).LT.180) EDIR='W '
      IF (ETR(3).GT.180) EDIR='E '
      IF ((ETR(3).GT.135).AND.(ETR(3).LT.225)) EDIR='N '
      IF ((ETR(3).GT.315).OR.(ETR(3).LT.45)) EDIR='S '
      EDIP=90-EPL(3)
C  PRINT OUT FOLIATION DATA.
  145 WRITE(6,150)IXK,IYK,ESTR,EDIP,EDIR,EPL(1),ETR(1),
     +NCT,K,C
  150 FORMAT(3(I3,1X),I2,1X,A2,3X,I3,1X,I3,3X,I3,1X,
     +F6.3,1X,F6.3)
      DO 170 I4=1,6
  170 M(I4)=0
      NCT=0
      GO TO 26
  200 CONTINUE
      STOP
      END
```

```
      PROGRAM DSEARCH(INPUT,OUTPUT,TAPE5=INPUT,TAPE6=OUTPUT)
C
C     THIS PROGRAM IS FOR USE IN A DOMAIN BOUNDARY SEARCH.
C  AN ESTIMATED PLUNGE (PD) AND TREND (TD) OF A DOMAIN B
C  AXIS IS OBTAINED BY EIGENVALUE ANALYSIS OF AN ARBITRARY
C  INITIAL DOMAIN. THIS IS INPUT INTO THIS PROGRAM WHERE IT
C  IS COMPARED TO A GIVEN FILE OF FOLIATION DATA. ALL
C  FOLIATIONS THAT ARE COMPATABLE WITH THAT AXIS (I.E.
C  CONTAIN THAT AXIS WITHIN A SPECIFIED DEVIATION) ARE THEN
C  OUTPUT AS A LIST. THE LIST CAN THEN BE USED TO DEFINE
C  A NEW DOMAIN AREA. A NEW B AXIS CAN THEN BE CALCULATED
C  FOR THE NEW DOMAIN, AND THE PROCESS REPEATED UNTIL THE
C  DOMAIN BOUNDARIES ARE STABLE.
C                                   -F.W.VOLLMER, U. OF MN., 1984
C
      INTEGER PD,TD,PL,TR,STR,DIP,AZ
      CHARACTER*10,LABEL1,LABEL2,LABEL3
      CHARACTER*2,DIR
C  INPUT PLUNGE AND TREND OF DOMAIN B AXIS.
      PD=73
      TD=107
      R=0.017453293
      READ(5,10)LABEL1
      READ(5,10)LABEL2
      READ(5,10)LABEL3
      WRITE(6,20)LABEL1,PD,TD
   20 FORMAT(A10/1H ,I2,1H-,I3)
   10 FORMAT(A10)
C  READ IN DATA TYPE CODE, AND NUMBER OF MEASUREMENTS.
      READ(5,*)TYPE,NUM
      DO 50 I=1,NUM
C  READ IN FOLIATION DATA.
      READ(5,25) IX,IY,STR,DIP,DIR
   25 FORMAT(I3,1X,I3,1X,I3,1X,I2,1X,A2)
C  CONVERT STRIKE TO TREND OF FOLIATION NORMAL.
      TR=STR+90
      IF (TR.GT.360) TR=TR-360
      IF (DIR.EQ.'N ') AZ=0
      IF (DIR.EQ.'NE') AZ=45
      IF (DIR.EQ.'E ') AZ=90
      IF (DIR.EQ.'SE') AZ=135
      IF (DIR.EQ.'S ') AZ=180
      IF (DIR.EQ.'SW') AZ=225
      IF (DIR.EQ.'W ') AZ=270
      IF (DIR.EQ.'NW') AZ=315
      IF (DIR.EQ.'  ') AZ=0
      ANG=ABS(TR-AZ)
      IF (ANG.GT.180) ANG=360-ANG
      IF (ANG.LT.90) TR=TR+180
      IF (TR.GT.360) TR=TR-360
```

```
C  CONVERT DIP TO PLUNGE OF FOLIATION NORMAL.
      PL=90-DIP
C  CALCULATE ANGLE BETWEEN FOLIATION NORMAL AND B AXIS.
      ANG=ACOS((COS(PD*R)*COS(TD*R)*COS(PL*R)*COS(TR*R))+
     +(COS(PD*R)*SIN(TD*R)*COS(PL*R)*SIN(TR*R))+(SIN(PD*R)
     +*SIN(PL*R)))
      IF (ANG.LT.0.0) ANG=ANG+360*R
      IF (ANG.GT.180*R) ANG=ANG-180*R
      IF (ANG.GT.90*R) ANG=180*R-ANG
C  REJECT IF ANGLE WITH FOLIATION NORMAL IS LESS THAN 80.
      IF (ANG.GT.R*80) THEN
         ANG=ANG/R
         WRITE(6,60)IX,IY,STR,DIP,DIR,ANG
      ENDIF
   50 CONTINUE
   60 FORMAT(I3,1X,I3,1X,I3,1X,I2,1X,A2,2X,F4.1)
      STOP
      END
```

```
      PROGRAM STGRAPH(INPUT,OUTPUT,TAPE5=INPUT,TAPE6=OUTPUT)
C     THIS PROGRAM PRODUCES EQUAL-AREA LOWER HEMISPHERE
C   STEREOGRAPHIC PROJECTIONS FOR STRUCTURAL ORIENTATION
C   DATA. THE NETS ARE 10 CENTIMETERS IN DIAMETER.
C
C     DATA TYPES:
C      1='+', 2='O', 3='Z', 4='S'  (LINEATIONS)
C      6='+', 7='O', 8='*'  (FOLIATIONS)
C      5='+'                (EIGENVECTORS)
C
C     THREE LABELS PROCEED DATA FOR EACH PLOT, FOLLOWED BY
C   DATA TYPE CODE AND NUMBER. THE LAST DATA TYPE ON A PLOT
C   MUST BE FOLLOWED BY 0,0. FOLLOWING THIS ARE THREE MORE
C   LABELS (E.G. EIGENVALUES). THE FIRST PLOT WILL BE IN THE
C   UPPER LEFT; SUBSEQUENT PLOTS WHOSE DATA LISTS ARE
C   PROCEEDED BY A 2, 3, OR 4, WILL BE IN THE UPPER RIGHT,
C   LOWER LEFT AND LOWER RIGHT RESPECTIVELY. THE FINAL
C   PLOT DATA MUST BE TERMINATED BY A 0.
C                 -F.W. VOLLMER, 1984, U OF MN
C
      INTEGER TYPE,PL,TR,STR,DIP,AZ,ANG
      CHARACTER*1,SYM
      CHARACTER*2,DIR
      CHARACTER*10,LABEL1,LABEL2,LABEL3,LABEL4,LABEL5,LABEL6
      CALL BGNCOR(0,0,1,0)
      CALL BGNVSF(0)
      CALL VSFON(0)
      CALL SWINDO(-15.0,15.0,-15.0,15.0)
      CALL SVPOR2(0.0,0.420168,0.420168,0.840336)
    5 READ(5,10) LABEL1
      READ(5,10) LABEL2
      READ(5,10) LABEL3
   10 FORMAT(A10)
      CALL CRTSEG
   20 READ(5,*) TYPE,NUM
      IF (TYPE.EQ.0) GO TO 100
      IF (TYPE.EQ.1) SYM='+'
      IF (TYPE.EQ.2) SYM='O'
      IF (TYPE.EQ.3) SYM='Z'
      IF (TYPE.EQ.4) SYM='S'
      IF (TYPE.EQ.5) SYM='+'
      IF (TYPE.EQ.6) SYM='+'
      IF (TYPE.EQ.7) SYM='O'
      IF (TYPE.EQ.8) SYM='*'
      SIZE=0.3
      IF (TYPE.EQ.5) SIZE=0.8
      CALL SCSIZE(SIZE,SIZE)
      CALL SCJUST(5)
      IF (TYPE.GT.5) GO TO 40
C   READ IN LINEATION DATA.
      DO 30 I=1,NUM
      READ(5,25) IX,IY,PL,TR
   25 FORMAT(I3,1X,I3,1X,I2,1X,I3)
C   CALCULATE PLOTTING COORDINATES.
```

```
      R=14.1421*SIN(0.785398-PL*0.00872665)
      X=R*COS((90-TR)*0.0174533)
      Y=R*SIN((90-TR)*0.0174533)
      CALL MOVA2(X,Y)
   30 CALL TEXT(SYM,1)
      GO TO 20
C  READ IN FOLIATION DATA.
   40 DO 60 I=1,NUM
      READ(5,50) IX,IY,STR,DIP,DIR
   50 FORMAT(I3,1X,I3,1X,I3,1X,I2,1X,A2)
C  CONVERT STRIKE TO TREND OF NORMAL.
      TR=STR+90
      IF (TR.GT.360) TR=TR-360
      IF (DIR.EQ.'N ') AZ=0
      IF (DIR.EQ.'NE') AZ=45
      IF (DIR.EQ.'E ') AZ=90
      IF (DIR.EQ.'SE') AZ=135
      IF (DIR.EQ.'S ') AZ=180
      IF (DIR.EQ.'SW') AZ=225
      IF (DIR.EQ.'W ') AZ=270
      IF (DIR.EQ.'NW') AZ=315
      IF (DIR.EQ.'  ') AZ=0
      ANG=ABS(TR-AZ)
      IF (ANG.GT.180) ANG=360-ANG
      IF (ANG.LT.90) TR=TR+180
      IF (TR.GT.360) TR=TR-360
      PL=90-DIP
C  CALCULATE PLOTTING COORDINATES.
      R=14.1421*SIN(0.785398-PL*0.00872665)
      X=R*COS((90-TR)*0.0174533)
      Y=R*SIN((90-TR)*0.0174533)
      CALL MOVA2(X,Y)
   60 CALL TEXT(SYM,1)
      GO TO 20
C  DRAW NET OUTLINE AND LABEL NET.
  100 READ(5,10) LABEL4
      READ(5,10) LABEL5
      READ(5,10) LABEL6
      CALL MOVA2(0.0,10.0)
      DO 110 K=1,360
      X=10*COS((90-K)*0.0174533)
      Y=10*SIN((90-K)*0.0174533)
  110 CALL LINA2(X,Y)
      CALL LINA2(0.0,10.2)
C  ADJUST LETTERING WIDTH AND HEIGHT.
      CALL SCSIZE(0.5,0.7)
      CALL SCJUST(9)
      CALL TEXT('N',1)
      CALL MOVA2(0.0,0.3)
      CALL LINA2(0.0,-0.3)
      CALL MOVA2(0.3,0.0)
      CALL LINA2(-0.3,0.0)
      CALL SCSIZE(0.5,0.6)
      CALL SCJUST(8)
```

```
      CALL MOVA2(8.0,-9.0)
      CALL TEXT(LABEL1,10)
      CALL MOVA2(8.0,-10.0)
      CALL TEXT(LABEL2,10)
      CALL MOVA2(8.0,-11.0)
      CALL TEXT(LABEL3,10)
      CALL MOVA2(-10.0,11.0)
      CALL TEXT(LABEL4,10)
      CALL MOVR2(0.0,-1.0)
      CALL TEXT(LABEL5,10)
      CALL MOVR2(0.0,-1.0)
      CALL TEXT(LABEL6,10)
      CALL CLTSEG
      READ (5,*) IQUAD
      IF (IQUAD.EQ.0) GO TO 200
      IF (IQUAD.EQ.2) CALL SVPOR2(0.42017,0.84034,0.42017,
     +0.84034)
      IF (IQUAD.EQ.3) CALL SVPOR2(0.0,0.42017,0.0,0.42017)
      IF (IQUAD.EQ.4) CALL SVPOR2(0.42017,0.84034,0.0,
     +0.42017)
      GO TO 5
  200 CALL VSFOFF(0)
      CALL TRMVSF(0)
      CALL TRMCOR
      STOP
      END
```

```
      PROGRAM LINEPL(INPUT,OUTPUT,TAPE5=INPUT,TAPE6=OUTPUT)
C     THIS PROGRAM IS DESIGNED TO PLOT LINEATION OR FOLIATION
C  DATA FOR THE MAP AREA. THE ORIENTATION DATA FILE MUST
C  CONTAIN GRID COORDINATES. DATA TYPES LESS THAN 6 ARE
C  PLOTTED AS LINEATIONS; DATA TYPES GREATER THAN 5
C  ARE PLOTTED AS FOLIATIONS.
C                              - F.W.VOLLMER, U. OF MN., 1984
C
      CHARACTER*2,DIR
      CHARACTER*10,LABEL1,LABEL2,LABEL3
      REAL LD,LS
      INTEGER TYPE,PL,TR,STR,DIP,AZ,ANG
      R=0.0174533
      CALL BGNCOR(0,0,1,0)
      CALL BGNVSF(0)
      CALL VSFON(0)
C  SCALEING FACTORS IN SWINDO AND SVPOR2 GIVE 1:50000.
      CALL SWINDO(-1.0,16.0,-1.0,16.0)
      CALL SVPOR2(0.0,0.9501,0.0,0.9501)
      CALL CRTSEG
      READ(5,10) LABEL1
      READ(5,10) LABEL2
      READ(5,10) LABEL3
   10 FORMAT(A10)
      READ(5,*)TYPE,NUM
      LD=1.0
      LS=0.1
      DO 50 I=1,NUM
      IF (TYPE.GT.5) GO TO 20
      READ(5,*) IX,IY,PL,TR
      GO TO 30
   20 READ(5,25) IX,IY,STR,DIP,DIR
   25 FORMAT(I3,1X,I3,1X,I3,1X,I2,1X,A2)
C  CONVERT STRIKE TO TREND OF NORMAL.
      TR=STR+90
      IF (TR.GT.360) TR=TR-360
      IF (DIR.EQ.'N ') AZ=0
      IF (DIR.EQ.'NE') AZ=45
      IF (DIR.EQ.'E ') AZ=90
      IF (DIR.EQ.'SE') AZ=135
      IF (DIR.EQ.'S ') AZ=180
      IF (DIR.EQ.'SW') AZ=225
      IF (DIR.EQ.'W ') AZ=270
      IF (DIR.EQ.'NW') AZ=315
      IF (DIR.EQ.'  ') AZ=0
      ANG=ABS(TR-AZ)
      IF (ANG.GT.180) ANG=360-ANG
      IF (ANG.GT.90) TR=TR+180
      IF (TR.GT.360) TR=TR-360
      PL=DIP
C  CONVERT GRID COORDINATES TO PLOT COORDINATES.
   30 IF (IX.LT.010) IX=IX+1000
      XPLOT=(IX-890.0)/10.0
      YPLOT=(IY-150.0)/10.0
```

```
      DPL=LD*COS(PL*R)
      IF (TYPE.GT.5) DPL=0.025
      XT=SIN(TR*R)*DPL
      YT=COS(TR*R)*DPL
      IF (TYPE.LT.6) GO TO 40
C     PLOT STRIKE AND DIP FOR FOLIATION.
      XS1=SIN((TR+90)*R)*LS
      YS1=COS((TR+90)*R)*LS
      XS2=SIN((TR+270)*R)*LS
      YS2=COS((TR+270)*R)*LS
      CALL MOVA2(XPLOT+XS1,YPLOT+YS1)
      CALL LINA2(XPLOT+XS2,YPLOT+YS2)
   40 CALL MOVA2(XPLOT,YPLOT)
      CALL LINR2(XT,YT)
      IF (TYPE.GT.5) GO TO 50
C     PLOT ARROW FOR LINEATION.
      XS1=SIN((TR-160)*R)*LS
      YS1=COS((TR-160)*R)*LS
      XS2=SIN((TR+160)*R)*LS
      YS2=COS((TR+160)*R)*LS
      CALL LINR2(XS1,YS1)
      CALL MOVA2(XPLOT+XT,YPLOT+YT)
      CALL LINR2(XS2,YS2)
   50 CONTINUE
C     PLOT MAP OUTLINE.
      CALL MOVA2(0.0,0.0)
      CALL LINA2(0.0,15.05)
      CALL LINA2(12.0,15.05)
      CALL LINA2(12.0,0.0)
      CALL LINA2(0.0,0.0)
C     LABEL MAP COORDINATES.
      CALL SCSIZE(0.2,0.25)
      CALL MOVA2(0.0,5.0)
      CALL LINA2(0.2,5.0)
      CALL SCJUST(7)
      CALL TEXT('20',2)
      CALL MOVA2(12.0,5.0)
      CALL LINA2(11.8,5.0)
      CALL MOVA2(1.0,15.05)
      CALL LINA2(1.0,14.85)
      CALL MOVA2(11.0,15.05)
      CALL LINA2(11.0,14.85)
      CALL MOVA2(1.0,0.0)
      CALL LINA2(1.0,0.2)
      CALL SCJUST(9)
      CALL TEXT('90',2)
      CALL MOVA2(11.0,0.0)
      CALL LINA2(11.0,0.2)
      CALL TEXT('00',2)
C     TITLE.
      CALL MOVA2(0.0,15.05)
      CALL SCJUST(8)
      CALL TEXT(LABEL1,10)
      CALL MOVA2(2.1,15.05)
```

```
      CALL TEXT(LABEL3,10)
      CALL CLTSEG
      CALL VSFOFF(0)
      CALL TRMVSF(0)
      CALL TRMCOR
      STOP
      END
```

```
      PROGRAM SHEATH(OUTPUT, TAPE6=OUTPUT)
C     THIS PROGRAM IS DESIGNED TO PLOT THE TOPOGRAPHY OF A
C  DOUBLE SINE SURFACE (DOME AND BASIN PATTERN) DEFORMED IN
C  SIMPLE SHEAR. SECTIONS OR THREE-DIMENSIONAL PROJECTIONS
C  MAY BE SPECIFIED. AN ADDITIONAL SIMULATION OF BACK-
C  SHEARING MAY BE ADDED.
C                                  - F.W. VOLLMER, U. OF MN., 1983
C
      DIMENSION X(-16:16,-128:128),Y(-16:16,-128:128),
     +Z(-16:16),GAMMA(4)
      CHARACTER*100 LABEL
C  SPECIFY INITIAL ROTATION AND SIMPLE SHEAR FOR FOUR PLOTS.
      RI=2.0*0.0174533
      GAMMA(1)=0.0
      GAMMA(2)=10.0
      GAMMA(3)=20.0
      GAMMA(4)=20.0
C  FINAL ROTATION FOR BACK-SHEARING IN FOURTH PLOT, OR ALL
C  SECTIONS.
      RF=20.0*0.0174533
C  SPECIFY SECTION, 1, OR PLOT, 0; NUMBER OF LAYERS (ODD).
      NXSECT=0
      NLAYER=1
C  SPECIFY CROSS-SECTION NORMAL (VECTOR POINTS TOWARDS EYE).
      SVX=0.0
      SVY=1.0
      SVZ=0.364
C  SPECIFY PLOT VIEW DIRECTION (VECTOR POINTS TOWARDS EYE).
      VX=-0.6
      VY=1.6
      VZ=2.2
C  LENGTH PARAMETER FOR X DIRECTION (32 TO 128).
      NL=64
C  INITIATE PLOTTING ROUTINE
      CALL BGNCOR(0,0,0,0)
      CALL BGNVSF(0)
      CALL VSFON(0)
      CALL SREFRM(0)
      IF (NXSECT.EQ.0) GO TO 30
      CALL SVPNOR(-SVX,-SVY,-SVZ)
      CALL SWINDO(-7.5,7.5,-7.5,7.5)
      IF (ABS(SVY).GT.ABS(SVX)) CALL SVUP3 (0.0,0.0,-1.0)
      CALL SPROJ(0,SVX,SVY,SVZ)
      GO TO 40
   30 CALL SVPNOR(-VX,-VY,-VZ)
      CALL SWINDO(-7.5,7.5,-7.5,7.5)
C  FOR ORTHOGRAPHIC PROJECTIONS USE 0; 1 FOR PERSPECTIVE.
      CALL SPROJ(0,20*VX,20*VY,20*VZ)
   40 DO 2000 NPLOT=1,4
C  SET UP VIEW AREAS ON FINAL PLOT.
      IF ((NPLOT.EQ.4).AND.(NXSECT.EQ.1)) GO TO 2000
      IF (NPLOT.EQ.1) CALL SVPOR2(0.0,0.5,0.35,0.85)
      IF (NPLOT.EQ.2) CALL SVPOR2(0.5,1.0,0.35,0.85)
      IF (NPLOT.EQ.3) CALL SVPOR2(0.0,0.5,0.0,0.5)
```

```
      IF (NPLOT.EQ.4) CALL SVPOR2(0.5,1.0,0.0,0.5)
      IF (NXSECT.EQ.0) GO TO 45
C  DISTO IS THE DISTANCE OF THE SECTION FROM ORIGIN.
      DISTO=(NPLOT-1.0)*0.5
      CALL SVDPTH(DISTO-0.00001,DISTO+0.00001)
      CALL SFPCLP(1)
      CALL SBPCLP(1)
   45 CALL CRTSEG
      IF (GAMMA(NPLOT).EQ.0.0) LABEL='INITIAL PERTURBATION$'
      IF (GAMMA(NPLOT).EQ.1.0) LABEL='GAMMA=1$'
      IF (GAMMA(NPLOT).EQ.5.0) LABEL='GAMMA=5$'
      IF (GAMMA(NPLOT).EQ.10.0) LABEL='GAMMA=10$'
      IF (GAMMA(NPLOT).EQ.20.0) LABEL='GAMMA=20$'
      IF (GAMMA(NPLOT).EQ.30.0) LABEL='GAMMA=30$'
      IF (GAMMA(NPLOT).EQ.40.0) LABEL='GAMMA=40$'
      IF (GAMMA(NPLOT).EQ.50.0) LABEL='GAMMA=50$'
      IF (GAMMA(NPLOT).EQ.60.0) LABEL='GAMMA=60$'
      IF (GAMMA(NPLOT).EQ.100.0) LABEL='GAMMA=100$'
      IF (GAMMA(NPLOT).EQ.500.0) LABEL='GAMMA=500$'
      IF ((NPLOT.EQ.4).AND.(RF.NE.0.0)) LABEL='BACK-SHEAR$'
      DO 1000 NLAY=-(NLAYER-1)/2,(NLAYER-1)/2
C  CALCULATE INITAL STATE POINT COORDINATES
      DO 10 M=-16,16
      Z(M)=M*0.19635
      DO 20 N=-NL,NL
      X(M,N)=N*0.19635
      Y(M,N)=0.06283*(COS(X(M,N))+COS(Z(M)))
     ++NLAY*0.2
C  INITIAL ROTATION
      IF (RI.EQ.0.0)  GO TO 5
      XTEMP=X(M,N)
      X(M,N)=XTEMP*COS(RI)+Y(M,N)*SIN(RI)
      Y(M,N)=-XTEMP*SIN(RI)+Y(M,N)*COS(RI)
C  SIMPLE SHEAR
    5 X(M,N)=X(M,N)+GAMMA(NPLOT)*Y(M,N)
C  SECOND ROTATION AND BACKTHRUSTING.
      IF (RF.EQ.0.0) GO TO 20
      IF ((NXSECT.EQ.0).AND.(NPLOT.LT.4)) GO TO 20
      XTEMP=X(M,N)
      X(M,N)=XTEMP*COS(RF)+Y(M,N)*SIN(RF)
      Y(M,N)=-XTEMP*SIN(RF)+Y(M,N)*COS(RF)
      IF (ABS(X(M,N)).LE.0.7854) Y(M,N)=Y(M,N)+SIN(X(M,N)*2)
      IF (X(M,N).GT.0.7854) Y(M,N)=Y(M,N)+1.0
      IF (X(M,N).LT.-0.7854) Y(M,N)=Y(M,N)-1.0
   20 CONTINUE
   10 CONTINUE
C  PLOT 'X' LINES
      IF (NXSECT.EQ.0) ISTEP=2
      IF (NXSECT.EQ.1) ISTEP=1
      DO 100 I=-16,16,ISTEP
      NCT=0
      DO 200 J=-NL,NL
      IF ((ABS(X(I,J))).GT.6.284) GO TO 250
   50 NCT=NCT+1
```

```
      IF (NCT.GT.1) GO TO 300
      CALL MOVA3(X(I,J),Y(I,J),Z(I))
      GO TO 200
  300 CALL LINA3(X(I,J),Y(I,J),Z(I))
      GO TO 200
  250 NCT=0
  200 CONTINUE
  100 CONTINUE
C  PLOT 'Z' LINES
      DO 400 L=-NL,NL,ISTEP
      MCT=0
      DO 500 K=-16,16
      IF ((ABS(X(K,L))).GT.6.284) GO TO 550
   60 MCT=MCT+1
      IF (MCT.GT.1) GO TO 600
      CALL MOVA3(X(K,L),Y(K,L),Z(K))
      GO TO 500
  600 CALL LINA3(X(K,L),Y(K,L),Z(K))
      GO TO 500
  550 MCT=0
  500 CONTINUE
  400 CONTINUE
 1000 CONTINUE
C  PLOT BOX OUTLINE
      IF (NXSECT.EQ.1) CALL SFPCLP(0)
      IF (NXSECT.EQ.1) CALL SBPCLP(0)
      CALL MOVA3(-6.283,2.0,-3.1416)
      CALL LINR3(0.0,-4.0,0.0)
      CALL LINR3(0.0,0.0,6.283)
      CALL LINR3(12.566,0.0,0.0)
      CALL LINR3(0.0,0.0,-6.283)
      CALL LINR3(-12.566,0.0,0.0)
      IF (NXSECT.EQ.1) GO TO 800
C  LABEL PLOT
      CALL SCSIZE(0.3,0.4)
      CALL SCPLAN(0.0,0.0,-1.0)
      CALL MOVA3(-6.0,2.0,-3.1416)
      CALL TEXT(LABEL,100)
  800 CALL CLTSEG
 2000 CONTINUE
      CALL VSFOFF(0)
      CALL TRMVSF(0)
      CALL TRMCOR
      STOP
      END
```

```
      PROGRAM SHEAROR(OUTPUT, TAPE6=OUTPUT)
C  THIS PROGRAM GIVES ORIENTATION DATA FOR A DOUBLE SINE
C  SURFACE (DOME AND BASIN PATTERN) DEFORMED IN SIMPLE SHEAR.
C  OUTPUT IS A LIST OF THE PLUNGES AND TRENDS OF SURFACE
C  NORMALS.
C                              - F.W. VOLLMER, U. OF MN., 1983
C
      DIMENSION X(-8:8,-256:256),Y(-8:8,-256:256),Z(-8:8)
      INTEGER PL,TR,PLO,TRO
      REAL LU,MU,NU,LI,MI,NI,LNTH
      K2=K3=PLO=TRO=0
C  SPECIFY INITIAL ROTATION AND SIMPLE SHEAR.
      RI=2*0.0174533
      GAMMA=20.0
C  CALCULATE INITAL STATE POINT COORDINATES
      DO 10 M=-8,8
      Z(M)=M*0.19635
      DO 20 N=-256,256
      X(M,N)=N*0.00613592
      Y(M,N)=0.062832*(COS(X(M,N))+COS(Z(M)))
C  INITIAL ROTATION
      IF (RI.EQ.0.0)  GO TO 5
      XTEMP=X(M,N)
      X(M,N)=XTEMP*COS(RI)+Y(M,N)*SIN(RI)
      Y(M,N)=-XTEMP*SIN(RI)+Y(M,N)*COS(RI)
C  SIMPLE SHEAR
    5 X(M,N)=X(M,N)+GAMMA*Y(M,N)
   20 CONTINUE
   10 CONTINUE
C  CALCULATE VECTOR COMPONENTS IN SURFACE.
      DO 500 I=-8,7
      DO 600 J=-256,255
      AX=X(I,J+1)-X(I,J)
      AY=Y(I,J+1)-Y(I,J)
      BX=X(I+1,J)-X(I,J)
      BY=Y(I+1,J)-Y(I,J)
      BZ=Z(I+1)-Z(I)
C  CALCULATE DIRECTION COSINES OF SURFACE NORMAL.
      LI=-AY*BZ
      MI=BZ*AX
      NI=AX*BY-BX*AY
      LNTH=SQRT(LI**2+MI**2+NI**2)
      LU=LI/LNTH
      MU=MI/LNTH
      NU=NI/LNTH
C  CALCULATE PLUNGE AND TREND OF NORMAL.
      PL=NINT(ASIN(MU)/0.017453)
      TR=NINT(ATAN2(NU,LU)/0.017453+270)
      IF (PL.LT.0) TR=TR+180
      IF (PL.LT.0) PL=-PL
      IF (TR.GT.360) TR=TR-360
C  K2 GIVES TOTAL NUMBER OF SURFACE NORMALS.
      K2=K2+1
      IF ((PL.EQ.PLO).AND.(TR.EQ.TRO)) GO TO 600
```

```
      PLO=PL
      TRO=TR
C  K3 GIVES NUMBER OF PLOTTED SURFACE NORMALS.
      K3=K3+1
      WRITE(6,555) PL,TR
  555 FORMAT(7H000 000,1X,I2,1X,I3)
  600 CONTINUE
  500 CONTINUE
      WRITE(6,666) K2,K3
  666 FORMAT(3I6)
      STOP
      END
```

```
S2
DOMAIN 4
N=18
7,9
968 268 216 73 E  S2
969 270 207 71 E  S2
969 271 205 88 W  S2
969 271 219 88 SE S2
968 272 208 84 SE S2
969 274 212 86 SE S2
989 219 203 83 SE S2
990 239 157 60 SW S2
995 207 136 62 SW S2
6,9
975 271 102 50 S  AP
975 271 067 85 SE AP
975 271 086 75 S  AP
975 271 170 75 W  AP
972 281 142 65 SW AP
974 290 161 71 SW AP
990 223 202 88 SE AP
990 223 205 87 W  AP
990 223 203 88 W  AP
5,3
000 000 00 112
000 000 29 022
000 000 61 203
0,0
S1=.6756
S2=.3087
S3=.0157
00-112
29-022
61-203
2
S2
DOMAIN 5
N=3
7,2
992 257 147 57 W  S2
007 287 215 40 NW S2
6,1
009 269 120 18 SW AP
5,3
000 000 58 075
000 000 13 186
000 000 29 283
0,0
S1=.7959
S2=.1279
S3=.0762
58-075
13-186
29-283
0
```

REFERENCES

Bally, A.W., 1981, Thoughts on the tectonics of folded belts, p. 13-32, in, McClay, K.R., and Price, N.J., eds., Thrust and Nappe Tectonics: Blackwell, Oxford, 539 p.

Barth, T.F.W., 1938, Progressive metamorphism of sparagmite rocks of southern Norway: Norsk Geologisk Tidskrift, v.18, p. 189-198.

Bartley, J.M., 1982, Limited basement involvement in Caledonian deformation, Hinnoy, north Norway, and tectonic implications: Tectonophysics, v. 83, p. 185-203.

Bell, T.H., 1978, Progressive deformation and reorientation of fold axes in a ductile mylonite zone: the Woodroffe thrust: Tectonophysics, v. 44, p. 285-320.

Bell, T.H., and Hammond, R.L., 1984, On the internal geometry of mylonite zones: Journal of Geology, v. 92, p. 667-686.

Bingham, C., 1974, An antipodally symmetric distribution on the sphere: Ann. Stats., v. 2, p. 1201-1225.

Biot, M.A., 1961, Theory of folding of stratified viscoelastic media and its implications in tectonics and orogenesis: Geological Society of America Bulletin, v. 72, p. 1595-1620.

Boyer, S.E., and Elliott, D., 1982, Thrust systems: American Association of Petroleum Geologists Bulletin, v. 66, p. 1196-1230.

Budd, W.F., 1970, The longitudinal stress and strain-rate gradients in ice masses: Journal of Glaciology, v. 9, p. 19-27.

Carswell, D.A., 1973, The age and status of the Basal Gneiss Complex of north-west southern Norway: Norsk Geologiske Tidsskrift, v. 53, p. 65-78.

Carter, N.L., Anderson, D.A., Hansen, F.D., and Kranz, R.L., 1981, Creep and creep rupture of granitic rocks, p. 61-82, in, Carter, N.L., Friedman, M., Logan, J.M., and Stearns, D.W., eds., Mechanical Behavior of Crustal Rocks: American Geophysical Union Monograph 24, 326 p.

Chapman, T.J., Milton, N.J. and Williams, G.D., 1979, Shape fabric variations in deformed conglomerates at the base of the Laksefjord Nappe, Norway: Journal of the Geological Society of London, v. 136, p. 683-691.

Charlesworth, H.A.K., Langenberg, C.W., and Ramsden, J., 1976, Determining axes, axial planes, and sections of macroscopic folds using computer-based methods: Canadian Journal of Earth Sciences, v. 13, p. 54-65.

Cobbold, P.R., 1979, Sheath folds and large strains (abstract), p. 338, in, White, S., Large strain deformation: report on a Tectonic Studies Group discussion meeting held at Imperial College, London on 14 November 1979: Journal of Structural Geology, v. 1, p. 333-339.

Cobbold, P.R., and Quinquis, H., 1980, Development of sheath folds in shear regimes: Journal of Structural Geology, v. 2, p. 119-126.

Coward, M.P., and Kim, J.H., 1981, Strain within thrust sheets, p. 275-292, in, McClay, K.R., and Price, N.J., eds., Thrust and Nappe Tectonics: Blackwell, Oxford, 539 p.

Cuthbert, S.J., Harvey, M.A., and Carswell, D.A, 1983, A tectonic model for the metamorphic evolution of the Basal Gneiss Complex, western south Norway: Journal of Metamorphic Geology, v. 1, p. 63-90.

Dahlstrom, C.D.A., 1970, Structural geology in the eastern margin of the Canadian Rocky Mountains: Bulletin of Canadian Petroleum Geology, v. 18, p. 332-406.

Daly, R.A., Manger, G.E., and Clark, S.P., Jr., 1966, Density of rocks, p. 19-26, in, Clark, S.P., Jr., ed., Handbook of Physical Constants: Geological Society of America Memoir 97, 587 p.

Davis, D., Suppe, J., and Dahlen, F.A., 1983, Mechanics of fold-and-thrust belts and accretionary wedges: JGR, v. 88, p. 1153-1172.

Dewey, J.F., 1969, Evolution of the Appalachian/Caledonian orogen: Nature, v. 222, April 12, p. 124-129.

Dyrelius, D., Gee, D.G., Gorbatschev, R., Ramberg, H., and Zachrisson, E., 1980, A profile through the central Scandinavian Caledonides: Tectonophysics, v. 69, p. 247-284.

Escher, A., and Watterson, J., 1974, Stretching fabrics, folds and crustal shortening: Tectonophysics, v. 22, p. 223-231.

Flinn, D., 1962, On folding during three-dimensional progressive deformation: Quarterly Journal of the Geological Journal of London, v. 118, p. 385-433.

Gale, G.H., and Roberts, D., 1974, Trace element geochemistry of Norwegian Lower Paleozoic basic volcanics and its tectonic implications: Earth and Planetary Science Letters, v. 22, p. 380-390.

Gee, D.G., 1975a, A tectonic model for the central part of the Scandinavian Caledonides: American Journal of Science, v. 275A, p. 468-515.

Gee ,D.G., 1975b, A geotraverse through the Scandinavian Caledonides - Østersund to Trondheim: Sverges Geologiska Undersökning, series C, v. 717, 66 p.

Gee, D.G., 1977, Extension of the Offerdal and Särv nappes and Seve supergroup into northern Trøndelag: Norsk Geologiske Tidsskrift, v. 57, p. 163-170.

Gee, D.G., 1978, Nappe displacement in the Scandinavian Caledonides: Tectonophysics, v. 47, p. 393-419.

Gee, D.G., 1980, Basement-cover relationships in the central Scandinavian Caledonides: Geologiska Föreningens i Stockholm Förhandlingar, v. 102, p. 455-474.

Ghosh, S.K., 1982, The problem of shearing along axial plane foliations: Journal of Structural Geology, v. 4, p. 63-67.

Grocott, J., and Watterson, J., 1980, Strain profile of a boundary within a large ductile shear zone: Journal of Structural Geology, v. 2, p. 111-118.

Haller, J., 1971, Geology of the East Greenland Caledonides: Wiley Interscience, New York, 413 p.

Hansen, E.C., 1963, Strain facies of the metamorphic rocks in Trollheimen, Norway: PhD thesis, Yale University, 194 p.

Hansen, E.C., 1971, Strain Facies: Springer-Verlag, New York, 220 p.

Hatcher Jr., R.D., Thrusts and nappes in the North American Appalachian orogen, p. 491-500, in, McClay, K.R., and Price, N.J., eds., Thrust and Nappe Tectonics: Blackwell, Oxford, 539 p.

Henriksen, N., 1978, East Greenland Caledonian fold belt, p. 105-109, in, Caledonian-Appalachian Orogen of the North Atlantic Region: Geological Survey of Canada Paper 78-13, 242 p.

Henriksen, N. and Higgins, A.K., 1976, East Greenland Caledonian fold belt, p. 183-246, in, Escher, A., and Watt, W.S., eds., Geology of Greenland: Grønlands Geologiske Undersøgelse, 603 p.

Hobbs, B.E., Means, W.D., and Williams, P.F., 1976, An Outline of Structural Geology: Wiley, New York, 571 p.

Hodges, K.V., Bartley, J.M., and Burchfiel, B.C., 1982, Structural evolution of an A-type subduction zone, Lofoten-Rombak area, northern Scandinavian Caledonides: Tectonics, v. 1, p. 441-462.

Holmson, P., 1955, Trekk av Opdalfeltets geologi: Norsk Geologiske Tidsskrift, v. 35, p. 135-150.

Holmsen, P., 1960, Caledonized basal gneisses in a northwestern area (Oppdal-Sunndal): Norges Geologiske Undersøkelse, v. 2121, 31 p.

Holtedahl, O., 1938, Geological observations in the Oppdal-Sunndal-Trollheimen district: Norsk Geologiske Tidsskrift, v. 18, p. 29-53.

Holtedahl, O., and Dons, J.A., 1960, Gelogisk kart over Norges - 1:1.000.000: Norges Geologiske Undersøkelse.

Hossack, J.R., 1968, Pebble deformation and thrusting in the Bygdin area (southern Norway): Tectonophysics, v. 5, p. 315-339.

Hossack, J.R., 1983, A cross-section through the Scandinavian Caledonides constructed with the aid of branch-line maps: Journal of Structural Geology, v. 5, p. 103-112.

Huber, M., Ramsay, J.G., and Simpson, C., 1980, Deformation in the Maggia and Antigorio nappes. Lepontine Alps: Eclogae Geol. Helv., v. 73, p. 593-606.

Hudleston, P.J., 1973, An analysis of "single-layer" folds developed experimentally in viscous media: Tectonophysics, v. 16, p. 189-214.

Hudleston, P.J., 1976, Recumbent folding in the base of the Barnes Ice Cap, Baffin Island, Northwest Territories, Canada: Geological Society of America Bulletin, v. 87, p. 1684-1692.

Hudleston, P.J., and Hooke, R.L., 1980, Cumulative deformation in the Barnes Ice Cap and implications for the development of foliation: Tectonophysics, v.66, p. 127-146.

Hurst, J.M., and McKerrow, S.W., 1981, The Caledonian nappes of eastern North Greenland: Nature, v. 290, n. 5809, p. 772-774.

Jaeger, J.C., 1969, Elasticity, Fracture and Flow with Engineering and Geological Applications: Chapman & Hall, London, 268 p.

Jager, J.C., and Cook, N.G.W., 1979, Fundamentals of Rock Mechanics, Third Edition: Chapman & Hall, London, 593 p.

Koch, P.S., Christie, J.M., and George, R.P., 1980, Flow law of "wet" quartzite in the α-quartz field (abstract): EOS, Transactions of the American Geophysical Union, v. 61, p. 376.

Kohlstedt, D.L., and Weathers, M.S., 1980, Deformation-induced microstructures, paleopiezometers, and differential stresses in deeply eroded fault zones: JGR, v. 85, p. 6269-6285.

Krill, A.G., 1980a, Tectonics of the Oppdal area, central Norway: Geologiska Föreningens i Stockholm Förhandlingar, v. 102, p. 523-530.

Krill, A.G., 1980b, Tectonics of N.E. Dovrefjell, central Norway: PhD thesis, Yale University, 178 p.

Krill, A.G., 1983a, Rb-Sr study of dolerite dikes and psammite from the Western Gneiss Region of Norway: Lithos, v. 16, p. 85-93.

Krill, A.G.,, 1983b, Rb-Sr study of rapakivi granite and augen gneiss of the Risberget Nappe, Oppdal, Norway: Norges Geologiske Undersøkelse, v. 380, p. 51-65.

Krill, A.G., in press, Relationships between the Western Gneiss Region and the Trondheim region: stockwerk-tectonics reconsidered, in, IGCP Symposium, Uppsala: Wiley.

Krill, A.G., and Röshoff, K., in press, Basement-cover relationships in the central Scandinavian Caledonides excursion B-5: Uppsala Caledonide Symposium.

Langenberg, C.W., Rondeel, H.E., and Charlesworth, H.A.K., 1977, A structural study in the Belgian Ardennes with sections constructed using computer-based methods: Geologie en Mijnbow, v. 56, p. 145-154.

Lisle, R.J., 1974, Deformed lineations as finite-strain structures: Tectonophysics, v. 21, p. 165-179.

Lisle, R.J., 1984, Strain discontinuities within the Seve-Köli Nappe Complex, Scandinavian Caledonides: Journal of Structural Geology, v. 6, p. 101-110.

Lundqvist, T., 1979, The Precambrian of Sweden: Sverges Geologiska Undersökning, series C, n. 768, 87 p.

Løset, F., 1977, Three fold phases in the northern part of Trollheimen in the Norwegian Caledonides: Norsk Geologiske Tidsskrift, v. 57, p. 121-131.

Magnusson et al., 1960 Magnusson, N.H., Thorslund, P., Brotzen, T., Asklund, B., and Kulling, O., eds. Description to Accompany the Map of the Pre-Quaternary Rocks of Sweden: Sverges Geologiska Undersökning, series Ba, n. 16, 177 p.

Mancktelow, N.S., 1981, A least squares method for determining the best-fit point maximum, great circle, and small circle to nondirectional orientation data: Journal of the International Association for Mathematical Geology, v. 13, p. 507-521.

Mardia, K.V., 1972, Statistics of Directional Data: Academic Press, New York.

Mardia, K.V., and Zemroch, P.J., 1977, Table of maximum likelihood estimates for the Bingham distribution: Journal Statist. Comput. Simul., v. 6, p. 29-34.

Mase, G.E., 1970, Continuum Mechanics: McGraw-Hill, New York, 221 p.

Mattauer, M., Collot, B., and Van den Driessche, J., 1983, Alpine model for the internal metamorphic zones of the North American Cordillera: Geology, v. 11, p. 11-15.

Means, W.D., Hobbs, B.E., Lister, G.S., and Williams, P.F., 1980, Vorticity and non-coaxiality in progressive deformations: Journal of Structural Geology, v. 2, p. 371-378.

McClay, K.R., and Coward, M.P., 1981, The Moine thrust zone. An overview, p. 241-282, in, McClay, K.R., and Price, N.J., eds., Thrust and Nappe Tectonics: Blackwell, Oxford, 539 p.

McClay, K.R., and Price, N.J., 1981, eds., Thrust and Nappe Tectonics: Geological Society of London Special Publication No. 9, Blackwell Scientific Publications, Oxford, 539 p.

Minnigh, L.D., 1979, Structural analysis of sheath-folds in a meta-chert from the Western Italian Alps: Journal of Structural Geology, v. 1, p. 275-282.

Muret, C., 1960, Partie S.E. de la culmination du Romsdal, Chainne Caledonienne, Norvege: Int. Geol. Congr. Norden, n. 19, p. 28-32.

Mykkeltveit, S., Husebye, E.S., and Oftedahl, C., 1980, Subduction of the Iapetus Ocean crust beneath the Møre Gneiss Region, southern Norway: Nature, v. 288, n. 5790, p. 473-475.

Nye, J.F., 1951, The flow of glaciers and ice sheets as a problem in plasticity: Proceedings of the Royal Society of London, Series A, v. 207, p. 554-472.

Nye, J.F., 1957, The distribution of stress and velocity in glaciers ice-sheets: Proceedings of the Royal Society of London, Series A, v. 239, p. 113-133.

Oftedahl, C., 1980, Geology of Norway: Norges Geologiske Undersøkelse, n. 356, p. 3-114.

Platt, J.P., 1983, Short note: progressive refolding in ductile shear zones: Journal of Structural Geology, v. 5, p. 619-622.

Ramsay, J.G., 1967, Folding and Fracturing of Rocks: McGraw-Hill, New York, 568 p.

Ramsay, J.G., 1980, Shear zone geometry: a review: Journal of Structural Geology, v. 2, p. 83-100.

Ramsay, J.G., and Pfiffner, O.A., 1982, Constraints on geological strain rates: arguments from finite strain states of naturally deformed rocks: JGR, v. 87, p. 311-321.

Roberts, D., and Gale, G.H., 1978, The Caledonian-Appalachian Iapetus Ocean, p. 255-342, in, Tarling, D.H., ed., Evolution of the Earth's Crust: Academic Press, London.

Roberts, D., and Sturt, B.A., 1980, Caledonian deformation in Norway: Journal of the Geological Society of London, v. 137, p. 241-250.

Roberts, D., and Wolff, F.C., 1980, Tectonostratigraphic development of the Trondheim region Caledonides, central Norway: Journal of Structural Geology, v. 3, p. 487-494.

Rosenqvist, I.T., 1943, Metamorphism and metasomatism in the Opdal area: Norges Geologiske Undersøkelse , v. 22, p. 106-202.

Röshoff, K., 1978, Structure of the Tännäs Augen Gneiss Nappe and its relation to under- and overlying units in the central Scandinavian Caledonides, Sverges Geologiska Undersökning, Series C, v. 739, p. 1-35.

Sanderson, D.J., 1973, The development of fold axes oblique to the regional trend: Tectonophysics, v. 16, p. 55-70.

Scott, W.H., 1967, Evolution of folds in the metamorphic rocks of western Dovrefjell, Norway: PhD thesis, Yale University, 111 p.

Sherwin, J., and Chapple, W.M., 1968, Wavelengths os single layer folds: a comparison between theory and observation: American Journal of Science, v. 266, p. 167-179.

Sibson, R.H., 1977, Fault rocks and fault mechanisms: Journal of the Geological Society of London, v. 133, p. 191-213.

Simpson, C., and Schmid, S.M., 1983, An evaluation of criteria to deduce the sense of movement in sheared rocks: Geological Society of America Bulletin, v. 94, p. 1281-1288.

Skjernaa, L., 1980, Rotation and deformation of randomly oriented planar and linear structures in progressive simple shear: Journal of Structural Geology, v. 2, p. 101-110.

Smith, R.B., 1975, Unified theory of the onset of folding, boudinage, and mullion structure: Geological Society of America Bulletin, v. 86, p. 1601-1609.

Smith, R.B., 1977, Formation of folds, boudinage, and mullions in non-Newtonian materials: Geological Society of America Bulletin, v. 88, p. 312-320.

Solheim, S., 1980, Geochronological investigations in the Oppdal area, central Norway, Norsk Geologiske Tidsskrift, v. 60, p. 175-188.

Steiger, R.H., Hansen, B.T., Schuler, C.H., Bar, M.T., and Henriksen, N., 1979, Polyorogenic nature of the southern Caledonian fold belt in East Greenland: an isotopic study: Journal of Geology, v. 87, p. 475-495.

Strand, T., 1961, The Scandinavian Caledonides, a review: American Journal of Science, v. 259, p. 161-172.

Sturt, B., 1978, The Norwegian Caledonides - Introduction, p. 13-15, in, Caledonian-Appalachian Orogen of the North Atlantic Region: Geological Survey of Canada Paper 78-13, 242 p.

Talwani, M., and Eldholm, O., 1977, Evolution of the Norwegian-Greenland Sea: Geological Society of America Bulletin, v. 88, p. 969-999.

Thompson, J.B., Jr., Robinson, P.R., Clifford, T.N., and Trask, N.J., 1968, Nappes and gneisse domes in west-central New England, p. 203-218, in, Zen, E., White, W.S., and Hadley, J.B., eds., Studies of Appalachian Geology: Northern and Maritime: Wiley, New York, 475 p.

Törnebohm, A.E., 1888, Om fjällproblemet: Geologiska Föreningens i Stockholm Förhandlingar, v. 10, p. 328-336.

Törnebohm, A.E., 1896, Grundragen af det centrala Skandinaviens berggyggnad: Kgl. Svenska Vetensk. Akad. Handl., v. 28(5), 212 p.

Treagus, S.H., 1973, Buckling instability of a viscous single-layer system, oblique to the principal compression: Tectonophysics, v. 19, p. 271-289.

Treagus, J.E., and Treagus, S.H., 1981, Folds and the strain ellipsoid: a general model: Journal of Structural Geology, v. 3, p. 1-17.

Trümpy, R., 1980, Geology of Switzerland: Wepf & Co., Basel, 334 p.

Tullis, T.E., and Wood, D.S., 1975, Correlation of finite strain from both reduction bodies and preferred orientations of mica in slate from Wales: Geological Society of America Bulletin, v. 86, p. 632-638.

Turner, F.J., and Weiss, L.E., 1963, Structural Analysis of Metamorphic Tectonites: McGraw-Hill, New York, 545 p.

Vollmer, F.W., and Bosworth, W., 1985, Formation of melange in a foreland basin overthrust setting: example from the Taconic Orogen, p. 53-68, in, Raymond, L.A., ed., Melanges: Their Nature, Origin and Significance: Geological Society of America Special Paper 198.

Watson, G.S., 1965, Equitorial distributions on a sphere: Biometrika, v. 52, p. 193-203.

Watson, G.S., 1966, The statistics of orientation data: Journal of Geology, v. 74, p. 786-797.

Wegmann, C.E., 1935, Zur deutung der migmatite: Geologische Rundschau, v. 26, p. 305-350.

Wegmann, C.E., 1959, La flexure axiale de la Driva et quelques problemes structuraux des Caledonides Scandinaves: Norsk Geologiske Tidsskrift, v. 39, p. 25-74.

Weiss, L., and Gay, 1974, The relationship between principal stress directions and the geometry of kinks in foliated rocks: Tectonophysics, v. 21, p. 287-300.

Wheeler, R.L., 1973, Folding history of the metamorphic rocks of eastern Dovrefjell, Norway: PhD thesis, Princeton University, 233 p.

White, S.H., Burrows, S.E., Carreras, J., Shaw, N.D., and Humphreys, F.J., 1980, On mylonites in ductile shear zones, Journal of Structural Geology, v. 2, p. 175-188.

Whitten, E.H.T., 1966, Structural Geology of Folded Rocks: Rand McNally, Chicago, 663 p.

Williams, G.D., 1978, Rotation of contemporary folds into the X direction during overthrust processes in Laksefjord, Finnmark: Tectonophysics, v. 48, p. 29-40.

Williams, P.F., 1970, A criticism of the use of style in the study of deformed rocks: Geological Society of America Bulletin, v. 81, p. 3283-3296.

Winkler, H.G.F., 1976, Petrogenesis of Metamorphic Rocks, Fourth Edition: Springer-Verlag, New York, 334 p.

Wise, D.U., Dunn, D.E., Engelder, J.T., Geiser, P.A., Hatcher, R.D., Kish, S.A., Odom, A.L., Schamel, S., 1984, Fault-related rocks: suggestions for terminology: Geology, v. 12, p. 391-395.

Wolff, F.C., 1976, Beskrivelse til geologisk kart over Norges - 1:250.000 Trondheim: Norges Geologiske Undersøkelse Kartserie.

Wolff, F.C., and Roberts, D., 1980, Geology of the Trondheim Region: Norges Geologiske Undersøkelse, n. 356, p. 117-128.

Woodcock, N.H., 1977, Specification of fabric shapes using an eigenvalue method: Geological Society of America Bulletin, v. 88, p. 1231-1236.

Zoback, M.D., 1983, State of stress in the lithosphere: Reviews of Geophysics and Space Physics, v. 21, p. 1503-1511.

Asklund, B., 1960, The geology of the Caledonian mountain chain and of adjacent areas in Sweden, in, Magnusson, N.H., Thorslund, P., Brotzen, T., Asklund, B., and Kulling, O., eds. Description to Accompany the Map of the Pre-Quaternary Rocks of Sweden: Sverges Geologiska Undersökning, series Ba, n. 16, 177 p.